Department of Chemistry

Electrochemical Studies Toward Proteomic Analysis

Eva Maria Alvarez de Eulate Diaz de San Martin

This thesis is presented for the Degree of
Doctor of Philosophy
of
Curtin University

February 2014

Declaration

To the best of my knowledge and belief this thesis contains no material previously published by any other person except where due acknowledgment has been made.

This thesis contains no material which has been accepted for the award of any other degree or diploma in any university.

Eva Maria Alvarez de Eulate Diaz de San Martin

Table of contents

“I prefer drawing to talking.

Drawing is faster, and leaves less room for lies.”

– Le Corbusier

Acknowledgements

I would like to express my sincere gratitude to Prof. Damien W. M. Arrigan for offering me the great opportunity of forming part of his research group. I will always be grateful for his supervision, guidance, encouragement and enthusiasm during these three years. He has played a very important role in the development of my professional career and more importantly in my personal life. You have been present in some of the most significant events of my life and I will always be grateful for being that kind of support which only some are lucky to receive from their supervisor. You have become part of my Perth family and I wish you the best in your future.

To the electrochemistry and sensors group, who have been there for the entire journey, Debbie, Michael, Shane, Junnie, Krish, Masniza, Salmah, Yang and Ghulam. Dr. Debbie S. Silvester for introducing me to the Ionic Liquid world which became an important and challenging part of my PhD. To Shane O'Sullivan for showing me the magic of how to prepare the organogel and sharing with me the good and bad moments, especially during our coffee breaks. And thanks to Krish and Junnie for all the electrochemistry discussions and lunches in Karawara. More importantly and above all, for their support and friendship.

I would like to thank Prof. Hubert H. Girault who adopted me in his group for several weeks at EPFL in Lausanne. He and his collaborators made me feel at home from the first day. I am still thrilled that I had the opportunity to learn from someone that I have cited and read countless times throughout my PhD. Special thanks to other collaborators including, Dr Michael Scanlon (EPFL) for bringing the opportunity to collaborate in H. H. Girault's group, sharing all his knowledge in his thesis *'The ITIES bible'* and taught me how Swiss eat cheese. Also thanks to Dr. Liang Qiao (EPFL) who guided me in the ESTASI-MS world during my stay at EPFL in Lausanne.

I would like to thank Lauren Serl, project students who assisted with the work presented in Chapter 6. To the following project students, Sharon Fletcher and Yiu

Hang Yuen who also helped in work published in 2013, which is not included in this thesis. I thank all of them for their time and help.

I would also like to thank all the PhD students at Curtin University who have shared the cheerful and painful moments during this time. Thanks for not killing us in the lab and for all the tequila parties, birthday parties, beers at Hippo Creek, footy and cricket private workshops, boot camp sessions, barbeques...

To my Perth family members who cared and looked after me, Lucia, Miguel, Zoe and Araceli. Thanks for being how you are. To '*the Spagnoli'* neighbours, the South Perth community, my Adelaide-Vigo family and my ex-housemates in Wellington St. who became my special little family in the city.

I do not want to forget all the people that I left 14,489 km away from Perth, family and friends from Pamplona who are always there for my return, my Uni friends who are always *'en la cresta de la ola'*, the '*majisísismo*' IBEC group and my Irish family who are distributed all over the world.

Finalmente, me gustaría dedicar esta tesis a mi familia. Sé que no es fácil dejar a una hija, hermana, cuñada o tía irse tan, tan lejos. Más cuando parece imposible irse más allá. Por eso y por todo el apoyo y amor recibido en la distancia, os quiero agradecer y dedicar esta parte de mi vida que nunca habría sido capaz de alcanzar sin vosotros. Papá y mamá, gracias por ser como sois y haberme enseñado a ver la vida y el mundo con vuestros ojos porque me ha hecho la persona que soy hoy. Gracias familia Calle-Alvarez de Eulate por el apoyo incondicional y por ser mi modelo a seguir aparte de tener los mejores sobris del mundo. Gracias JADE por haberme enseñado ese espíritu aventurero y luchador. Gracias a la familia barcelonesa por tener siempre un hueco en vuestras vidas para la Evita. Y gracias Elios por ser mi compañero de viaje y formar parte de esta '*crazy*' familia. Gracias por ser así, os quiero.

GRACIAS

Glossary of symbols and abbreviations

Roman symbols

Symbol	Meaning	Units
A	area	cm^2
a_i	activity of species i	-
C	capacitance	F
C_i	concentration of species i	mol cm^{-3}
d	centre-to-centre separation in microdiscs or micropores	cm
D_i	diffusion coefficient of species i	cm^2 s^{-1}
e	elementary charge in spectrometry	-
e^-	electrons	-
E	potential	V
	electric field strength in spectrometry	V m^{-1}
E_{eq}	equilibrium potential	V
$E^{0'}$	formal potential	V
F	Faraday constant	C
i	current	nA
i_{lim}	limiting current	nA
J	flux	-
L	recessed depth in microelectrodes	cm

	or micropores	
m	mass	g mol^{-1}
n	number of electrons in solid electrode electrochemistry	-
N_i	number of moles of species i	-
o	organic phase at liquid – liquid interfaces	-
O	oxidised species in redox reactions	--
Q	charge	C
r	radius	cm
R	reduced species in redox reactions	-
	resistance	Ω
	universal gas constant	J K^{-1} mol^{-1}
R_s	resistance of solution	Ω
t	time	s
T	temperature	K
V	potential difference	V
w	water / aqueous phase at liquid – liquid interfaces	-
z_i	charge of species i	-
Z	impedance	Ω
Z_{im}	imaginary component of impedance	Ω
Z_{re}	real component of impedance	Ω

Greek symbols

Symbol	Meaning	Units
α	aqueous phase of a liquid – liquid system	-
β	organic phase of a liquid – liquid system	-
Δ	difference	-
δ	diffusion zone	-
ε	relative permittivity of a solvent	$A^2\ s^4\ kg^{-1}\ m^{-3}$
γ_i^{α}	activity coefficient for species i in phase α	-
$\varphi 0'$	formal potential	V
$\bar{\mu}_i^{\alpha}$	electrochemical potential of species i in phase α	$kJ\ mol^{-1}$
μ_i^{α}	chemical potential of species i in phase α	$kJ\ mol^{-1}$
$\mu_i^{\alpha,0}$	standard chemical potential of species i in phase α	$kJ\ mol^{-1}$
v	scan rate in voltammetry	$V\ s^{-1}$
	velocity of ions in spectrometry	$m^2\ s^{-1}\ V^{-1}$

Standard abbreviations

Abbreviation	Meaning
ACT	Aqueous complexation followed by transfer
ACV	Alternating current voltammetry
AdSV	Adsorptive stripping voltammetry
AOT	Bis(2-ethylhexyl) sulfosuccinate

ASV	Anodic stripping voltammetry
BTPPA	Bis(triphenylphosphoranyliden)ammonium, organic cation
BESI	Biphasic electrospray ionisation
BSA	Bovine serum albumin
CE	Capillary electrophoresis Counter electrode
CSV	Cathodic stripping voltammetry
CV	Cyclic voltammetry
DESI	Desorption electrospray ionisation
DB18C6	Dibenzo-18-crown-6
1,2-DCE	1,2-dichloroethane
1,6-DCH	1,6-dichlorohexane
2-DGE	Two dimensional gel electrophoresis
DHB	2,5-dihydroxy benzoic acid
DNNS	Dinonylnaphthalenesulfonate
DPPC	L-α-dipalmitoyl phosphatidylcholine
ESI	Electrospray ionisation
EIS	Electrochemical impedance spectroscopy
ESTASI	Electrostatic spray ionisation
ET	Electron transfer
FAP	Tris(pentafluoroethyl)trifluorophosphate, room temperature ionic liquid anion

FIT	Facilitated ion transfer
FT-ICR	Fourier transform ion cyclotron resonance
GC	Gas chromatography
HEWL	Hen-egg-white-lysozyme
IHP	Inner Helmholtz plane
IT	Ion transfer
ITIES	Interface between two immiscible electrolyte solutions
LC	Liquid chromatography
MALDI	Matrix-assisted laser desorption ionisation
MD	Molecular dynamics
MS	Mass spectrometry
NALDI	Nano-assisted laser desorption ionisation
NB	Nitrobenzene
OHP	Outer Helmholtz plane
$P_{14,6,6,6}$	Trishexyl(tetradecyl)phosphonium, room temperature ionic liquid cation
PVC	Polyvinyl chloride
QELS	Quasi laser light scattering
RE	Reference electrode
RTIL	Room temperature ionic liquid
SECM	Scanning electrochemical microscopy
SICM	Scanning ion-conductance microscopy

SIMS	Secondary ion mass spectrometry
SPE	Solid phase extraction
SV	Stripping voltammetry
TBA	Tetrabutyl ammonium, organic cation
TIC	Transfer by interfacial complexation
TID	Transfer by interfacial dissociation
TOC	Transfer to the organic phase followed by complexation
TOF	Time of flight
TPB	Tetraphenylborate, organic anion
TPBCl	Tetrakis(4-chlorophenyl)borate, organic anion
TPFB	Tetrakis(4-fluorophenul)borate, organic anion

Abstract

The understanding of the behaviour of biomolecules at liquid – liquid interfaces is of considerable importance for investigating fundamental biological processes and therapeutics. Electrochemistry at the interface between two immiscible electrolyte solutions (ITIES) is based on charge transfer across the polarised soft interface formed when bringing two electrolyte solutions (aqueous and organic) into contact. This provides the possibility for detecting biomolecules such as proteins in a label-free manner. Several pre-treatment steps used in proteome analysis such as protein pre-concentration and digestion were implemented at the liquid – liquid interfaces in order to investigate the possibilities of this methodology as a tool for the detection and identification of proteins.

For this purpose, lysozyme, a model protein was investigated. Electroadsorption of this protein was studied at an array of thirty micro-interfaces between two immiscible electrolyte solutions (μITIES). Optimum adsorption of lysozyme was achieved at an applied potential of 0.95 V, which was followed by voltammetric desorption to lower potentials. The desorption peak recorded at *ca.* 0.68 V was dependent on the adsorption time and on the concentration of the protein in the aqueous phase. The slow process to reach saturation or equilibrium indicated that the multilayer formation and/or protein re-organisation at the interface was the rate-determining step and not the diffusion to the interface. For high concentrations and long adsorption times, the formation of multilayers of lysozyme at the gelled liquid – liquid interface was suggested when analysing surface coverage values obtained from the voltammetric data. The maximum surface coverage measured (550 pmol cm^{-2}) corresponds to several layers of the protein if a single monolayer is 13 pmol cm^{-2}. The implementation of this adsorption approach followed by voltammetric detection for lysozyme detection demonstrated a linear dynamic range of 0.05 – 1 μM and a limit of detection of 30 nM, for 300 seconds adsorption which is a more than ~15-fold improvement over previous lysozyme detection methods at the ITIES.

Based on the mechanism proposed for lysozyme detection at the ITIES (adsorption followed by facilitated transfer of organic phase anions), mass

spectrometry (MS) analyses were carried out via electrostatic spray ionisation (ESTASI-MS) on the hydrophobic gel after protein accumulation by adsorption was implemented electrochemically at the gelled liquid – liquid interface. This step was performed in a single millimetre-size interface when the organogel was placed in a glass pipette (0.075 cm radius). The gel was exposed to the aqueous phase in a hemispherical configuration which corresponds to 0.035 cm^2. The ESTASI spectra demonstrate the presence of protein at the organogel which is enhanced when applied potential, pre-concentration time and concentration of lysozyme in solution are increased. Moreover, complexes such as $[Lysozyme\text{-}1TPBCl+9H]^{+8}$, $[Lysozyme\text{-}1TPBCl+10H]^{+9}$, $[Lysozyme\text{-}1TPBCl+11H]^{+10}$ and $[Lysozyme\text{-}2TPBCl+12H]^{+10}$ were found between the positively charged protein and one or two anions of the electrolyte (tetrakis(4-chlorophenyl)borate). This is the first time that ESTASI-MS has been employed directly at a hydrophobic gel following electrochemistry at the ITIES and confirms the formation of interfacial complexes at the polarisable interfaces. Additionally, multilayer formation is also proven as for a monolayer (13 pmol cm^{-2}) the amount of lysozyme will be 0.45 pmol which is lower than the reported limit of detection for ESTASI-MS on a hydrophilic gel used in electrophoresis (1.63 pmol). Therefore multilayers are necessary in order to me detected via ESTASI-MS.

Lysozyme behaviour was also explored at water / room temperature ionic liquid (W/RTIL) microinterfaces. Adsorption of the protein at the soft interface was possible with a surface coverage of 311 pmol cm^{-2} achieved implementing AdSV when inducing adsorption at the positive limit of the available potential window (*ca.* 0.1 V). Similar to the gelled liquid – liquid approach, lysozyme was detected down to ~2.5 μM in the aqueous phase for 60 second pre-concentration. Thus, W/RTIL provides a new interface for the non-redox detection of biomolecules in a label-free manner. Furthermore, a parallel phenomenon was identified under acidic conditions where lysozyme is fully protonated. Hydronium cation transfer was reported with the formation of a net-neutral capacitive layer at the interface, as this process was confirmed by electrochemical impedance spectroscopy and biphasic electrospray ionisation - mass spectrometry (BESI-MS). BESI spectra signal for the RTIL anion (tris(pentafluorethyl)trifluorphosphate -FAP-) when the ionic liquid is in contact with

either hydrochloric acid or acetic acid, decreased significantly (99.8%) which suggest the formation of neutral species at the interface.

The behaviour of haemoglobin, a more complex protein was evaluated at the gelled μ-ITIES in order to examine the potential of AdSV for analytical purposes. Utilising a 60 s adsorption step (0.975 V) and linear sweep voltammetry, haemoglobin showed a linear response over the range 0.01 – 0.5 μM. The calculated detection limit based on three times the standard deviation was 48 nM for 60 s adsorption time, while the relative standard deviation was 13.3 % for 6 successive measurements at 0.1 μM haemoglobin. This data supports the methodology using lysozyme which can be utilised as a simple and fast preconcentration step. The difference in amino acid sequence, size, charge and structure between lysozyme and haemoglobin translates in different electroactivity which in this case was favourable for haemoglobin as it is believed that the higher degree of charge of the protein and the lack of disulfide bonds enhances the electrostatic interactions at the soft interface with the anions from the organic phase.

Furthermore, lysozyme, myoglobin, bovine serum albumin and haemoglobin were investigated under similar conditions for pepsin and trypsin proteolysis which resulted in eight unique voltammograms. This showed the potential of electrochemistry at the μ-ITIES as a tool for the identification of proteins. The specific fragments produced after digestion present different electrochemical behaviour at the soft micro-interfaces. For this purpose, the effect of several proteases (pepsin, trypsin and endoproteinase Glu-C) was investigated for lysozyme digestion. Complimentary techniques such as matrix-assisted laser desorption ionisation – time of flight – mass spectrometry (MALDI-TOF/TOF-MS), liquid and gas chromatography - mass spectrometry (LC-MS and GC-MS) were evaluated for an extensive analysis of the lysozyme digest composition which would affect the voltammetric signal. The results indicate that the protein digest signal varies depending on the enzyme used, which cleaves in different parts of the amino acid sequence of the protein. Additionally, the degree of pepsinisation is influenced by the acidity of the aqueous solution. Then the results open up a new avenue for simple, label-free identification and biosensing tool.

These results provide the basis for a new analytical approach for simple, portable and rapid label-free protein detection based on adsorptive stripping voltammetry (AdSV) at the μ-ITIES and identification when combined with proteolysis steps prior to electrochemical analysis. ESTASI-MS has also confirmed the detection mechanism which can be used as a new tool to optimise the electroactivity of biomolecules for their detection at the ITIES.

1 Introduction

The principles of dynamic electrochemistry at solid electrodes introduce the fundamental concepts of electrochemistry for an increased understanding of electrochemistry at liquid-liquid interfaces. The processes at these interfaces are governed by the Gibbs free energy of transfer of charged species in solution. These processes can be subdivided into ion transfer, assisted ion transfer and electron transfer. This enables label-free detection of ionised molecules. The advantages and importance of using micro-interfaces in this research are discussed from an analytical perspective. An extensive literature review on the most relevant research carried out at the Interface between Two Immiscible Electrolyte Solutions (ITIES) is presented at the end of this chapter, followed by the scope and relevance of this research.

1. 1. Fundamentals of electrochemistry

Electrochemistry examines chemical reactions based on charge transfer between an electrified surface and an ionic conductor (electrolyte) solution.[1] The focus of this section is to provide a brief overview of electrochemistry before exploring in more detail the principles behind electrochemistry at the Interface between Two Immiscible Electrolyte Solutions (ITIES), also called liquid-liquid electrochemistry.

1.1.1. Solid electrode electrochemistry

Solid electrode electrochemistry involves electron transfer between a carbon, metal or semiconductor and a chemical species in solution.

1.1.2. Electron transfer reactions

Electron transfer occurs at the solid electrode surface causing oxidation or reduction of the electroactive species in solution. Oxidation involves the loss of electrons from the chemical species to the electrode (anodic process, Equation 1.1.1) whilst reduction results in the gain of electrons from the electrode (cathodic process, Equation 1.1.2). In both equations, R is the reduced and O is the oxidised species.[2]

$$R \rightarrow O + ne^- \qquad (1.1.1)$$

$$O + ne^- \rightarrow R \qquad (1.1.2)$$

The equilibrium electrode potential is given by the Nernst equation (Equation 1.1.3) when electron transfer is thermodynamically or kinetically favourable:[3, 4]

$$E_{eq} = E^{o\prime} + \frac{RT}{nF} ln \frac{C_O(0,t)}{C_R(0,t)} \qquad (1.1.3)$$

where E_{eq} is the equilibrium potential, $E^{o'}$ is the formal potential of the redox couple, T is the Kelvin temperature, n the number of electrons transferred in the redox reaction, R the universal gas constant (8.314 J K^{-1} mol^{-1}), F the Faraday constant, the magnitude of electric charge per mole of electrons (96,487 C), $C_O(0,t)$ and $C_R(0,t)$ are the concentration of the electroactive species (O and R) at the surface $(x=0)$ at time t.

1.1.3. Faradaic and non-faradaic processes

The current resulting from the oxidation-reduction of the electroactive species is the *faradaic* current. This current obeys Faraday's law (Equation 1.1.4) and is a direct measure of the rate of these chemical reactions.[1]

$$Q = \int_0^t i dt = nN_i F \qquad (1.1.4)$$

where Q is the charge, i is the Faradaic current and N_i is the number of moles of species i in the system.

Conversely, *non-faradaic* current is the current generated at the electrode from processes that do not involve chemical reactions, e.g. adsorption and desorption which result in charge accumulation at the interface. This structure formed at the solid interface is known as the electrical double layer (see Section 1.1.4).

1.1.4. Electric double layer

As faradaic and non-faradaic processes occur simultaneously, the non-faradaic contribution has to be taken into account in the study of electrode reactions. Helmholtz[1, 4] was the first to introduce the term electrical double layer in order to explain the non-faradaic charging current observed at electrode reactions. In Helmholtz's model, the electrode/solution interface itself is believed to be an electrical double layer composed of the electrical charge at the surface of the electrode and the charge of the ions disbursed in the solution at a small distance from the electrode surface. This double layer is formed when a potential is applied to the electrode and causes a charging current (non-Faradaic current) to pass through the cell. The electrode/solution interface is analogous to a capacitor (see Figure 1.1.1).

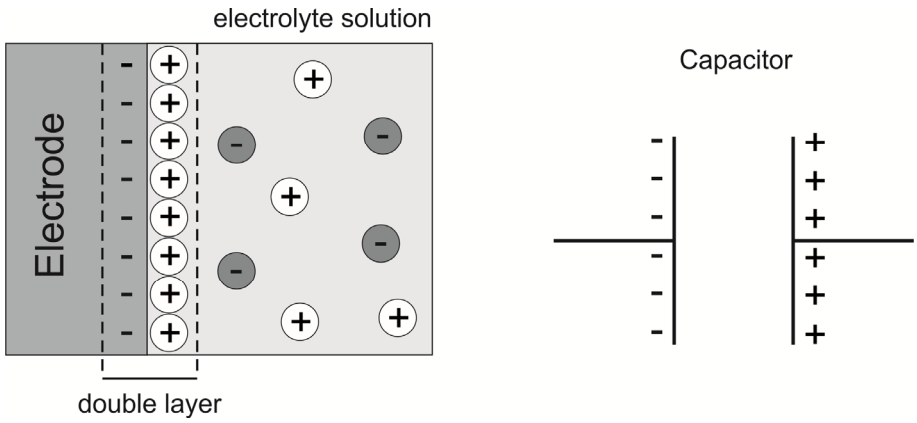

Figure 1.1.1. a) Helmholtz's model of electric double layer and b) capacitor representation.

A capacitor is an electrical component which consists of two metal electrodes facing each other. When a potential is applied to the capacitor, charges rearrange and accumulate on its metal plates as shown in Figure 1.1.1.b, according to Equation 1.1.5.

$$C = \frac{Q}{E} \qquad (1.1.5)$$

where Q is the charge, E the potential and C the capacitance.

The phenomenon of the electrical double layer has been explained and modified throughout the years. Gouy and Chapman's theory[1] introduced the concept of diffuse layer and demonstrates that the charge in solution cannot be confined to the electrode surface. At low concentrations, there are fewer charge carriers present in solution, therefore a thicker layer would be necessary to neutralise the charge of the electrode. The extension of this layer is called the *diffuse layer*. The concentration gradient of counter ions would decrease as the distance from the electrode surface increases as the electrostatic forces weaken. Furthermore, the potential applied has also a great impact on the thickness of this diffuse layer; the higher the potential, the greater the electrostatic forces therefore the diffuse layer result in a reduction of its thickness.

Neither the model proposed by Helmoltz nor Gouy-Chapman, are realistic approaches because both consider the ions as point-charges that can approach the surface arbitrarily. Nevertheless, Stern modified the theory defining a plane of

closest approach known as Outer Helmholtz Plane (OHP) for the centres of ions, at a distance x_2 (Figure 1.1.2).

Grahame also made a contribution introducing the term Inner Helmholtz Plane (IHP) for adsorbed species which may be tightly bound to the surface. This plane is defined as the distance x_1 from the centre of the species to the metallic surface as shown in Figure 1.1.2.

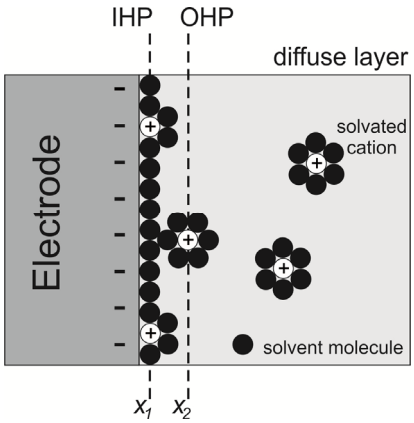

Figure 1.1.2. Illustration of the electric double layer including the Inner and Outer Helmoltz Plane proposed by Stern and Grahame.

1.1.5. Mass transport

Mass transport in an electrochemical cell is the movement of electroactive species in solution towards or away from the electrode. Mass transport which is commonly measured as the flux (*J*), can be due to three mechanisms in solution: *(1) diffusion* - movement of species due to a concentration gradient; *(2) migration* - movement of charged species under the influence of an electric field and *(3) convection* - movement of species due to mechanical forces such as stirring or temperature gradient.[1, 5]

The flux of a species *i* to the electrode is described by a differential equation, the Nerst-Planck equation:

$$J_i(x) = -D_i \frac{\partial C_i(x)}{\partial x} - \frac{z_i F}{RT} D_i C_i \frac{\partial \emptyset(x)}{\partial x} + C_i v(x) \qquad (1.1.6)$$

where x is the distance, D is the diffusion coefficient (cm^2s^{-1}), $\frac{\partial C_i(x)}{\partial x}$ is the concentration gradient, $\frac{\partial \emptyset(x)}{\partial x}$ is the potential gradient, $\nu(x)$ is the hydrodynamic velocity, z_i is the charge and C_i the concentration.

The equation can be simplified by suppressing the migration and convection effect by adding an excess of electrolyte and conducting the experiment under stationary conditions. Then the movement of the electroactive species is limited by diffusion. The first Fick's law describes the flux of a species i (J_i) as a function of the change in its concentration C_i with the position, x, from the electrode at a time t:

$$J_i(x,t) = -D_i \frac{\partial C_i(x,t)}{\partial x} \qquad (1.1.7)$$

Fick's second law describes the dependence of the diffusional flux with the time:

$$\frac{\partial C_i(x,t)}{\partial t} = D_i \frac{\partial^2 C_i(x,t)}{\partial x^2} \qquad (1.1.8)$$

In addition the current (i) is directly proportional to the flux, in other words, it measures the rate of flow of the charge:

$$i = -nFAJ(x,t) \qquad (1.1.9)$$

As a result of the combination of equations (1.1.9) and (1.1.7) we obtain the equation (1.1.10), when migration and convection are suppressed;

$$i = nFAD \frac{\partial C_i(x,t)}{\partial x} \qquad (1.1.10)$$

where n is the number of electrons exchanged in the process, F the Faraday constant and A the area of the electrode.

1. 2. Electrochemistry at the Interface between Two Immiscible Electrolyte Solutions (ITIES)

1.2.1. Introduction

The interface between two immiscible electrolyte solutions, ITIES, is formed when an aqueous phase containing a hydrophilic electrolyte and an organic solution with a hydrophobic electrolyte present are brought in contact.[6]

In the early 1900s Nernst and Riesenfield described the transfer of coloured ions across the interfaces water-phenol-water.[7] In the 1970s electrochemistry at the ITIES gained renewed interest after decades of research purely focused on salt distribution within the immiscible phases.[4, 7] Gavach et al. demonstrated that the ITIES can be polarised, therefore, the Galvani potential difference between the immiscible solutions can be used as a driving force for charge transfer reactions.[8] Cremer in 1906 was the first to advise the analogy between the water/oil/water interfaces and the cell membrane.[4] Following Gavach's work, Koryta et al. established the theory of the transport across the liquid-liquid interface and postulated the similarity to conventional redox reactions on solid electrodes.[9] This enabled the use of electrochemical techniques in the study of charge transfer reactions at the ITIES. In 1977, Samec et al. designed a four-electrode set-up in order to compensate the ohmic drop to study kinetics of these processes.[10] Since then there has been a wide range of investigations carried out.[10] Several studies have also highlighted that the ITIES could serve as an approximation of half of the lipid bilayer cell membrane.[11] In cells, this membrane is composed of a double phospholipid layer where the polar heads are oriented to the outer part of the cell (exposed to the extracellular aqueous media and the oil-like lipid structure facing the inner intracellular membrane). This has increased the interest on electrochemical studies of biomolecules at the ITIES. Recently, a broad range of biomolecules has been successfully characterised via electrochemistry at the ITIES.[12, 13] Relevant biomolecules in biological processes such as dopamine (neurotransmitter),[14] amylin[15] and insulin[16] involved in Alzheimer's disease and diabetes have been reported to be electrochemically active at the liquid - liquid interfaces. Drugs such as propranolol[17] and warfarin[18] have been reported to transfer across polarised interfaces. At the same time, there has been an increasing interest on the application of ITIES for scanning electrochemical microscope (SECM) analysis.[19] Other recent work is focused on other aspects of

electrochemistry, from hydrogen evolution via catalysis at polarised interfaces,[20] nanoparticle assembly at the ITIES[21] to photocurrent analysis at the liquid - liquid interfaces.[22]

1.2.2. Theory

At the ITIES, the two electrically conducting solutions have different Galvani potentials: $\emptyset^w$ is the potential of aqueous phase *(w)* and $\emptyset^o$ is the potential of the organic phase *(o)*. The equilibrium Galvani potential difference, $\Delta_o^w\emptyset$, across the interface is defined according to the following equation.[2, 6]

$$\Delta_o^w\emptyset = \emptyset^w - \emptyset^o \qquad (1.2.1)$$

The conditions for equilibrium for an ion *i* at the ITIES are such that their electrochemical potentials are equal:

$$\bar{\mu}_i^w = \bar{\mu}_i^o \qquad (1.2.2)$$

In thermodynamics, the work required to transfer a species *i* from a vacuum phase to a phase α is defined as $\bar{\mu}_i^\alpha$, the electrochemical potential:

$$\bar{\mu}_i^\alpha = \mu_i^\alpha + z_i F\emptyset^\alpha \qquad (1.2.3)$$

Equation 1.2.3 illustrates the chemical (μ_i^α) and electrical ($z_i F\emptyset^\alpha$) contribution in the electrochemical potential equation. When $z = 0$ (neutral species) in solution the electrochemical potential is equal to the chemical potential and can be written as follows:

$$\mu_i^\alpha = \mu_i^{0,\alpha} + RTlna_i^\alpha \qquad (1.2.4)$$

$$a_i^\alpha = \gamma_i^\alpha C_i^\alpha \qquad (1.2.5)$$

being a_i, c_i and γ_i are the activity, concentration and activity coefficient of the ion *i* respectively.

The standard Gibbs free energy to transfer an ion *i* from the aqueous to the organic solution ($\Delta G_{tr,i}^{w\to o}$) can be related to the standard potential of ion transfer by Equation 1.2.6:

$$\Delta_o^w \emptyset_i^0 = \frac{\Delta G_{tr,i}^{w \to o}}{z_i F} = \frac{\mu_i^{0,o} - \mu_i^{0,w}}{z_i F} \qquad (1.2.6)$$

where $\mu_i^{0,\alpha}$ is the standard chemical potential of *i* in phase α. α can be either the organic, oil phase (*o*) or aqueous, water phase (*w*). z_i is the charge of species *i* and *F* the Faraday constant.

Hence the distribution of species at the interface can be formulated in an analogous equation to solid electrodes. This equation is known as the Nernst-type equation:

$$\Delta_o^w \emptyset = \emptyset^w - \emptyset^o = \Delta_o^w \emptyset_i^0 + \frac{RT}{z_i F} ln\left(\frac{a_i^o}{a_i^w}\right) \qquad (1.2.7)$$

Since $\Delta_o^w \emptyset_i^o$ remains constant when the interfacial potential is changed, the ratio (a_i^o / a_i^w) will change when an external energy source is applied. The resulting movement of ions across the interface to equilibrate the system, translates in an electrical current across the interface. This means the current can be measured as function of the potential applied. The potential difference at the liquid-liquid interface can be also manipulated by changing the relative activities of a common ion on either side of the interface.

The Nernst-type equation (1.2.7) can be also expressed in terms of concentration and activity coefficients of species *I*, which can be related by $a_i^\alpha = \gamma_i^\alpha C_i^\alpha$:

$$\Delta_o^w \emptyset = \Delta_o^w \emptyset_i^0 + \frac{RT}{z_i F} ln\left(\frac{\gamma_i^o C_i^o}{\gamma_i^w C_i^w}\right) \qquad (1.2.8)$$

Finally Equation 1.2.8 can be rearranged by replacing the standard Galvani ion transfer potential and activity coefficients with the formal Galvani ion transfer potential ($\Delta_o^w \emptyset_i^{0'}$).

$$\Delta_o^w \emptyset_i^{0'} = \Delta_o^w \emptyset_i^0 + \frac{RT}{z_i F} ln\left(\frac{\gamma_i^o}{\gamma_i^w}\right) \qquad (1.2.9)$$

Thus the following equation is expressed solely in terms of the concentration of species *i* in either phase (*w* or *o*):

$$\Delta_o^w \emptyset = \Delta_o^w \emptyset_i^{0'} + \frac{RT}{z_i F} ln\left(\frac{C_i^o}{C_i^w}\right) \qquad (1.2.10)$$

1.2.3. Interfacial structure

The first theoretical model of the structure of the interface formed at the ITIES was proposed by Verwey and Niessen[23] based on an adaptation of Gouy-Chapman's model published in 1910.[5] The interface at the ITIES was defined as two back-to-back diffuse layers independent of each other. In 1977 Gavach et al. incorporated the compact inner layer hypothesis[8] introducing the concept of an ion-free inner layer of orientated molecules which are surrounded by ions in the diffuse layer. Further research led by Samec et al. followed this idea but including ion penetration in the diffuse layer,[10] which is known as the Verwey-Niessen model. In 1985, Girault and Schiffrin proposed the idea that the inner layer is a mixed solvent layer, constantly changing composition (see interface between the organic and aqueous solutions in Figure 1.2.2).[24] After this, Schmickler pointed out that the thickness of the mixed solvent depends on the solubility of the two solvents.[25]

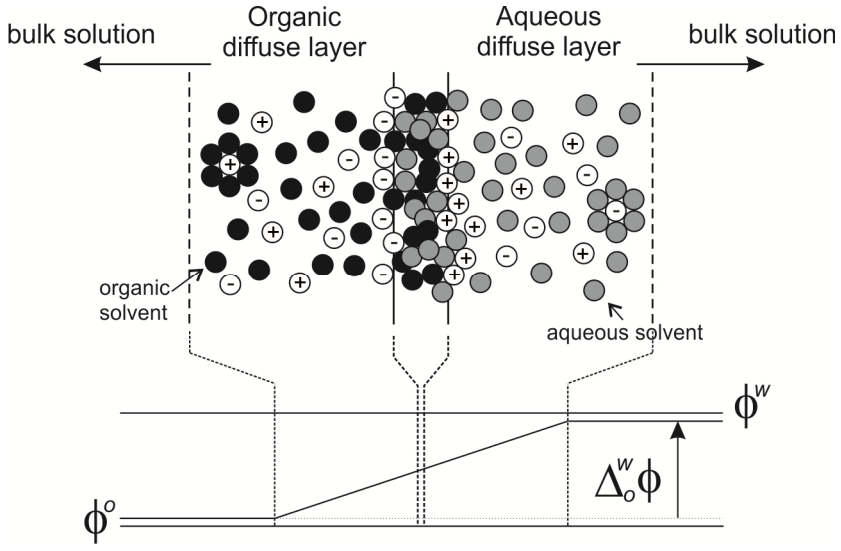

Figure 1.2.2. Schematic representation of structure of the electric double layer formed at the ITIES.

The latest work performed to elucidate the thickness and characteristics of the double layer used techniques such as X-ray reflectivity and neutron reflection and have provided experimental data which are in agreement with theoretical simulations performed by molecular dynamics (MD).[26] The combination of MD with experimental data introduces the possibility to describe the distribution near the charged interface at a molecular scale which was ignored in the mean field theory.[27,

[28] Mitrinovic et al. reported the interfacial thickness of water – alkane interfaces to be 3.5 – 6 Å[29] by X-ray reflectivity measurements and experimental results obtained by Strutwolf et al. via neutron reflection revealed that the water – dichloroethane interface thickness is 10 Å.[30] To comprehend the complex interfacial structure, ion-ion correlations and ion-solvent interactions have to be considered at the nano-scale because these affect thickness and structure of the ionic double layer, as shown by the different theoretical and experimental studies when changing the ion distribution and varying the organic phase.

1.2.4. Polarisable and non-polarisable ITIES

Polarisation of a liquid-liquid interface formed between two immiscible solutions occurs when there is a charge excess in each of the phase, positive in one and negative in the other.[31] Thus the interface acts as a working electrode where the process of interest takes place. The polarisation of the ITIES was illustrated in Figure 1.2.2 in previous section (1.2.3). The polarisability of the interface depends on the electrolyte components of the two immiscible phases.

An ideal polarisable interface refers to ionic electrolytes with infinite Gibbs energies of transfer. In reality, real ions have finite Gibbs energy of transfer and this is the reason why the electrolytes used will define the polarisability of a system. A polarisable interface is formed when a very hydrophilic electrolyte (A^+, B^-) is present in the water phase and a very hydrophobic electrolyte (C^+, D^-) in the oil phase, see Figure 1.2.3. The interface is polarised within a certain potential window which is defined by the formal ion transfer potentials of the electrolytes.

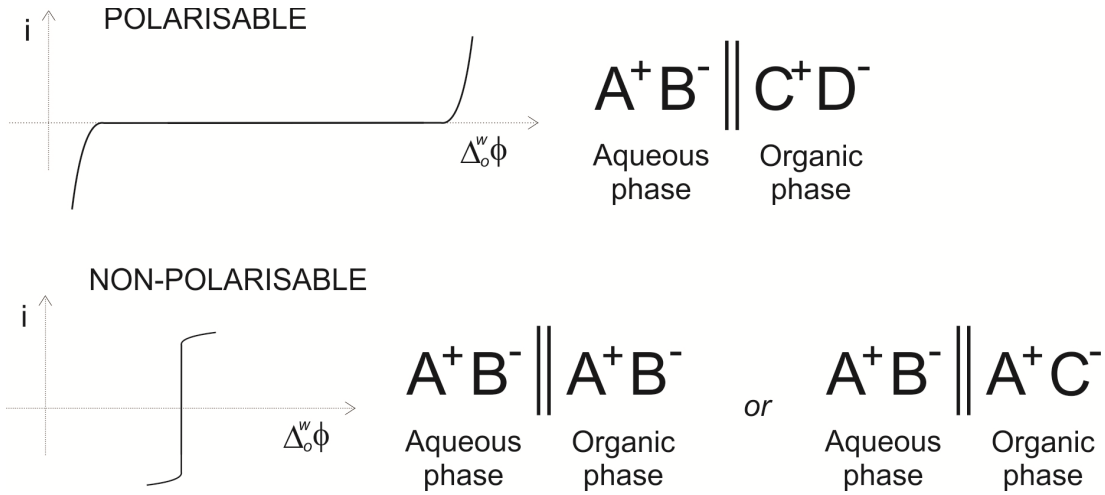

Figure 1.2.3. Diagram of a polarisable and a non-polarisable interface between two immiscible solutions. In the polarisable case A^+B^- and C^+D^- are very hydrophilic and hydrophobic respectively. However, in the non-polarisable interface there are two cases; A^+B^- are common ions in both solutions or A^+ is a common cation in both solutions and B^- is highly hydrophilic and C^- is a very hydrophobic anion.

A non-polarisable interface is formed if a single binary 1:1 electrolyte (A^+ B^-) is present in both phases (see Figure 1.2.3). Thus the Nernst equation can be written as follows for each of the ions:

$$\Delta_o^w \emptyset = \Delta_o^w \emptyset_{A^+}^0 + \frac{RT}{F} ln\left(\frac{a_{A^+}^o}{a_{A^+}^w}\right) \qquad (1.2.11)$$

$$\Delta_o^w \emptyset = \Delta_o^w \emptyset_{B^-}^0 - \frac{RT}{F} ln\left(\frac{a_{B^-}^o}{a_{B^-}^w}\right) \qquad (1.2.12)$$

being $z_{A^+} = +1$ and $z_{B^-} = -1$ for the cation A^+ and anion B^- respectively.

As A^+ solubility is different in both phases, there is a distribution potential established across the interface which is independent of the concentration. Therefore, the Nernst equation can be re-written in terms of activity coefficients as shown in the following expression:

$$\Delta_o^w \emptyset = \frac{\Delta_o^w \emptyset_{A^+}^{0'} + \Delta_o^w \emptyset_{B^-}^{0'}}{2} + \frac{RT}{2F} ln\left(\frac{\gamma_{A^+}^o \gamma_{B^-}^w}{\gamma_{A^+}^w \gamma_{B^-}^o}\right) \qquad (1.2.13)$$

Alternatively, there is another form of non-polarisable interface as shown in Figure 1.2.3. This process occurs when there is a common ion (A^+) in both immiscible phases and B^- is really hydrophilic and C^- is sufficiently hydrophobic, that both ions remain in the aqueous and organic phase, respectively. As a result A^+ is able to transfer across the interface in any direction resulting in the Galvani potential difference controlled by the activity of A^+:

$$\Delta_o^w \emptyset = \Delta_o^w \emptyset_{A^+}^0 + \frac{RT}{F} ln \left(\frac{a_{A^+}^o}{a_{A^+}^w} \right) \qquad (1.2.14)$$

1.2.5. Potential window

For a better understanding of how the electrochemical signal is generated at the ITIES to form a polarisable interface, cyclic voltammetry data obtained when using 10 mM HCl as the aqueous electrolyte and bis(triphenylphosphoranyliden)ammonium tetrakis(4-chlorophenyl)borate (BTPPA TPBCl) is shown below in Figure 1.2.4. In this example, deionised water and 1,6-dichlorohexane (1,6-DCH) were the aqueous and organic phase respectively. When conducting cyclic voltammetry, the current is measured while voltage is scanned forward and backward between two potential limits. Normally, the voltage is scanned from a low initial voltage to a more positive potential on the forward scan and then back to the initial potential (see Section 2.4 where electrochemical techniques are explained in detail). Thus the convention is that if the current measured on the forward scan is more positive when the applied potential is positive (right side of the graph) then this represents the transfer of positively charge ions from the aqueous phase to the organic and/or the transfer of anions from the organic to the aqueous solution. On the contrary, a negative current on the reverse scan represents the back-transfer of positively charged ions from the organic to the aqueous phase and/or the transfer of negatively charged ions from the aqueous into the organic.

In the example shown in Figure 1.2.4, when the potential applied is between 0.05 and 0.2 V, $BTPPA^+$ transfers from the organic to the aqueous solution and Cl^- transfers from the aqueous to the organic. Scanning to more positive potentials (0.2 – 0.8 V), no electrolyte is transferred and this region is called the *potential window* or *polarisation region* where there is no background electrolyte transfer which could mask the analyte signal. Finally on the more positive region, H^+ transfers from the

aqueous to the organic and $TPBCl^-$ from the organic to the aqueous phase. On reversing the potential, the ions previously transferred (H^+ and $TPBCl^-$ from 1 to 0.8 V) back transfer to the aqueous and organic respectively and scanning down from 0.2 to 0.05 V, $BTPPA^+$ will transfer from the aqueous to the organic and Cl^- from the organic to the aqueous solution. Therefore it can be said that the potential window is limited by the transfer of both background electrolytes. From the experimental point of view, it is desirable to have a wide potential window in order to observe transfer processes without any interference from the background electrolyte. This is the reason why a very hydrophilic electrolyte (HCl) in the water phase and a very hydrophobic electrolyte (BTPPA TPBCl) in the oil phase are required. Their low solubility in each other phase determines the energy required for them to transfer across the ITIES and, therefore, the potential window for that system.

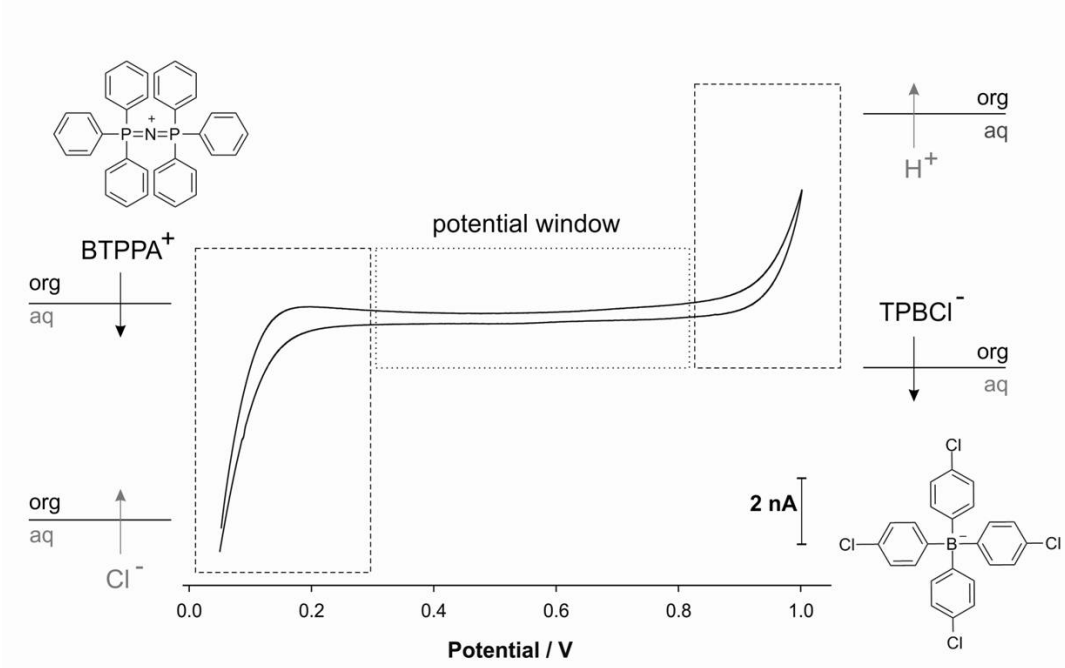

Figure 1.2.4. Cyclic voltammetry of 10 mM HCl in the aqueous phase and 10 mM BTPPA·TPBCl in the gelled organic solution (10 % w/v polyvinylchloride/1,6-dichlorohexane). Dashed boxes on the left and right side represent the electrolyte transfer across the liquid-liquid microinterface formed with an array of 30 interfaces of 22.4 μm diameter. Dotted box in the middle shows the potential window where there is no background electrolyte transfer.

1.2.6. Types of charge transfer processes

The simplest charge transfer process is ion transfer (IT). IT consists of the movement of ions from both phases across the interface until the accomplishment of the concentration ratio defined by Nernst equation. As explained previously, this movement is forced by applying an external potential difference across the interface. The transfer of an ion across the ITIES occurs when the applied potential difference overcomes the Gibbs energy of transfer of that ion across the polarised interface.[6] This process is measurable if the potential required is within the potential window limited by the transfer of the background electrolytes.

Another charge transfer reaction is facilitated ion transfer (FIT)[6] which can be classified into four different categories, (i) TIC stands for Transfer by Interfacial Complexation, (ii) TID for Transfer by Interfacial Dissociation, (iii) ACT for Aqueous Complexation followed by Transfer, and (iv) TOC for Transfer to the Organic phase followed by Complexation. These four assisted ion transfer processes are classified based on the mechanism of complexation and charge transfer between the ion and the ionophore and are fully described in Figure 1.2.5.

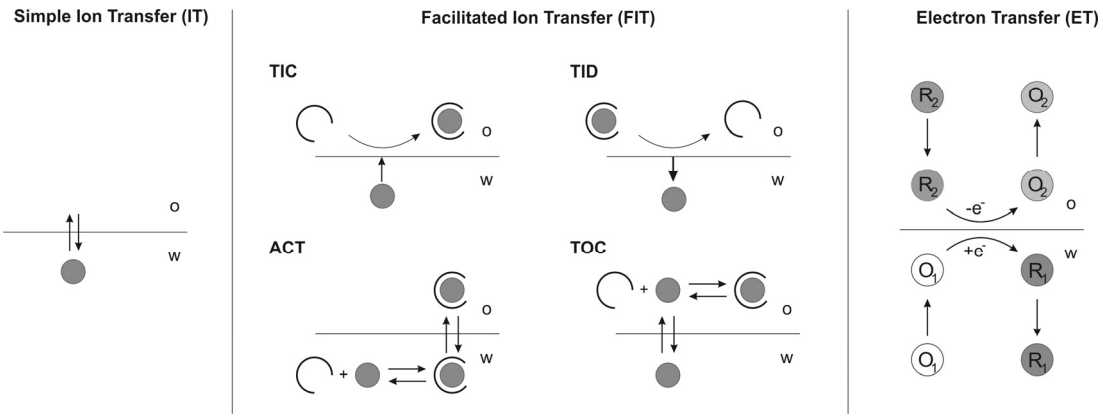

Figure 1.2.5. Representation of the three possible charge transfer processes; ion transfer (IT), facilitated ion transfer (FIT) which can be subdivided in four different complexation reactions – transfer by interfacial complexation (TIC), transfer by interfacial dissociation (TID), aqueous complexation followed by transfer (ACT) and transfer to the organic phase followed by complexation (TOC) - and electron transfer (ET).

Electron transfer (ET) is a significantly more complex process at liquid-liquid interfaces than at metallic surfaces. It requires two redox couples (species 1 and 2), one each located in the adjacent immiscible phases. If the reaction at equilibrium is:

$$O_1^w + R_2^o \leftrightarrow R_1^w + O_2^o \qquad (1.2.15)$$

Then the Nernst equation for ET will be:

$$\Delta_o^w \emptyset = \Delta_o^w \emptyset_{ET}^0 + \frac{RT}{F} ln\left(\frac{a_{R_1}^w a_{O_2}^o}{a_{O_1}^w a_{R_2}^o}\right) \qquad (1.2.16)$$

1. 3. Micro-ITIES

1.3.1. Advantages of minitiurising the ITIES

Miniaturisation of the ITIES brings some advantages with respect to larger liquid-liquid interfaces. Smaller interfaces provide lower currents and therefore reduce the Ohmic potential drop caused by the resistive organic phase.[4] When the potential is measured between the working and the reference electrode, there will be a voltage drop observed that is equivalent to iR_s, as given by Ohm's law (Equation 1.3.1). Ohm's law states that the current (i) that flows through a conductor between two points is directly proportional to the potential difference (V) across those two points and the constant of proportionality is the resistance (R).

$$i = \frac{V}{R} \qquad (1.3.1)$$

Thus in the ITIES electrochemical cell R is the resistance of the solution (R_s):

$$V = iR = iR_s \qquad (1.3.2)$$

Figure 1.3.1 illustrates the current flow through a conductor, the resistance of the solution and double layer capacitance at the solid – liquid interface and the similar equivalent circuit at a liquid – liquid interface. These last two representations enable the comprehension of the Ohmic potential drop at the liquid – liquid interface. Note that the aqueous phase presents a high ability to carry current in comparison to hydrophobic organic solutions which posses low permittivity values. Therefore the contribution of R_s at the ITIES is greater in the case of the organic solution and this is

the reason why the resistance from the aqueous solution is not represented in the liquid – liquid diagram.

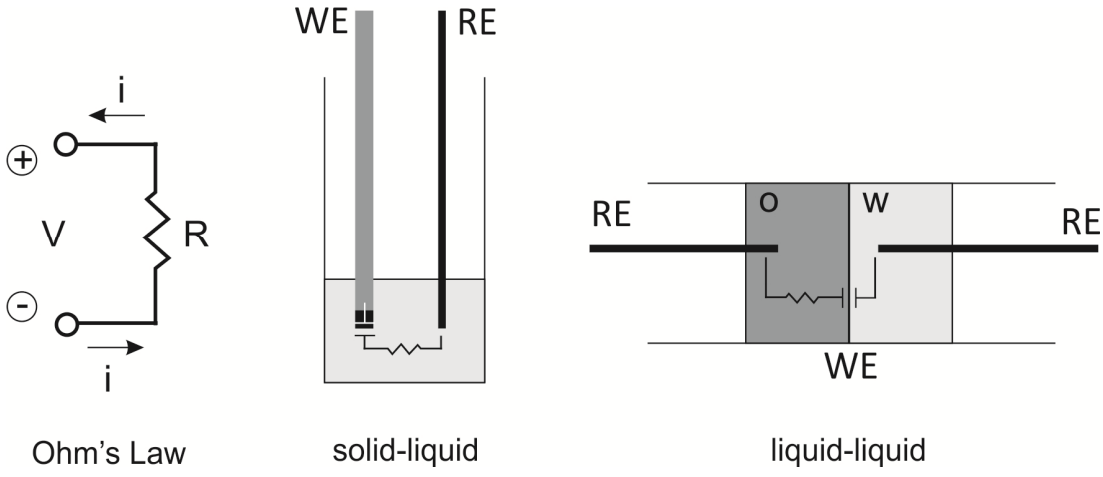

Figure 1.3.1. Representation of current flow to explain Ohm's law (left side), resistance of the solution and double layer capacitance in a solid – liquid system (centre) and resistance of the organic solution at the liquid - liquid interface and the corresponding double layer capacitance (right side).

If R_s in the system is small (1 – 2 mV) then a two electrode cell can be used because a smaller area greatly reduces the current, which reduces the overall value of iR_s.[4] Additionally, smaller interfaces cause an increase in the mass transport flux.

Another important aspect is the fact that minimising the size of the interfaces brings a wide range of possibilities in terms of portability, cost, applications and integration with other techniques.

Taylor and Girault introduced micrometer-sized ITIES supported at glass pipette tips in the late 1980s.[32] Subsequently, the development of micro-ITIES via micro-pipettes and micro-holes has been widely studied in the last decades. Regarding the fabrication method, the combination of photolithography, electron beam lithography and chemical etching was developed on silicon and silicon nitride materials for micro- and nano-porous membranes.[33, 34] Different materials have been considered such as silicon,[34, 35] silicon nitride,[36] glass[37] and polymers.[38, 39] Nano-size glass pipettes have been also developed and are normally fabricated by CO_2-laser-based glass pullers.[37, 40] At present, glass nano-pipettes are extensively used as a probe for

scanning electrochemical microscope (SECM) and scanning ion-conductance microscope (SICM). In this field, dual micro and nano-pipettes were developed by Shao and Mirkin[41] in the late 1990s as a novel electrochemical generator/collector technique which is in use as an SECM probe.[19]

1.3.2. Effect of interface arrangement on the electrochemical signal

In the previous section, the importance of the interface size was described and here the effect of interface geometry and arrangement on the diffusion profile is discussed. In solid electrode electrochemistry, microelectrodes show different voltammetric response when during the fabrication process they present altered features such as a hemispherical, inlaid disc[42] or recessed disc electrodes[43, 44] (see Figure 1.3.2). In Chapter 2, Section 2.2, voltammetric techniques and analysis are shown.

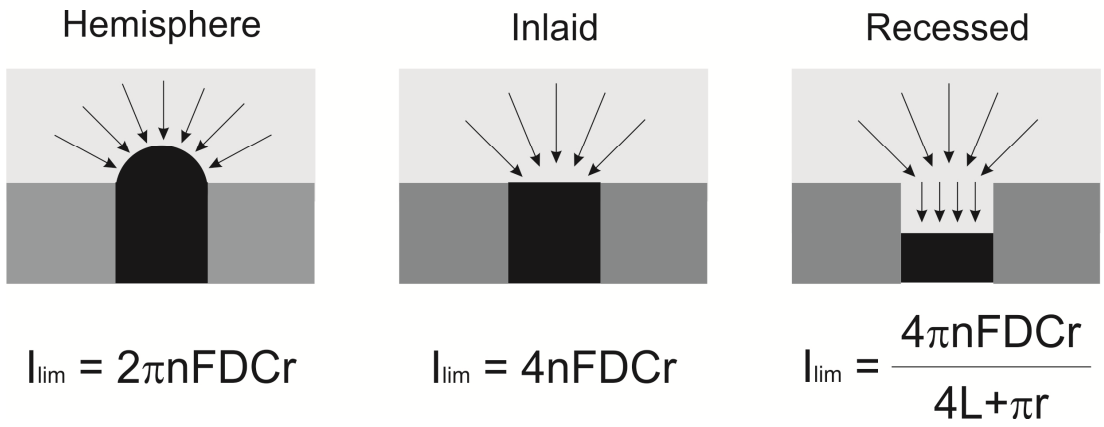

Figure 1.3.2. Diffusion modes and limiting current equations for a microelectrode where the electrode presents different geometries (hemispherical, inlaid and recessed). I_{lim} is the limiting current, n is the number of electrons transferred, F the Faraday constant, D the diffusion coefficient, C the concentration, r the radius of the electrode and L the recessed depth.

Similarly, charged soft interfaces formed within micropores act as microdisk thus the limiting current equations shown in figure 1.3.2 can be used for characterisation purposes. Note that n needs to be replaced by charge number of the ion transferred. In this particular research, a microporous membrane has been used for the electrochemical analysis at the ITIES. The experimental set-up and the electrochemical characterisation of the micro-arrays via simple ion transfer

demonstrates that the pores are filled with the organic phase in an inlaid mode therefore showing radial diffusion when the ion is transferred from the aqueous to the organic phase and planar diffusion when the ion is back-transferred to the aqueous solution.[35] Figure 1.3.2 is a representation of the diffusion profile of a single micropore filled with organic phase, leading to an inlaid disc micro-interface.

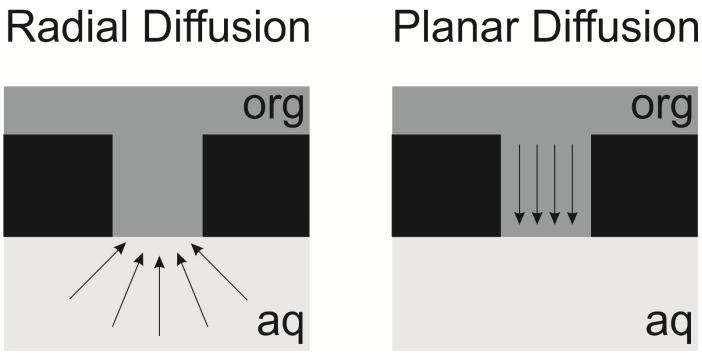

Figure 1.3.2. Diffusion profile for a single microinterface where the organic solution fills the micropore. The figure on the left shows radial diffusion for the transfer from the aqueous to the organic solution whilst illustration on the right presents planar diffusion for the transfer from the organic to aqueous phase.

When each electrode in an array operates at the same potential the overall signal depends on the density of the electrode distribution and the dimensions of the micro-electrodes. If interfaces in the array are too close together, it can result in an overlap of the diffusion zones therefore resulting in a decrease in current. The geometry is not the unique limiting factor, pore dimensions (radius and depth), pore centre-to-centre separation; the experimental time scale and diffusion coefficient of the transferring species are also parameters to take into account.[35]

When microinterfaces are too close to each other in a micropore array, overlapping diffusion layers are present and this is the reason why the geometrical disposition of the interfaces in an array plays an important role. For an optimum voltammetric performance, the centre-to-centre separation in microinterfaces as in the case of microdisc electrode arrays, needs to be separated enough to avoid diffusion zone overlap or shielding. Davies et al. published in 2005 experimental[45] and simulated[46] values for microelectrode arrays when using a cubic, hexagonal and random arrangement. Figure 1.3.3 represents the cubic and hexagonal arrangement

for micro-electrodes. In this thesis, the hexagonal packing is used due to a minimal overlapping of the diffusion zones.[35]

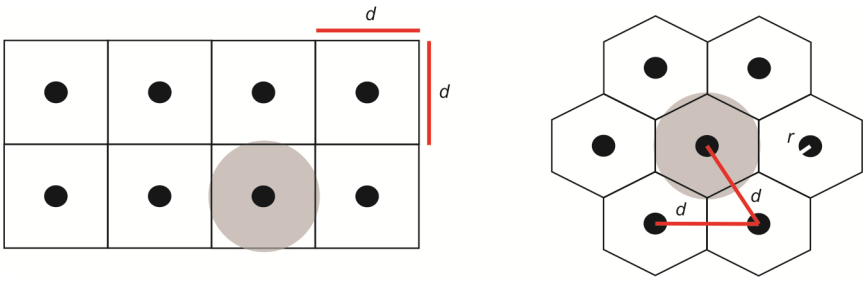

Figure 1.3.3. Cubic (left hand side) and hexagonal (right hand side) arrays of microdiscs where d is the distance between pores and r the pore radius. The grey zone corresponds to the diffusion zone for a single micro-electrode.

As a result, when designing arrays it is important to ensure that the micropores are sufficiently separated so that the individual diffusion zones remain independent for an optimum current signal.

In Figure 1.3.4, different diffusion profiles are detailed for an array of microinterfaces. Figure 1.3.4 A) represents the linear diffusion when ion is transferring from the organic phase to the aqueous phase, B) shows radial diffusion for the transfer of ions from the aqueous to the organic solution, C) describes the shielding effect (diffusion overlapping) and D) is the same case as C but when the overlapping is an extensive overlap leading to an overall linear diffusion from the organic to the water phase.[35]

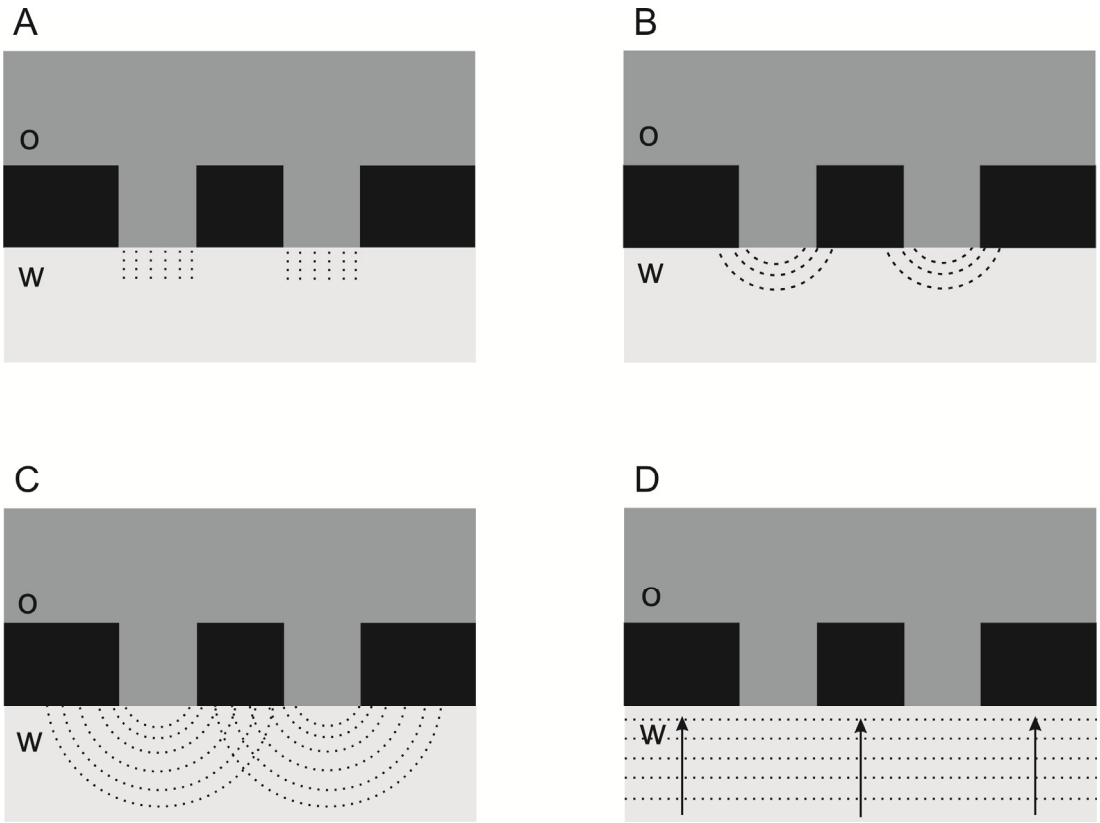

Figure 1.3.4. Diffusion profile A) linear diffusion from organic to aqueous, B) non-linear diffusion from aqueous to organic, C) overlapping diffusion layers and C) heavily overlapping diffusion layers resulting in linear diffusion (*o*→*a*).

Saito[47] studied diffusion overlapping at a microdisc electrode and proposed an expression based on the assumption of purely steady-state response at microelectrodes then independent of the scan rate. Shielding occurs when microdisc centre-to-centre separation (d) is lower than 12 times the radius of the electrode (r):

$$d > 12r \qquad (1.3.3)$$

Many other groups attempted unsuccessfully to provide a universal formula to predict accurately the optimum electrode centre-to-centre separation and radius relation for electrochemical analysis. Fletcher and Horne reported the following approximation:[48]

$$d \geq 20r \qquad (1.3.4)$$

And Davies and Compton also formulated an equation to estimate the diffusion zone (δ) at microelectrode arrays.[46]

$$\delta > \sqrt{2D_i \frac{\Delta\left(\Delta_\beta^\alpha \phi\right)}{v}} \qquad (1.3.5)$$

where *D* is the diffusion coefficient of the species *i*, *v is* the scan rate, and $\Delta\left(\Delta_\beta^\alpha \phi\right)$ is the potential range from the onset faradaic current to the steady state current or attainment of a peak.

Equation (1.3.5) shows the dependence on the time via scan rate potential but not individual electrode or pore size unlike Equation 1.34 and 1.35 and this is because for this expression (Equation 1.3.5), the diffusion is assumed to be unidimensional.

All the expressions presented (Equation 1.3.3 to 1.35) have been proven to be unsuitable for $r < 1$ μm.[46-48] As a consequence, no universal equation allows us to estimate accurately the relation between *d* and *r* for optimum voltammetric analysis.

Arrigan's group has characterised silicon micropore arrays varying the arrangement of the pores and sizes. Strutwolf *et al.* demonstrated that experimental values using water/gelled 1,6-DCH micro-interfaces were in agreement with simulations performed with the program COMSOL. These were used to locate the interface within the pores and analyse the possible diffusion overlapping in the membrane array. For some of the designs studied, diffusion overlapping was observed when equation 1.3.3 was not fulfilled. Also designs that did not meet the criteria of equation 1.3.5 showed diffusion overlapping resulted in a peak-shaped wave on the forward scan instead of steady-state currents (radial diffusion-controlled).[35]

The micropore arrays used in this thesis were composed of 30 pores of *ca.* 10 μm pore radius, 200 μm pore centre-to-centre distance and 100 μm depth. The pores are displayed in a hexagonal arrangement design which fulfils Equation 1.3.3 and 1.3.4 as *d* is 20 times the pore radius ($d = 20r$).

1. 4. Bioelectrochemical analysis at the ITIES

Since 1984, there has been a wide range of investigations targeting biomolecules at polarisable soft interfaces. That year, Vanysek et al. reported for the first time ovalbumin and bovine serum albumin adsorption at the ITIES in Cs^+ transfer studies at the water/nitrobenzene interface.[49] The variety of articles published after this discovery ranges from mimicking the cell membrane, adsorption studies, extraction and detection of drugs, DNA hybridization and finally label-free detection of biological molecules.

In 1998, Horrocks and Mirkin established a new approach to characterise ion-binding to *DNA*. They reported DNA detection by non-redox facilitated ion transfer by interfacial binding to oligonucleotides.[50] Since then, very little work has been carried out to develop the electrochemical studies of DNA at the ITIES. Osakai et al. showed how the transfer of the surfactant dimethyldistearylammonium tetraphenylborate from the organic phase to the aqueous phase was facilitated by DNA adsorbed at the water/1,2-dichloroethane (W/1,2-DCE) interface.[51] Vagin et al. employed impedance spectroscopy to detect DNA hybridisation down to 0.01 μM using an organic film shielded electrode.[52] Then Kivlehan et al. presented the interaction of acridine-calix[4]arene with DNA at the ITIES. This study also takes advantage of sensitive impedance measurements to assess the DNA interactions at low nanomolar level of double stranded DNA.[53]

In terms of *small molecules* which are involved in biological processes, the oxidation of L-ascorbic acid was studied at the electrified liquid – liquid interfaces as a synergistic antioxidant effect between L-ascorbic acid and α-tocopherol at the cell membranes is well known and studied.[54] Also the redox process between β-nicotinamide adeninedinucleotide (NADH) and quinone derivatives were also addressed in 1998.[55] This process is considered essential in energy accumulation at the mitochondrial inner membrane. Other types of low molecular weight molecules which have an important role in biology have been also investigated at the ITIES. Dopamine, a neurotransmitter, was successfully detected by facilitated protonated dopamine transfer using different ionophores[56] such as dibenzo-18-crown-6 (DB18C6) across the liquid – liquid interface.[56] Arrigan's group evaluated the effect of ascorbate and other interference using DB18C6 in the organic phase.[57] In this work, the lowest detectable concentration of dopamine when performing differential

pulse voltammetry followed by background subtraction, corresponded to 2 μM.[57] Further research when using micro-sized interfaces was probed to lower the measurable dopamine concentration down to 0.5 μM.[14] Latest work carried out by Pereira's group has also shown the electroactivity of another neurotransmitter, noradrenaline, when using DB18C6 at the W/1,6-DCH interface.[58]

Determination of the Gibbs energy of transfer of *drugs* across liquid - liquid interfaces via electrochemistry has become of interest in pharmacokinetics studies. Propranolol detection in artificial saliva[17] and in the presence of bovine serum albumin,[59] has been reported by Collins and Arrigan. In 2012, propranolol and warfarin were measured at rotating liquid - liquid interfaces.[18] Chiral discrimination of propranolol enantiomers was achieved by using α_1-acid-glycoprotein[60] at the water/1,2-DCE interfaces. This protein has the ability to bind stereoselectively to enantiomers and through these experiments, S-propranolol has been found to bind more strongly to α_1-acid-glycoprotein than the R enantiomer.

Carbohydrates e.g. heparin (average molar mass of ~12KDa) used clinically as anticoagulant, interacts with antithrombin III via ionic forces. Samec et al. proposed ITIES as a new strategy to study heparin.[61] The first report demonstrated the activity of heparin when using polyvinyl chloride (PVC) – 1,6-dichlorohexane membranes,[61] Amemiya's group used 1,2-dichloroethane[62] and the latest publication includes the use of room temperature ionic liquids to promote the extraction of heparin.[63]

A model of half *cell membrane* was studied by Mendez et al. when forming a lipidic monolayer at the water/1,2-dichloroethane interface.[64] This provided a platform to analyse melittin, a cell membrane peptide with antimicrobial activity. Under these conditions, melittin undergoes adsorption at the interfaces, then interacts with a monolayer of L-α-dipalmitoyl phosphatidylcholine (DPPC) disrupting the phospholipid layer.[65] Previous work also performed by Mendez et al. showed the peptide-lipid complex formation when DPPC was present in the organic solution. Angiotensin III and Leuenkephalin are two small peptides formed by 7 and 5 amino acids, respectively. These small peptides (molecular weight < 1 KDa) interact with receptors embedded in the cell membrane and are linked to regulation of blood pressure and inflammatory immune response by acting as neurotransmitters.[64]

Single *amino acids* and *small oligopeptides* are also electrochemically active at water/1,2-dichloroethane or water/1,6-dichlorohexane interfaces. The ionophore

DB18C6 is added in the organic phase and this crown-ligand complexes the amino acids facilitating the transfer of amino acids[66] and small peptides.[34] These studies highlight the fact that amino acid position in the peptide sequence and composition are key factors in order to determine their electrochemical activity across the ITIES.

As mentioned at the beginning of this section, in 1984, Vanysek et al. reported for the first time the influence of large biomolecules (ovalbumin and bovine serum albumin) at the water/nitrobenzene interface.[49, 67] It was until 2002 that the study of *large proteins* at the ITIES took a new avenue. The use of more hydrophobic solvents such as 1,6-dichlorohexane and the incorporation of surfactants into the organic phase, opened up a new approach to study protein behaviour and explore the potential of label-free protein detection at the ITIES for analytical purposes.

In 2002, Dryfe's group evaluated the electron transfer process between cytochrome c and 1,1′-dimethylferrocene at the electrified liquid - liquid interfaces. This redox reaction is analogous to the in vivo situation where cytochrome c acts as an electron transfer protein (redox carrier) within the membrane in the mitochondrial electron transfer chain.[68] A year after this publication, Amemiya et al. published the electrochemical behaviour of protamines at the water/1,2-dichloroethane interface. This protein is an arginine-rich small protein (~4 KDa) which is highly positively charged and was reported to transfer across the interface.[69] Further research led by Amemiya determined the effect of the addition of different organic electrolytes and anionic surfactants (DNNS).[70] Following this research, Vagin et al characterised the influence of different surfactants in the organic phase: cationic, anionic or neutral molecules in the presence of proteins such as α-chymotrypsin, soybean trypsin inhibitor and lysozyme. Micelles formation was reported when bis(2-ethylhexyl) sulfosuccinate (AOT) and cetyltrimethylammonium bromide (CTAB) were present in the organic phase whilst neutral polyoxyethylen(4)-laurylether (Brij-30) and polyoxyethylen(2)-cetylether (Brij-52) did not show the same protein-surfactant interactions.[71] Shinshi et al. observed similar behaviour in the case of cytochrome c, protamines and ribonuclease A at the W/(1,2-DCE + AOT) interfaces.[72] Trojanek's work on protamines by changing the organic electrolytes and characterizing the water/1,2-dichloroethane by quasi-elastic laser light scattering (QELS) showed the complex mechanism composed of facilitated protamine transfer with an intermediate adsorption step.[73]

Recent work presents the use of surfactants as an approach to enhance the protein detection signal. O'Sullivan and Arrigan analysed myoglobin,[74] cytochrome c and haemoglobin using an anionic surfactant (AOT) which can complex with the positively charged protein, increasing the signal by 17-fold in terms of interfacial coverage.[75] Matsui et al. have also implemented these surfactant-protein interactions for the detection of albumin in urine in a flow cell. In this case, they employed dinonylnaphthalenesulfonate ($DNNS^-$) and achieved a limit of detection of 1.2 μM in the artificial urine sample.[76]

On the contrary, Arrigan's research has mainly focused on the analytical perspective of the methodology. Most of this group's publications present surfactant-free organic phases for the detection of molecules such as insulin,[77] lysozyme,[78, 79] and haemoglobin.[80, 81] Herzog et al. carried out voltammetric measurements after haemoglobin was chemically denatured[82] and digested with enzymes resulting in a peptide mixture in solution.[83] The results open-up a new strategy in protein detection and identification via electrochemistry at polarisable liquid - liquid interfaces.

As it is been detailed in this section (1.5), a small range of proteins (3.2 - 66 KDa.) has been investigated during recent decades. Additional examples not described in the section are summarised in Table 1.4.1.

Table 1.4.1. Large biomolecules electrochemical studies at liquid – liquid interfaces.

Biomolecule	Size / KDa	pH	Aqueous electrolyte	Organic electrolyte	Organic Solvent	Surfactant / Ionophore	Interface Size / cm^2	Technique	Mechanism	[Protein] / µM	Reference
Amino acids											
Amino acids (Aa)	20 Aa	1	5 mM Mg_2Cl + H_2SO_4	TBATPBCl	1,2-DCE	DB18C6	2×10^{-6}, 3×10^{-6} and 8×10^{-7}	CV	Transfer by interfacial complexation/dissociation	0.02 – 0.2	[66]
Oligopeptides											
Oligopeptides	2-4 Aa	2	10 mM HCl	BTPPA TPBCl	1,6-DCH + PVC	DB18C6	0.785 and 1.7×10^{-4} (8 µpore array)	CV DPSV	Oligopeptides transfer assisted by DB18C6	0.4	[34]
Proteins											
Rat-amylin	3.2	2	10 mM HCl 1 mM PBS	BTPPATPBCl	1,6-DCH (gel)	-	1.18×10^{-4} (30 µpore array)	CV	Amylin transfer	2	[15]
Protamine	4 – 4.25	7.4 (Tris)	0.1 M LiCl 0.05 M Tris buffer	TDDATPBCl	1,2-DCE	$DNNS^-$	$1.3 – 2.8\times10^{-7}$, 3×10^{-6} and 1.5×10^{-5}	CV Chronoampe rometry	Facilitated transfer of protamine through interfacial complexation with DNNS	16	[70]
		3.4 - 7	0.1 M KCl	TPnAAOT TPnATPB	1,2-DCE	AOT	0.05	CV	Protein extraction by reverse micelle formation	10	[72]
		-	0.1 M LiCl	TBA TPB TPeA TFPB BTPPA TPBCl	1,2-DCE	-	0.189	CV QELS	Facilitated protamine transfer with intermediate adsorption step	50 2.5	[73]
		-	10 mM LiCl	TBA TPB	NB 1,2-DCE 1,6-DCH	-	$\sim 8\times10^{-7}$	CV	Facilitated protamine transfer with intermediate adsorption step	12	[69]
Insulin	6	7.4	10 mM PBS	BTPPA TPFB	1,2-DCE	-	1.3	CV Interfacial impedance	Adsorption kinetics	0.1	[84]
		1-9.7	10 mM LiCl ± HCl /NaOH	BTPPA TPBCl BTPPA TPB BTPPA TFPB	1,2-DCE	-	0.785	CV SWSV	Ion-pairing interactions + adsorption	1 2	[77]

Table 1.4.1. Large biomolecules electrochemical studies at liquid – liquid interfaces.

Biomolecule	Size / KDa	pH	Aqueous electrolyte	Organic electrolyte	Organic Solvent	Surfactant / Ionophore	Interface Size / cm^2	Technique	Mechanism	[Protein] / µM	Reference
Insulin	6	2	10 mM HCl	BTPPATPBCl	1,6-DCH (gel)	-	2.12×10^{-5} (8 µpore array)	CV	Adsorption + FIT of anion from organic phase Comparable to dendrimer DAB-AM-4 behaviour	1	[79]
		2	10 mM HCl 1 mM PBS	BTPPATPBCl	1,6-DCH (gel)	-	1.18×10^{-4} (30 µpore array)	CV AdSV	Adsorption + FIT of TPBCl	0.01	[16]
Cytochrome c	13	3.4 - 7	0.1 M KCl	TPnA AOT TPnA TPB	1,2-DCE	AOT	0.05	CV	Protein extraction by reverse micelle formation	10	[72]
		-	10 mM Borate buffer	BTPPA TPB	1,2-DCE	-	1.13	CV	Direct e^- transfer, between cytochrome *c* and a ferrocene derivative	400	[68]
		3-7.1	0.1 M KCl	TPnAX' TPnATPB	1,2-DCE	DNNS AOT BDFHS BEHP	0.0278	CV	Adsorption/desorption of the proteins	100	[85]
		2	10 mM HCl	BTPPA TPBCl	1,6-DCH (gel)	AOT	1.03×10^{-5} (8 µpore array)	CV	Protein adsorpt-interaction AOT, enhances signal	6	[75]
Ribonuclease A	13.7	3.4 - 7	0.1 M KCl	TPnAAOT TPnATPB	1,2-DCE	AOT	0.05	CV	Protein extraction by reverse micelle formation	10	[72]
	13.7	3-7.1	0.1 M KCl	TPnAX' TPnATPB	1,2-DCE	DNNS AOT BDFHS BEHP	0.0278	CV	Adsorption/desorption of the proteins	100	[85]
Lysozyme	14.3	7.4	10 mM PBS	TBA TPB	1,2-DCE	AOT CTAB Brij-30/52 PVS-St	0.38	CV	Ionic surfactants facilitates micelles formation	~14	[71]
Lysozyme	14.3	0.9 – 11.9	10 mM HCl 1-100 mM LiCl	BTPPA TPBCl BTPPA TPB BTPPA TFPB	1,2-DCE	-	1	CV	Adsorption + FIT of anion from organic phase	10	[78]

Table 1.4.1. Large biomolecules electrochemical studies at liquid – liquid interfaces.

Biomolecule	Size / KDa	pH	Aqueous electrolyte	Organic electrolyte	Organic Solvent	Surfactant / Ionophore	Interface Size / cm^2	Technique	Mechanism	[Protein] / µM	Reference
Lysozyme	14.3	2	10 mM HCl	BTPPA TPBCl	1,6-DCH (gel)	-	2.12×10^{-5} (8 µpore array)	CV	Adsorption + FIT of anion from organic phase Comparable to dendrimer DAB-AM-4 behaviour	0.5	[79]
Lysozyme	14.3	2	10 mM HCl	BTPPA TPBCl	1,6-DCH (gel)	-	1.18×10^{-4} (30 µpore array)	CV AdSV	Adsorption and facilitated transfer of TPBCl	0.03	Chapter 3
		2	10 mM HCl	BTPPA TPBCl	RTIL	-	1.18×10^{-4} (30 µpore array)	CV AdSV	Adsorption and facilitated transfer of the organic anion	2.5	Chapter 5
Myoglobin	16.7	-	10 mM HCl 1-100 mM LiCl	BTPPATPBC	1,6-DCH (gel)	-	1.03×10^{-5} (8 µpore array)	CV	Adsorption and facilitated transfer of TPBCl	1	[74]
		2	10 mM HCl	BTPPATPBCl	1,6-DCH (gel)	AOT	1.03×10^{-5} (8 µpore array)	CV	Protein adsorpt-interaction AOT, enhances signal	1	[75]
Soybean trypsin inhibitor	22		0.01 – M KCl 20 mM Acetic Acid	Shielded electrode PPTA	n-octane	AOT^- DAP^+	0.25	CV Impedance	Adsorption on shielded electrodes	120	[86]
		7.4	10 mM PBS	TBATPB	1,2-DCE	AOT^- $CTAB^+$ Brij-30/50 PVS-St	0.38	CV	Ionic surfactants facilitates micelles formation	~10	[71]
α-Chymotrypsin	24	7.4	10 mM PBS	TBATPB	1,2-DCE	AOT^- $CTAB^+$ Brij-30/50 PVS-St	0.38	CV	Ionic surfactants facilitates micelles formation	~8	[71]
Ovalbumin	45	-	10 mM LiCl	TBA TPB	NB	-	0.18	CV AC impedance	Adsorption of protein disrupts Cs^+ transfer	~0.09	[49]

Table 1.4.1. Large biomolecules electrochemical studies at liquid – liquid interfaces.

Biomolecule	Size / KDa	pH	Aqueous electrolyte	Organic electrolyte	Organic Solvent	Surfactant / Ionophore	Interface Size / cm^2	Technique	Mechanism	[Protein] / µM	Reference
Haemoglobin	64.5	2 7.4	10 mM HCl 0.1 M PBS	BTPPA TPBCl BTPPA TPB BTPPA TFPB	1,2-DCE	-	0.785 and 1.7×10^{-4}	CV	Adsorption forming multilayer + facilitated transfer of organic anion	0.55	[80]
		2	10 mM HCl	BTPPA TPBCl BTPPA TPB BTPPA TFPB	1,2-DCE	-	1.16	CV ACV	Adsorption + facilitated transfer of organic anion	1.25 0.1	[81]
		2	10 mM HCl	BTPPA TPBCl	1,2-DCE 1,6-DCH (gel)	-	0.785 and 1.7×10^{-4}	CV DPSV	Peptide detection after digestion	0.55	[83]
		2	10 mM HCl + urea	BTPPA TPBCl	1,2-DCE	-	1.12	CV DPSV	Chemical denaturation (Unfolding)	0.1	[82]
		2	10 mM HCl	BTPPA TPBCl	1,6-DCH (gel)	AOT	1.03×10^{-5} (8 µpore array)	CV	Protein adsorption-interaction AOT, enhances signal	6	[75]
		2	10 mM HCl	BTPPA TPBCl	1,6-DCH (gel)	-	1.18×10^{-4} (30 µpore array)	CV AdSV	Adsorption and facilitated transfer of TPBCl	0.048	Chapter 6
Bovine Serum Albumin	66	-	10 mM LiCl	TBA·TPB	NB	-	0.18	CV AC impedance	Adsorption of protein disrupts Cs^+ transfer	~0.02	[49]
		2 – 7.6	10 mM LiCl	TBA·TPB	NB	-	0.0314	CV AC impedance	Adsorption	~0.02	[67]
		3.4	Urine control	TPnA TPB	1,2-DCE	$DNNS^-$	0.023	Amperometry	Protein complexation with $DNNS^-$	1.2	[76]

[Protein] *refers to the lowest measured protein concentration or the limit of detection*

NB: nitrobenzene, 1,2-DCE: 1,2-dichloroethane, 1,6-DCH: 1,6-dichlorohexane

Tables 1.4.1 detail the most relevant work performed at the ITIES towards biological processes elucidation. This thesis focuses on large proteins and this review highlights the importance of parameters such as aqueous and organic electrolytes, organic solvent, interfacial dimensions, the electrochemical techniques employed and the presence of ionophores or surfactant all serve to enhance complexation of the biomolecule at the interface. The size of the protein, number of charged amino acids and hydrophobic component defines its Gibbs energy of transfer of the protein to cross the polarisable interface. Early studies used nitrobenzene which posses a high dielectric constant (ε = 34.8),[87] however the trend has been to increase the hydrophobicity of the organic solvent in order to widen the potential window to measure charge transfer processes. The most common solvents are 1,2-dichloroethane (ε = 10.45), 1,6-dichlorohexane (ε = 8.83)[87] and gelled-1,6-DCH by adding PVC. From the mechanistic point of view, it is been proven that ionic ionophores and surfactants are able to complex the charged protein in a similar way than the organic electrolyte employed at the ITIES. Thus, the selection of the ionophore/organic electrolyte will affect protein behaviour at liquid – liquid interfaces. Recently, Girault's group in Switzerland have implemented electrospray ionisation mass spectrometry techniques to confirm the formation of complexes at the liquid – liquid interfaces. Their result illustrates the strong interactions between protein and organic electrolyte after creating a chemical imposed potential difference across the liquid – liquid interfaces formed when using a microchip prior ionisation. This techniques is known as biphasic electrospray ionisation mass spectrometry (BESI-MS) and has been applied to angiotensin III and leuenkephalin,[64] melittin[65] and lysozyme[88] showing complexes such as [DPPC-angiotensin III], [DPPC-melittin] or [lysozyme – TPBCl or TPFB] at different charge states.

It is clear the need for complementary techniques at the ITIES to fully comprehend biomolecule interactions at the soft interfaces and the improvement in terms of sensitivity and selectivity across this field of electrochemistry. This could be achieved by simply integrating established methodology employed in proteomics such as capillary electrophoresis, sample preparation strategies and mass spectrometry which has been the driving purpose of this thesis.

1. 5. Proteomics

Proteomics is the science that investigates biological processes through the analysis of proteins expressed in a cell or tissue. It determines, characterises, identifies and quantifies gene and cellular functions at protein level. Before Tanaka[89] and Fenn[90] gave "Electrospray Wings for Molecular Elephants"[91] with the development of soft ionisation techniques for mass spectrometry in the detection of large biomolecules, the available techniques in proteomics were limited to genetic experiments, cell imaging, and light and electron microscopy amongst others. Since the 1980s with the breakthrough of soft ionisation techniques including the ionisation of bovine albumin via matrix-assisted laser desorption ionisation (MALDI) achieved by Karas and Hillenkamp,[92] mass spectrometry-based techniques such as matrix-assisted laser desorption ionisation – time of flight (MALDI-TOF), electrospray ionisation (ESI-MS), liquid chromatography (LC), two-dimensional gel electrophoresis (2-DGE) and capillary electrophoresis (CE) separation prior to MS have become indispensable analyses for molecular and cellular biology studies.[93]

1.5.1. Mass spectrometry

Mass spectroscopy in proteome research can be classified as *bottom-up* or *top-down*. Bottom-up proteomics or "shotgun" proteomics requires trypsin or other enzymatic digestion of the protein and then the peptide fragments generated can be identified in a protein database.[94] The protein digestion is typically coupled to liquid chromatography or capillary electrophoresis for peptide separation followed by tandem MS. This process can be automated and with a high throughput and sensitivity. However, the identification of the proteins is based on the identification of a low number of peptides. This low peptide sequence coverage is the main disadvantage of bottom-up proteomics. On the contrary, top-down proteomics primarily separates the proteins present in the sample. Then high resolution MS is used to determine molecular weight accurately. The inconvenience is the expensive mass spectrometers required, low throughput and the difficulties obtaining a complete separation especially in samples with low levels of the target protein.

1.5.2. Shotgun proteomics, sample preparation

As discussed in section 1.5.1, bottom-up proteomic analysis requires digestion of the protein as a first step towards identification of the target molecule. This step provides a large amount of small peptides which can be evaluated using mathematical algorithms and identified from sequence databases. Proteins, unlike deoxyribonucleic acid (DNA), possess a high degree of complexity, they are heterogeneous in terms of size, charge and structure which make them very challenging to be isolated. Another aspect to consider when preparing the target molecule is the possible low level of protein in the original sample. For this reason, separation, pre-fractioning and enrichment of the protein are essential in proteomics.[95] Other techniques applied in proteomics such as optical methods, and structural proteomics also require extensive sample preparation.[95] These pre-treatment steps depend on the sample and method employed and they can be very tedious, time consuming and costly. Sample preparation steps can be classified into cell disruption, de-salting, purification, enrichment, fractioning, separation, protein solubilisation, enzymatic digestion and sample labelling.[95]

For shotgun protein identification and quantification, LC, ESI and MALDI-MS are routinely performed after an extensive treatment of the sample. Figure 1.5.1 illustrates several steps required in proteome analysis prior to identification or quantification. In some cases, denaturation, reduction and alkylation are required in order to prevent reoxidation of intra- and intermolecular disulfide bonds.[95]

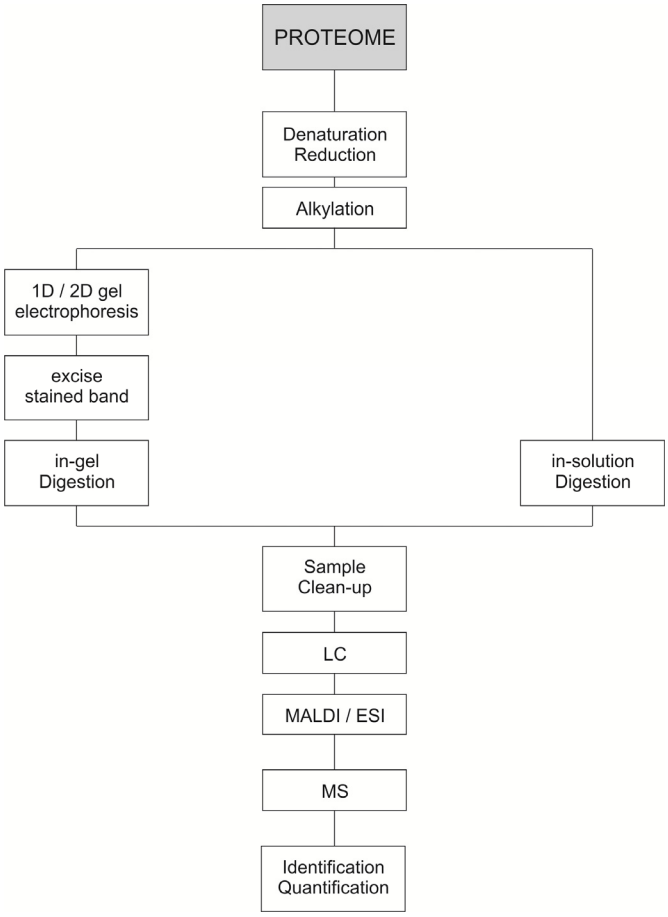

Figure 1.5.1. Scheme of the sample preparation in bottom-up proteome analysis.

The advantages of using this methodology are the possibility to detect amino acid substitutions or post-translational modifications. In addition, MS provides high resolution measurements and the capability to be integrated with separation techniques such as LC and CE. Further separation and enrichment can be also obtained by incorporating solid phase extraction (SPE) columns prior to analysis. An example of this is the work of Wang et al.,[96] a multifunctional chip fabricated for protein detection. The chip integrates trypsin digestion, solid phase extraction and capillary electrophoresis separation which is coupled to ESI-MS for mass analysis.[96] However, as mentioned previously, one of the disadvantages in this technology is the low sequence coverage which makes difficult the determination of the target biomolecules and the low levels of the protein of interest in the sample.

Consequently, bioelectrochemistry at liquid - liquid interfaces could be an alternative or complementary technology in label-free detection of biological

molecule. For this reason, combination of electrochemical methods and advanced sample preparation methods such as enzymatic digestion has been assessed in this thesis with a view to developing a new proteomic analysis technology.

The next sections explore the instrumentation routinely used in proteomics as a way of understanding the advantages, disadvantages and challenges faced by mass spectrometry.

1.5.3. Mass spectrometer

A mass spectrometer consists of an ion source, a mass analyser and a detector.[93, 97] The mass analyser measures the mass-to-charge ratio (*m/z*) of the ionized analytes and the detector registers the number of ions at each *m/z* value. The ionisation methods most commonly used for proteins and peptides are electrospray ionisation (ESI) and MALDI. There are four types of mass analysers:[93, 98] ion-trap, TOF, quadrupole and Fourier transform ion cyclotron resonance (FT-ICR), which can be also be put in tandem to enhance resolution and sensitivity. Finally, there are several types of detectors available for ion detection after being separated by their mass/charge ratio in the mass analyser. Commonly an ion detector requires an electron multiplier due to the low ion current measured.

1.5.3.1. Ionisation Methods

Soft ionisation of large biomolecules includes ESI and MALDI as the most widely used technique in proteomics.

Electrospray ionisation consists in pumping the liquid sample through a needle at high voltage to electrostatically disperse (electrospray) small droplets (see Figure 1.5.2a). The solvent rapidly evaporates imparting the charge onto the analyte. This ionisation occurs at atmospheric pressure and is therefore a gentle process with no fragmentation in the gas phase.[99] The liquid sample is composed of the analyte which is dissolved in an acidified aqueous solution with a high concentration of organic solution (i.e. 1% acetic acid in 49% water and 50% methanol). This acidic solution facilitates the protonation of the protein and its transfer into the gas phase. When proteins are electrosprayed using ESI, they become multiply protonated and

they normally appear as a series of different peaks in the spectrum which correspond to different charge states of the protein.[95]

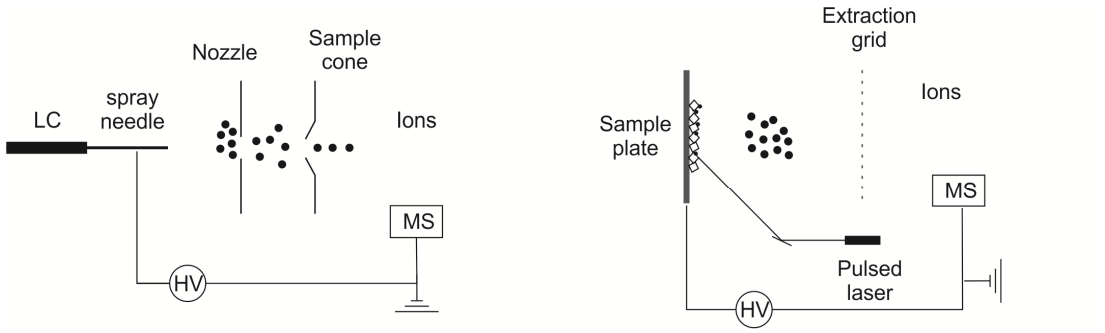

a) Electrospray ionization (ESI) **b)** Matrix-assisted laser desorption/ionization (MALDI)

Figure 1.5.2. Ionisation process in a) ESI and b) MALDI prior to MS

In the case of MALDI ionisation, the sample (protein or peptides) is deposited on a metallic plate and co-crystallized with a high concentration of matrix solution (low molecular weight organic compound, for instance 2,5-dihydroxybenzoic acid, α-cyano-4-hydroxy-cinnamic acid and sinapinic acid).[100] This matrix is typically added in excess (matrix to analyte volume ratio of 1000:1 or larger) to absorb the laser energy and disperses the sample. After deposition, a pulsed laser of known wavelength is applied to the cocrystallite resulting in desorption of the analyte into the gas phase and its ionisation (see Figure 1.5.2b). Upon irradiation, a photo-chemical process (photo-ablation and photo-ionisation) takes place although the precise ionisation mechanism is still unknown.[99] Then the charged ions produced are accelerated via an electric field between the sample plate and the detector. Unlike ESI, this method produces mainly single charged ion peaks in the *m/z* spectrum.[95]

Recent research has been focused on different ionisation methods that have opened up a new way to analyse samples. New strategies consist in direct ionisation onto different substrates. These are also known as imaging mass spectrometry techniques.[101, 102] Amongst mass spectrometry imaging, such as electrostatic spray ionisation (ESTASI),[103] desorption electrospray ionisation mass spectrometry (DESI),[104] matrix-assisted laser desorption ionisation mass spectrometry imaging (MALDI-MSI) and time of flight secondary ion mass spectrometry (TOF-SIMS), the sample preparation steps has been reduced considerably due to the possibility to measure via MS directly onto the sample. Qiao et al. have demonstrated the versatility of ESTASI which has been tested in different geometries (polymer coated

silica capillaries, plastic micropipette tips and polyimide microchips).[105] Their latest publication reports the combination of isoelectric gel electrophoresis with MS via ESTASI.[103] TOF-SIMS has been used in biomedical imaging analysis for decades[106, 107] such as lipid composition imaging in cell membranes.[108] MALDI[102] and DESI also provide a new platform for mass determination on biological tissues with minimal pre-treatment of the sample. For instance, Eberlin et al. have published a classification method to discern between gliomas (malignant tumour with origin in the brain or spine) and meningiomas (usually benign tumour) to delimit the tumour boundaries by using DESI-MS. This could be of use to provide diagnostic information and guide decision making during brain tumour surgery.[109] They also published a study of nano-assisted desorption ionisation mass spectrometry (NALDI)[110] to image lipid biomarkers in melanoma tumours[111] and nano-DESI for tissue imaging .[112]

1.5.3.2. Mass analyser

There are four main types of mass analyser: ion trap, quadrupole, time of flight and Fourier transform ion cyclotron resonance mass spectrometer.

In the first type (ion trap), the ions produced by previous ionisation are trapped when various radio frequency voltages are applied. The motion of the ions depends on the voltage applied and their (*m/z*) ratios. Then the steam of ions is focused to the detector to produce the mass spectra. The Fourier transform ion cyclotron resonance (FT-ICR) mass spectrometer is also a trapping mass spectrometer. The main difference is that it captures the ions under high vacuum in a high magnetic field. In the case of the quadrupole, oscillating electric fields are applied through four metallic cylindrical rods. Those four rods are connected two opposite to each other and the potential applied between both affects the motion of the ions towards the detector allowing the determination of the mass-to-charge ratio. However, TOF analysers measure the time ions require to reach the detector after being accelerated by an electric field of known strength, therefore the mass-to-charge (*m/z*) ratio can be determined using the following expression:[113]

$$v = \sqrt{2Eed}\sqrt{\frac{z}{m}} \qquad (1.4.1)$$

where v is the velocity of the ions, E is the electric field strength, e is the elementary charge and d the width of the electric field.

Figure 1.5.3 presents a scheme of the four mass spectrometers described above.

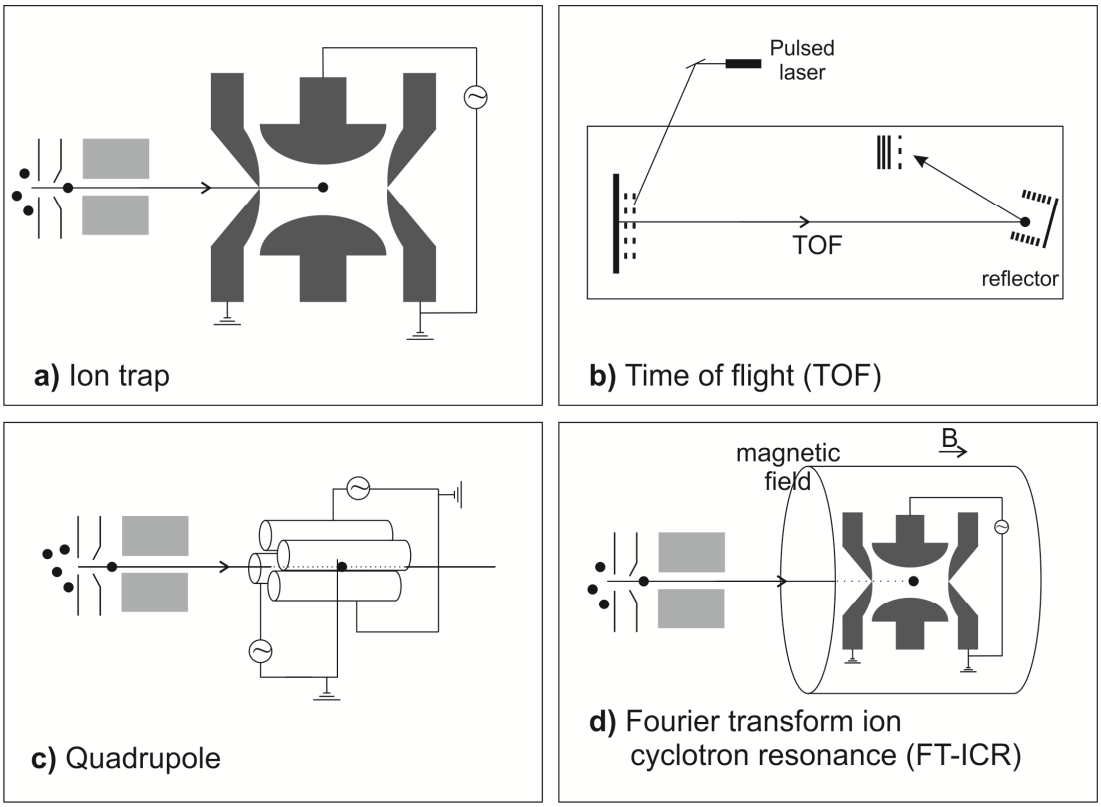

Figure 1.5.3. Mass analyser types used in mass spectrometry.

1.5.3.3. Ion detector

The mass of each ion produced by ionisation is accelerated through the mass analyser towards the detector. The detector generates a signal from the incident ions by either generating secondary electrons which are further amplified or by inducing a current generated by a moving charge which can be then related to the ions *m/z*.

Complex and costly instrumentation is required in routine proteomic analysis and extensive sample preparation becomes indispensable in bottom-up proteomics for protein identification. Therefore implementation of bioelectrochemistry at the ITIES

could be an alternative for the label-free detection of biological molecules. Preparation procedures employed at shotgun proteomics have been also evaluated in this thesis.

1. 6. Aims

The aim of this work is to study the pre-concentration of proteins at liquid – liquid interfaces via electrochemical adsorption. This method has been evaluated as an electrochemical enhancement of the protein signal followed by label-free voltammetric detection and also as a pre-treatment step prior to more complex analysis such as electrostatic spray ionisation. This methodology was tested in different conditions either different organic phases or protein of interest. In addition, combination of advanced sample preparation methods such as enzymatic digestion with electrochemistry at the ITIES, was targeted and has been assessed with a view to developing a new proteomic analysis technology.

Adsorptive stripping voltammetry (AdSV) was implemented in order to achieve lower limits of detection when enriching the interfacial protein concentration via electrochemistry at the liquid – liquid μ-interfaces. These results are described in Chapter 3.

In Chapter 4, electrostatic spray ionisation – mass spectrometry (ESTASI-MS) has been used as a complementary technique in order to elucidate the mechanism of lysozyme detection proposed in Chapter 3 when implementing AdSV. In addition, a proof-of-principle study is also presented in this chapter which consisted in the coupling of a gelled hydrophobic phase after electrochemical protein pre-concentration with this soft ionisation technique prior to MS.

In Chapter 5, a new organic phase, room temperature ionic liquid (RTIL), was investigated for lysozyme detection via adsorptive stripping voltammetry. Using cyclic voltammetry at the water (W) – RTIL μ-interfaces, lysozyme detection was unsuccessful. However when performing AdSV, lysozyme was successfully detected. In parallel to this work, proton interactions at the W-RTIL interfaces were observed when a positive potential difference was applied.

Following this work, haemoglobin, a bigger protein molecule (almost 6-folds bigger in molecular weight than lysozyme), highly charged and with a quaternary structure, was studied under similar conditions reported in Chapter 1, consisting of electrochemical adsorption as a protein pre-concentration step prior to electrochemical analysis. The results are detailed in Chapter 6.

Chapter 7 presents the effect of protein digestion prior to electrochemical analysis. This pre-treatment step was implemented to mimic proteomic sample preparation steps for protein identification. This approach was carried out as a new label-free fingerprint platform.

Finally, general conclusions and future work are discussed in Chapter 8.

2 Experimental section

This chapter contains a general summary of the procedures performed in this study. The electrochemical cells employed and several electrochemical characterisation tools such as cyclic voltammetry, adsorptive stripping voltammetry, alternating current voltammetry and electrochemical impedance spectroscopy are fully described. There is also a detailed description of the silicon membranes used to form the liquid-liquid microinterfaces, showing the importance of the geometric arrangement of the micropores. The methodology for electrospray ionisation – mass spectrometry of the gel after protein pre-concentration at the gelled liquid - liquid interfaces is also described. Finally information regarding the enzymatic digestion of biomolecules and complementary analysis carried out in order to mimic proteomic methods prior to electrochemical characterisation are illustrated. In this case, small peptides were analysed via liquid chromatography – mass spectrometry and single amino acids were measured by gas chromatography – mass spectrometry after a derivatisation step.

2. 1. Electrochemical cell

An electrochemical glass cell is commonly used in a four–electrode configuration to perform electrochemical measurements at liquid – liquid interfaces as represented in Figure 2.1.1. It consists of two reference and two counter electrodes, one of each in a different phase.[4] Platinum-mesh is usually employed as the counter electrode and silver/silver chloride electrode as the reference electrode.

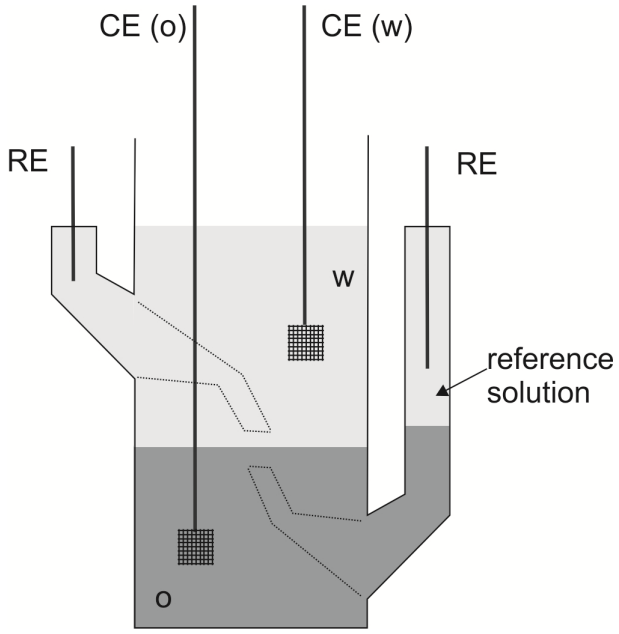

Figure 2.1.1. Representation of a four-electrode set-up at the ITIES where *w* and *o* refer to the respective aqueous and organic phase, RE is the reference electrode and CE the counter electrode in the water phase (*w*) and organic solution (*o*).

The above cell is extensively used for millimetre- or centimetre-scale ITIES because it compensates the Ohmic drop caused by the resistive organic solution. However in the experiments performed and shown in this thesis, a two–electrode cell was used to conduct all the electrochemical measurements. This is only possible since the size of the interfaces are drastically decreased which translates into a reduction of the Ohmic drop. In the case of a two-electrode cell, two reference electrodes (Ag/AgCl) serve as both reference and counter electrodes, one in each phase. All the voltammograms shown in Chapter 3 to 7 correspond to the signal obtained at the μ-ITIES array when using a microporous membrane sealed onto a

glass cylinder. The organic phase is introduced into this glass cylinder and then immersed in a beaker containing the aqueous solution.[34] Therefore microinterfaces are formed at the edge of the membrane when both (aqueous and organic) phases come into contact. Figure 2.1.2 is a schematic of the two-electrode electrochemical cell when using the microporous membrane to define the μ-ITIES array. Both the reference solution in which the Ag/AgCl is immersed and the organic phase contain a common cation ($BTPPA^+$), resulting in a non-polarisable interface between the reference solution and the organic phase.

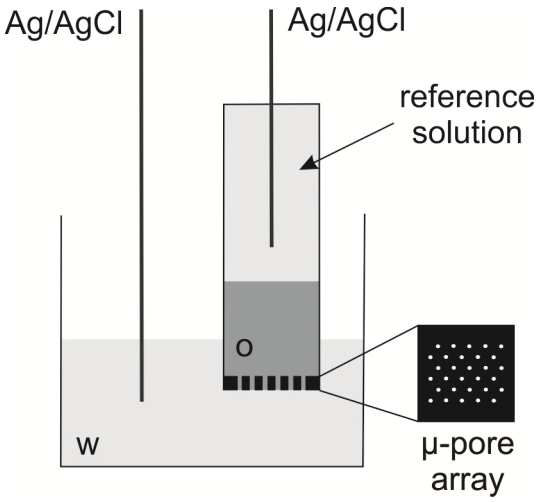

Ag | AgCl	*x* μM ANALYTE in 10 mM electrolyte	10 mM $BTPPA^+TPBCl^-$ in gellified 1,6-DCH	10 mM $BTPPA^+Cl^-$ in 10 mM LiCl	AgCl | Ag

Figure 2.1.2. Two-electrode set-up of the liquid-liquid electrochemical cell. The analyte and electrolyte used in each experiment will be specified in the following chapters for specific measurements. *w* and *o* refer to the aqueous and organic solutions.

In order to improve the mechanical stability of the organic phase during the electrochemical characterisation, polyvinyl chloride (PVC) was added to the organic solution (1,6-dichlorohexane). This results in a hydrophobic 10% w/v gel.[79, 114] In addition, the organic electrolyte (BTPPA TPBCl) present in the gelled 1,6-DCH was kept at a concentration of 10 mM. The organic electrolyte salt was synthesized via metathesis.[38] The protocol for the organic electrolyte preparation is outlined in more details in Appendix A.

The cell described in Figure 2.1.2 was modified in order to perform the room temperature ionic liquid – water (RTIL/w) interface experiments. The properties of the hydrophobic ionic liquid selected (trihexyl(tetradecyl) phosphonium tris(pentafluoroethyl) trifluorophosphate) limited the cell characteristics requiring a fritted glass tube to support the reference solution (trihexyl(tetradecyl) phosphonium chloride in 10 mM LiCl) and position of the immiscible solutions having to be inverted.[115] Now the RTIL rests at the bottom of the beaker and the aqueous phase remains in the glass cylinder. Figure 2.1.3 shows a scheme of the two-electrode cell used. The same micro-pore array design was sealed onto a glass tube which is then immersed in the ionic liquid.[34] The silicon membrane design and fabrication is described in the next section (Section 2.2).

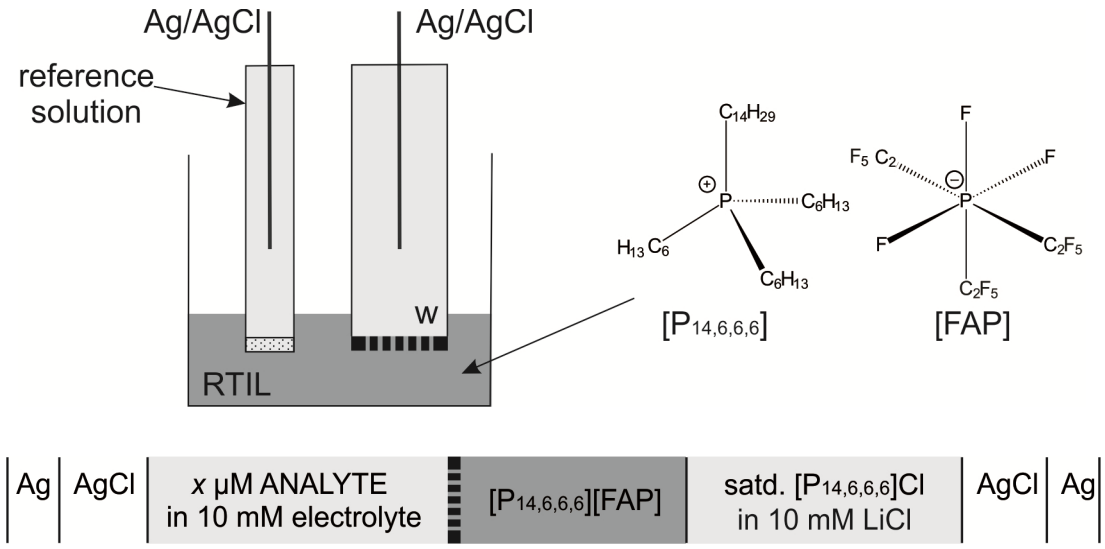

Figure 2.1.3. Two-electrode set-up of the electrochemical cell when using a room temperature ionic liquid (RTIL) as an alternative organic phase. The very hydrophobic ionic liquid employed in this research is known as $[P_{14,6,6,6}][FAP]$, trihexyl(tetradecyl) phosphonium tris(pentafluoroethyl) trifluorophosphate.

All electrochemical measurements were performed using an Autolab PGSTAT302N electrochemical analyser (Metrohm Autolab, Utrecht, The Netherlands).

2. 2. Micropore arrays

The liquid-liquid microinterfaces were formed using a silicon membrane consisted of 30 micropores of 22.4 µm diameter which provides a total geometric cross-sectional area of $1.18 \cdot 10^{-4}$ cm^2 (see scanning electron microscopy images in Figure 2.2.1). The 30 micropores were fabricated through a combination of dry and wet etching. During the pore fabrication by deep reactive ion etching (DRIE), the inner part of the pores was coated with a fluorocarbon film to create a hydrophobic layer on the walls of the micropore array.[33, 35]

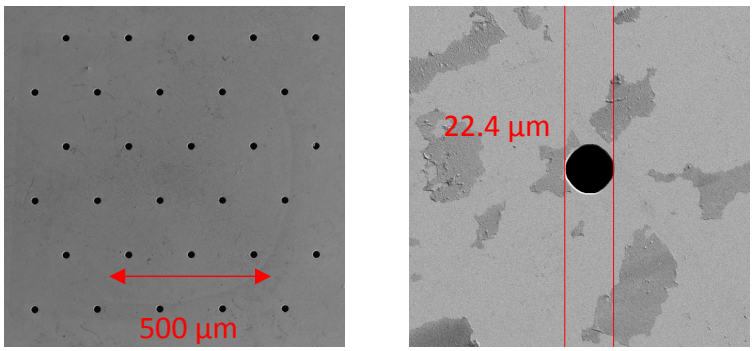

Figure 2.2.1. Scanning Electron Microscopy (SEM) images of the silicon membrane. SEM images were recorded using a Zeiss Neon 40 EsB FIBSEM microscope (Carl Zeiss Nano Technology Systems) and were taken with a beam of 5 kV, using the In Lens secondary electron detector at Curtin University.

In Section 1.3.2, the design and filling of the pores have been shown to determine the voltammogram shape and behaviour due to their impact on the mass transport profile. For this reason, the design illustrated in Figure 2.2.1 is been shown to provide an optimum arrangement of the pores to prevent diffusion overlap. The pores in the membrane are etched in a hexagonal distribution (see Figure 2.2.2) with a pore-to-pore distance of twenty times the pore radius or ten times the pore diameter.

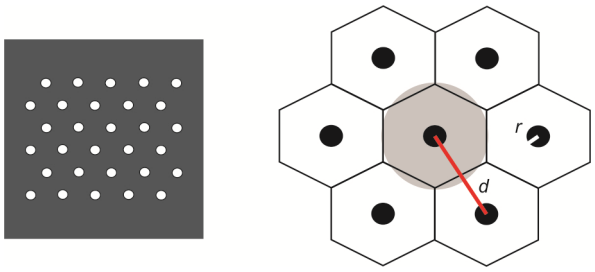

Figure 2.2.2. Scheme of the hexagonal arrangement of the micropore array where *r* is the pore radius and *d* the pitch *(d = 20r)*.

2. 3. Reference electrodes

The reference electrodes utilised in this research were silver/silver chloride electrodes:

$$AgCl(s) + e^- \rightarrow Ag(s) + Cl^-(aq) \qquad (2.3.1)$$

These electrodes provide a stable and reproducible potential which behaviour approaches that of an ideal non-polarisable electrode. There are a wide variety of reference electrodes such as saturated calomel electrode ($Hg/Hg_2Cl_2/KCl$ (saturated)) and silver/silver salt ($Ag/AgX/X^-$ where X is an ion of charge -1). High stability is reached when the concentration ratio of the redox species is constant.[4, 116] The Nernst equation for Ag/AgCl (Equation 2.3.2) shows the dependence of the potential of Ag/AgCl on the activity (a) of the Cl^- ions.

$$E_{Ag/AgCl} = E^0_{Ag/AgCl} - \frac{RT}{F} ln a_{Cl^-} \qquad (2.3.2)$$

The standard potential (E^0) of Ag/AgCl when measured against a standard hydrogen electrode (considered 0 V at 1 atmosphere and 25 ˚C) is + 0.222 V:

$$Ag \mid AgCl \mid K^+ Cl^- \parallel Cl^- H^+ \mid H_2 \mid Pt \qquad \Delta E_{cell}{}^0 = +\, 0.222V$$

Therefore if the concentration of Cl^- is constant, the electrode possesses a stable potential and this potential corresponds to the standard potential of the Ag/AgCl.

2. 4. Electrochemical techniques

2.4.1. Cyclic Voltammetry (CV)

Cyclic voltammetry (CV) is one of the most common techniques in electrochemistry. This technique allows to scan the system on a forward linear scan from an initial potential (E_1 in Figure 2.4.1) to a different potential (E_2 in Figure 2.4.1) and scan back towards the initial potential (E_1) in a cycle.[116] Cyclic voltammetry can provide information about reversibility, kinetics, diffusion, adsorption, lipophilicity and number of electrons or charge transferred in a charge transfer reaction.[5, 116]

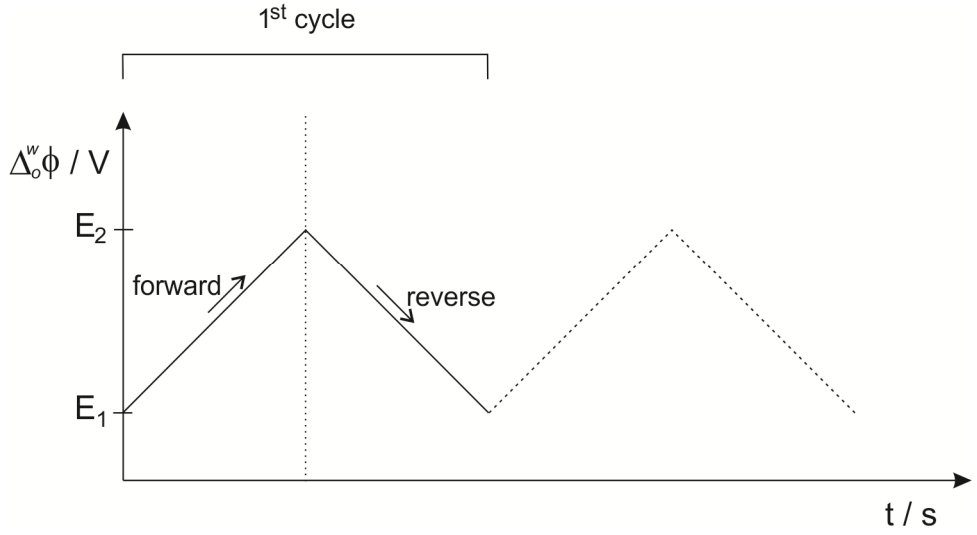

Figure 2.4.1. Cyclic voltammetry waveform when representing the applied potential versus time.

At the ITIES, the initial and final applied potential (E_1 and E_2) will be determined by the organic and aqueous background electrolytes. As previously discussed in Chapter 1, the transfer of the background electrolytes limit the potential window where charge transfer reactions are detectable. Scanning to potentials where background electrolyte transfers provides little information on the analyte ion of interest due to the analyte transfer being masked by the background electrolyte current.

Figure 2.4.2 shows two different voltammograms of the reversible transfer a cation (A^+) at the ITIES: a) in the case of a purely planar diffusion transfer at a

millimetre-interface and b) in the case of an asymmetric diffusion of A^+ across the polarisable interface at a micro-interface.

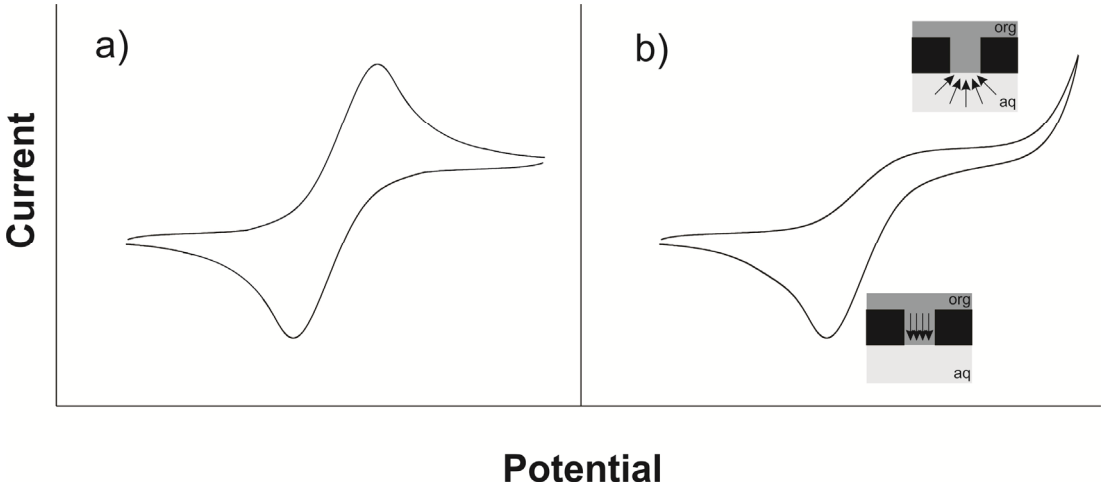

Figure 2.4.2. CV of a) A^+ transfer at an interface and b) A^+ transfer at a micro-interface. The arrows refer to the transfer from aqueous to organic (aq → *org*) via radial diffusion or organic to aqueous (*org* → *aq*) via linear diffusion.

In the case of linear diffusion, peak current is described by the Randles-Sevcik equation (2.4.1) for an electrochemically reversible process:

$$i_p = (2.69 \cdot 10^5) z_i^{3/2} A D_i^{1/2} C_i v^{1/2} \qquad (2.4.1)$$

where i_p is the peak current, z_i the charge of ion i, D_i the diffusion coefficient of species i, C_i the concentration of species i and A the area of the interface. Peak current is proportional to the square root of the scan rate ($v^{1/2}$) making the assumption that one-dimensional diffusion is occurring, that the interface is flat and there is a large excess of supporting electrolyte. Nonetheless, quasi-reversible processes can be described with the following equation which includes α as the transfer coefficient, z_a the charge involved in the charge transfer step and $\alpha = nFv/RT$.

$$i_p = (2.99 \cdot 10^5) z (\alpha z_i)^{1/2} A D_i^{1/2} C_i v^{1/2} \qquad (2.4.2)$$

In the case of an adsorption process, equation 2.4.3 shows the proportional relationship between the peak current and the scan rate.

$$i_p = \frac{z^2 F^2 \Gamma A v}{4RT} \qquad (2.4.3)$$

where z is the number of charges transferred, F is the Faraday constant, Γ is the surface coverage, R is the universal gas constant and T the temperature.

Experimentally, if the peak measured is integrated when current is plotted versus time, the charge can be calculated in Coulombs. This charge can then provide more information about the adsorption process. Equation (2.4.4) shows that this charge *(Q)* is directly proportional to the surface area, surface coverage, the Faraday constant and z_i the charge of the species i.

$$Q = z_i F A \Gamma \qquad (2.4.4)$$

In radial diffusion, the characteristic steady state current for a radial diffusion process (see forward scan in Figure 2.4.2.b) in which the diffusion characteristic in an interface is similar to that around and inlaid electrode described by:

$$I_{lim} = n4z_i FDCr \qquad (2.4.5)$$

where n is the number of microinterfaces, F the Faraday constant, z_i the number of charges of species i transferred, D and C are the diffusion coefficient and bulk concentration of the transferring species, and r is the radius of one interface.

However when the organic is recessed L distance within the pore, the analogue equation is:

$$I_{lim} = n\frac{4\pi z_i FDCr}{4L+\pi r} \qquad (2.4.6)$$

And in the case of a hemispheric organic phase (see Figure 2.4.3), the limiting current is described as follows:

$$I_{lim} = n2\pi z_i FDCr \qquad (2.4.7)$$

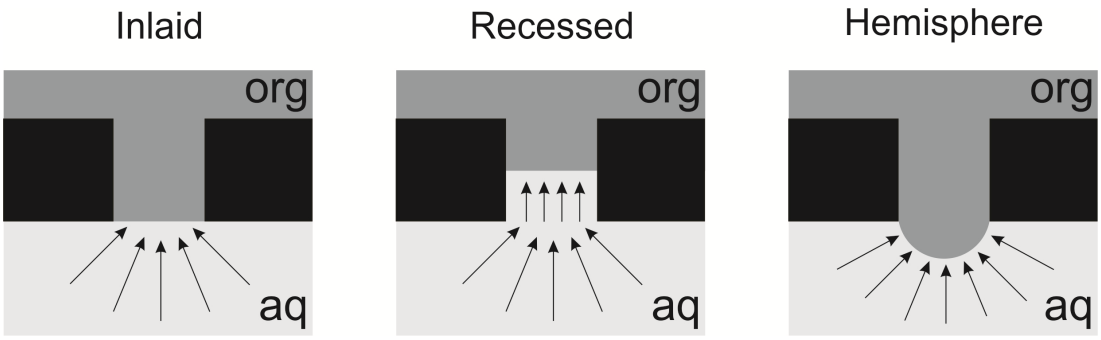

Figure 2.4.3. Diffusion profiles for a micropore where the organic phase presents different geometries (hemispherical, inlaid and recessed).

All cyclic voltammograms presented in this thesis were generally implemented at a scan rate of 5 mV s^{-1} due to the analysis of slow processes. Higher scan rates were normally applied for mechanism elucidation and will be indicated in the corresponding sections of this document when necessarily.

2.4.2. Stripping Voltammetry (SV)

Stripping voltammetry (SV) is a two-step technique, *(1) pre-concentration* and *(2) detection step*. The *pre-concentration* step involves holding the applied potential for a period of time which causes the extraction or adsorption of the analyte of interest.[5] Then the second step is also known as the *stripping step* which consists in scanning in the positive/negative direction causing the back transfer of the analyte into the aqueous phase. Figure 2.4.4 illustrates the two-step waveform of the SV.

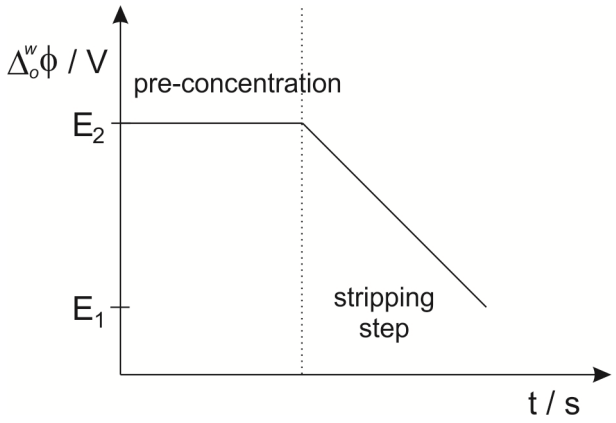

Figure 2.4.4. Galvani potential-time waveform used in stripping voltammetry.

Stripping techniques have been widely used for metal detection at electrode electrochemistry, in particular at mercury electrodes in polarography. SV can be divided into: *anodic* stripping voltammetry (ASV) which consists of a cathodic deposition and the potential is scanned positively in the detection step; *cathodic* stripping voltammetry (CSV) involves anodic deposition of the analyte followed by stripping in a negative potential scan (cathodic detection step); and *adsorptive* stripping voltammetry (AdSV) which is based on the accumulation of a surface/interface active analyte. The response is directly related to the analyte concentration, amongst other parameters and to surface concentration in the case of AdSV.[5]

The applied potential and pre-concentration time were optimised for each set of experiments when adsorptive stripping voltammetry was performed (see details in the corresponding chapters (3, 4, 5 and 6)) being the scan rate 5 mVs^{-1}.

2.4.3. Alternating Current Voltammetry (ACV)

Alternating current voltammetry (ACV) allows the investigation of non-faradaic processes e.g. adsorption. The initial (E_1) and final (E_2) applied potential is limited by the background electrolytes in both immiscible phases. A sinusoidal alternative voltage is applied across the liquid-liquid interface from E_1 to E_2 at a fixed frequency and amplitude (see Figure 2.4.5). Thus ACV can give information on the charging current, how the capacitance of the ionic double layer is altered when adsorption occurs at a potential between E_1 and E_2.[117]

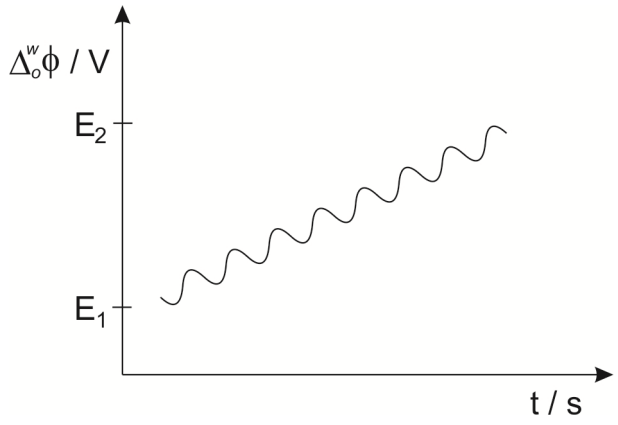

Figure 2.4.5. Potential versus time waveform for alternating current voltammetry at a fixed frequency and amplitude.

ACV has the ability to scan the frequency domain to excite different processes with different time constants. The excitation signal *V(t)* is defined as it follows:

$$V(t) = V_o\, sin(\omega t) = V_o e^{i\omega t} \qquad (2.4.8)$$

where *Vo* is amplitude, *t* is the time, ω is the radial frequency ($\omega = 2\pi f$) and *f* the frequency. As a result, the sinusoidal current *I(t)* generated is described in equation 2.4.9 where θ is the phase difference between the voltage and the current and is zero for purely resistive behaviour.[4, 117]

$$I(t) = I_o\, sin(\omega t + \theta) = I_o e^{i\theta} e^{i\omega t} \qquad (2.4.9)$$

Due to the non-faradaic nature of the current measured, this is directly related to Ohm's law. Consequently, impedance can be written as the alternating current resistance of an electric conductor (see Equation 2.4.10).[4, 117]

$$Z = \frac{V}{I} = \frac{V_o}{I_o} e^{i\theta} \qquad (2.4.10)$$

Impedance is also associated to the capacitance (*C*) in a RC (resistor/capacitor) circuit:

$$Z = \frac{1}{j\omega C} \qquad (2.4.11)$$

where *j* is a complex number, $\sqrt{-1}$. Then the impedance (*Z*) was given by Z_{re} and Z_{im} which are the real and imaginary parts of the impedance respectively.

$$Z = Z_{re} + Z_{im} \qquad (2.4.12)$$

$$\theta = tan^{-1} \frac{Z_{im}}{Z_{re}} \qquad (2.4.13)$$

Alternating current voltammetry was performed for adsorption analysis at the liquid-liquid microinterfaces when a very hydrophobic room temperature ionic liquid (trihexyl(tetradecyl)phosphonium tris(pentafluorethyl)trifluorphosphate) was used as an alternative organic phase. All ACV measurements were carried out at 6 Hz (frequency), 5 mV (amplitude) and scanned at phases angles of 0˚ and 90˚and are described and discussed in Chapter 5.3.

2.4.4. Electrochemical Impedance spectroscopy (EIS)

Electrochemical impedance spectroscopy (EIS) is a complex technique that involves the measurement of impedance obtained when a sinusoidal potential of a certain amplitude is superimposed on a fixed DC potential (E_1) as function of frequency.[117] Figure 2.4.6 represents the profile of the potential versus time waveform. Equations 2.4.8 to 2.4.13 are of interest for impedance characterisation.

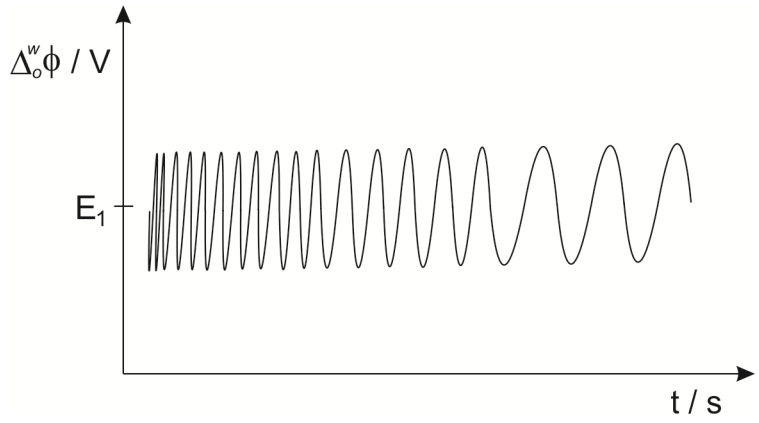

Figure 2.4.6. Potential-time waveform for electrochemical impedance spectroscopy at a fixed potential (E_1) and Amplitude (A).

In this work, EIS was performed at an amplitude of 5 mV over the frequency range from 100 kHz to 0.1 Hz. The DC potential was also fixed and varied depending on the process under study. In addition, ZView software from Scribner Associates Inc. (North Caroline, USA) was used to fit the impedance data to equivalent electrical circuits to provide a better understanding of the processes taking place at the liquid – liquid interfaces.

2. 5. Enzymatic reactions

One of various pre-treatment methods in proteomics for protein identification is the study of multiple enzymatic digestions to increase the sequence coverage and therefore to enhance the probabilities for determining the unknown protein.[95] In this investigation, the same approach was evaluated by electrochemistry at liquid – liquid interfaces. Protein digestions were carried out according to published procedures.[83] The enzyme-to-protein molar ratio was fixed at 1:25 for the different enzymatic

reactions. For *peptic* digestion, the protein and pepsin were dissolved in hydrochloric acid (HCl) at the required pH of 1.3 or 2, and the mixture was incubated at 37 °C for 2 h. In the case of *tryptic* digestion, the mixture was prepared in 0.2 g L^{-1} of ethylenediaminetetraacetic acid (EDTA) at pH 7.0-7.6. Then the enzyme-protein mixture was incubated at 37 °C for 16 h. In addition, the *endoproteinase Glu-C* – protein mixture was incubated in phosphate buffered saline (PBS) at pH 7.8 or employing 10 mg mL^{-1} of ammonium bicarbonate at pH 8. Both incubations were carried out at 37 °C for 16h.

The protein digest was then separated from undigested material by filtration using 3 kDa centrifugal filter devices (see Figure 2.5.1).

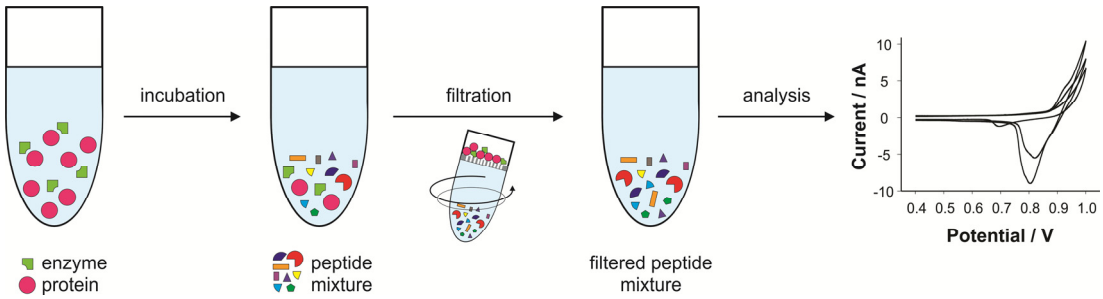

Figure 2.5.1. Schematic representation of the enzymatic digestion prior to analysis.

In the literature, the preferential cleavage sites of the enzymes employed for this study has been reported and this information is summarised in Figure 2.5.2. This table also shows the amino acid structure and the incubation conditions specified above. Pepsin exhibits preferential cleavage for hydrophobic amino acids, in particular aromatic amino acids. Trypsin cleaves predominately at the carboxylic site of arginine and lysine except when they are bound to a C-terminal proline whilst in the case of endoproteinase Glu-C, the enzyme also hydrolyzes peptide bonds at the carboxylic side in the presence of ammonium at the glutamic and aspartic acid and only aspartic acid in the absence of ammonium ions in solution.[118, 119]

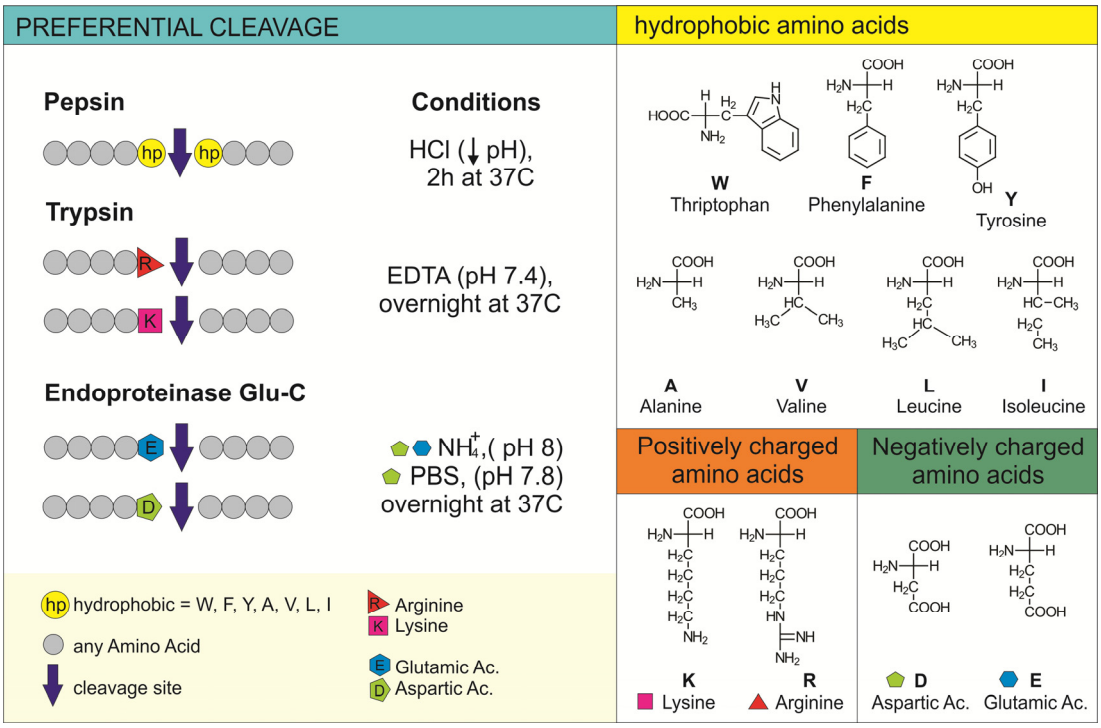

Figure 2.5.2. Representation of the preferential cleavage sites (blue arrow) depending on the different enzymes used under different incubation condition. A list of 11 amino acids which determine the preferential cleavage is shown on the right side of the diagram and is divided in 3 groups (hydrophobic, positively and negatively charged amino acids).

2. 6. Mass Spectrometry

Mass spectrometry (MS) is an analytical technique that can provide quantitative and qualitative information on ionizable analytes. The development of soft ionisation techniques such as electrospray ionisation (ESI) and matrix-assisted laser desorption ionisation (MALDI) opened up a new form to study biomacromolecules.[120] For this reason, such systems are the perfect candidates for a full characterisation of the proteins and peptides investigated in this research. Gas and liquid chromatographic techniques (GC and LC) were also combined in order to separate the compounds prior to mass analysis. In terms of mass determination of the sample, numerous mass analysers can be used that can isolate the ions based on their mass-to-charge ratio (*m/z*) and are described in the corresponding chapters.

Table 2.6.1 summarizes the different mass spectrometry techniques which have been applied during this research. All the MS measurements were performed as a

complementary investigation for further understanding of complex processes at the ITIES or, as in the case of the electrostatic spray ionisation, the integration of electrochemical protein pre-concentration on an organic gel with mass spectrometry via electrospray ionisation. This table also provides the nature of the sample, the pre-treatment required and the chapter where the results will be discussed.

Table 2.6.1. Summary of the mass spectrometry analysis performed in this thesis, sample nature, pre-treatment and location of the results and discussion.

Technique	Sample	Sample preparation	Chapter
ESTASI-MS*	Protein	Electrochemical protein pre-concentration on the gelled organic phase as detailed in Chapter 3	4
MALDI-TOF*	Protein	Protein extraction from organogel after electrochemical pre-concentration using the method explained in Chapter 3	4
BESI-MS*	Room temperature ionic liquid	No sample preparation required	6
GC-MS	Single amino acids	Enzymatic digestion prior analysis followed by derivatisation using EZFaast kit from Phenomenex	7
MALDI/TOF-TOF	Peptides	Enzymatic digestion prior analysis	7
LC-MS	Peptides	Enzymatic digestion prior analysis	7

**ESTASI – Electrostatic spray ionisation*

**TOF - Time of flight*

**BESI – Biphasic electro spray ionisation*

2.6.1. ElectroSTAtic Spray Ionisation – Mass Spectrometry (ESTASI-MS)

Most of the electrochemical measurements presented in this thesis have been performed at the gelled liquid – liquid interfaces. When coupling this technique with mass spectrometry via electrostatic spray ionisation, the organogel was fixed on a 0.2 mm GelBond®PAG film from Lonza Group Ltd. (Basel, Switzerland) after electrochemical protein pre-concentration. The ESTASI-MS was performed as illustrated in Figure 2.6.1. A gold electrode was placed beneath the bottom plastic

layer (GelBond®PAG film) and the gel was placed close to the MS inlet to induce the electrostatic spray ionisation.[103] The electrode was connected with a DC high voltage (9 kV) source via switch 1 or grounded via switch 2. A special LabView program controls the switches in order to synchronize their work.

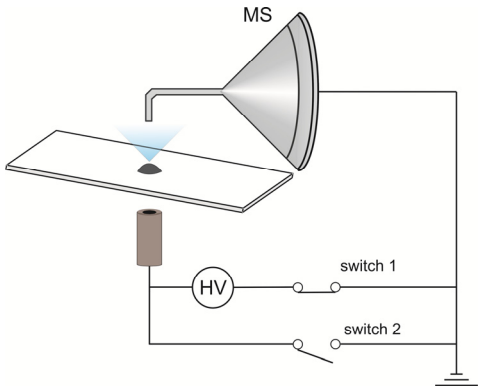

Figure 2.6.1. Illustration of ESTASI-MS set-up.

Drops of an acidic buffer (50% methanol, 49% water and 1% acetic acid) were deposited manually on top of the gel.[103] During ESTASI, the spray voltage of the internal power source of the LTQ Velos (mass analyser from Thermo Fisher Scientific Inc., Hampton, New Hampshire) was set to 0 although an external power source (explained above) was used to apply a high voltage of 9 kV to induce the spray. An enhanced ion trap scan rate (10,000 [1]Th/s) was selected to obtain a good spectral resolution.

Electrospray ionisation - mass spectrometry work was performed at Prof. Hubert Girault's Laboratory of Physical and Analytical Electrochemistry (LEPA), École Polytechnique Fédérale de Lausanne (EPFL) in Lausanne, Switzerland.

2.6.2. Matrix-Assisted Laser Desorption Ionisation – Time of flight (MALDI-TOF)

[1] Th stands for Thomson and is the unit of mass-to-charge ratio proposed by Cooks and Rockwood. Th = 1.036 x 10^{-8} Kg C^{-1} Cooks and Rockwood, The Thomson - A suggested unit for mass spectroscopists. In *Rapid Commun. Mass Spectrom.*, 1991; Vol. 5, pp 93-93.

The MS analyses were performed on a positive mode Microflex MALDI-TOF instrument (Bruker Daltonics GmbH, Faellanden, Switzerland) equipped with a nitrogen laser (wavelength 337 nm). Two microliters of the extracted protein solution from the organogel was deposited on a steel target plate and left to dry at room temperature. The extraction procedure after electrochemical pre-concentration on the gel consists in dissolving the gel in 5 µL of 1,6-dichlorohexane and swirl with a vortex for 5 minutes. Due to the high hydrophobicity of the solvent chosen for extraction, 1 µl of the matrix solution (10 mg/mL 2,5-dihydroxy benzoic acid (DHB) in 50% acetonitrile, 0.1% trifluoroacetic acid, and 49.9% water) was added after the 1,6-dichlorohexane was evaporated. Normally, DHB is deposited at the same time than the sample so the protein co-crystallises with the matrix but in this case the solvents are incompatible. After this addition, the sample was also left to dry at room temperature prior to measurements. Finally, data analysis was performed using flexAnalysis software from Bruker in the range of 4,000 - 85,000 *m/z*.

Matrix-assisted laser desorption ionisation - mass spectrometry work was performed at Prof. Hubert Girault's Laboratory of Physical and Analytical Electrochemistry (LEPA), École Polytechnique Fédérale de Lausanne (EPFL) in Lausanne, Switzerland.

2.6.3. Biphasic Electrospray Ionisation – Mass Spectrometry (BESI-MS)

For the biphasic electrospray ionisation mass spectrometry (BESI-MS) analysis, a three-channel microchip fabricated on polyimide (PI) was used as a mixing reactor and an emitter in ESI-MS. This microchip was fabricated via laser ablation performed on a PI substrate which was then laminated with 25/10 µm polyethylene/polyethylene terephthalate (PE/PET) composite sheets (Morane Ltd., Banbury, UK).[122, 123] The microchannels are 50 µm in depth and 100 µm in width and the electrode was fabricated by filling one of the microchannels with carbon ink and placed 2 mm from the solution channel to induce electrospray.[123] Figure 2.6.2 shows the microchip design where the tip of the microchannel shows a V-shape to facilitate electrospray ionisation and the dimensions of the chip.

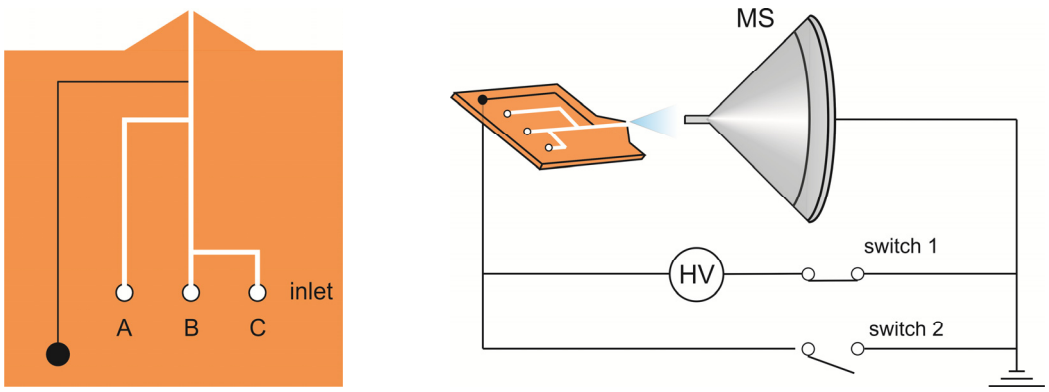

Figure 2.6.2. BESI microchip design (diagram on the left) and integration of the microchip with the mass spectrometer (diagram on the right).

The BESI-MS experiments were performed on a Thermo LTQ Velos mass spectrometer as in ESTASI-MS (see section 2.6.1). During ESI, the spray voltage of the internal power source of the LTQ Velos was set to 0 V although an external power source was used to apply a high voltage of 9 kV to induce the spray. An enhanced ion trap scan rate (10,000 Th/s) was selected to obtain a good spectral resolution. MS data were processed using the program Xcalibur from Thermo.

Biphasic electrospray ionisation - mass spectrometry work was performed at Prof. Hubert Girault's Laboratory of Physical and Analytical Electrochemistry (LEPA), École Polytechnique Fédérale de Lausanne (EPFL) in Lausanne, Switzerland. Figure 2.6.3 illustrates the BESI-MS set-up at EPFL on the left hand side whilst on the right side, there is a comparison between the polyimide microchip and an Australian dollar coin of 20.50 mm diameter.

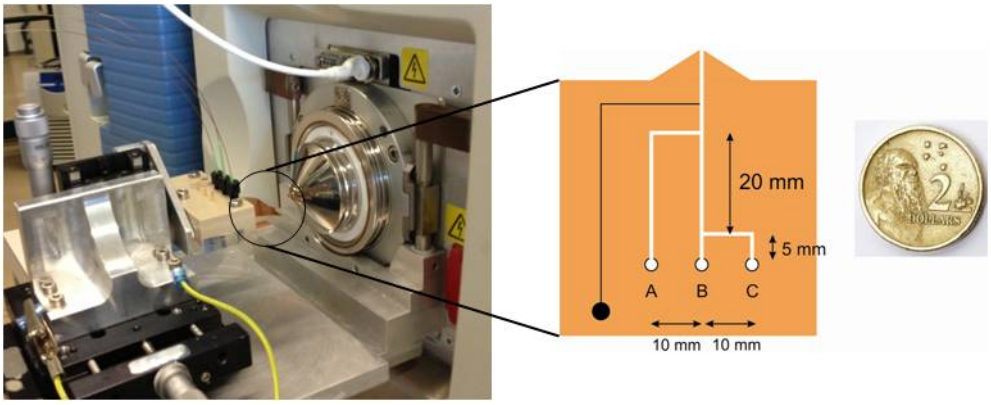

Figure 2.6.3. Image of the PI microchip and the ionisation source (left hand side). This picture was taken in the laboratory at EPFL, Lausanne, Switzerland. On the right side, comparison between the microchip dimensions and a $2 Australian dollar coin.

2.6.4. Gas Chromatography - Mass Spectrometry (GC-MS)

In order to determine the single amino acid content of some protein digested samples (see Chapter 7), gas chromatography mass spectrometry was performed. This technique can provide quantitative and qualitative information of analyte of low molecular weight and volatile compounds. For this reason, the samples are treated prior to GC-MS analysis. The pre-treatment consisted of the addition of a chloroformate agent (see Figure 2.6.4) which derivates the amines, carboxylic and hydroxyl groups. This reaction produces derivatives of amino acids more volatile and therefore easier to detect via mass spectrometry (see Figure 2.6.4). The Kit:EZFaast from Phenomenex Inc. (Australia) was used to carry out the sample preparation. This kit provides all the reagents necessary to accomplish the derivatisation, addition of an internal standard (norvaline), separation from more complex analyte and extraction of the amino acid derivates in 15 minutes.

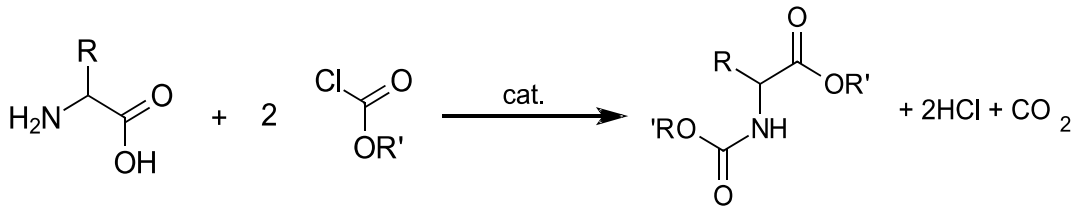

Figure 2.6.4. Schematic diagram illustrating the derivatisation reaction using the EZFaast kit for GC-MS.

To finally assess the amino acid content, gas chromatography – mass spectrometry (GC-MS) was carried out using a gas chromatograph from Agilent equipped with a ZB-AAA (10 m x 0.25 mm) Amino Acid Analysis GC Column that was directly connected to a 7000 Series GC/Triple Quad mass spectrometer. The injection volume was 2 µL at a carrier gas flow of 1.1 ml min^{-1} helium with a split ratio of 1:15 with hot needle (250 °C). The initial oven temperature of 110 °C was raised to 320 °C at 30 °C min^{-1}. Other settings were 240 °C ion source temperature and auxiliary of 310 °C. Mass spectra were analysed in the range of 45-450 *m/z* at a sampling rate of 2², 3.5 scans s^{-1}. MS data were processed using the program MassHunter from Agilent Technologies Australia Pty. For quantification purposes, a mixture of 23 amino acid standards was prepared as described previously using the EZFaast kit.

Mass spectrometry work was performed by the Centre for Metabolomics at the faculty of Life and Physical Sciences at the University of Western Australia.

2.6.5. Matrix-Assisted Laser Desorption Ionisation / Time of Flight – Time of Flight (MALDI/TOF-TOF)

In the case of peptide identification, matrix-assisted laser desorption ionisation followed by tandem time of flight (MALDI/TOF-TOF) was selected to determine the amino acid sequence of the digested proteins of interest. The protein samples were enzymatically digested and peptides extracted according to Figure 2.5.1. Peptides were then analysed by MALDI/TOF-TOF mass spectrometer using a 5800 Proteomics Analyser from AB Sciex Australia Pty Ltd. (Mt Maverley, Victoria, Australia). Spectra were analysed to identify protein of interest using Mascot sequence matching software (Matrix Science Ltd., London, UK) with Ludwig NR Database and Taxonomy set to metazoa (June 2012, 3831323 sequences). The search parameters for use on the mass spectrometer were: ± 0.4 of peptide tolerance (tol) and MS/MS tol ± 0.4, peptide charge of +1, monoisotopic, one miss cleavage and trypsin digestion.

The proteomics analyses were performed in facilities funded by the (WA) Lotterywest State Biomedical Facility – Proteomics Node, Western Australian Institute for Medical Research, Perth, Australia. The proteomics data analyses were

performed with the support of the facilities at the Australian Proteomics Computational Facility.

2.6.6. Liquid Chromatography - Mass Spectrometry (LC-MS)

For a complementary amino acid sequence coverage of the peptides produced after trypsinisation, LC-MS was carried out using the Ultimate 3000 nano HPLC system (Dionex, Thermo Fisher Scientific) coupled to a 4000 Q TRAP mass spectrometer from Applied Biosystems (Life Technologies Australia Pty Ltd., Mulgrave, Australia). Tryptic peptides were loaded onto a C18 PepMap100, 3 µm (LC Packings) and separated with a linear gradient of water/acetonitrile/0.1% formic acid (v/v). Spectra were analysed to identify proteins of interest using Mascot sequence matching software with Ludwig NR database and Taxonomy set to metazoa (September 2012, 3958669 sequences).

The proteomics analyses were performed in facilities funded by the (WA) Lotterywest State Biomedical Facility – Proteomics Node, Western Australian Institute for Medical Research, Perth, Australia. The proteomics data analyses were performed with the support of the facilities at the Australian Proteomics Computational Facility.

3 Electrochemical detection of lysozyme via adsorptive stripping voltammetry at liquid – liquid microinterfaces

Electrochemical adsorption and voltammetry of hen-egg-white-lysozyme (HEWL) was studied at an array of micro-interfaces between two immiscible electrolyte solutions (μITIES). Adsorption of the protein was achieved at an optimal applied potential of 0.95 V, after which it was desorbed by a voltammetric scan to lower potentials. The voltammetric peak recorded during the desorption scan was dependent on the adsorption time and on the aqueous phase concentration of lysozyme. The slow approach to saturation or equilibrium indicated that protein re-organisation at the interface was the rate-determining step and not diffusion to the interface. For higher concentrations and longer adsorption times, a lysozyme multilayer surface coverage of 550 pmol cm^{-2} was formed, based on the assumption that a single monolayer corresponded to a surface coverage of 13 pmol cm^{-2}. Implementation of adsorption followed by voltammetric detection as an adsorptive stripping voltammetric approach to lysozyme detection demonstrated a linear dynamic range of 0.05 – 1 μM and a limit of detection of 0.03 μM, for 5 minutes preconcentration in unstirred solution; this is a more than ten-fold improvement over previous lysozyme detection methods at the ITIES. These results provide the basis for a new analytical approach for label-free protein detection based on adsorptive stripping voltammetry at the μ-ITIES.

3. 1. Introduction

Proteins are essential components of organisms and participate directly or indirectly in every process within a biological cell. The understanding and control of the fundamental processes in which proteins are involved is of great importance and may lead to new applications in biomedical diagnostics and therapy.[124]

Lysozyme is a compact globular protein consisting of 129 amino acid residues stabilized by four cysteine disulfide bonds.[125-127] Hen-egg-white lysozyme (HEWL) possesses a molecular weight of ~14,600 g mol^{-1} [128] and has an ellipsoid structure.[129] At physiological pH, lysozyme is positively charged due to its isoelectric point (pI) of 11.35.[130] The primary function of lysozyme is to promote the hydrolysis of polysaccharides in the cell walls of Gram-positive bacteria.[131] It is present in mucosal secretions such as saliva, mucus, tears and human milk.[132] Increased levels of lysozyme can be used as indicators of some diseases, for instance Crohn's disease,[133] breast cancer,[134] gastric cancer,[135] leukaemia, meningitis.[136] In contrast, some studies have suggested that lysozyme has potential in HIV treatment[137] and as an anti-cancer drug[138].

Electrochemistry at the interface between two immiscible electrolyte solutions (ITIES), or at the liquid-liquid interface,[139-142] has been shown to offer an excellent capability for label-free biomolecular detection and quantification. Over the past 30 years, bioactive molecules such as neurotransmitters, carbohydrates, drugs, peptides and DNA have been studied at the ITIES.[12] Amemiya et al. have reported the transfer of the highly charged polypeptide protamine across the water/1,2-dichloroethane interface.[69] Facilitated transfer of amino acids[66] and peptides[64, 66] in the presence of dibenzo-18-crown-6-ether (DB18C6) has been used as a method for their detection. Vagin and co-workers reported the spontaneous formation of micelles at polarized interfaces and used these as carriers to transfer proteins into the organic phase[71, 143] whilst Osakai *et al*. have recently studied the effect of surfactants and micelle formation at the water/oil interface in the presence of polypeptides and proteins including protamine, lysozyme, albumin, myoglobin and alpha-lactalbumin.[72, 85] They have suggested that adsorption is dependent on the relative densities of charged, polar and nonpolar regions of the protein.[85] Lysozyme has already been subjected to a number of studies at the ITIES. Scanlon *et al*. studied its electrochemical behaviour at the ITIES and demonstrated adsorption at both liquid

ITIES and at a gel-supported μITIES array. The detection mechanism was proposed to involve protein adsorption in its cationic state at the ITIES and facilitated transfer of organic phase anion across the ITIES to form a complex with the protein on the aqueous side of the interface,[78, 79] as suggested for protamine by Samec et al.[144] The interfacial formation of complexes of lysozyme and hydrophobic anions was recently confirmed using an on-line mass spectrometry approach by Hartvig et al.[88] Other proteins and polypeptides were seen to undergo a similar detection mechanism at the ITIES, such as haemoglobin[81, 145] and insulin.[77] In the case of haemoglobin, multilayer adsorption at the ITIES was suggested and independent evidence for the interaction of cationic haemoglobin with hydrophobic anions was obtained using acoustic sensor technology.[146]

To-date, the detection limits for proteins based on voltammetric detection at the ITIES have been in the low micro-molar range, with one report of the detection of 0.5 μM lysozyme [79] using background-subtracted cyclic voltammetry at a μITIES array. For detection in biomedical areas, such as disease diagnostics, detection limits orders of magnitude lower are needed. In voltammetric methods of analysis, a widely-used strategy for improving detection limits is to preconcentrate the target analyte onto or into the working electrode surface prior to the voltammetric measurement. This approach is referred to as stripping voltammetry, with variants such as anodic, cathodic, adsorptive, abrasive and catalytic adsorptive stripping voltammetry. The use of adsorption as a preconcentration step has been widely studied for detection of organic, inorganic and biological molecules[147] at especially mercury electrodes via the method of adsorptive stripping voltammetry (AdSV). A prime example of the AdSV approach is the detection of trace nickel by its adsorptive preconcentration as a complex with dimethylglyoxime.[148] Such an approach was suggested by Amemiya and co-workers for detection of heparin, a mixture of sulphated carbohydrates, at a micropipette-based μITIES. [62]

Although the adsorption of proteins at the ITIES has been studied with various methods, examination of adsorptive accumulation as a way to improve protein detection limits has not been addressed. Consequently, the purpose of the work reported here is to examine the adsorption of lysozyme at the ITIES, in this particular case at the gelled μITIES array, as a basis for preconcentration prior to voltammetric detection, and to assess any improvement in detection limits brought about by this adsorption.

3. 2. Experimental Section

3. 2. 1. Reagents

All the reagents were purchased from Sigma-Aldrich Australia Ltd. and used as received unless indicated otherwise. The organic phase was gelled and prepared using bis(triphenylphosphoranylidene) tetrakis(4-chlorophenyl)borate ($BTPPA^+TPBCl^-$, 10mM) in 1,6-dichlorohexane (1,6-DCH) and low molecular weight poly(vinyl chloride) (PVC)[79, 114]. The $BTPPA^+TPBCl^-$ salt was prepared by metathesis of bis(triphenylphosphoranylidene)ammonium chloride ($BTPPA^+Cl^-$) and potassium tetrakis(4-chlorophenyl)borate (K^+TPBCl^-), se Appendix A. Stock solutions of hen-egg-white lysozyme (HEWL) were prepared in 10mM HCl of pH 2 on a daily basis. Tetraethylammonium (TEA^+) chloride was also dissolved in 10 mM HCl of pH 2. All the aqueous solutions were prepared in purified water, from a USF Purelab plus UV, with a resistivity of 18 MΩ cm.

3. 2. 2. Apparatus

All experiments were performed using an AUTOLAB PGSTAT302N electrochemical analyser (Metrohm, The Netherlands). The micropore arrays used to form the micro-ITIES array were fabricated in silicon.[33] The fabrication procedure provided hydrophobic micropore walls so that the organic phase filled the pores.[33, 35] The micropore array consisted of thirty micropores arranged in a hexagonal close-packed arrangement, each with a diameter of 22.4 μm and a pore centre-to-centre distance of 200 μm. These microporous silicon membranes were sealed onto the lower orifice of a glass cylinder using a silicone rubber (Acetic acid curing Selleys glass silicone (Selleys Australia & New Zealand)). The gelled organic phase solution was introduced into the silicon micropore array via the glass cylinder,[34] and the organic reference solution was placed on top of the gelled organic phase. The silicon membrane was then immersed into the aqueous phase (10mM HCl, lysozyme in 10mM HCl and/or TEA^+ in 10 mM HCl). The electrochemical cell employed is summarised in Scheme 3.2.2.1. Contact angle measurements were performed with a contact angle goniometer (KSV Instruments LTP, Finland) on a glass slide spin-coated with a film of gelled organic phase.

Ag | AgCl	*x* μM HEWL and / or *x* μM TEA^+ in 10mM of HCl pH 2	10mM $BTPPA^+TPBCl^-$ in gellified 1,6-DCH	10mM $BTPPA^+Cl^-$ in 10mM LiCl	AgCl | Ag

Scheme 3.2.1. Electrochemical cell.

3. 2. 3. Electrochemical measurements

The interfacial potential difference was applied and measured between a pair of Ag/AgCl electrodes. The geometric area of the micro-interfaces was 1.18 x 10^{-4} cm^2. Cyclic voltammetry (CV), linear sweep voltammetry (LSV) and linear sweep stripping voltammetry (LSSV) were carried out at a sweep rate of 5 mV s^{-1}, unless otherwise stated, and parameters such as protein concentration, applied potential and duration of the adsorption stage were varied.

3. 3. Results and Discussion

3. 3. 1. Distortion of simple ion transfer by adsorption

A qualitative indication of whether a macromolecule is adsorbed at the μITIES can be obtained by not only examination of the CV of the macromolecule at the interface, but also by comparison of the voltammetric response for a simple ion transfer process in the presence and absence of the macromolecule.[79, 149] If the macromolecule is adsorbed at the μITIES, then the CV for simple ion transfer should be distorted, depending on the extent of adsorption. Figure 3.3.1 shows CVs for lysozyme adsorption at the μITIES array. Figure 3.3.1(A) shows the background CV response, obtained when both phases contain only the background electrolyte species. The rise in current at the positive end of the voltammogram is indicative of background electrolyte transfer across the ITIES.[79] Figure 3.3.1(B) shows the situation when the aqueous phase contains 15 μM lysozyme. There are differences between the CV in the presence and absence of lysozyme, which indicates that lysozyme can be detected, most easily by the reverse scan peak, which may be attributed to desorption of lysozyme from the interface. The broad increase in current between *ca*. 0.6 and 0.9 V is due to the adsorption of lysozyme at the interface but it is not useful for detection purposes because of its broadness. The response of

lysozyme at the ITIES is complex and, as discussed previously,[78, 79, 88] is a combination of lysozyme adsorption at the interface and its facilitation of the transfer of background electrolyte anion from the organic phase to the aqueous phase where it forms a complex with the cationic protein. In contrast to the complex nature of lysozyme detection, the transfer of TEA^+ (Figure 3.3.1(D)) is a simple ion-transfer process dominated by mass transport: radial diffusion on the forward (positive-going) scan provides a steady-state voltammogram and linear diffusion (in the micropores used to form the μITIES) on the reverse scan (negative-going) produces a peak-shaped response.[79] However, this ideal response to TEA^+ is severely distorted in the presence of aqueous phase lysozyme (Figure 3.3.1(C)). Although a transfer current for TEA^+ can be discerned on the forward scan, it is smaller and less well-defined than that in the absence of lysozyme (Figure 3.3.1(D)). A peak for the reverse transfer of TEA^+ can be seen at *ca*. 0.6 V. The peak at *ca*. 0.7 V is due to desorption of lysozyme from the interface. Transfer of the TEA^+ from the aqueous phase to the organic phase in the presence of lysozyme was distorted from the expected steady-state response for TEA^+ transfer across the interface. This behaviour indicates an adsorbed protein layer is formed. The reverse sweep for TEA^+ in the presence of lysozyme was affected also, despite apparent desorption of protein before the TEA^+ reverse peak potential. This is because the adsorbed protein results in a decreased concentration of TEA^+ for the reverse transfer in comparison to that in the absence of protein. Also, as discussed by Hartvig et al.,[88] adsorption of protein may occur at potentials positive of the potential of zero charge so that protein adsorption occurs over a wide potential range.

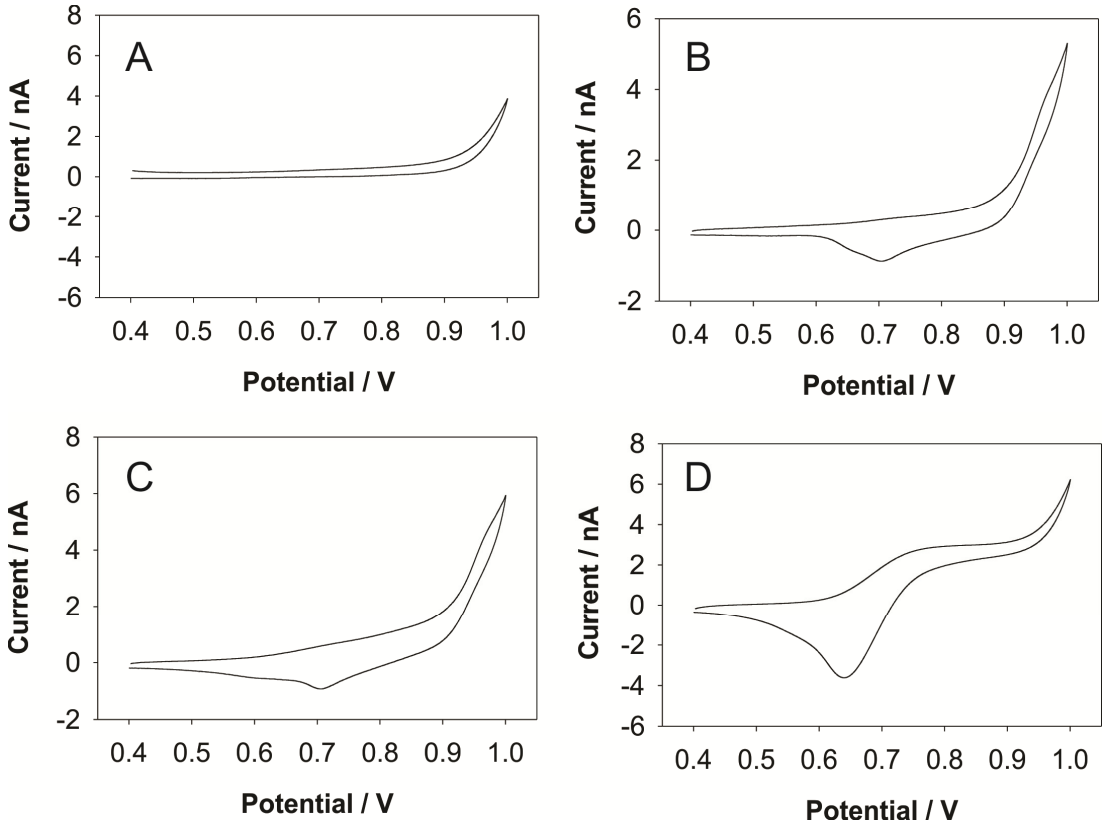

Figure 3.3.1. Cyclic voltammetry of the μITIES array in the absence and presence of aqueous phase lysozyme and TEA^+. (A) Aqueous phase: 10 mM HCl, (B) aqueous phase: 15 μM lysozyme + 10 mM HCl, (C) aqueous phase: 15 μM lysozyme + 15 μM TEA^+ + 10 mM HCl, (D) aqueous phase: 15 μM TEA^+ + 10 mM HCl. In all cases the organic phase was as described in Scheme S-1. Scan rate for all experiments: 5 mV s^{-1}.

3. 3. 2. Potential-dependent adsorption of lysozyme

The influence of applied potential on lysozyme adsorption at the μITIES array was investigated by holding the applied potential at pre-determined values for a certain time, followed by scanning to lower potentials in order to desorb the protein and produce a stripping voltammogram. The influence of the applied potential on lysozyme adsorption is shown in Figure 3.3.2 Since the potential for protein adsorption was close to the region where background electrolyte transfer occurs, the optimum potential was assessed by examining both the peak current and the ratio of peak height : half-peak width for the desorption voltammogram. The optimum protein adsorption potential is a compromise between the maximum desorption current and the minimum background signal. The optimum adsorption potential was

determined to be 0.95 V for lysozyme. At this adsorption potential, the peak current reaches a shoulder, but continues to rise at higher applied potentials (due to contributions from background electrolyte transfer). In contrast, the ratio of peak height:half-peak width reaches a plateau at this potential, indicating there is no added benefit to applying higher applied potentials during the adsorption process.

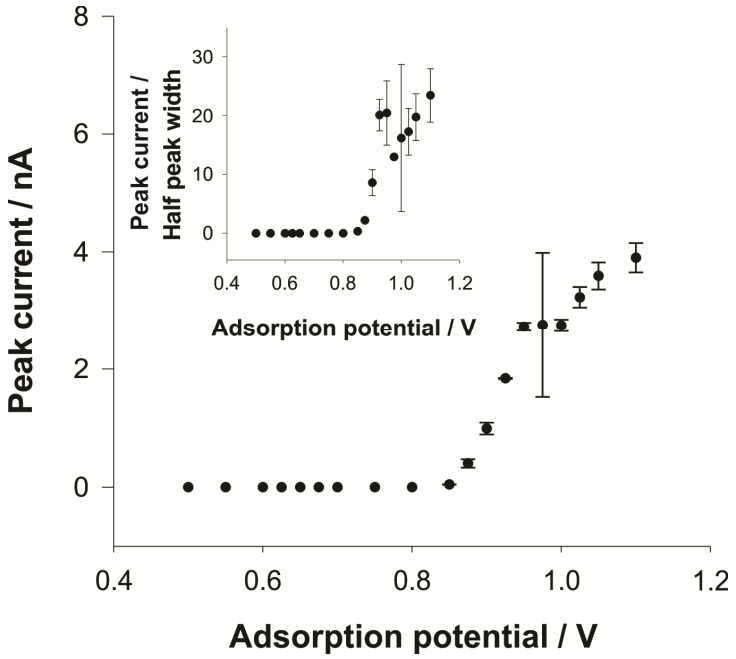

Figure 3.3.2. Influence of the applied potential during the adsorption step on the peak current and ratio of peak current: peak half-width. Concentration of lysozyme: 10 μM in 10mM HCl. Adsorption time: 60 s, without stirring. The organic phase was as described in Scheme 3.2.1.

Interestingly, at potentials ≤0.8 V, the peak currents are low, indicating that the amount of lysozyme adsorbed to the interface at these applied potentials is not high. This suggests that the simple ion transfer of TEA^+ (Figure 3.3.1(C)) should be evident at potentials ≤0.8 V. It may well be that the minute amounts of lysozyme adsorbed at these potentials are sufficient to distort the TEA^+ transfer described above. Indeed, low surface coverages for protamine, a polypeptide of lower RMM than lysozyme, were determined[73] in an equivalent potential region, where no charge transfer current was measured. Protamine surface coverages of *ca*. 8 x 10^{-11} mol cm^{-2}, consistent with a monolayer or so of this polypeptide, were found. Similar adsorption of a monolayer of lysozyme in this potential region (≤0.8 V) would also distort the TEA^+ voltammogram.

3. 3. 3. Scan rate dependence

The influence of the scan rate on the voltammetric desorption peak was examined, following adsorption at constant potential from unstirred solution (see Figure 3.3.3). The shift in the stripping peak potential is attributed to the uncompensated resistance in the cell. The linear dependence of the desorption peak current on the scan rate was as expected for a charge transfer process involving an adsorbed species. Consequently, the peak current is directly proportional to the surface coverage (Γ) as well as the potential scan rate (υ), according to the equation 3.3.1:[5]

$$i_p = \frac{z_i^2 F^2 \Gamma A \upsilon}{4RT} \qquad (3.3.1)$$

where i_p is the peak current, z_i is the number of charges transferred per molecule, F is the Faraday constant, R is the universal gas constant, T is the temperature and A is the total interfacial area, 1.18 x 10^{-4} cm^2. At a temperature of 21 °C and assuming that the number of ions transferred per molecule is the same as the protein charge, +17,[150] the surface coverage obtained from the slope of the line of the inset graph in Figure 3.3.3 is 4 pmol cm^{-2}, for a 0.5 μM lysozyme aqueous concentration and a 60 second adsorption time.

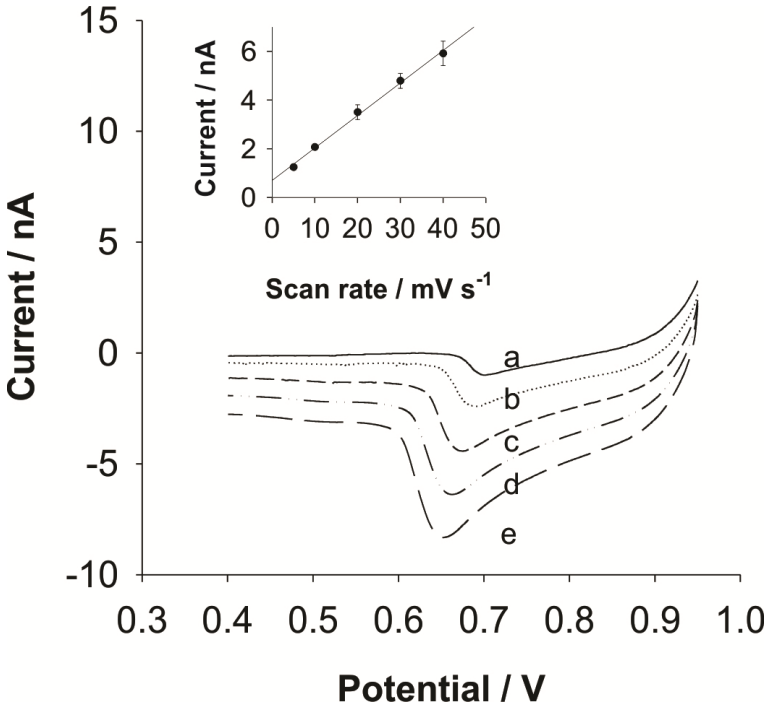

Figure 3.3.3. Influence of the voltammetric scan rate on the desorption peak: stripping voltammograms of 0.5 μM lysozyme in 10 mM HCl at a) 5, b) 10, c) 20, d) 30 and e) 40 mV

s^{-1} scan rates following 60s adsorption from unstirred solution. The organic phase was as described in Scheme 3.2.1. Inset: the linear dependence of the peak current on the scan rate.

3. 3. 4. Time dependence

Figure 3.3.4 shows the influence of adsorption time on the voltammetric desorption response. Without any time for adsorption (i.e. 0 s adsorption), it was not possible to detect 0.1 μM lysozyme in the aqueous phase. However, LSV following adsorption of lysozyme at the μITIES for times longer than 60 s provided stripping peaks at this low concentration. Figure 3.3.5 indicates that after each desorption voltammogram, the protein is stripped away from the interface, so that there is no carryover between experiments.

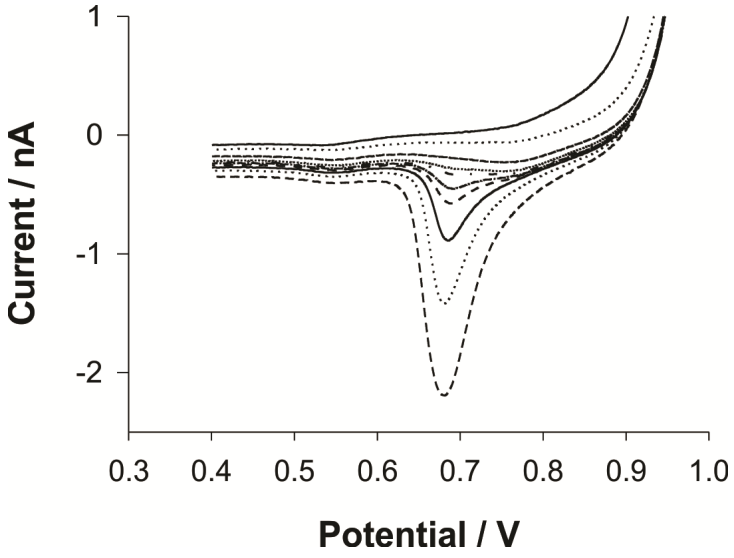

Figure 3.3.4. AdSV of 0.1 μM lysozyme at different preconcentration times from 0 s (—) to 1800 s (- -) via times of 5, 60, 150, 180, 240, 300, 480 and 900 s.

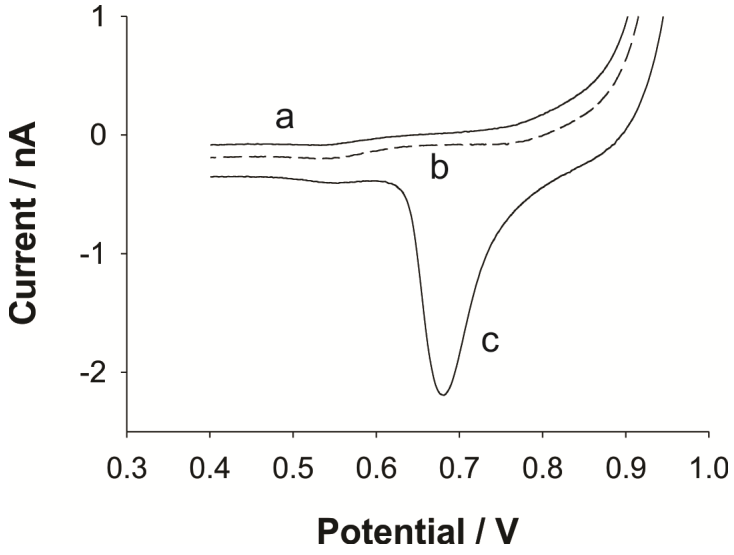

Figure 3.3.5. LSV of 0.1 μM lysozyme in 10mM HCl before (a) and after (b) preconcentration steps where dotted line (c) is LSV of 0.1 μM lysozyme after a preconcentration time of 1800 s at 0.95 V.

The kinetics of the adsorption process was examined across a range of aqueous phase lysozyme concentrations by varying the adsorption time prior to initiation of the LSV desorption step. For these results, the charge under the voltammetric peak was determined and this is plotted in Figure 3.3.6 as a function of the adsorption time and the aqueous phase concentration of lysozyme. It can be seen that the charge for lysozyme desorption from the μITIES array increased with the adsorption time at an applied potential of 0.95 V. The electrochemical data revealed that the adsorption of lysozyme at the ITIES can be controlled by the solution concentration and the adsorption time. The charge required for desorption of the protein from the surface for any given adsorption time, Q_t , is given by[5]

$$Q_t = Q_e[1 - e^{-KCt}] \qquad (3.3.2)$$

where Q_e is the equilibrium surface charge passed, K is the adsorption rate constant, C is the concentration and t is the time. For the fitting of the data to this equation (Figure 3.3.6), R^2 values between 0.83 and 0.99 were obtained, while values of K obtained from the fitting increased with the aqueous phase concentration of lysozyme. It is clear from Figure 3.3.6 that long adsorption times are needed in order to reach a saturation or equilibrium surface coverage at any given aqueous concentration. This may be reflected in the transport of protein molecules to the

interface and their subsequent adsorption and reorientation within the adsorbed layer.[151, 152] Furthermore, the possibility for structural rearrangements when the protein is present in low pH solutions was noted by Kleijn et al.[152] A purely diffusion-controlled adsorption process seems unlikely given the long times involved to reach saturation/equilibrium, together with the fact that the experiments are implemented with microinterface arrays. Under such conditions, with radial diffusion to the interface, surface saturation/equilibration should be reached quickly for a diffusion-controlled process. As discussed later, multi-layer adsorption of lysozyme L may occur at the interfaces employed here.

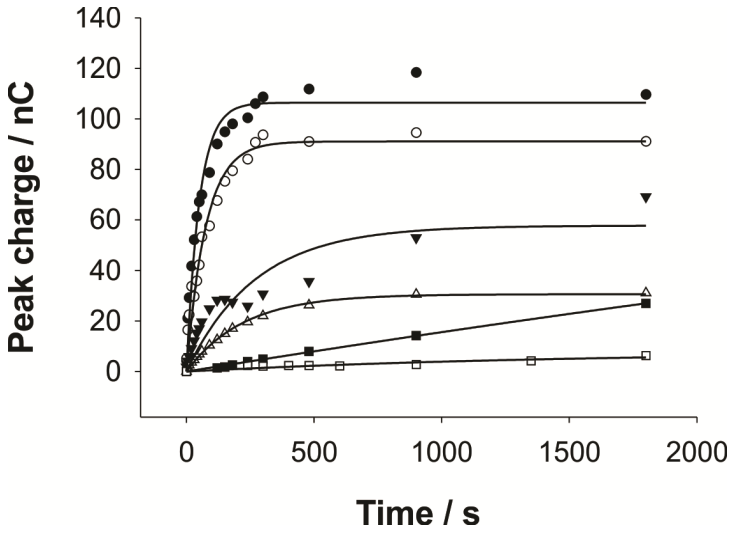

Figure 3.3.6. Kinetics of lysozyme adsorption at the μITIES array at different concentrations: (□) 0.05 μM, (■) 0.1 μM, (Δ) 0.5 μM, (▼) 1.0 μM, (○) 5 μM, (●) 10 μM lysozyme, in aqueous 10mM HCl. The solid lines (—) are the best fits to equation 3.3.2.

3. 3. 5. Concentration dependence

The adsorption of lysozyme at the μITIES was analysed as a function of the concentration of lysozyme in the aqueous phase. As above, the analytical signal may be taken as the charge under the voltammetric peak. Figure 3.3.7 shows charge versus concentration plots for five sets of experiments in which different adsorption times were used, from 0 to 300 seconds, at an adsorption potential of 0.95 V. The lysozyme concentration in the aqueous phase was varied between 0.05 μM and 10 μM.

After a period of 5 minutes adsorption at elevated lysozyme concentrations, the amount of adsorbate at the ITIES reached a saturation point (see Figure 3.3.7). However at lower concentrations, up to *ca*. 1 μM, a linear dependence between the desorption charge and the concentration of lysozyme in the aqueous phase exists, which can be clearly used for analytical purposes. The surface saturation charge, *ca*. 100 nC, is reached for the higher concentrations and longer adsorption times (Figures 3.3.6 and 3.3.7).

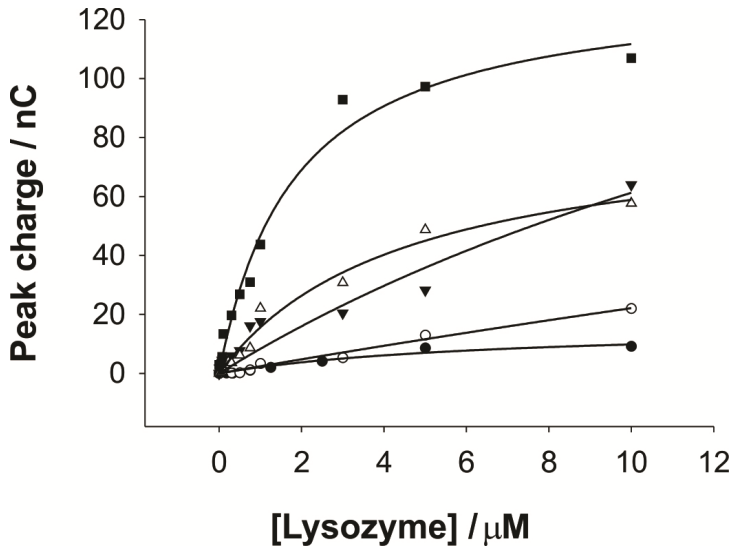

Figure 3.3.7. Concentration-dependence of lysozyme in 10 mM HCl determined by voltammetry following adsorption for various times: (●) 0 s, (○) 30 s, (▼) 60 s, (Δ) 120 s and (■) 300 s. Experiments were performed in unstirred solutions. The organic phase was as specified in Scheme 1. The solid lines (—) are guides to the eye.

3. 3. 6. Sensitivity and detection limits

The adsorption process at the gelled μITIES array has been studied as it may provide a means to better analytical performance via adsorptive preconcentration prior to voltammetric measurement. Peak current values plotted versus lysozyme concentration show the same features as Figure 3.3.7, reaching a saturation current value of 5 nA for a maximum preconcentration time of 300 seconds. The linear range for the stripping current response to lysozyme concentration was between 0.05 and 1 μM lysozyme. As shown in Table 3.3.1, the longer preconcentration times provided a greater calibration graph slope (sensitivity) and lower calculated limits of detection (LOD) (based on 3σ). With this AdSV approach at the μITIES array, a

preconcentration time of 300 seconds enabled a LOD of 0.03 μM lysozyme to be achieved, which corresponds to 0.44 μg ml^{-1}. Concentrations of 0.05 μM lysozyme were detected, compared to 0.5 μM detection with CV at a similar μITIES array[79] or to even higher concentrations at ITIES[77, 78, 81] This is the lowest concentration of a protein detected by electrochemistry at the ITIES to-date.

Table 3.3.1. Analytical characteristics for AdSV of lysozyme at μITIES array.

Pre-concentration times / s	Sensitivity (calibration graph slope) / nA μM^{-1}	Limit of detection (LOD) / μM	Linear range / μM	Correlation coefficient (r)
30	0.22	0.10	0 - 1	0.928
60	0.91	0.06	0 - 1	0.978
120	1.41	0.05	0 - 1	0.977
300	4.31	0.03	0 - 1	0.989

3. 3. 7. Surface coverage

In this discussion we aim to relate the voltammetric desorption charges reported above to surface coverages for lysozyme at the μITIES array. Table 3.3.2 summarizes the surface coverages for lysozyme monolayers on a variety of interfaces. A variety of interfaces have been studied but not aqueous-organic interfaces. The pH values of data reported in the literature are far from the acidic conditions used in this study. Most of the surfaces employed are highly hydrophilic, with contact angle values lower than 10°. Materials such as mercury exhibit a reactive surface where the disulfide groups within the protein can react with mercury. In contrast, Su *et al.*[151] employed a silicon dioxide surface modified with a self-assembled monolayer of octadecyltrichlorosilane (OTS), forming a hydrophobic surface with a contact angle of 110°.[151] In the present study, the organogel phase forms one side of the adsorbing interface while lysozyme is present initially in the aqueous phase under acidic conditions, where is has a charge of +17. The water contact angle of the organogel surface was determined to be ~80°, confirming the hydrophobic property of the organic phase. Therefore the ITIES employed here is more like the SiO_2-OTS surface than the other interfaces presented in Table 3.3.2.

The monolayer surface coverage on SiO_2-OTS may be taken as that for the protein at the ITIES, noting that there are differences, such as the ITIES is charged and electrified as well as soft, and the aqueous phase is acidic. Such differences may alter the way the protein interacts and folds/unfolds at the interface. The soft interface nature of the ITIES may lead to its being deformed or changed upon protein adsorption. Nevertheless, for now, the surface coverage of a lysozyme monolayer at the μITIES is assumed to be 13 pmol cm^{-2}.

Table 3.3.2. Surface coverage values for lysozyme adsorption on solid - liquid and mercury - liquid interfaces.

Substrate	pH	Surface Coverage		Technique	Reference
		Side-on pmol/cm^2	End-on pmol/cm^2		
Mercury	7	9		AC polarograms	[153]
Mercury	5	9		Electrochemistry	[154]
Silica	4	34		Streaming potential	[155]
Silica	7.4	17		Dual polarization interferometry	[156]
SiO_2	4 / 7	12		Spectroscopic Ellipsometry	[151]
SiO_2-OTS	7	13		Spectroscopic Ellipsometry	[151]
Germanium	7.4	10		Fourier Transform Infrared Spectroscopy (FTIR)	[151, 156, 157]
Gold	7	12	19	* lysozyme dimensions / orientation	[152]
Quartz	7	14	21	* lysozyme dimensions / orientation	
Silica	7	16	31	Forster Resonance Energy Transfer (FRET)	[139, 155, 156]
Silica	4	1	16	Dual polarization interferometry	[156]
Silica	7	5	22	Dual polarization interferometry	[156]
Si(Ti)O_2	8	15	21	Optical Waveguide Light mode Spectroscopy (OWLS)	[158]

***** *Hexagonal packing (lysozyme dimensions* 4.6 x 3.0 x 3.0 nm^3)[159]

From Figures 3.3.6 and 3.3.7, the maximum charges (Q) measured can be related to surface coverage (Γ) by equation (3) [5]

$$Q = z_i F A \Gamma \qquad (3.3.3)$$

Taking into account the charge of the protein (z_i) at pH 2, +17,[150] the area (A) of the interface array, as patterned by the geometric area of the micropore array, 1.18 x 10^{-4} cm^2, and the value of the Faraday constant (F), the surface coverage can be calculated. The corresponding maximum surface coverage values determined from Figures 3.3.6 and 3.3.7 are 550 pmol cm^{-2}. If, as discussed above, we take a monolayer of adsorbed lysozyme to be 13 pmol cm^{-2}, then *ca*. forty monolayers of lysozyme are formed at the liquid-liquid interface for a five minute preconcentration period. Such a multilayer formation at the gelled μITIES array requires that the proteins have attractive interactions with each other. As the protein is highly charged (+17 charges), presumably the positive interactions come from exposure of the hydrophobic amino acid residues and then hydrophobic interactions drive the attachment of the protein to the interface and to each other. The acidic nature of the aqueous phase may contribute to partial unfolding of the lysozyme, exposing the internal hydrophobic regions and thus promoting multilayer adsorption at the ITIES. Furthermore, Herzog et al. [81] suggested *ca*. seven monolayers of haemoglobin formed at the aqueous–1,2-dichloroethane ITIES during a single CV cycle, without a preconcentration step as used here. Thus employing a preconcentration step at an optimum applied potential for five minutes may indeed result in an order of magnitude increase in protein adsorption at the interface. As discussed by Wei et al., the non-equilibrium nature of the adsorptive process may also promote multilayer build-up of lysozyme.[157] Furthermore, the formation of lysozyme multilayers on hydrophilic solid surfaces such as mica,[160] germanium crystal[157] and Si(Ti)O_2[158] and on a hydrophobic surface (quartz modified with octadecyl trichlorosilane)[161] have been reported, as have the multilayer formation of two other proteins, albumin and cytochrome c, under the influence of applied potential.[162]

Figure 3.3.8 summaries the pre-concentration process at the μITIES. According to the results, this pre-treatment step is pre-concentrating the protein at the liquid-liquid interface of the microporous membrane where desorption is observed after AdSV was performed toward the open circuit potential of the system. This reversible system does not require further cleaning steps as it is been demonstrated in Figure 3.3.5.

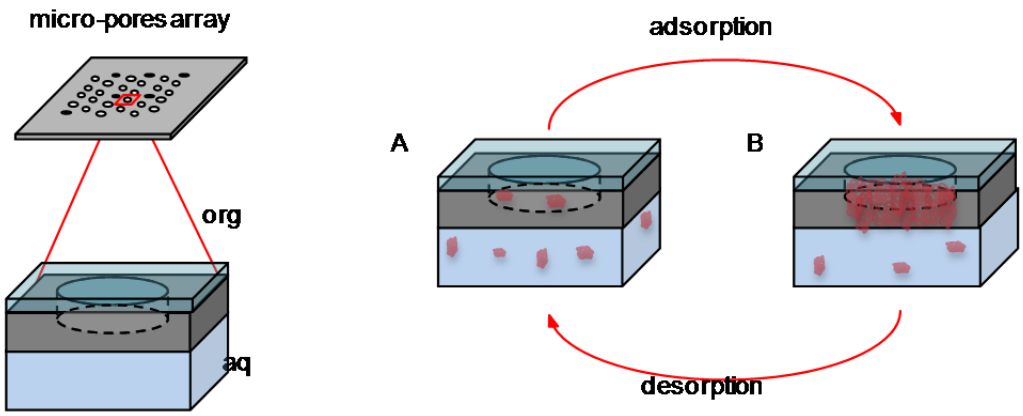

Figure 3.3.8. Reversible adsorption-desorption process proposed for a pre-concentration step of lysozyme at the liquid-liquid interface. A) Diagram of lysozyme in solution and B) diagram showing the adsorption and accumulation of protein on the micro-pore interface after a certain potential applied during a X period of time.

3. 4. Conclusions

Adsorption of the protein lysozyme at miniaturised liquid-liquid interfaces has been investigated as a preconcentration strategy prior to voltammetric detection by desorption of the adsorbed material. Studies as a function of adsorption potential and adsorption time revealed that maximum protein adsorption occurs at higher positive potentials, just below the potential limit set by background electrolyte transfer. This is consistent with protein adsorbing at potentials positive of the potential of zero charge. The time-dependence of the adsorption indicated that it was a slow process, associated with multi-layer formation and molecular re-orientations within the adsorbed film. This may be promoted by the acidic nature of the aqueous phase employed. Using a preconcentration (adsorption) time of 300 s, a LOD of 0.03 µM lysozyme was achieved, which is the lowest concentration of protein detected by electrochemistry at the ITIES to-date. The results of this study show that the limit of detection at µITIES has been improved by preconcentrating the protein at the interface. Prospective lower LODs may be achieved using advanced electrochemical methods in conjunction with the adsorptive preconcentration, such as differential pulse voltammetry and square wave voltammetry.

4 Electrochemical lysozyme pre-concentration at the gelled liquid – liquid interface studied by ESTASI-MS

Based on the mechanism of lysozyme detection at the liquid-liquid interfaces, which is believed to follow an initial protein adsorption process at the polarized interface followed by facilitated transfer of organic phase anions, adsorption of lysozyme at the interface was implemented as a pre-concentration step by applying an optimum adsorption potential prior to electrochemical analysis. In order to confirm the protein adsorption and the detection mechanism proposed at the gelled liquid – liquid micro-interfaces, mass spectrometric (MS) analyses were performed by electrostatic spray ionisation (ESTASI) from the surface of the organogel where protein was previously electrochemically pre-concentrated. The spectra demonstrate the presence of protein at the organogel which is enhanced when applied potential, pre-concentration time and concentration of lysozyme in solution are increased. Moreover, complexes between the charged protein and one or two anions of the electrolyte ($[Lysozyme\text{-}1TPBCl+(x+1)H]^{+x}$ where x can be 8, 9 or 10 and $([Lysozyme\text{-}2TPBCl+12H]^{+10}$) were detected by ESTASI-MS. This is the first time that ESTASI-MS has been employed directly at a hydrophobic gel following electrochemistry at the ITIES. The combination of these two techniques provides a new platform for label-free biomolecule detection and elucidation of complex processes occurring at soft liquid – liquid interfaces, which are difficult to characterise.

4. 1. Introduction

Adsorption of protein at the liquid – liquid interfaces was first reported in 1984 by Vanysek et al., when bovine serum albumin was observed to interfere in ion transfer studies at the water/nitrobenzene interface.[49] Since then, several publications have addressed the electroactivity of biomacromolecules such as proteins at the interface between two immiscible electrolyte solutions (ITIES) from different perspectives, from mimicking the cell membrane, DNA hybridization, label-free detection of biological molecules to adsorption studies.[12] Hen-egg-white-lysozyme was characterised at the ITIES by Scanlon et al.[78] The detection mechanism was believed to undergo two sequential steps, adsorption and facilitation of anion transfer from the organic phase to the aqueous via interfacial complexation of the charged protein with the negatively charged organic electrolyte.[78] A different approach based on this proposed mechanism was implemented (see Chapter 3) in order to enhance the electrochemical signal to achieve better sensitivity in a label-free form. This consisted in pre-concentrating lysozyme at its optimum adsorption potential for a period of time followed by stripping voltammetry, also called adsorptive stripping voltammetry (AdSV). A detection limit of 30 nM was achieved.

However the study of interfacial complexes and interfacial adsorption at the ITIES is a challenging task. For this reason very limited techniques mainly electrochemical techniques such as electrochemical impedance spectroscopy,[49, 67, 84, 86] alternating current voltammetry[81, 84] and classic voltammetry have been used to evaluate the capacitive properties of the soft liquid-liquid interfaces containing adsorbed protein.

Electrospray ionisation - mass spectrometry (ESI-MS) is a highly sensitive strategy which can softly ionize macromolecules and providing information such as protein molecular weight, protein 3D structures, posttranslational modifications, amino acid sequence and non-covalent interactions.[93, 97] For instance non-covalent complexes such as protein-DNA, protein-low molecular ligand supramolecules and double-stranded oligonucleotides have been studied via ESI-MS.[163] Biphasic electrospray ionisation (BESI) was implemented recently to investigate non-covalent interfacial complexes that can be formed at the liquid – liquid interfaces.[88, 164, 165] Several complexes between lysozyme and different organic electrolyte anions were reported via BESI-MS.[88] In addition, the complex formation between peptides such

as melittin[65] and the phospholipids have been also elucidated via BESI-MS by Mendez et al.[64, 65]

Previous attempts induced a potential difference by tuning the electrolyte concentrations in the immiscible solutions[88] whilst in this study, the potential difference is induced by applying a voltage. For this reason, the use of electrostatic spray ionisation – mass spectroscopy (ESTASI-MS) was thought to provide an alternative in the study of forced adsorption on the gelled liquid - liquid interface. The advantage of ESTASI-MS versus conventional ESI-MS are the possibility to ionize directly from a soft surface and the contactless approach which avoids electrochemical reactions[166] occurring at the electrode used to electrospray the sample. ESTASI-MS was developed and implemented by Qiao et al. in different set-ups and geometries (microfluidic chip, micropipette and microdroplets).[105] More recent work have proven the potential of this methodology with the publication of isoelectric focusing electrophoresis (IFE) coupled trough ESTASI-MS.[103]

The aim of this work is to study via ESTASI-MS the electrochemical adsorption process at the hydrophobic gelled liquid – liquid interface including interfacial complexes formation and the influence of parameters such as applied potential, time and protein concentration in the adsorption of lysozyme. In particular, it was anticipated that the approach would enable direct detection of protein-anion complexes, in order to help confirm an aspect of the protein detection mechanism at ITIES and gelled ITIES.

4. 2. Experimental Section

4. 2. 1. Reagents

The organic phase was gelled and prepared using bis(triphenylphosphoranylidene) tetrakis(4-chlorophenyl)borate ($BTPPA^+TPBCl^-$, 10 mM) in 1,6-dichlorohexane (1,6-DCH) and low molecular weight poly(vinyl chloride) (PVC). The $BTPPA^+TPBCl^-$ salt was prepared by metathesis of bis(triphenylphosphoranylidene)ammonium chloride ($BTPPA^+Cl^-$) and potassium tetrakis(4-chlorophenyl)borate (K^+TPBCl^-) as indicated in Appendix A. Hen-egg-white-lysozyme (HEWL) solutions were freshly prepared in 10 mM HCl of pH 2 prior to electrochemical experiments. All these reagents were purchased from Sigma-Aldrich Switzerland Ltd. and all the aqueous

solutions were prepared in purified water, from alpha Q Millipore system (Zug, Switzerland).

4. 2. 2. Apparatus

All electrochemical experiments were performed using an Autolab PGSTAT302N electrochemical analyser (Metrohm Autolab, Utrecht, The Netherlands). The millimetre size interface was formed using a glass pipette of 0.075 cm radius. The total geometric area of the water/organogel interface was calculated to be 0.035 cm^2 assuming that the droplet formed is a perfect hemisphere. The electrochemical cell is summarised in Scheme 4.2.1, where *x* is the concentration of lysozyme in the aqueous phase.

Ag	AgCl	*x* μM Lysozyme in 10mM of HCl pH 2	10mM $BTPPA^+TPBCl^-$ in gelled 1,6-DCH	10mM $BTPPA^+Cl^-$ in 10mM LiCl	AgCl	Ag

Scheme 4.2.1. Diagram of the electrochemical cell.

4. 2. 3. Electrochemical measurements

A three-electrode system was employed for all measurements. Electrochemical pre-concentration at a fixed potential was implemented before ESI-MS from the gel. In contrast to Chapter 3, the protein adsorbed at the interface was not stripped away by Stripping Voltammetry (SV) so the protein remained on the organogel for further studies via mass spectrometry. Therefore, no voltammograms are presented in this chapter.

4. 2. 4. ESTASI-MS

After pre-concentration of lysozyme at the water/organogel interface, the gel was cut and fixed on a 0.2 mm GelBond®PAG film (Lonza), as shown in Figure 4.2.1 for ionisation. In addition, drops (1-2 μL) of an acidic buffer consisted of 1% acetic acid in a 50:50 water:methanol solution were deposited manually on top of the organogel. For electrostatic ionisation a gold electrode was placed underneath the plastic layer (GelBond®PAG film) and the gel was placed close to the MS inlet to induce the

electrostatic spray ionisation.[103] The electrode was then connected with a DC square wave with maximum high voltage (9 kV) source via switch 1 or grounded via switch 2 (0 V) to reduce the surface charge that cannot be consumed by the electrode. For this, a LabView program controls the switches in order to synchronize their application. The spray voltage of the internal power source of the LTQ Velos was set to 0 V. An enhanced ion trap scan rate (10,000 Th/s) was selected to obtain a good spectral resolution. These experiments were performed on a dual pressure ion trap Thermo LTQ Velos mass spectrometer and all the MS data were processed using the program Xcalibur from Thermo Fisher Scientific Inc. (Hampton, New Hampshire, USA).

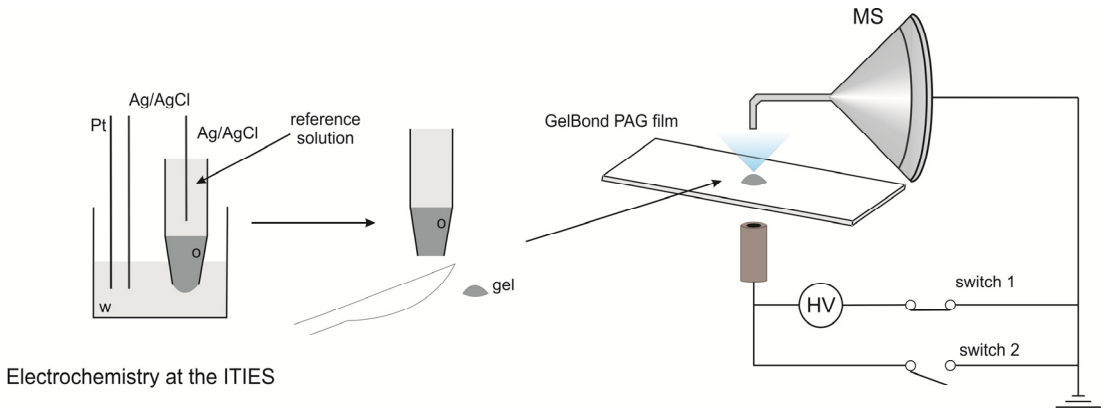

Figure 4.2.1. Three electrode set-up electrochemical cell.

ESTASI-MS experiments were carried out in Prof. Hubert Girault's Laboratory of Physical and Analytical Electrochemistry (LEPA) at École Polytechnique Fédérale de Lausanne (EPFL) in Lausanne, Switzerland.

4. 2. 4. MALDI-TOF

Firstly, extraction of lysozyme electrochemically adsorbed at the organogel was performed by dissolving the gel in 5 µL of 1,6-dichlorohexane and swirl with a vortex for 5 minutes. After that, 2 µL of the extracted protein solution from the organogel was deposited on a steel target plate and left to dry at room temperature. Then 1 µL of the matrix solution (10 mg/mL 2,5-dihydroxy benzoic acid (DHB) in 50% acetonitrile, 0.1% trifluoroacetic acid, and 49.9% water) was added after the 1,6-dichlorohexane was evaporated. After this second addition, the sample was left again to dry at room temperature prior to measurements. Matrix-assisted laser

desorption ionisation - mass spectrometry (MALDI-TOF) analyses were performed on a positive mode Microflex MALDI-TOF instrument (Bruker Daltonics GmbH, Faellanden, Switzerland) equipped with a nitrogen laser (wavelength 337 nm). Data analysis was performed using flexAnalysis software from Bruker in the range of 4,000 - 85,000 *m/z*.

MALDI-TOF experiments were carried out in Prof. Hubert Girault's Laboratory of Physical and Analytical Electrochemistry (LEPA) at École Polytechnique Fédérale de Lausanne (EPFL) in Lausanne, Switzerland.

4. 3. Results and Discussion

ESTASI is a contactless spray ionisation technique which prevents from electrochemical reactions from occurring at the electrode/solution interface as happens in traditional ESI-MS when a high voltage is applied between the electrode and the mass analyser (counter electrode). By applying a DC high voltage between the electrode placed at a small distance from the sample and the mass spectrometer (Figure 4.3.1.a), two capacitors are formed: C_1) electrode-insulator-sample solution and C_2) sample solution-gas-MS inlet (see Figure 4.3.1.b). After the application of high voltage, charges accumulate at the solution/gas interface (see Figure 4.3.1.b) and electrostatic spray is induced when the charge accumulated at this interface is too large and the electrostatic pressure (p_e) is greater than the Laplace pressure between the solution and the gas phase.

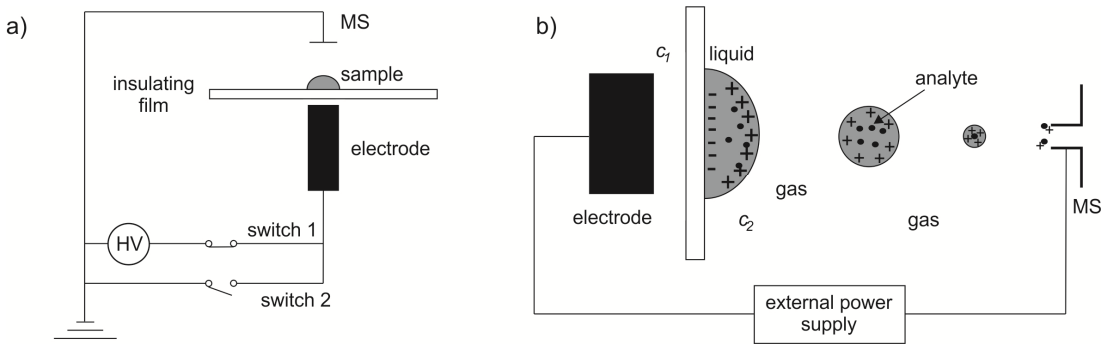

Figure 4.3.1. Sketch of the electrostatic spray ionisation (a) and an amplification of the ionisation processes followed by evaporation of the liquid and charged molecules reaching the mass analyser (b). C_1 and C_2 are the capacitors formed when applying the potential difference at the electrode-insulator-sample and the sample-gas-MS.

Laplace pressure (p_L) is defined as the pressure difference between the spherical meniscus formed between a hemispherical solution droplet and the gas phase, which is caused by surface tension, see Equations 4.3.1 and 4.3.2.

$$p_e = \sigma^2/2\varepsilon_0 \qquad (4.3.1)$$

$$p_L = 2\gamma/r \qquad (4.3.2)$$

where σ is the surface charge density, ε_0 the permittivity of vacuum and the γ is the surface tension of the solution and r is the radius of the droplet hemisphere. Then when electrostatic spray is forced, the surface charge density must be larger than $4\gamma\varepsilon_0/r$ as described in Equation 4.3.3.

$$\sigma^2 > 4\gamma\varepsilon_0/r \qquad (4.3.3)$$

After electrospray the electrode is disconnected and grounded to discharge both capacitors and avoid counterion charge build-up once the sample is ionized. In this case, the gel is placed on the insulating polymer film and a drop of acidic buffer is added on top of the gel to provide an acidic medium that enables protonation of the protein and also facilitates the transfer of the molecule into the gas phase. Figure 4.3.2 illustrates the new set-up showing the hydrophobic gel on the insulating film and the acidic solution deposited onto the organogel.

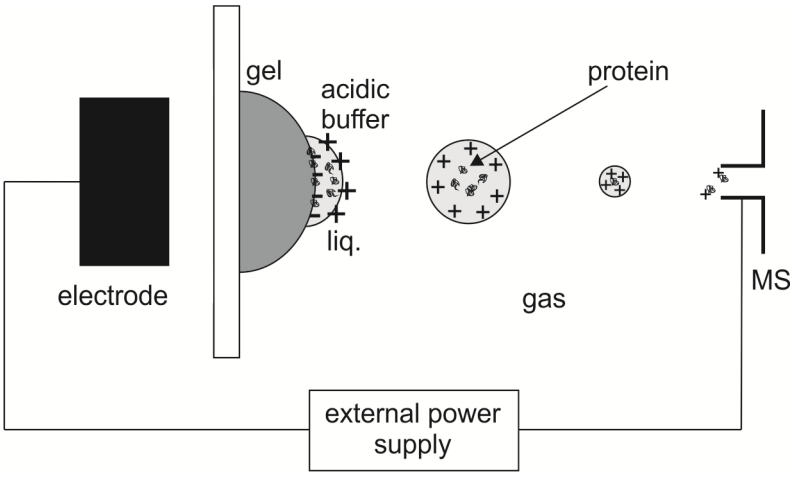

Figure 4.3.2. Schematic representation of the electrostatic spray ionisation.

Consequently this technique was the ideal candidate to characterise the gelled organic phase after electrochemical pre-concentration of lysozyme as this methodology enables the direct analysis of the electro-adsorbed protein.

4. 3. 1. Organic electrolyte in the gel

Firstly, the organogel was prepared with different concentrations of organic electrolyte (1, 5 and 10 mM) in order to evaluate signal via ESTASI-MS. The organic electrolyte, bis(triphenylphosphoranylidene) tetrakis(4-chlorophenyl)borate ($BTPPA^+$ $TPBCl^-$), was dissolved in 1,6-dichoroheaxene and then gelled by adding polyvinyl chloride (10%w/v). Then a droplet of the organogel was placed on the GelBond®PAG film. As mentioned in Section 4.2.4, 1-2 µL of 1% acetic acid in 49% water and 50% methanol were deposited manually on top of the gel to facilitate the protonation and also the transfer of the analytes into gas phase. Figure 4.3.3.a and Figure 4.3.3.b show the spectra of the organogel containing 10 mM BTPPA TPBCl. The results for lower concentrations are not shown as the signal for the organic ions was either non-existent or not as intense as that observed for 10 mM organic electrolyte. In Figure 4.3.3.a, a sharp peak corresponding to the cation of the electrolyte ($BTPPA^+$) was detected at a mass-to-charge ratio of 538.26 which correspond to the molecular weight of bis(triphenylphosphoranylidene)ammonium with one charge. In the negative mode, the anion of the organic electrolyte was also detected when the electrolyte concentration in the gel was 10 mM. Figure 4.3.3.b represents the percentage relative intensity over the mass-to-charge ratio (*m/z*) measured for the 10 mM BTPPA TPBCl organogel in the negative mode. The peak observed at *m/z* 457.16 corresponds to tetrakis(4-chlorophenyl)borate with z = -1, which is in agreement with the monoisotopic molecular mass of tetrakis(4-chlorophenyl)borate (TPBCl).

In addition, no interference was observed from the gel composed of low molecular weight polyvinyl chloride (averaged molecular mass 48,000 g mol^{-1}) in 1,6-dichlorohexane. This is attributed to its low solubility in the acidic buffer. Assuming that the polymer (PVC) was ionised, repetitive peaks with interval of *m/z* 62.5/n, where n is the charge number, should be observed to present the different polymerization states of the PVC, as the molecular mass of the PVC monomer (–CH_2CHCl–) is 62.5 g mol^{-1}. They were not observed in any of the mass spectra

obtained by ESTASI-MS on the organogel, implying that PVC was not detected by this ESTASI-MS method.

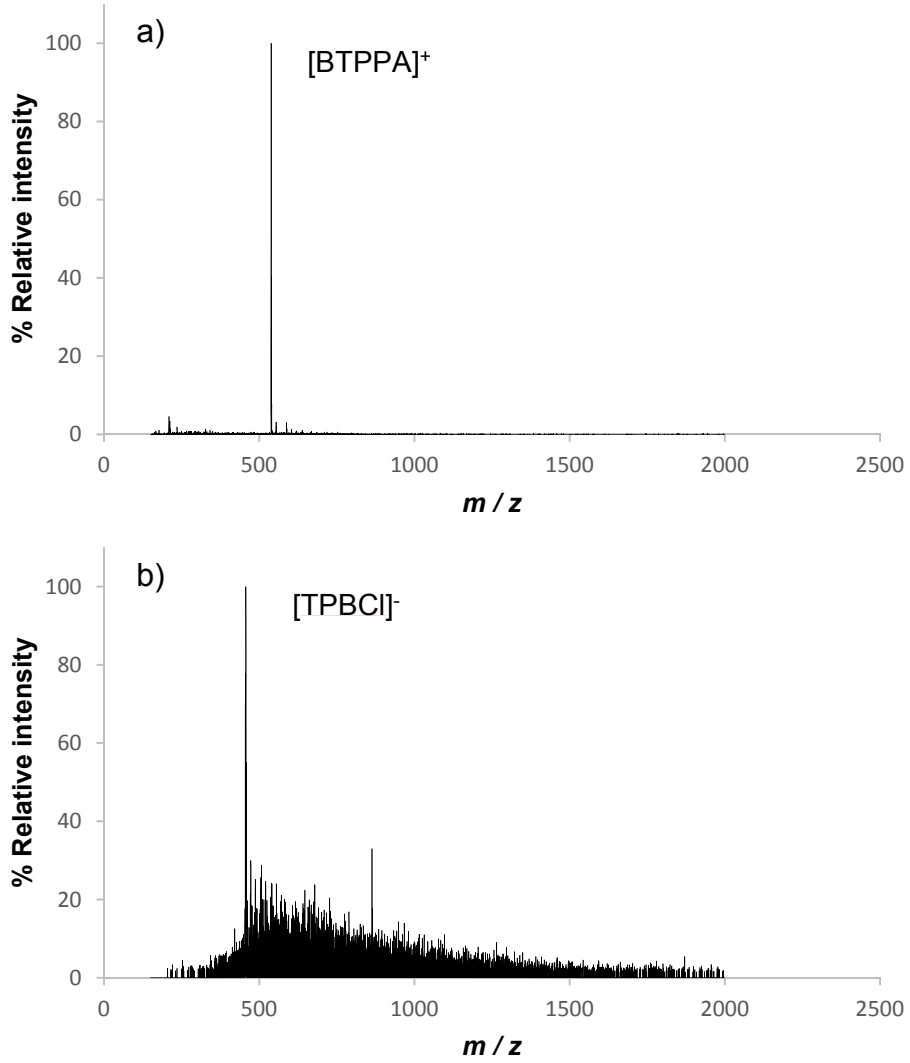

Figure 4.3.3. Electrostatic-spray spectra of 10% w/v organogel (10 mM BTPPA TPBCl in PVC/1,6-DCH); a) in the positive mode and b) in the negative mode.

4. 3. 2. Lysozyme in solution

Before characterizing the organogel with electro-adsorbed protein via mass spectrometry, lysozyme in an acidic buffer solution was characterised by ESTASI-MS. A drop (1 µl) of 10 µM lysozyme in 1% acetic acid in water:methanol (50:50) was placed on the plastic film for ionisation. This experiment was performed to evaluate the lysozyme spectrum when this protein is softly ionized via ESTASI.

Lysozyme has been reported to show several protonated states depending on the unfolding conformation of the protein.[167, 168] In the case of lysozyme, higher charged states have been reported when the four disulfide bonds in lysozyme molecules were reduced by dithiothreitol (DTT), which led to unfolding of the protein and consequently exposing the buried residues of the protein in its native compact structure.[167] Another study on lysozyme fibril formation reported protonated states of lysozyme up to +15 charges when lysozyme was denatured at a low pH and high temperatures (65˚C for 14 and 96 h).[168] These reports indicate that low charge states (7+ to 10+) of lysozyme correspond to its native conformation with intact disulfide bridges. The unfolded conformation present peaks in the mass spectra corresponding to lysozyme protonated with 9 to 16 protons. In Figure 4.3.4, the spectrum obtained for lysozyme illustrates four charge states of the protonated protein. Hen-egg-white-lysozyme has been reported to be charged with 17 positive charges at pH 2 when carrying out acid-base titration curves.[150] However, based on the amino acids sequence of the protein, lysozyme is expected to present +18 charges (11 arginine, 6 lysine and 1 histidine residues)[169] if within the protein, all the possible protonatable sites (arginine, lysine and histidine) are protonated with one proton (+ $1H^+$). In soft ionisation techniques such as ESTASI – MS, the charge states measured in the mass analyser depends on the physical conformation of the protein due to the gentle ionisation.

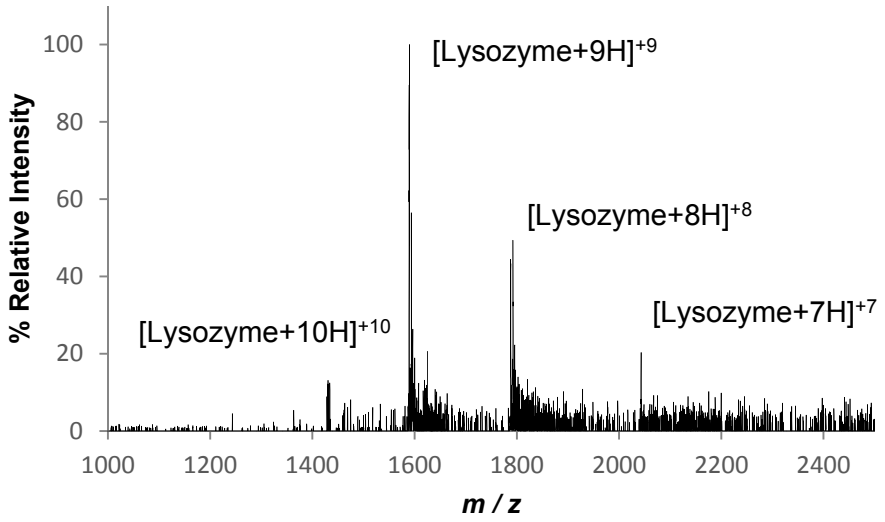

Figure 4.3.4. Spectrum of 1 µl of 10 µM lysozyme in 1% acetic acid in water:methanol (50:50) deposited on the plastic film which theoretically corresponds to 10 pmoles.

The spectrum in Figure 4.3.4 is dominated by one peak at 1590 *m/z* followed by 1787, 2043 and 1430 mass-to-charge ratio values. ESI-MS protein spectra normally possess broad multiple charge peaks when protonated (positive mode) which correspond to different charge states of the protein when ionized in an acidic medium. Moreover, the broadness of the peaks is attributed to isotopic peaks detected in the large biomolecule, which is mainly composed of carbon, nitrogen, oxygen and hydrogen and a low percentage of sulfur when methionine and/or cysteine residues are present in the amino acid sequence of the protein.

In order to confirm that the peaks obtained in the spectrum (Figure 4.3.4) correspond to lysozyme, mathematical deconvolution was performed using ProMass (Thermo Fisher Scientific Inc., Hampton, USA). Equation 4.3.4 and 4.3.5 are a summary of the mathematical expressions employed to develop the algorithm that can resolve the convoluted date obtained from the mass analyser and detector.

$$m/z = (M + zA)/z \qquad (4.3.4)$$

For adjacent peaks $z_1 = z_2 + 1$ for protonated proteins (+1 hydrogen), then;

$$z_2 = (mz_1 - A)/(mz_2 - mz_1) \qquad (4.3.5)$$

m/z is the mass-to-charge peak from the spectrum, *z* is the charge, *M* is the mass of the protein and *A* is the adduct providing charge. In the case of a protonated protein, the adduct corresponds to the sum of the molecular mass of the protein and n ($A=M+n$), being n the number of hydrogen (~1 g mol^{-1}). When cations such as potassium or sodium are present in the sample, the adducts could correspond to the mass of the protein plus the atomic mass of these cations which therefore would form the charged molecule detectable via mass spectrometry.

From the ProMass deconvolution, the calculated mass was 14,296 g mol^{-1} whilst the monoisotopic molecular mass of lysozyme ($C_{613}H_{951}N_{193}O_{185}S_{10}$) would correspond to 14,295.8 g mol^{-1}.[170] Then the peaks detected via ESTASI-MS correspond to lysozyme protonated with 10 protons (*m/z* = 1430 being *z* = +10), 1590 is $[Lysozyme+9H]^{+9}$, 1787 corresponds to lysozyme protonated with 8H+ and the peak at *m/z* 2043 is the signal obtained for $[Lysozyme+7H]^{+7}$ complex.

These data also reveal that the protein in the acidic buffer remains in its native configuration as the *m/z* values correspond to low charge states of the protein which is in agreement with a 3D compact conformation of lysozyme; i.e. it is not denatured.

4. 3. 3. Effect of the applied potential

Before exploring the effect of pre-concentration of lysozyme at the organogel surface via electrochemistry at the ITIES, a control experiment was performed in triplicate in order to determine the possible natural adsorption of the protein under open-circuit conditions at the gelled liquid – liquid interface. After immersing the organogel in a 10 μM lysozyme aqueous solution for 30 minutes at open circuit, there was no detectable protein in the spectrum (see spectrum in Figure 4.3.5).

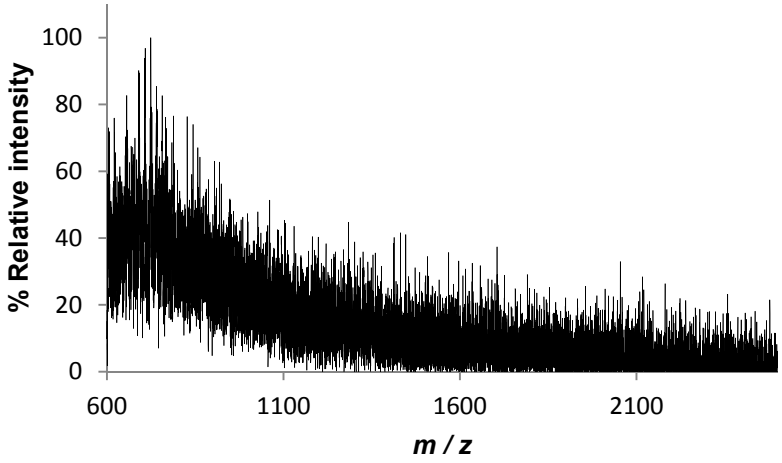

Figure 4.3.5. Spectrum of the organogel (10 mM BTPPA TPBCl in 10%w/v PVC in 1,6-DCH) after incubation in 10 μM lysozyme acidic solution (10 mM HCl) for 30 minutes under open-circuit conditions.

Based on previous experiments (see Chapter 3), adsorption of lysozyme at liquid-liquid micro-interfaces has been demonstrated to be concentration and time-dependent. In addition, the results showed that the maximum protein adsorption potential was 0.95 V. Thus, this adsorption phenomenon could be tuned by changing the pre-concentration conditions. For this reason, adsorption of lysozyme was implemented, as described in Chapter 3, but was not followed by electrochemistry but by ESTASI-MS. Figure 4.3.6 illustrates the difference between the approach

utilized in Chapter 3 (Adsorptive Stripping Voltammetry, AdSV) and the electrochemical pre-concentration prior to ESTASI-MS. Figure 4.3.6.a represents the adsorption of lysozyme at a constant potential (E_{ads}) for a period of time (t), which is the pre-concentration step, followed by the desorption of the protein back to the aqueous phase via stripping. In this step the potential is scanned back to the potential of open-circuit potential. On the contrary, Figure 4.3.6.b shows the electrochemical pre-concentration step which is then interrupted after a period of time and subjected to ESTASI-MS on the organogel. There is no electrochemical characterisation prior to the ESTASI step. This prevents electrochemical desorption of the protein from the interface which would lead to the loss of the biomolecule from the interface.

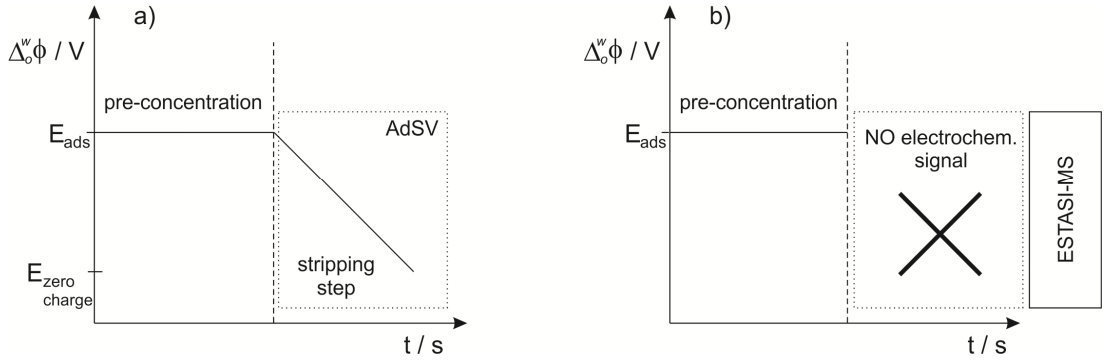

Figure 4.3.6. Diagram of a) Adsorptive Stripping Voltammetry (AdSV) and b) electrochemical adsorption at E_{ads}, without a desorption step, followed by ESTASI-MS.

The influence of different applied potentials was studied between 0.6 and 1.0 V, as this range which was reported in Chapter 3 (Section 3.3.2) as the potential region where the charged protein undergoes adsorption and complexation with $TPBCl^-$ from the organic phase. The gelled organic phase was immersed in 10 μM lysozyme in 10 mM HCl and a constant potential was applied for 30 minutes. Immediately following the electrochemical adsorption, the organogel was removed from solution and placed onto the insulating film located between the electrode and the mass analyzer inlet (Figure 4.3.2). For 0.6, 0.7 and 0.8 V, no MS signal distinguishable from background signal was detected. This data is in agreement with the electrochemical response when AdSV was implemented (see Figure 3.3.2). However from 0.85 V upwards to 1.0 V, the *m/z* signal increased in intensity. Figure 4.3.7 shows the spectra for 10 μM lysozyme in the aqueous solution after pre-concentrating the protein for 30 minutes at 0.85 (Figure 4.3.7.a), 0.95(Figure 4.3.7.b) and 1.0 V (Figure 4.37.c). For an

adsorption potential of 0.85 V, the charge states of the protein are more difficult to distinguish from the background noise, although peaks corresponding to $[Lysozyme+10H]^{+10}$ and $[Lysozyme+9H]^{+9}$ were observed at 1430 and 1590 *m/z*. At 0.95 V, $[Lysozyme+8H]^{+8}$ was detectable and $[Lysozyme+7H]^{+7}$ appeared at 2044 *m/z* for 30 minutes pre-concentration at 1.0 V. It was also noticed that for 0.95 and 0.975 V, there was a slight increase in the intensity of peaks at *ca.* 1641 and 1847 *m/z* which were hard to isolate from the background signal; these peaks correspond to Lysozyme-1TPBCl complexes in their +9 and +8 protonated state, respectively. $[Lysozyme\text{-}1TPBCl+(n+1)H]^{+n}$ complexes for n = 10, 9 and 8 were identified at 1477, 1641 and 1847 *m/z,* respectively. However, for higher E_{ads} values such as 1.0 V, those peaks increased in intensity (see asterisks in Figure 4.3.7.c).

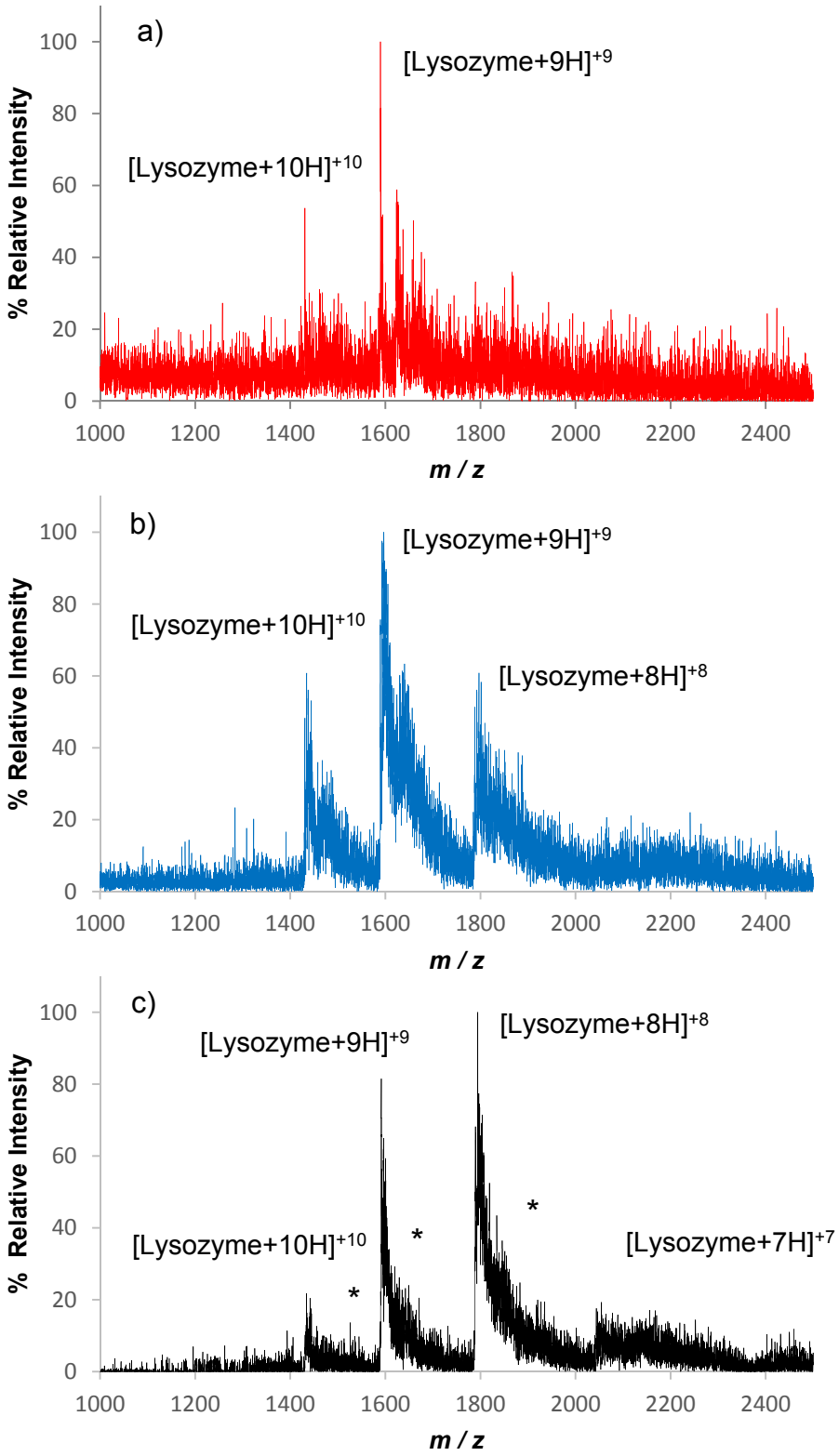

Figure 4.3.7. Mass spectra of the gel (10 mM BTPPA TPBCl in 10%w/v PVC in 1,6-DCH) after pre-concentration of 10 µM lysozyme aqueous solution for 30 minutes at: a) 0.85 V, b) 0.95 V and c) 1.0 V. *Complexes formed between lysozyme and $TPBCl^-$.

The most prominent peak in the spectrum is at *m/z* 1524 (see Figure 4.3.8), which corresponds to the complex formed between a positively charge molecule of lysozyme and 2 molecules of the anion from the organogel ($TPBCl^-$), i.e. $[Lysozyme\text{-}2TPBCl+12H]^{+10}$. Increasing the potential applied across aqueous – organogel interface increased the amount of protein detected at the organogel surface, as confirmed by the increased intensity of *m/z* peaks in the spectra. Additionally, new *m/z* peaks were observed at higher applied potentials, which is in agreement with the detection mechanism proposed in Chapter 3 for lysozyme detection at the ITIES. This consists of adsorption followed by complexation of the positively charged protein with the organic anion from the organogel; this complexation facilitates its transfer, resulting in changes in the current measured.

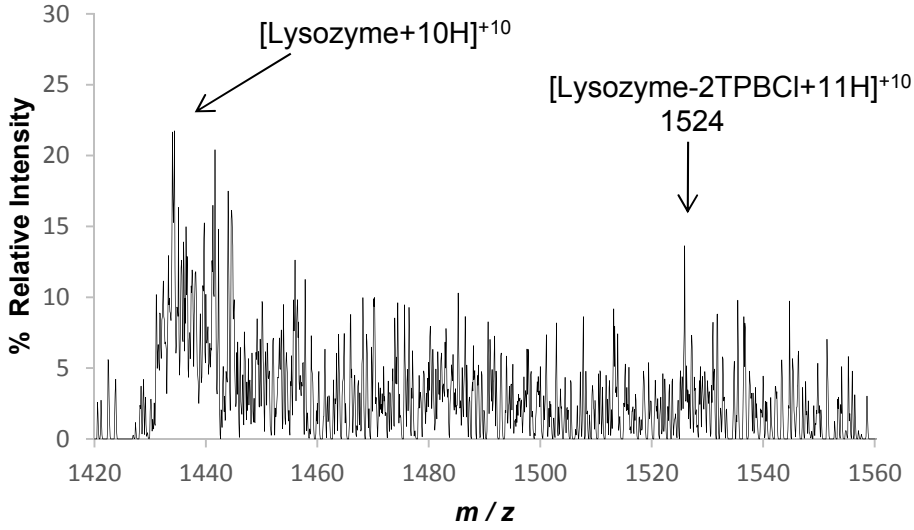

Figure 4.3.8. Spectra of the organogel after previous pre-concentration of 10 μM lysozyme for 30 minutes at 1.0 V. This figure corresponds to an expansion of a section of Figure 4.3.7.c.

Figure 4.3.9.a illustrates how the spectra have been analysed in order to study the signal-to-noise ratio evolution with the applied potential. The peak intensity of the signal is measured and the average of the noise calculated together with the corresponding standard deviation of the noise. Then the ratio (signal/noise) was calculated and normalised to a percentage, the signal-to-noise ratio of the data obtained at 1.0 V being set at 100%.

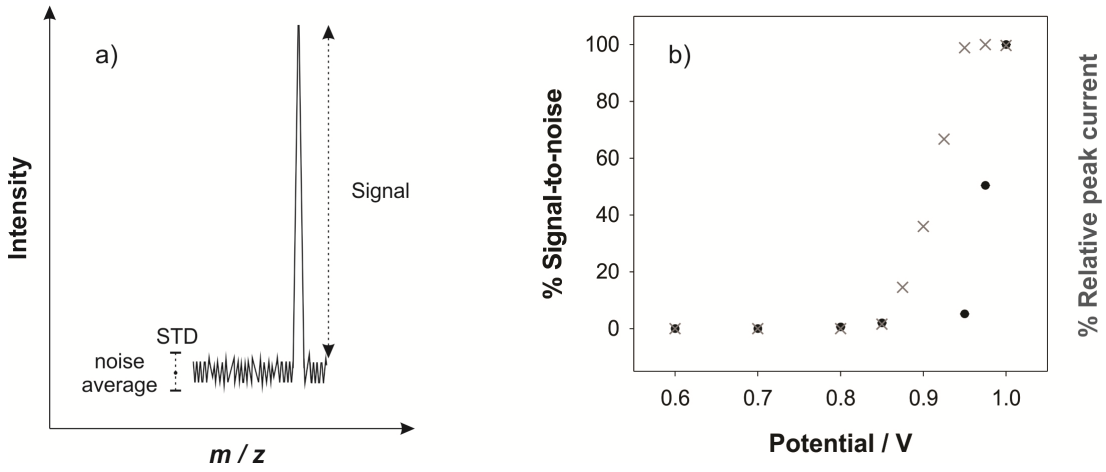

Figure 4.3.9. a) Sketch of how the signal-to-noise ratio was measured in the ESTASI-MS spectrum and b) percentage of signal-to-noise ratio against the applied potential for 30 minutes in a solution of 10 µM lysozyme (●) and percentage of height of the peak after performing adsorptive stripping voltammetry of 10 µM lysozyme for 60 s pre-concentration time (×) at liquid-liquid microinterfaces (30 micropore array, see results in Chapter 3, Section 3.3.2). Note that the error bars corresponding to the standard deviation (*STD*) of the noise are represented although they are lower than 0.01%.

The data illustrated in Figure 4.3.9b is based on the ESTASI-MS spectra for different applied potentials and electrochemical data obtained after pre-concentrating 10 µM lysozyme for 30 min and 60 s, respectively. In both cases, the intensity of the signal either ESTASI-MS or electrochemical increases rapidly from 0.85 V onwards. A summary of the raw data (peak current, ESTASI-MS signal and noise) is presented in table 4.3.1.

Table 4.3.1. Stripping voltammetry and ESTASI-MS values for the pre-concentration of lysozyme at liquid-liquid interfaces.

	Electrochemical data after AdSV at liquid-liquid μ-interfaces [a]		ESTASI-MS after pre-concentration on the gel [b]			
Adsorptive potential / V	**Peak current / nA**	**% Relative peak current**	**Signal ESTASI-MS peak / a.u.**	**Noise intensity / a.u.**	**ESTASI-MS signal-to-noise / a.u.**	**ESTASI-MS / % Relative intensity**
0.600	0.000	0.00	0.00	0.00	0.00	0.00
0.700	0.000	0.00	0.00	0.00	0.00	0.00
0.800	0.000	0.00	213.60	50.71	4.21	0.61
0.850	0.044	1.61	476.73	34.27	13.91	2.02
0.875	0.401	14.57	-	-	-	-
0.900	0.991	35.987	-	-	-	-
0.925	1.838	66.76	-	-	-	-
0.950	2.723	98.89	58.35	1.62	35.93	5.21
0.975	2.753	100.00	667.24	1.912	347.80	50.44
1.000	2.746	99.73	1473.85	2.14	689.56	100.00

[a] *Adsorptive Stripping Voltammetry data when pre-concentrating 10 μM lysozyme in solution for 60 s.*

[b] *30 min pre-concentration of 10 μM lysozyme in the aqueous solution with no desorption potential applied.*

The intensity of the signal (peak current or MS peak intensity) was measured and the average of the noise. Then the ratio (signal/noise) was calculated and normalised to a percentage where 100% corresponds to the strongest signal (peak current – 2.753 nA – and ESTASI-MS – 1473.85 a.u.).

Another remarkable feature found in the spectra was the shift in the intensity of the predominant peak in the ESTASI-MS spectra. At low adsorption potentials, the predominant peak corresponded to $[Lysozyme+9H]^{+9}$, however, $[Lysozyme+8H]^{8H+}$ becomes the most intense *m/z* peak at more positive potentials which could indicate that the charged protein adopted a more compact configuration when a higher quantity of protein is adsorbed onto the organogel. In the literature, larger charged ions of lysozyme measured via ESI-MS were attributed to an unfolded conformation of the protein[167, 168] which is attributed to the reduction of disulfide bonds in the molecule, leading to greater exposure of the amino acid residues of protein. Figure 4.3.10.a shows the spectrum of 10 μM lysozyme droplet in an acetate buffer obtained

by ESTASI-MS. For comparison, an ESTASI-MS spectrum showing the theoretical signal generated by unfolded lysozyme is depicted in Figure 4.3.10.b. These peaks represented in Figure 4.3.10.b have been generated based on previously reported studies[167] and allocating 100 % relative intensity to the peak corresponding to $[Lysozyme+13H]^{+13}$. The difference between Figure 4.3.10.a and 4.3.10.b indicates that the protein is not unfolded, at least to a significant extent, in the electrochemical adsorption-ESTASI-MS experiment reported here.

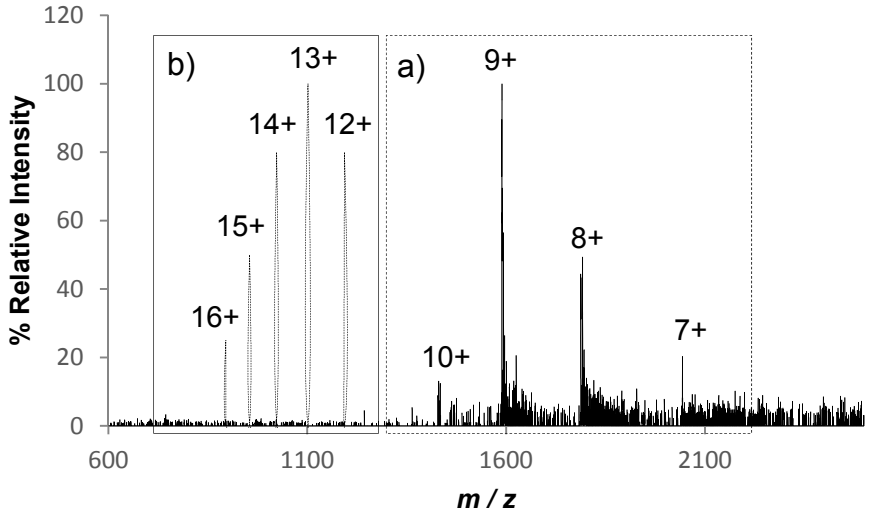

Figure 4.3.10. ESTASI-MS spectrum of a droplet of 10 µM lysozyme in 1% acetic acid in water:methanol (50:50) deposited on the plastic film (a) and the theoretical *m/z* peaks that the unfolded conformation of lysozyme would show (b) after electrostatic spray.

4. 3. 4. Pre-concentration time influence

The adsorption time was varied from 5, 10, 20 to 30 minutes at 1.0 V and 10 µM lysozyme as under these conditions the spectra obtained showed optimum results regarding sensitivity of the ESTASI-MS on the organogel. Figure 4.3.11 summarises the spectra acquired for several pre-concentration times after pre-concentrating 10 µM lysozyme onto the organogel then followed via ESTASI-MS or electrochemically at liquid-liquid microinterfaces. As demonstrated by results presented in Chapter 3, the *m/z* signal is enhanced significantly when the time of adsorption is increased as it is noted in Figure 4.3.11, the voltammetric analysis at the micro-interfaces is more sensitive to this variation.

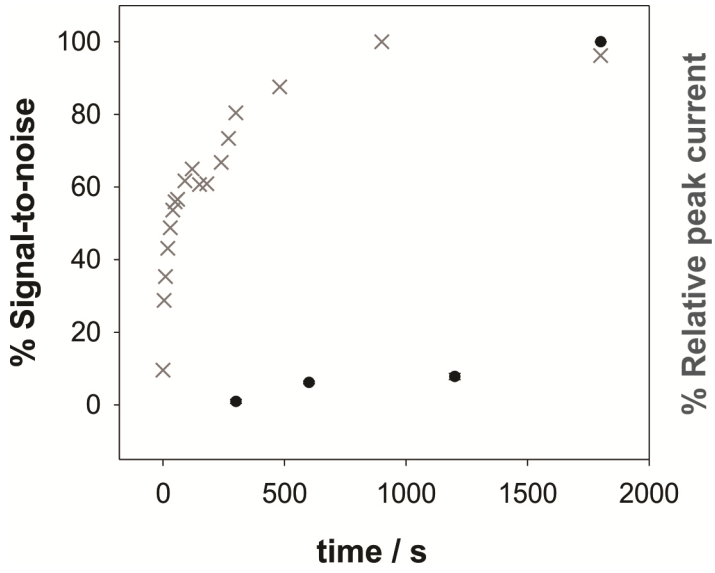

Figure 4.3.11. (●) Percentage of signal-to-noise ratio versus pre-concentration time of 10 μM lysozyme in 10 mM HCl at 1 V (optimum for ESTASI-MS) and (×) percentage of peak current after AdSV of 10 μM lysozyme at 0.95V at liquid-liquid microinterfaces (see Chapter 3, Section 3.3.4). Note that the error bars corresponding to the standard deviation (*STD*) of the noise are represented although they are lower than 0.01%.

Figure 4.3.12 shows an example of the data spectra used to produce the presented in Figure 4.3.11, which was obtained when pre-concentrating lysozyme in a solution of 10 μM in 10 mM HCl at a fixed potential of 1.0 V for 10 minutes. As mentioned previously, the signal-to-noise ratio is lower than the spectra obtained for longer adsorption times. On the other hand, larger charged states are present such as +11. This shift in the abundance of the different lysozyme ions detected at lower times and the possibility to measure more positively charged states could be related to the different adsorbed layers at the gelled organic phase. In Chapter 3, multilayer formation of protein at gelled liquid – liquid micro-interfaces was proposed as a slow process taking place under diverse conditions.

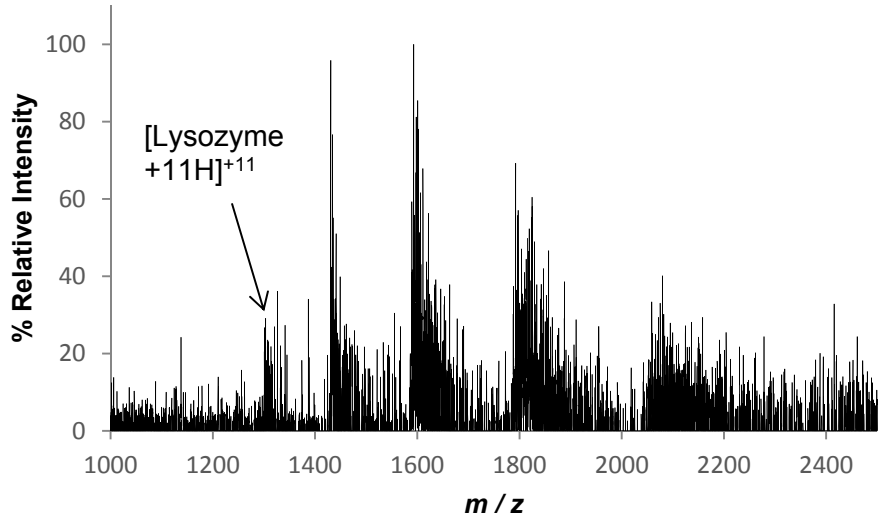

Figure 4.3.12. Spectrum of the organogel after pre-concentration of 10 μM lysozyme (aqueous phase) for 10 minutes at 1.0 V.

4. 3. 5. Concentration dependence

The adsorption of lysozyme was studied as a function of its concentration in the aqueous phase. Figure 4.3.13.a and b show two ESTASI-MS spectra for two sets of experiments (2.5 μM and 5 μM lysozyme in the aqueous phase) at a fixed adsorption potential of 1.0 V following 30 minutes adsorption. Again the lower charged ions were found to become more intense when the amount of lysozyme in the bulk solution was higher. This process satisfies the hypothesis of a higher surface coverage and possible multilayer formation linked to more compact proteins in the outer layer. This process is achieved at larger applied potential, concentration in solution and time required for electrochemical adsorption. Consequently, based on this investigation, the lower the degree of adsorption in terms of multilayer formation, the higher the charged peaks measured via MS which could show a direct correlation with the re-arrangement of the protein at the monolayer level.

Figure 4.3.14 is a summary of the different lysozyme concentrations analysed via ESTASI-MS after electrochemical adsorption. Pre-concentration time and potential was fixed at 30 minutes and 1.0 V, respectively, as these values were optimum for previous spectra.

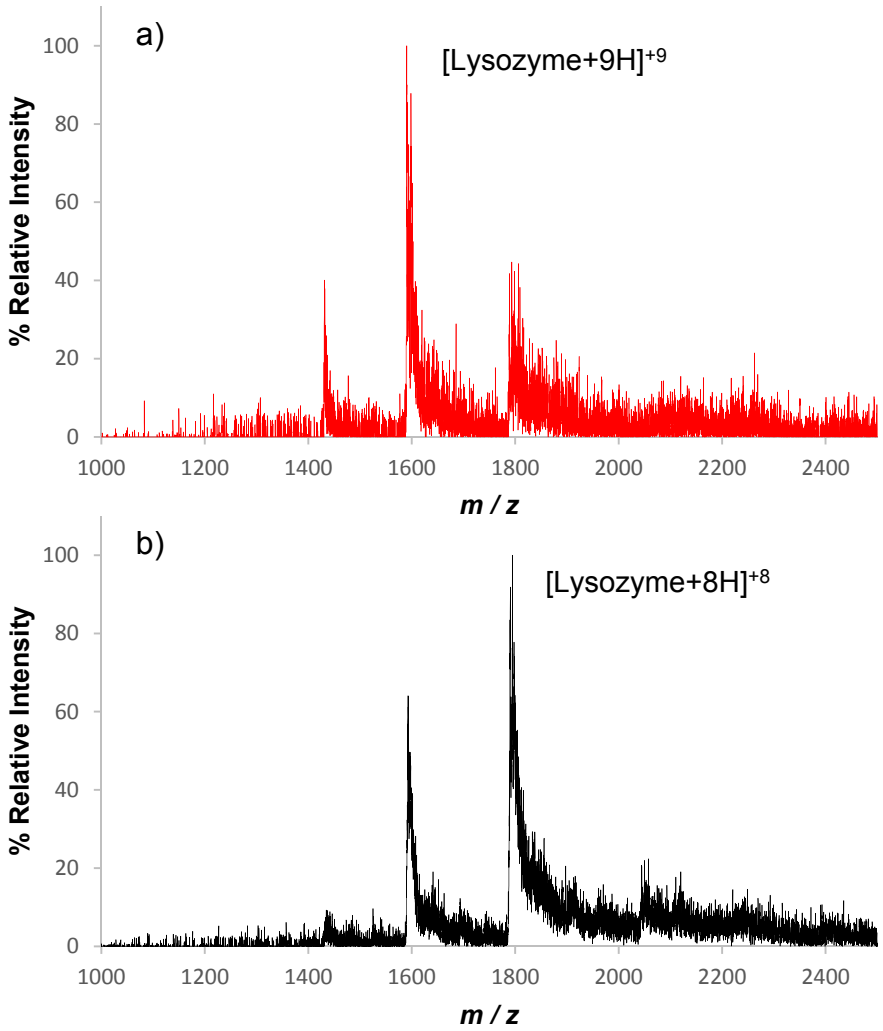

Figure 4.3.13. Spectra of the organogel after electrochemical pre-concentration of a) 2.5 µM and b) 5 µM lysozyme in the aqueous solution for 30 minutes at 1 V.

When lysozyme concentration was evaluated at 0.5 and 1 µM, the signal-to-noise ratio decreased considerably. Lower concentrations were studied although the protein signal was indistinguishable from the background signal. This behaviour is similar to the observed for different pre-concentration times. In comparison to the AdSV results presented in Chapter 3, the sensitivity of AdSV is greater than the obtained for ESTASI-MS based on the signal intensity for the various experiments although factors such as the interruption of the electric field has to be taken into account for a fully comparison.

From 2.5 µM and higher, it was found that *m/z* peaks corresponding to $[\text{Lysozyme-1TPBCl+(n+1)H}]^{+n}$ (being n = 8 – 10) increased slightly with the concentration of protein adsorbed.

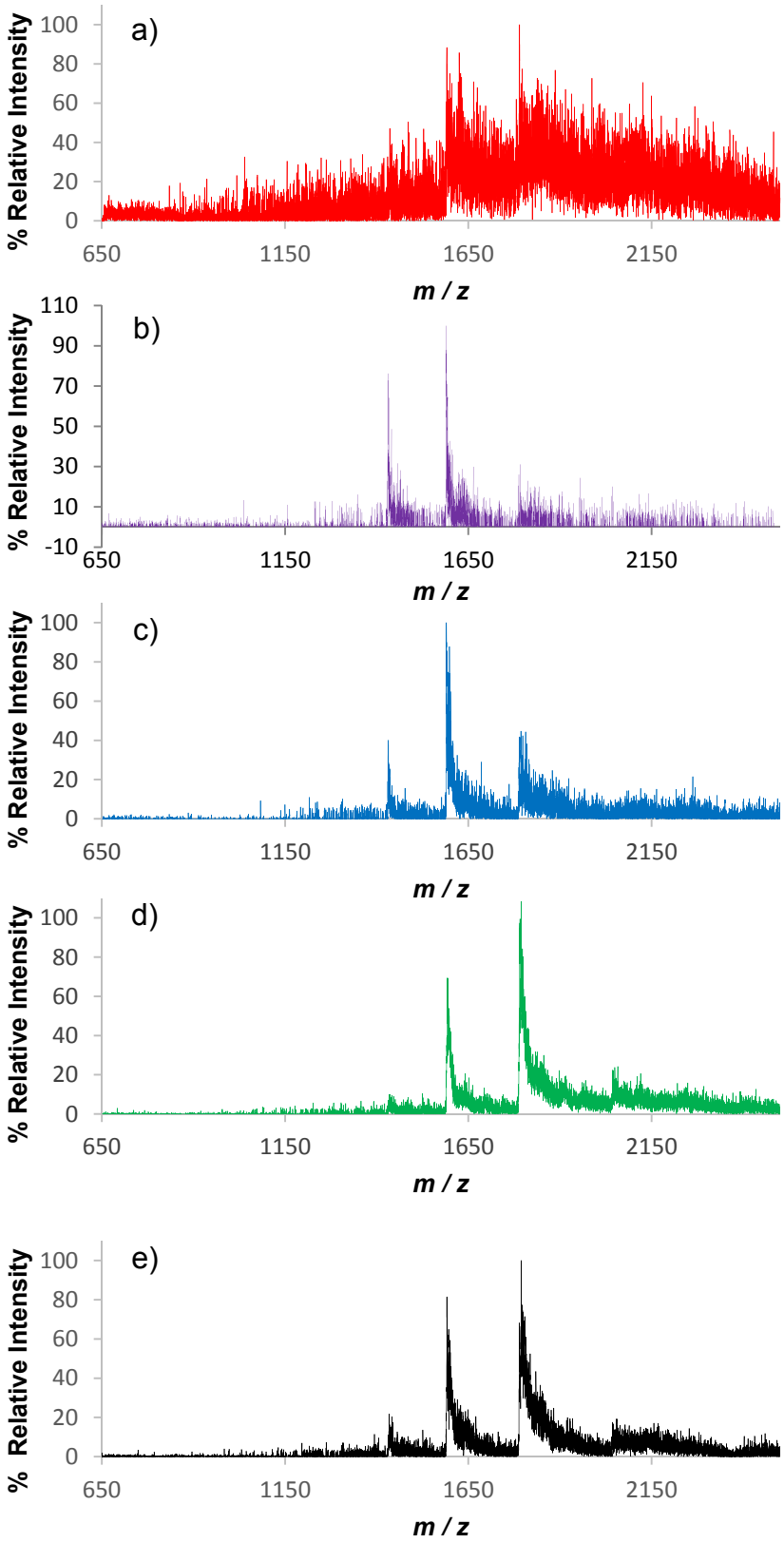

Figure 4.3.14. Mass spectra of the organogel after electrochemical pre-concentration of a) 0.5 µM, b) 1 µM, c) 2.5 µM, d) 5 µM and e) 10 µM lysozyme in the aqueous solution for 30 minutes at 1 V.

4. 3. 6. MALDI-TOF

Matrix-assisted laser desorption ionisation – time-of-flight (MALDI-TOF) experiments were carried out in order to evaluate the content of protein in the organogel and also to provide another platform to characterise the formation of complexes between the cationic form of the protein and the anion from the organic phase. The samples were treated under the same conditions as the gel used for ESTASI-MS. The only difference was the extraction of the protein from the gel by using 1,6-dichlorohexane. The sample was then deposited and co-crystallized with a high concentration of matrix solution (10 mg/ml 2,5-dihydroxy benzoic acid in 50% acetonitrile, 0.1% trifluoroacetic acid, and 49.9% water) on a metallic plate. A pulsed nitrogen laser of 337 nm wavelength was applied to the crystals deposited on the plate which resulted in desorption of the analyte into the gas phase and its ionisation. Finally, the charged ions are accelerated via an electric field between the sample plate and the mass detector. Unlike ESTASI-MS, this method produced low charged ion peaks in the *m/z* spectrum (see Figure 4.3.15). In this figure, lysozyme was detected in two forms, protonated with one or two protons, which corresponds to 14,336 and 7,231 *m/z* values, respectively. Acetonitrile and ethanol were also tested as alternative solvents to extract the protein and/or protein complexes from the gel although 1,6-dichlorohexane was the solvent with better results in terms of detectable ions.

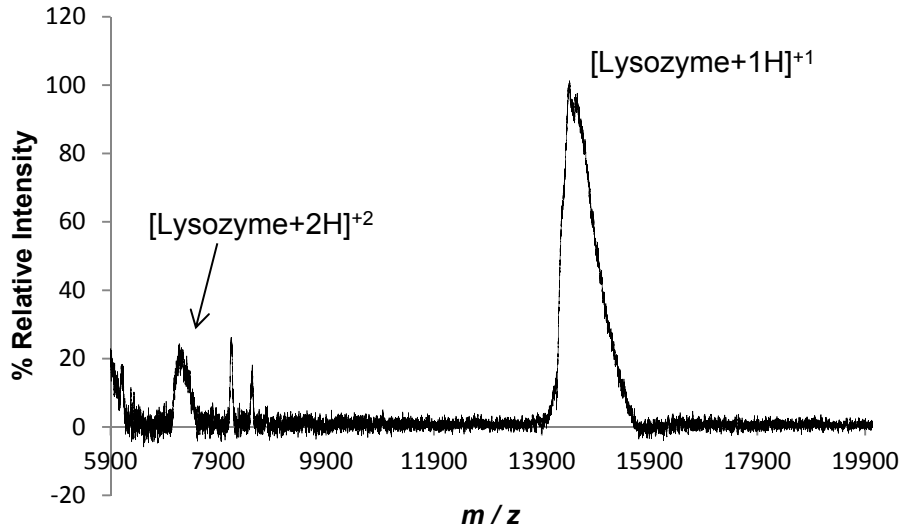

Figure 4.3.15. MALDI-TOF spectrum of the organogel after electrochemical pre-concentration of 10 μM lysozyme in the aqueous solution for 30 minutes at 1.0 V.

Lower concentrations in the aqueous solution used to pre-concentrate lysozyme under a constant potential applied were analysed via MALDI-TOF. Figure 4.3.16 illustrates similar information to Figure 4.3.15, although the main difference is the concentration which was lowered down to 0.5 μM of lysozyme in the aqueous phase.

A broad shoulder can be appreciated at *m/z* 14,772 which starts at 14,333 *m/z* and two peaks at 8,246 and 4058. This first peak 14,772 could be attributed to the protonated lysozyme and its complex with TPBCl although the signal is too broad and unresolved.

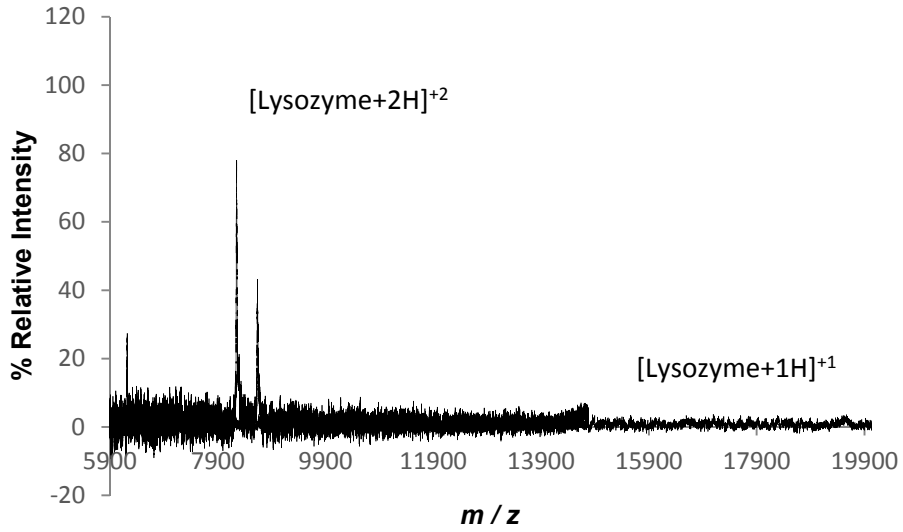

Figure 4.3.16. MALDI-TOF mass spectra of extracted 0.5 μM lysozyme in the aqueous solution for 30 minutes at 1 V.

4. 3. 7. Sensitivity and multilayer formation

Regarding the sensitivity of soft ionisation mass spectrometry, limits of detection of picomole and femtomole have been reported for electrospray ionisation (ESI-MS) when coupled with LC.[171-173] Nevertheless, the size of the molecule of interest can affect this figure of merit as larger molecules hit the detector with lower velocity, which results in a lower signal and therefore lower sensitivity. The limit of detection for isoelectric focusing gel electrophoresis coupled to ESTASI-MS analysis was reported to be in the picomole range and this system is the most similar to the approach presented here out of all the different set-ups studied via ESTASI-MS.[105] This could be a limitation in the study of electrochemical adsorption and could explain the high concentrations (0.5 to 10 μM lysozyme in solution) and times (30 minutes) required to detect the presence of the protein after pre-concentration at the organogel. If for a monolayer of lysozyme, the surface coverage corresponds to 13 pmol/cm^2 (see Chapter 3, section 3.3.7)[151] and assuming that a perfect hemispherical gel area (0.035 cm^2) is 100% exposed to ionisation, then the amount of lysozyme detected via MS will be 0.45 pmol of lysozyme. However, for the same monolayer but employing the 30-micropore array (1.18 x 10^{-4} cm^2) employed previously and reported in Chapter 3, the amount of lysozyme at the micro-interfaces would

correspond to 1.5 fmol. This corresponds to a 300-fold difference in sensitivity between both techniques which raises the potential of AdSV as a new analytical approach. The amount of protein calculated for a perfect monolayer form on the hemispheric gel (0.45 pmol) is below the limit of detection reported for this technique[103] and confirms the need for multiple layers of protein adsorbed via electrochemistry at gelled liquid – liquid interfaces. In addition, if we consider that the drop of acidic buffer occupied partially the area of the gel, this value will decrease considerably, then the lysozyme ionized will be orders of magnitude lower than the reported limit of detection (1.63 pmol)[103] when using polyacrylamide on the insulating film for ESTASI-MS. Moreover, using the experimental data presented in Chapter 3, Section 3.3.5 and 3.3.6, the maximum surface coverage (550 pmol/cm^2) data obtained from the charge under the desorption peak will represent 19.25 pmol of lysozyme on the gel with an area of 0.035 cm^2 which also corresponds to multilayers as proposed in Chapter 3. In addition, the abundance of the multiply charged states of the protein was found to shift with the three factors studied (potential, time and concentration). The lower the value of these parameters, the higher was the signal-to-noise ratio and also the more abundant was the protonated lysozyme with +10 and +11. In both extremes, the charges are still lower than those expected for unfolded lysozyme. However, this phenomenon may describe the difference in the adsorption process and the multilayer formation. When the applied potential, the time of adsorption and the concentration of protein in the aqueous solution is high, the lysozyme detected is more abundant in a more compact form, [Lysozyme+8H]$^{+8}$. This might provide some information regarding the conformation and orientation of lysozyme within the multilayer. This data suggest a more compact form of the protein in the outer layer in comparison with the values obtained for conditions when a lower of lysozyme was detected.

4. 4. Conclusions

For the first time, a highly hydrophobic gel has been used as a substrate to characterise lysozyme via ESTASI-MS after electrochemical pre-concentration. The formation of lysozyme-TPBCl interfacial complexes has been observed at the gelled liquid-liquid interfaces via ESTASI-MS, which confirms the proposed mechanism

for the detection of lysozyme at the ITIES.[78, 79, 88] This is the most direct study performed at the ITIES and serves as a new platform for further investigations combining electrochemistry at the liquid – liquid interfaces monitored by ESTASI-MS. It is also observed that higher charged states of the protein allows the detection of complexes with a larger number of anions from the organic phase. This data supports previous spectra reported when using biphasic electrospray ionisation – mass spectrometry (BESI-MS) in a microfluidic chip which put in contact 100 μM lysozyme in an acidic solution and 10 μM $TPBCl^-$ in 1,2-dichloroethane.[88] In that investigation,[88] the potential difference is achieved chemically whilst herein, the potential difference is produced electrochemically then measured directly via ESTASI-MS. It should be noted that the ionisation method differs to BESI-MS and the concentrations detected here are 10-fold lower in the aqueous solution than the work reported by Hartvig et al.[88] Moreover, the highly resistive nature of the gel could affect the efficiency of the electrochemical adsorption as the gel area was 0.035 cm^2 and probably a 4-electrode system would have reduced the resistance of the system. The low abundance of these interfacial complexes in the ESTASI-MS spectra could be explain due to the interruption of the electric field which promotes the interaction between the protonated lysozyme and tetrakis(4-chlorophenyl)borate. The interruption of the electric field after 30 minutes of constant potential applied at the gelled liquid – liquid interface, leads to a new equilibrium at the previously polarized interface. This equilibrium can be therefore altering the spectra obtained from the potential spectra that would be generated if the *m/z* could be analyzed straight after the electrochemical pre-concentration.

Moreover, mass spectrometry analyses also support the trend observed when adsorptive accumulation of lysozyme was followed by AdSV. Adsorption can be controlled by tuning the applied potential, the pre-concentration time and the concentration of lysozyme in solution. The minimum measurable protein via ESTASI-MS (0.5 μM lysozyme in aqueous solution) corresponds to several layers of lysozyme which is in agreement the limit of detection reported when using ESTASI-MS on polyacrylamide (1.63 pmol)[103] which corresponds to *ca.* 3 layers of lysozyme.

Therefore when the conditions promote submonolayer or monolayer coverage of the hemispherical gel surface, re-arrangement of the protein at the gelled liquid – liquid interface could explain the difference in the mass spectra as shift towards higher charge states is observe for low surface coverage. In Figure 4.3.17 the

multilayer formation is represented to show the differences in the protein structure within the various layers as proposed based on the different charge states observed in the spectra obtained.

Figure 4.3.17. Diagram of the proposed multilayer formed onto the hydrophobic gel. Note that the electrolyte present in the gel which interacts with the protein is not illustrated in this diagram.

Optimization of the gel geometry and the integration of ITIES and ESTASI-MS could improve the limit of the detection of this technology and elucidate interfacial processes which are particularly relevant in cell membrane biology.

5 Electrochemistry at the water – room temperature ionic liquid microinterfaces

Electrified interfaces between immiscible liquid phases provide a basis for the non-redox detection of ions and ionised molecules via interfacial transfer or adsorption processes. In this chapter, the behaviour of water / room temperature ionic liquid microinterfaces was explored in the presence of aqueous phase acid and protein (hen egg white lysozyme). Under voltammetric conditions, hydronium cation transfer was identified, with the formation of a net-neutral capacitive layer at the interface, as confirmed by electrochemical impedance spectroscopy and biphasic electrospray ionisation - mass spectrometry. It was possible to detect hydronium cation transfer at concentrations down to 10 mM although lithium cation transfer was not detectable. In the presence of lysozyme, adsorption of the protein at the interface was possible, with surface coverage of 311 pmol cm^{-2} achieved following potential-induced adsorption at the positive limit of the available potential window. Application of a subsequent voltammetric desorption enabled the detection of lysozyme at concentrations down to ca. 2.5 μM. The water / ionic liquid interface thus provides a new interface for the non-redox detection of ions and ionised biomolecules in a label-free manner.

5. 1. Introduction

The fundamental properties of room temperature ionic liquids (RTILs), such as low volatility, high thermal stability, high intrinsic conductivity, high polarity and the ability to dissolve a wide range of compounds,[174, 175] make them highly attractive for various studies, including electrochemistry,[176] where potential windows as wide as 6.8 V[177, 178] have been found at solid/liquid interfaces. These properties have focused a lot of attention on RTILs in different fields including the study of proteins.[176, 179, 180] For instance, recent work has shown an improvement in lysozyme crystallization using a hydrophilic ionic liquid as an additive.[181] RTILs have been tested as refolding enhancers of lysozyme and the anti-oxazolone single–chain antibody fragment[182] and as thermal- and activity-stabilizers[183] in protein liquid formulations.[184] Efficient and fast separation of basic proteins including lysozyme has also been achieved by employing ionic liquid-modified capillary electrophoresis (CE).[185] Haemoglobin extraction in the presence of a hydrophobic ionic liquid was first reported in 2008.[186] Since then, studies based on selective adsorption of proteins into RTILs have emerged and researchers have explored this phenomenon as a new extraction and separation methodology.[187] For example Zhao et al. employed a polymer (chloromethyl polystyrene resin), which was functionalized to expose methylimidazolium chloride on the polystyrene surface, to separate selectively haemoglobin.[188] In addition, the presence of co-extractants, such as dicyclohexano-18-crown-6, in the ionic liquid was shown to enhance the solubility of the protein of interest and to facilitate the extraction process.[189, 190] Ionic liquid matrices (ILMs)[191, 192] have also been investigated for the detection of biomolecules, such as oligodeoxynucleotides, peptides, and small proteins, by matrix-assisted laser desorption/ionisation time-of-flight mass spectrometry (MALDI-TOF-MS).[192] In the electrochemistry of biomolecules, RTILs have been used as immobilisation matrices to attach proteins to electrode surfaces[193, 194] and have been considered to be incorporated in biofuelcell as a replacement of aqueous media.[176] In addition, an ionic liquid - human serum albumin glassy carbon electrode was implemented to discriminate between fenoprofen enantiomers based on selective binding.[195]

The electrochemical behaviour of bioactive molecules at the interface between two immiscible electrolyte solutions (ITIES) has been undertaken recently as part of a better understanding of biological processes and as the foundations for new label-

free and sensitive detection tools. To-date, drugs, neurotransmitters, carbohydrates, proteins, peptides, amino acids and DNA have all been studied at this polarized interface.[12] For instance, proteins such as protamine[73] insulin,[77, 84] haemoglobin,[80] myoglobin,[74, 85] albumin[76] and lysozyme[78, 85] seem to undergo a similar detection mechanism. When the protein is present in the aqueous phase, it is a cationic species. It then undergoes adsorption to the interface at positive applied potentials and facilitates the transfer of anions from the organic phase to the aqueous side of the interface where it forms a complex with the cationic protein.[73, 77-81, 88] The transfer of the organic phase anions provides the charge transfer step that is detected by voltammetry at the ITIES. The two immiscible solutions consist of a water phase and an organic solvent phase, both containing dissolved electrolyte species. The electrochemical behaviour of proteins has been investigated at these polarized interfaces using solvents such as 1,2-dichloroethane,[66, 69, 78, 85] 1,6-dichlorohexane[79] and nitrobenzene[67, 69] as the organic phases. Recently, the electrochemistry of water - RTIL (W/RTIL) interfaces has become of interest after pioneering work published by Bard et al.[196] and further studies carried out by Samec and co-workers[197, 198] and Kakiuchi's group.[3, 178, 198, 199] Their work focused on simple and facilitated ion transfer across the polarisable water - ionic liquid interfaces when varying the ionic liquid under study and in the presence of ionophores such as dibenzo-18-crown-6.[178] Stockmann et al. compared the ferrocene/ferrocenium redox couple at a μ-W/RTIL interface formed within a 25 μm diameter borosilicate glass pipette to that observed at a micro-Pt electrode (with the same dimensions as the W/RTIL interface) and investigated simple ion transfer at the water/trihexyltetradecylphosphonium tetrakis(pentafluorophenyl)borate micro-interface.[200] Silvester and Arrigan studied an array of water – RTIL microinterfaces[115] using a commercially available hydrophobic RTIL at 25 °C (trihexyl(tetradecyl)phosphonium tris(pentafluorethyl)trifluorphosphate) and established the basis of the work presented in this chapter. Recent work has shown the electroactivity of heparin at the polarisable water/ ionic liquid membrane.[63] However, protein characterisation at the W/RTIL interface has not yet been addressed.

The purpose of the work reported in this chapter is to explore the behaviour of a model protein, hen-egg-white-lysozyme (HEWL), at the W/RTIL interface, building on the previous work on formation of a W/RTIL microinterface array[115] and on the behaviour of proteins at electrified water - organic interfaces as described in Chapter

3. The microinterface array helps to minimise the impact of cell resistance, critical in the case of highly viscous ionic liquids, and also increases the rate of mass transport, which is beneficial from a detection and mechanistic point of view. Since previous work on protein behaviour at water-organic ITIES identified that the best responses to proteins were obtained with acidic aqueous phases,[77, 78] the behaviour of the acidic aqueous – RTIL interface is also assessed here. Simultaneously, acidic μ-W/RTIL interfaces are also characterised. For the first time the interaction of acid species and ionic liquid at an aqueous – RTIL interface has been assessed.

5. 2. Experimental Section

5. 2. 1. Reagents

All the reagents were purchased from Sigma-Aldrich Australia Ltd. except the ionic liquid (Merck) and used as received. The ionic liquid used is trihexyl(tetradecyl)phosphonium tris(pentafluorethyl)trifluorphosphate $[P_{14,6,6,6}][FAP]$ (Figure 5.2.1) of ultra-high purity grade (halide content <100 ppm). Trihexyl(tetradecyl)phosphonium chloride $[P_{14,6,6,6}]Cl$ was purchased in highly pure form. Stock solutions of hen-egg-white-lysozyme (HEWL) were prepared in 10 mM HCl (pH 2) on a daily basis. Tetrapropylammonium ($TPrA^+$) chloride was also prepared in 10 mM HCl (pH 2). Different concentrations of aqueous hydrochloric acid and lithium chloride solutions were prepared in purified water (resistivity: 18 MΩcm), using water from a USF Purelab plus UV unit (Elga Lab Water, ThermoFisher Scientific Australia Pty Ltd).

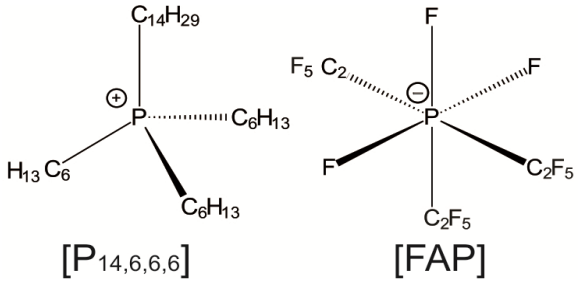

Figure 5.2.1. Room temperature ionic liquid structure used as organic phase at the ITIES: trihexyl(tetradecyl)phosphonium tris(pentafluorethyl)trifluorphosphate $[P_{14,6,6,6}][FAP]$.

5. 2. 2. Apparatus

All experiments were performed using an Autolab PGSTAT302N electrochemical analyser (Metrohm Autolab, Utrecht, The Netherlands). The microinterface array was formed using a silicon membrane containing micropore array of thirty micropores arranged in a hexagonal close-packed arrangement, each with a diameter of 22.4 μm and a pore-to-pore separation of 200μm. The fabrication of these membranes was previously reported.[33, 35] The fabrication procedure provided hydrophobic micropore walls. The silicon membranes were sealed onto the lower orifice of a glass cylinder using silicone rubber (Acetic acid curing glass silicone (Selleys Australia & New Zealand)). The aqueous phase solution was introduced into the glass cylinder, and the reference solution was placed in a fritted glass tube. The silicon membrane and fritted glass cylinder were then immersed into the ionic liquid as described previously.[115] The total geometric area of the W/RTIL microinterface array was 1.18 x 10^{-4} cm^2. The electrochemical cell is summarised as follows, where *x* is the concentration of HEWL or $TPrA^+$ in the aqueous phase:

Ag | AgCl	*x* μM HEWL and / or *x* μM $TPrA^+$ in 10mM of HCl or LiCl	RTIL $[P_{14,6,6,6}]^+[FAP]^-$	10mM LiCl +satd. $[P_{14,6,6,6}]^+Cl^-$	AgCl | Ag

Scheme 5.2.1. Electrochemical cell.

5. 2. 3. Electrochemical measurements

A two-electrode arrangement was employed for all measurements. Alternating Current Voltammetry (ACV) was carried out at 6 Hz (frequency) and 5 mV (amplitude); Cyclic Voltammetry (CV) was implemented at a scan rate of 5 mVs^{-1} unless specified; Adsorptive Stripping Voltammetry (AdSV) was implemented using parameters described in the text and figures. Electrochemical impedance spectroscopy (EIS) was performed at an amplitude of 5 mV over the frequency range from 100 kHz to 0.1 Hz.

5. 2. 4. Mass Spectrometry

Biphasic electrospray ionisation - mass spectrometry (BESI-MS) analyses were performed using a three-channel microchip fabricated via laser ablation. The microchip was fabricated on polyimide laminated with polyethylene/polyethylene terephthalate films (Morane Ltd., Banbury, UK). The microchannels are 50 and 100 μm in depth and width respectively.[122, 123] One of the channels was filled with carbon ink to induce the spray (see Chapter 2, Section 2.6.3). Then the carbon electrode is connected to an external power source to apply the high voltage required for electrospray ionisation (ESI) of the sample.[123] These modifications to the ionisation procedure have been reported by Girault's group.[122, 123] The microchip was fixed in a holder connected to a syringe pump (KDScientific, Holliston, MA, USA) and three 100 mL syringes (Hamilton, Bonaduz, Switzerland) were used to inject the different solutions. These experiments were performed on a Thermo LTQ Velos mass spectrometer. During ESI, the spray voltage of the internal power source of the LTQ Velos was set to 0 V although the external power source was set up to ± 9 kV. An enhanced ion trap scan rate (10,000 Th/s) was selected to obtain a good spectral resolution. All the MS data were processed using the program Xcalibur from ThermoThermo Fisher Scientific Inc. (Hampton, New Hampshire, USA).

BESI-MS experiments were carried out in Prof. Hubert Girault's Laboratory of Physical and Analytical Electrochemistry (LEPA) at École Polytechnique Fédérale de Lausanne (EPFL) in Lausanne, Switzerland.

5.3. Results and Discussion

5.3.1. Acidic W/RTIL

5.3.1.1. Cyclic voltammetry

Previous studies demonstrated that acidic conditions promote the best detection of proteins, because the protein is cationic and can interact with many organic phase anions at the interface, leading to more sensitive detection.[77] Hence the behaviour of the acidic W/RTIL interfaces was examined before the study of protein behaviour. Figure 5.3.1 shows CV at the micro-interface array formed between either aqueous 10 mM LiCl or aqueous 10 mM HCl and the room temperature ionic liquid,

$[P_{14,6,6,6}]^+[FAP]^-$. The potential window observed (~500 mV) is limited by chloride transfer at -0.45 V and by $[FAP]^-$ transfer at +0.10 V. An increase in current at -0.01 V in the forward CV sweep (Figure 5.3.1) of the 10 mM HCl W/RTIL interface suggests a charge transfer process takes place at this interface. This charge transfer is absent when the aqueous phase is comprised of 10 mM LiCl. It appears that the presence of aqueous phase protons results in voltammetry which is different from that of a cell with only background electrolytes present in each phase, i.e. a conventional organic phase like 1,2-dichloroethane with an acidic aqueous solution.[78, 79]

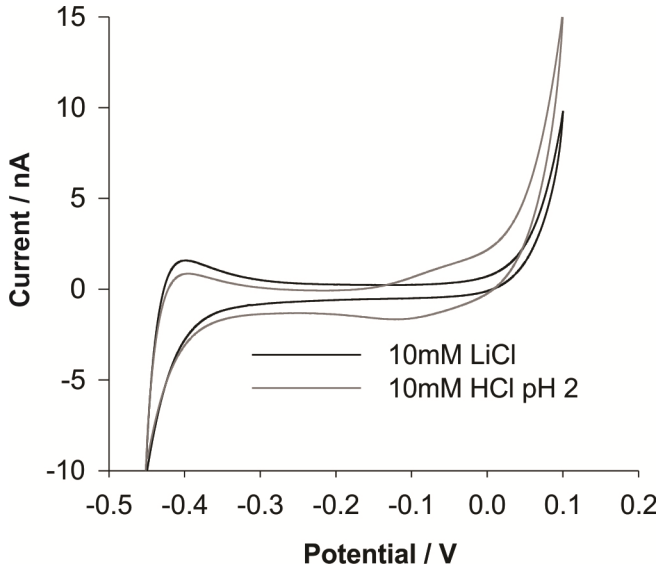

Figure 5.3.1. Cyclic voltammetry at the micro-interface array between water and the RTIL $[P_{14,6,6,6}][FAP]$. The aqueous phase is either 10 mM LiCl (black line) or 10 mM HCl at pH 2 (grey line). Scan rate: 5 mVs^{-1}.

The influence of the aqueous phase acid concentration on this charge transfer process was investigated. Concentrations of HCl between 1 mM and 500 mM were employed in the aqueous phase and CV experiments implemented. Figure 5.3.2 shows some of these results. In these experiments, the aqueous phase contained only HCl at the stated concentration, and no other electrolyte was intentionally added. It was not possible to detect HCl at 1 mM concentration, whereas at 5 mM a shoulder appeared towards the positive end of the potential window. As shown in Figure 5.3.2, concentrations of HCl at 10, 50 and 100 mM were easily detected on the forward sweep towards the upper limit of the potential window, and on the reverse sweep at the higher concentrations shown. Thus the forward current may be attributed to

transfer of a cation species, probably H_3O^+, and the reverse current to its back transfer.

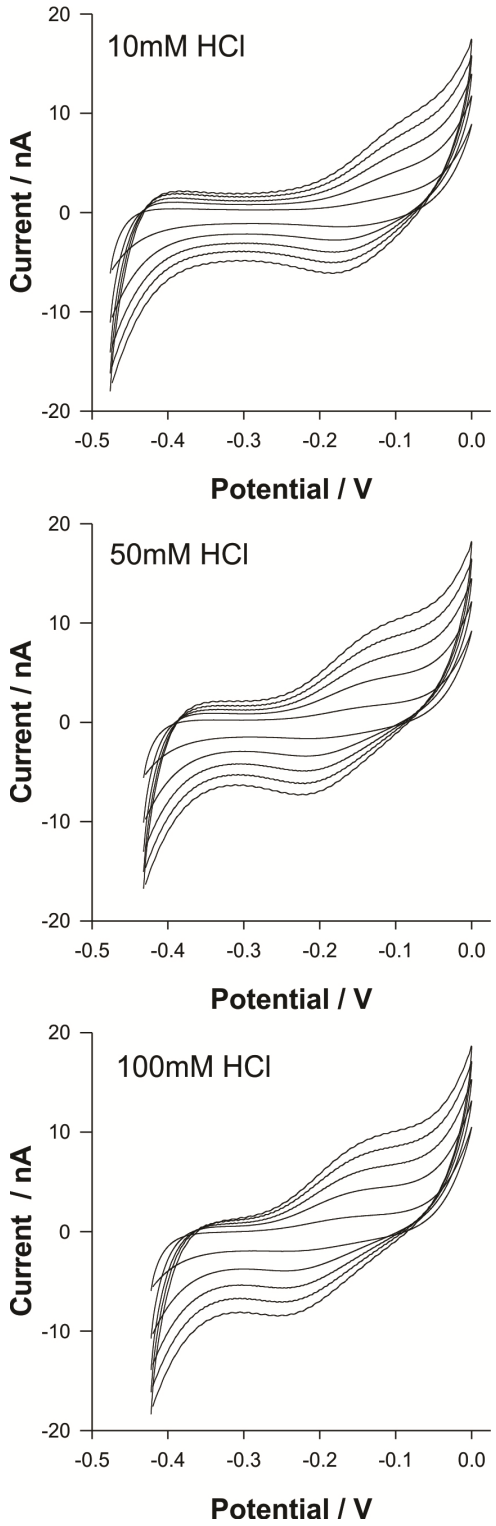

Figure 5.3.2. Cyclic voltammetry at the micro-interface array between water and the RTIL $[P_{14,6,6,6}][FAP]$. The aqueous phase is 10, 50 or 100 mM HCl at different scan rates: 5, 10, 25, 50, 75 and 100 mVs^{-1}.

The CVs in Figure 5.3.2 exhibit some notable features. The current on the forward sweep reaches a steady-state, which is consistent with radial diffusion to microinterfaces, whereas the reverse scans exhibit a peak-shaped voltammogram, consistent with linear diffusion or an adsorption/desorption process. Furthermore the steady-state forward current increases with the scan rate. The diffusion-limited steady-state current (I_{lim}) at a micro-interface array is described by the equation

$$I_{lim} = n4z_iFDCr \qquad (5.3.1)$$

(where n is the number of microinterfaces, z_i, D and C are the charge, diffusion coefficient and bulk concentration of the transferring species, and r is the radius of one interface). Thus for the diffusion-controlled transfer of hydronium species at a W/RTIL interface array consisting of 30 microinterfaces, the limiting current is expected to be 13μA, 65μA and 130μA at each of the concentrations shown in Figure 5.3.2 (10, 50 and 100 mM). These values are in disagreement with the experimental data which show limiting currents several orders of magnitude lower than the estimated for $D_{H3O+} \sim 10^{-4}$ cm^2s^{-1},[201] for hydronium in bulk solution. However, this does not fully explain the voltammetry obtained for acidic W/[$P_{14,6,6,6}$][FAP] interfaces which suggest hydronium reverse transfer on the reverse scan (see Figure 5.3.2 and 5.3.3) based on the shape of the reverse wave. If the reverse waveform was diffusion-controlled, a peak-shaped voltammogram would be generated according to the linear diffusion of the cationic species from RTIL to the aqueous phase.

Upon changing the acid concentration of the aqueous phase, it is notable that the width of the potential window decreased with increasing HCl concentration, consistent with the lower limit being marked by chloride transfer (see Figure 5.3.3a). However, by maintaining a constant total chloride concentration by preparation of mixtures of HCl and LiCl, a current wave on the forward CV scan was seen to increase with acid concentration (see Figure 5.3.3b).

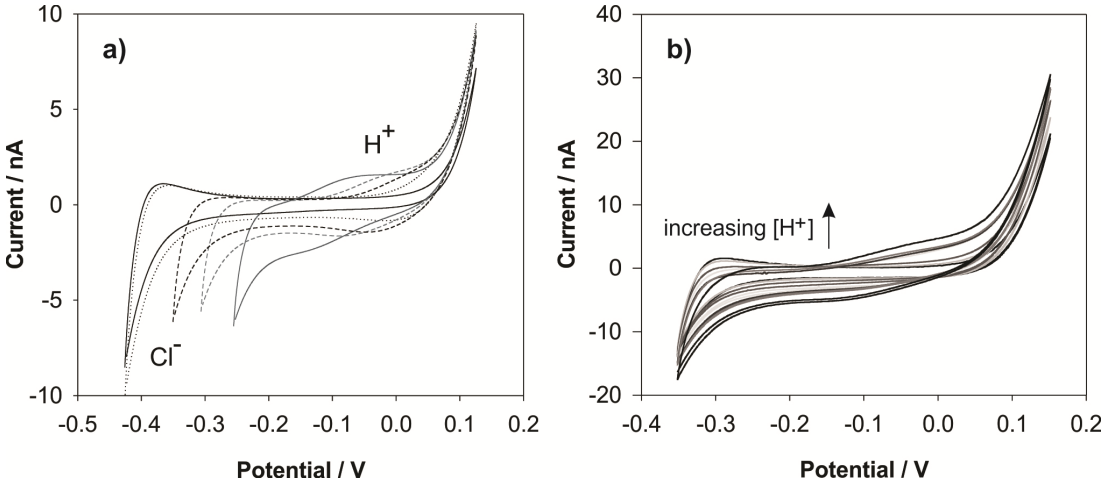

Figure 5.3.3. CVs at the W/[$P_{14,6,6,6}$][FAP] micro-interface array of a) different concentrations of HCl: 100 µM (—), 10 mM (····), 50 mM(- - -), 100 mM (- - -) and 500 mM (—) and b) different concentrations of HCl:LiCl solution with increasing concentrations of HCl as follows; 0:100, 0.1:99.9, 1:99, 10:90, 50:50 and 100:0 mM.

For simple ion-transfer voltammetry at µITIES such as used here, a forward transfer wave and a reverse transfer peak is expected for diffusion-controlled forward and reverse processes.[35, 115, 202] The shape of the voltammogram in Figure 5.3.3b suggests that there is radial diffusion of the transferring species, hydroniums, during the forward scan, but no linear diffusion of the transferring species during the reverse scan.

The data in Figure 5.3.2 show that under the conditions employed, the limiting currents change with scan rate. Although the charging current (before the transfer wave) also changes, the latter change is smaller than that occurring on the limiting current region. However, for a micro-interface such as used here, the limiting current is expected to be independent of the scan rate or square root of the scan rate, if radial diffusion is the controlled factor. The scan rate dependence of the reverse scans in Figure 5.3.2 is expected, if the process involves either linear diffusion or a desorption process. In addition, the shift in the half-peak potential was evaluated for different concentrations of HCl. Due to the short potential window and the simultaneous transfer of $TPrA^+$ and H_3O^+, the measurement of the half-peak potential of H_3O^+ transfer against $TPrA^+$ became challenging. For this reason, different concentrations of HCl were characterised in the presence and absence of $TPrA^+$. To quantity the shift in potential caused by the increase of hydroniums in solution, the potential

difference between the half-peak potential ($E_{1/2}$) of the H_3O^+ transfer and the potential corresponding to 5 nA on the forward current (E_{5nA}) was measured as shown in Figure 5.3.4a. Then these values were referred to the transfer potential of $TPrA^+$ (E_{TPrA+}) obtained from the CVs (see Figure 5.3.4b).

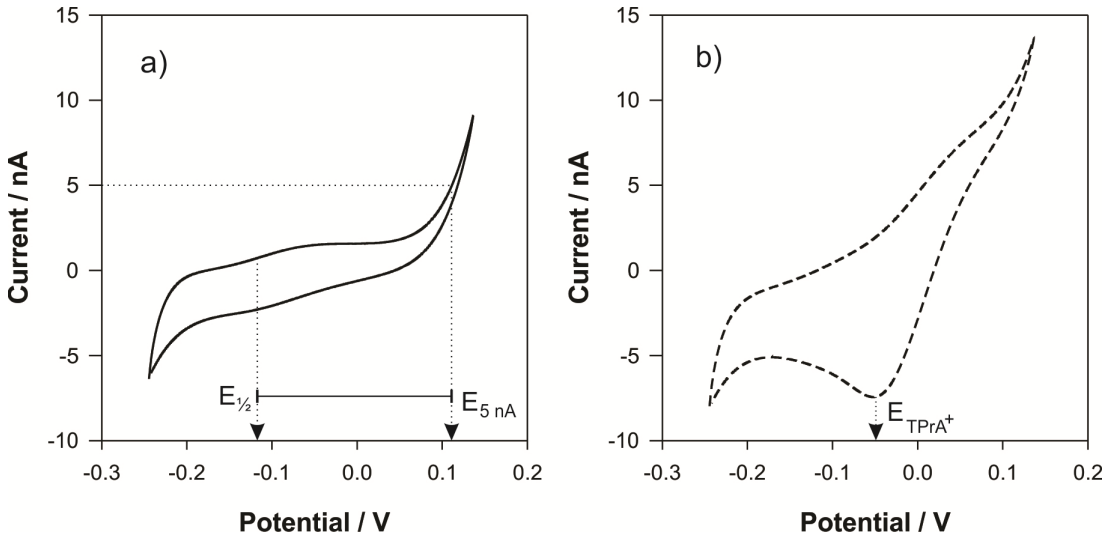

Figure 5.3.4. CVs at the W/[$P_{14,6,6,6}$][FAP] micro-interface array of a) 500 mM HCl in 1 mM LiCl (—) and b) 500 mM HCl in 1 mM LiCl + 100 µM $TPrA^+$ (- - -). $E_{1/2}$ is the half-peak potential of the H_3O^+ transfer, E_{5nA} is the potential corresponding to 5 nA on the forward current and E_{TPrA+} is the transfer potential of $TPrA^+$.

The half-peak potential ($E_{1/2}$) varies linearly with proton concentration which slope corresponds to 64mV, see Figure 5.3.5. The results of the forward potential shift as a function of pH (remember pH = -log[H_3O^+]), this shows the similarity to a one electron transfer in a redox reaction at solid electrodes (59 mV variation in the half cell potential per 10-fold change in the concentration of the species) which could be comparable to a one positively charge species (H_3O^+) transferring across the interface.

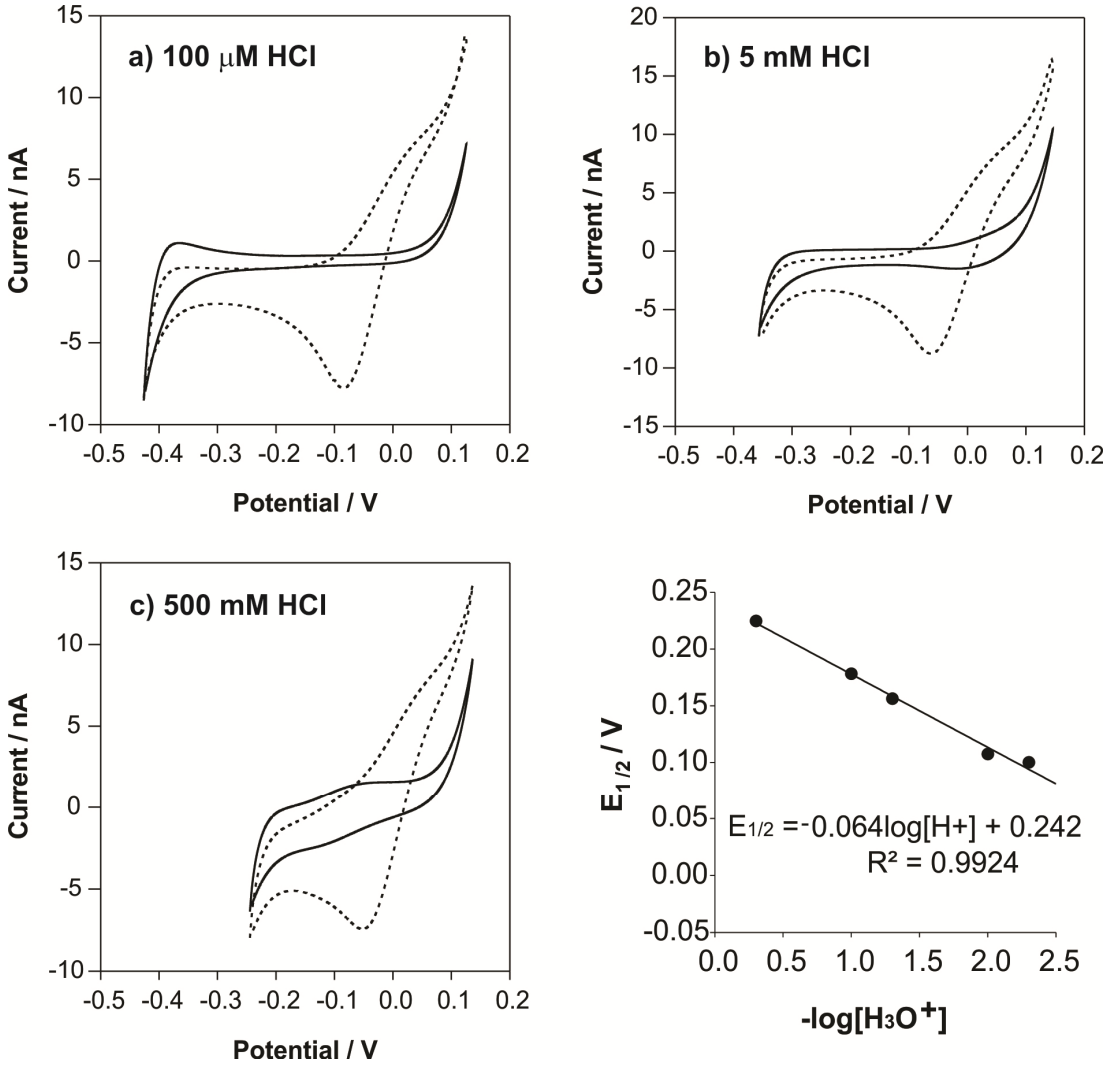

Figure 5.3.5. CVs at the W/[$P_{14,6,6,6}$][FAP] micro-interface array of a) 100 μM HCl in 1 mM LiCl (—) + 100 μM $TPrA^+$ (···), b) 5 mM HCl in 1 mM LiCl (—) + 100 μM $TPrA^+$ (···) and c) 500 mM HCl in 1 mM LiCl (—) + 100 μM $TPrA^+$ (···). The graph in the bottom right hand side represents half-peak potential of hydronium versus pH (pH = -log[H_3O^+]).

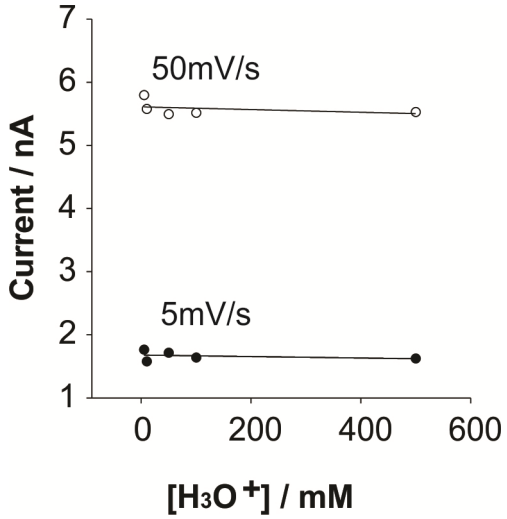

Figure 5.3.6. Current values of the forwards peaks at 5 and 50 mV/s versus the concentration of H_3O^+ and half-peak potential versus pH (pH = -log[H_3O^+]).

One possibility for the scan rate dependence shown by the forward limiting currents (Figure 5.3.6) is that the ion transfer process leads to the formation of a new phase at the interface which adds to the capacitance of the system. Studies using EIS and ACV were implemented to investigate this possibility.

5.3.1.2. Electrochemical impedance spectroscopy

Electrochemical impedance spectroscopy (see Figure 5.3.7) and alternating current voltammetry techniques were performed in order to elucidate the mechanism involved at the W/RTIL micro-interface array. Figure 5.3.7A shows a Nyquist plot of 50 mM HCl in 1 mM LiCl (dotted line) and 1 mM LiCl (solid line) in the absence of HCl at the W/RTIL interface polarised at -0.2 V which corresponds to a potential where there is no charge transfer process across the W/RTIL interface. Figure 5.3.7B presents the Nyquist plot of 50 mM HCl in 1mM LiCl at two different potentials: -0.2 V (dotted line) and 0.0 V (solid line) where the latter corresponds to the potential where protons are interacting at the polarized micro-interfaces. On the right side of both Nyquist plots, the corresponding equivalent circuits which best fit the experimental data are shown. The fitted equivalent circuit shows a series and parallel combination of resistances (Rs, Rm and Rdl) and capacitances (non-ideal CPm-CPdl and ideal capacitor Cnew). Rs corresponds to the resistance of the solution and Rm and CPm can be attributed to the membrane-pores because it is constant and

independent of the potential applied. Rdl and CPEdl correspond to a slower diffusion process at lower frequencies (right part of the Nyquist plot).

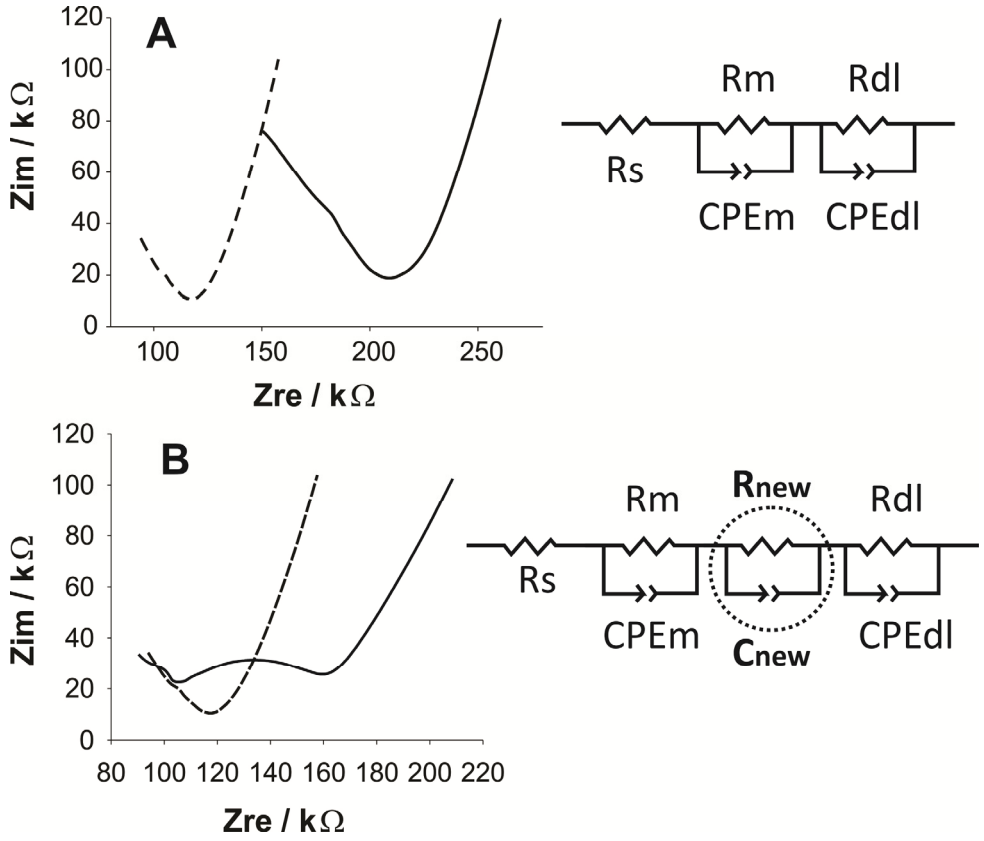

Figure 5.3.7. Electrochemical Impedance Spectroscopy (EIS) of: A) (–) 1 mM LiCl, and (- -) 50 mM HCl in 1 mM LiCl at a potential where there is no transfer processes involved (-0.2 V) and B) (- -) 50 mM HCl in 1 mM LiCl at -0.1 V where there is proton – ionic liquid interaction. Right hand side of the graphs correspond to the equivalent circuit which fits A) impedance at -0.2V and B) impedance at -0.1 V in the presence of HCl.

In the case of 50 mM HCl in 1 mM LiCl, where the impedance is measured at different excitation potentials, a new feature is observed. It consists of a round shoulder (camel-shaped) between 100 and 160 kΩ on the real impedance axis. This new rounded peak increases, reaching an impedance maximum of 30 kΩ. The new feature (Rnew and Cnew) occurs at high frequencies meaning that this is a fast process which is 2 or more orders of magnitude faster than the diffusion observed at lower frequencies (Rdl and CPdl). Similar experiments were carried out for different hydrochloric acid concentrations, all of which produced a similar Nyquist plot (see Figure 5.3.8). The camel-shaped peak is independent of the hydrochloric acid concentration above a certain concentration, perhaps due to saturation (Figure 5.3.8).

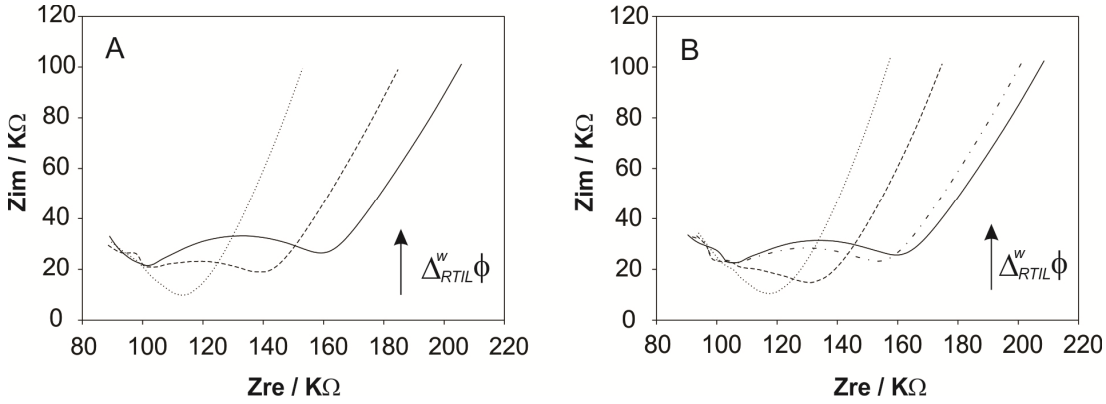

Figure 5.3.8. Electrochemical Impedance Spectroscopy (EIS) analysis of: A) 50 mM HCl in 1 mM LiCl at different applied potentials and B) 10 mM HCl in 1 mM LiCl different applied potentials from -0.3 V (···) to -0.05 V (—).

This new feature fits to a circuit with an additional capacitor, which suggests a change at the W/RTIL interface due to the transfer of hydronium cations and their interaction with $[P_{14,6,6,6}][FAP]$. Relative dielectric permittivity (ε_r) values reported in the literature for a wide range of ionic liquids vary between 8 and 16,[203, 204] although is not available for the RTIL used here. Assuming that the dielectric permittivity (ε_r) of $[P_{14,6,6,6}][FAP]$ is within this range and the geometric area (A) of the microinterface array is 1.18 x 10^{-4} cm^2 then the thickness of this capacitor can be calculated using Equation 5.3.2. The capacitance of the new capacitor (C) corresponds to 3.7 x 10^{-10} F which was obtained from the equivalent circuit (Cnew in Figure 5.3.7B) which best fit the experimental data. Therefore, the new capacitive layer at the W/RTIL microinterface array corresponds to a thickness of ~2.3 – 4.5 nm.

$$C = \frac{\varepsilon_0 \varepsilon_r A}{d} \qquad (5.3.2)$$

where C is the capacitance, ε_r is the relative dielectric permittivity, ε_0 is the electric constant (8.5 x 10^{-12} $F \cdot m^{-1}$), d is the thickness and A is the area.

Recently Fedorov and Kornyshev have suggested the formation of 'voids' in the ionic liquid structure in order to explain the camel-shaped capacitance of the electrical double layer at metal/RTIL interfaces.[205, 206] The idea of cavities is well-known in crystallography and it has been suggested that ionic liquids may contain voids which can accommodate small molecules. This theory is in accordance with

the transfer of hydronium cations across the W/RTIL microinterfaces to form a mixed-ionic liquid layer which introduces an additional capacitance into the electrochemical cell. Solvated lithium cations are approximately three times bigger in terms of hydrodynamic radius than solvated protons. If Li^+ is solvated with n number of water molecules (n = 1-6 and 8 H_2O),[207] the theoretical diameter for $Li(H_2O)_4^+$ would be *ca.* 6 Å assuming that Li-O bond length is 1.942 Å[208] and O-H distance is 1.1 Å.[209] For the hydronium, solvated proton, the diameter is ~ 2.8 Å.[210] If the anions $[FAP]^-$ are considered as spheres and the cation $[P_{14,6,6,6}]^+$ as an ellipsoid both surrounded by counter ions, the calculated voids based on a closed packing arrangement are approximately between 3 and 4 Å is diameter size. These data have been calculated based on bond length (C-P 1.87 Å, C-C 1.54 Å, C-F 1.33 Å, C-H 1.09 Å.[211]) and are only illustrative. Thus, H_3O^+ would fulfill the ionic liquid voids theory reinforcing the idea of a capacitive neutral layer formed at the water/ionic liquid interface which reduces the mobility of hydronium within the ionic liquid.

5.3.1.3. Alternating current shift potential

AC voltammetry of LiCl and HCl (see Figure 5.3.9) was also analysed at different phase angles (0° and 90°) as another qualitative analysis of interfacial behaviour. This method has been used previously to study adsorption at the ITIES of nanoparticles[212] and biomacromolecules.[81] A shift of the potential of zero charge (pzc) towards more negative potentials in the presence of acid in the aqueous solution suggests adsorption of hydronium ions at the water - $[P_{14,6,6,6}][FAP]$ microinterface. Studies of positively charged haemoglobin at water/organic solvent interfaces[213] suggest a shift of the pzc to more negative potentials, as indicated in this case. The dashed line in Figure 5.3.9 also reveals the reversibility of this process; AC voltammograms remain the same (with the same pzc) in a 10mM LiCl solution before and after W/RTIL was exposed to hydrochloric acid (solid and dotted lines). There is no potential shift at the LiCl/$[P_{14,6,6,6}][FAP]$interface after the exposure to a highly protonated solution. Another interesting feature is the shoulder which appears in the range of -0.2 to 0 V under acidic conditions. This increase in capacitance is in agreement when the transfer of hydronium cations at more positive potentials.

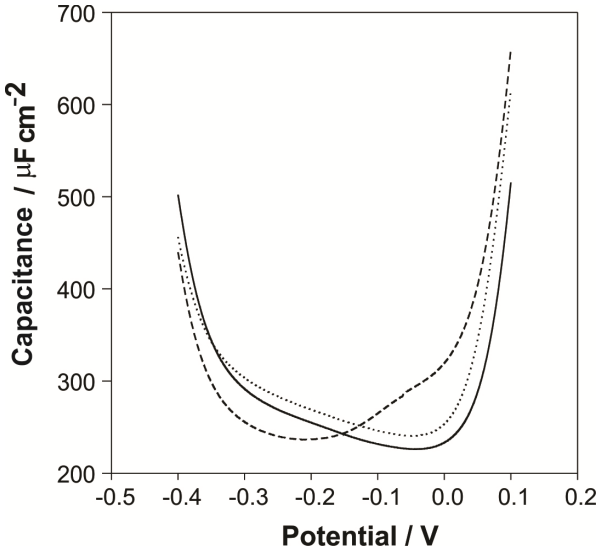

Figure 5.3.9. Alternating Current Voltammetry (AC) of 10 mM LiCl (solid line), 10 mM HCl (dashed) and 10 mM LiCl after ionic liquid exposure to HCl (dotted line).

The electrochemical results suggest a combination of hydronium cation transfer and association with the ionic liquid material to form a new capacitive layer at the interface. This may explain why the CV limiting current changes with scan rate but remains as a steady-state current. These interactions involve hydronium diffusion into $[P_{14,6,6,6}][FAP]$ up to a certain concentration where no more H_3O^+ can cross the interface. This saturation could be explained by the formation of a new layer, maybe of $[FAP]^-$ anions and H_3O^+ cations due to strong electrostatic interactions. Strong interactions between H^+ and $[FAP]^-$ have also been reported in an electrochemical study of hydrogen gas oxidation in a range of RTILs.[214] This hypothesis is in agreement with the formation of a new layer at the W/RTIL with capacitor properties which are observed in the EIS measurements. Additionally, cyclic voltammograms at different scan rates with hydrochloric acid have demonstrated H_3O^+ reversible transfer across the W/$[P_{14,6,6,6}][FAP]$ microinterfaces. However this process is not purely diffusion controlled. This diffusion limitation may be explained due to the strong interactions between the hydronium cations and $[FAP]^-$ anions from the ionic liquid which led to the formation of a net neutral layer.

5.3.1.4. IR and NMR spectroscopy

In order to assess this process, NMR and IR spectroscopy measurements were carried out after saturation of the ionic liquid with water or hydrochloric acid. In both case, the data did not reveal any change in the spectra of the RTIL under the different environments (see Appendix B).

5.3.1.4. Biphasic electrospray ionisation - mass spectrometry

Finally biphasic electrospray ionisation - mass spectrometry (BESI-MS) using a microfluidic device was used as another alternative to study charge interactions. Figure 5.3.10 illustrates the microfluidic chip and the ionisation process prior to MS. The solutions of RTIL, methanol and water, hydrochloric acid or acetic acid were injected at 40 µL/h and monitored in the negative mode to follow the interactions of the anion of the ionic liquid.

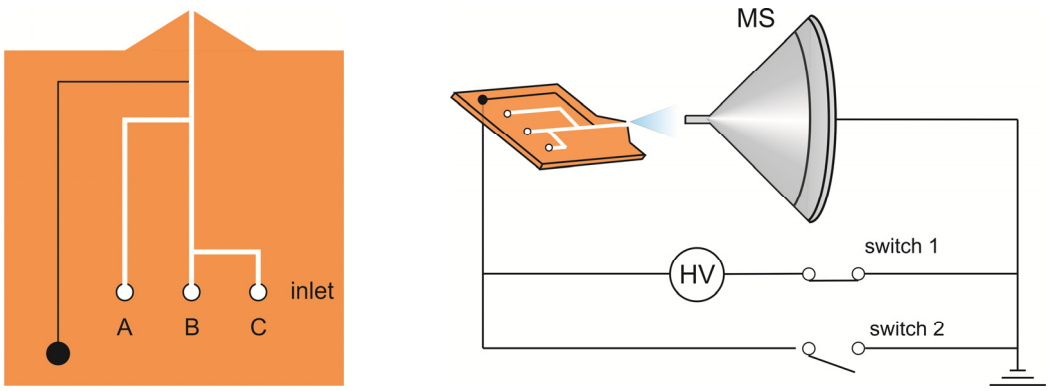

Figure 5.3.10. BESI microchip design (diagram on the left) and integration of the microchip with the mass spectrometer (diagram on the right).

The MS spectra plotted in Figure 5.3.11 show the *m/z* values for $[FAP]^-$, 445.09 and for $[FAP/P_{14,6,6,6}/FAP]^-$ 1,373.11 when the ionic liquid and water are in contact. When the ionic liquid is in contact with 0.5 M HCl, the spectrum is similar regarding the anionic composition.

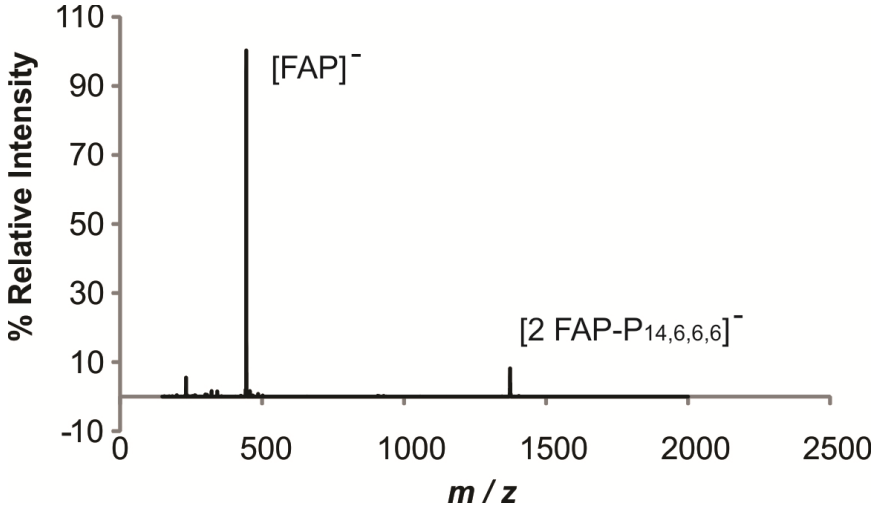

Figure 5.3.11. Mass spectrum of $[P_{14,6,6,6}][FAP]$ when electrosprayed with water.

However, the relative intensity of the ions with respect to the initial signal (Figure 5.3.11) when RTIL was exposed to HCl, decreased dramatically. There is a decrease in the signal of 99.8% in 2 minutes (see Figure 5.3.12a). In Figure 5.3.12b, similar data is shown. In this case (Figure 5.3.12b), the aqueous solution contained 1% of acetic acid instead of 0.5 M HCl. This information confirms the hypothesis of strong interactions between hydroniums and $[FAP]^-$ at the W/RTIL interface. As the hydroniums are present in the biphasic mixture, they interact neutralizing the anionic form of the ionic liquid which is not detectable form in MS. Thus, this results in a significant decrease in the signal intensity (99.8%), which is in agreement with the proposition of a neutral layer formation at the W/RTIL when performing electrochemical analysis.

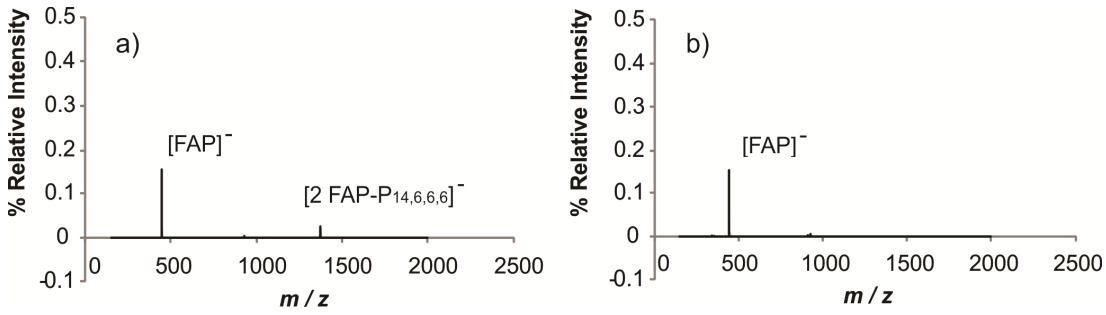

Figure 5.3.12. Spectra of $[P_{14,6,6,6}][FAP]$ in contact with a) 0.5 M HCl and b) 1% acetic acid (HAc) with respect to 100% relative intensity for RTIL and water.

Taking into account all the data obtained, a charge transfer process has been revealed to take place at the W/RTIL involving hydronium interactions with $[FAP]^-$, the anion present in the ionic liquid. Figure 5.3.13 summarises the suggested process taking place at the W/$[P_{14,6,6,6}][FAP]$ micro-array interface. Figure 5.3.13A corresponds to the interface composition at the equilibrium when there is no potential difference applied while Figure 5.3.13B shows the diffusion of hydronium molecules across the polarized interface forming a new H_3O^+ / RTIL layer which behaves as an electrical capacitor.

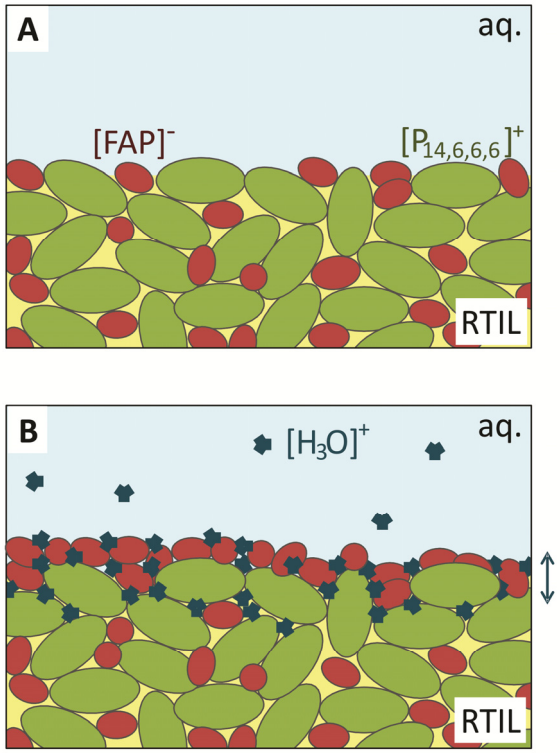

Figure 5.3.13. Sketch of the suggested process involved at the polarised interface between water and $[P_{14,6,6,6}][FAP]$. A) Shows the typical unpolarised W/RTIL interface and B) in the presence of protons at a certain potential applied where H_3O^+ interacts with the ionic liquid forming a new thin layer of H_3O^+ / RTIL.

5.3.2. Lysozyme at W / RTIL

Besides the phenomenon described in the previous section, the μ-W/RTIL interfaces were evaluated under acidic conditions in order to detect a model protein, hen-egg-white-lysozyme (HEWL) as reported in Chapter 3 and several publications.[77, 78] The possible interference of hydronium during protein analysis is also under study in this section.

5.3.2.1. Alternating current shift potential

Initial studies by cyclic voltammetry (CV) with lysozyme dissolved in an aqueous 10 mM LiCl phase did not reveal any charge transfer processes within the available potential window. However alternating current (AC) voltammetry (Figure 5.3.14) showed a shift (ca. 100 mV) in the potential of minimum capacitance to negative values when lysozyme was present. This negative shift is consistent with the adsorption of a cationic species at the interface.[81, 212] In such a case, it is possible that there is potential–dependent adsorption of lysozyme at the interface but no interfacial charge transfer, so that any changes are not easily detectable by CV.

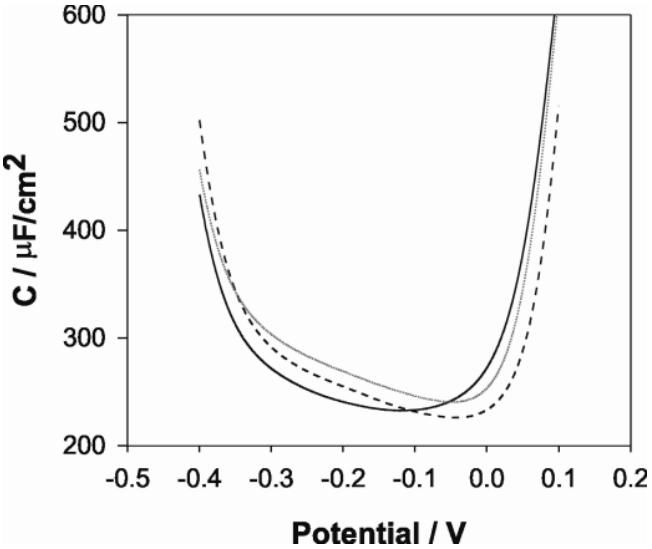

Figure 5.3.14. Alternating Current Voltammetry (ACV) at the μ-array W/[P14,6,6,6][FAP] interface of 10 mM LiCl (dashed line), 10 μM lysozyme (solid line), and 10 mM LiCl (grey line) after protein exposure.

5.3.2.2. Distortion of simple ion transfer by adsorption

In previous work,[79] the most sensitive detection of lysozyme at aqueous-organic interfaces was obtained when the aqueous phase was acidic, at a pH lower than the protein's isoelectric point. At pH 2, lysozyme is fully protonated (pI = 11.35) with 17 positive charges[150, 215] and the best sensitivity was obtained under these aqueous conditions at water-organic interfaces. When the aqueous phase is 10 mM HCl in the W/RTIL system, there was no obvious response in the CVs for 10 and 100 μM lysozyme. This could be because of the limited potential window at the W/RTIL interface, which is much narrower than that at aqueous/organic interfaces or the possible interference caused by the capacitive layer formed when hydroniums interact at the W/RTIL interface. However, a qualitative indication of some interactions of lysozyme with the interface under these conditions was obtained by undertaking CV of a simple ion transfer process in the absence and presence of lysozyme in the aqueous phase. Ion transfer CV of 100 μM tetrapropylammonium ($TPrA^+$), from the water phase to the hydrophobic ionic liquid $[P_{14,6,6,6}][FAP]$ phase, was undertaken in the absence and presence of 100 μM lysozyme (Figure 5.3.15). The ion transfer of $TPrA^+$ is dominated by mass transport, with radial diffusion on the forward scan producing a steady-state voltammogram, and linear diffusion on the reverse scan producing a peak-shaped voltammogram.[115] As shown in Figure 5.3.15, this ideal response is distorted to some extent by the presence of lysozyme in the aqueous phase (dotted line). This can be attributed to the presence of a layer of adsorbed protein material at the interface. Although no obvious charge transfer process was obtained by CV, it should be noted that even at aqueous/organic interfaces operated under conditions of a gelled organic phase and in a microinterface array format, no obvious voltammetric waves or peaks were observed on the forward CV scans (see Chapter 3, Section 3.3.1).

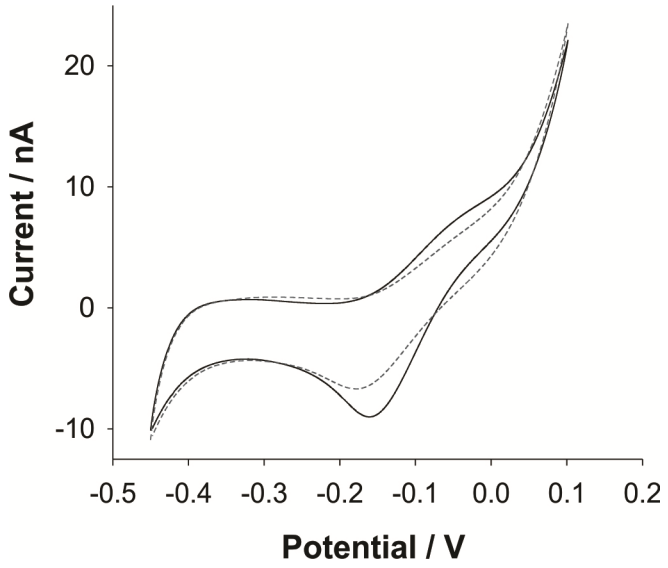

Figure 5.3.15. Cyclic voltammetry at the μ-array W/[P14,6,6,6][FAP] interface of aqueous phase 100 μM $TPrA^+$ in the presence (- - -) and absence (—) of aqueous phase 100 μM lysozyme in 10 mM HCl.

5.3.2. 3. Adsorption of lysozyme

The reverse scans of these CVs usually reveal a peak-shaped voltammogram due to desorption of the protein from the ITIES. Thus adsorptive-desorption strategies employing a constant-potential adsorption followed by a desorptive voltammetric scan can be employed to collect the protein at the W/RTIL interface and subsequently to detect it by desorption. A variety of potentials between -0.2 V and +0.1 V, at intervals of 50 mV, were investigated for lysozyme adsorption at the W/RTIL interface (Figure 5.3.16). It was found that only at the very positive edge of the potential window, where the RTIL anion $[FAP]^-$ commences transfer across the interface, was a peak recorded on the scan to lower potentials (Figure 5.3.16). Interestingly, another feature is observed at the voltammogram (-0.15 V) which could correspond to the hydronium desorption wave described in the previous section. Thus the peak at -0.02 V could potentially be attributed to lysozyme being desorbed from the water/ionic liquid interface.

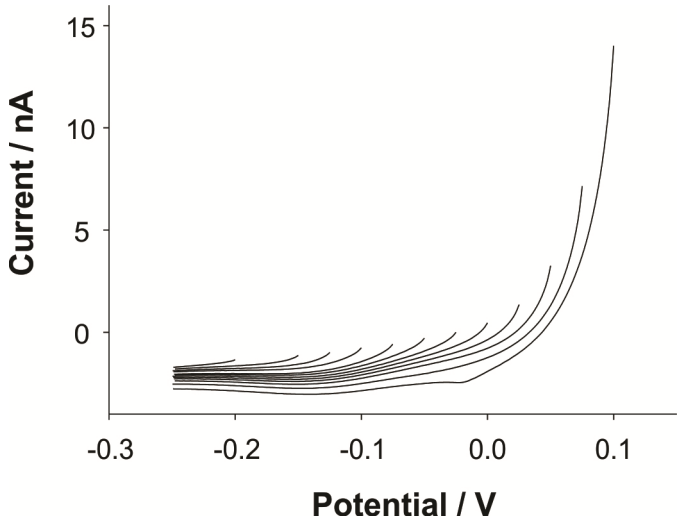

Figure 5.3.16. AdSV of 10 μM lysozyme after a constant potential adsorption of 60 s at different applied potential.

Implementation of this procedure for 10 μM lysozyme at different adsorption times is illustrated in Figure 5.3.17. When increasing the pre-concentration time at 0.1 V, the desorption peaks observed also increase in terms of peak height and area and the wave attributed to hydronium-[FAP] interactions remains constant under the different conditions.

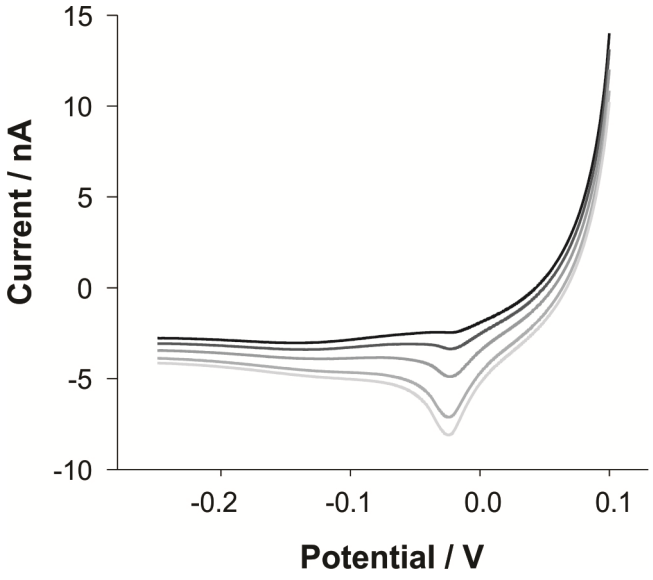

Figure 5.3.17. AdSV at the μ-array W/[$P_{14,6,6,6}$][FAP] interface of 10 μM lysozyme in the aq. phase (10 mM HCl) following constant potential adsorption for 60, 120, 240, 480 and 600 s at an adsorption potential of 100mV.

Similar experiments performed in the absence of aqueous phase lysozyme did not produce any peaks on the voltammetric scan to lower potentials, indicating that the peaks shown in Figure 5.3.16 and 5.3.17 were due to the presence of lysozyme. In separate experiments (Figure 5.3.18), in which the RTIL was dissolved in an organic phase of 1,6-dichloroethane and polyvinyl chloride, $[FAP]^-$ transfer from organic to aqueous phase was found to be the limiting process at the positive side of the available potential window; this means that application of sufficiently high potentials can be employed to drive $[FAP]^-$ transfer to the aqueous phase. However in the pure RTIL phase, reverse scan peaks were only obtained in the presence of aqueous phase lysozyme.

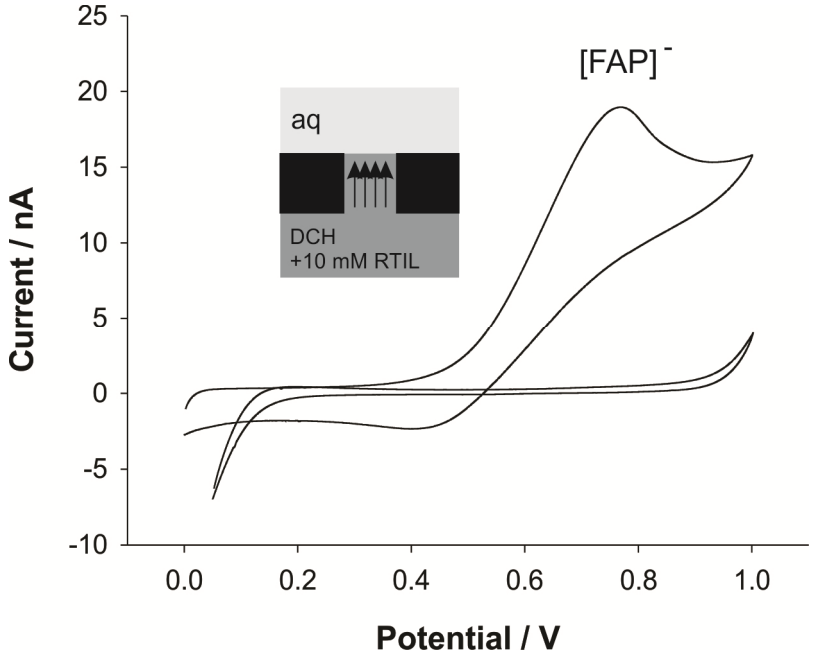

Figure 5.3.18. CV of 10 mM HCl at the W / gelled 1,6-DCH which contains 10 mM $[P_{14,6,6,6}][FAP]$. Peak-shaped is due to linear diffusion of $[FAP]^-$ from the organic phase to the aqueous phase. Flat voltammogram correspond to the signal of 10 mM HCl at the W / gelled 1,6-DCH when there is no RTIL present in the organic phase.

5.3.2.4. Scan rate dependence

The magnitude of these reverse-scan peaks was seen to vary with the voltammetric scan rate, with higher scan rates leading to larger peaks (Figure 5.3.19). It was found that the peak currents varied linearly with the square root of the scan rate ($i_p=0.443v^{1/2}+0.208$, $r=0.999$, where i_p is the peak current, v is the voltammetric

scan rate and *r* is the linear correlation coefficient), which is contradictory to expectations based on the bell-shaped peak obtained on the voltammetric scans towards lower potentials. These bell-shaped voltammetric curves are usually indicative of adsorption or desorption processes.

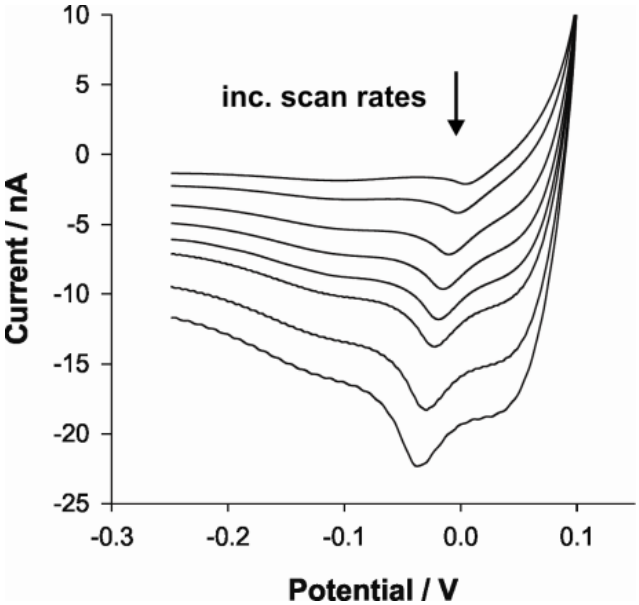

Figure 5.3.19. AdSV at W/[$P_{14,6,6,6}$][FAP] μ-interfaces of 100 μM lysozyme in 10 mM HCl (aqueous phase) at different scan rates (5, 10, 20, 30, 40, 50, 75 and 100 mV s^{-1}) following 60 s adsorption at an applied potential of 100 mV.

Nevertheless the background charging current also increased substantially when the scan rate was increased, making measurement of the peak currents at different scan rates difficult. As a result, these desorption peaks represent the disruption of the lysozyme-[FAP] complex that has formed at the interface during the constant-potential adsorption time and the removal of lysozyme from the interface back to the aqueous phase. By integration of the area under the peaks (Figure 5.3.17 or Figure 5.3.19), values of the surface coverage of lysozyme at the W/RTIL interface can be determined by relating the peak charge (Q) to the total moles of substance using Faraday's law ($Q = m \cdot z_i \cdot F$; m is the moles of substance, z_i is the charge transferred per molecule and F is Faraday's constant) and assuming that under these conditions the lysozyme is fully protonated (+17 charge) and that each of these charges on lysozyme is compensated by a $[FAP]^-$ anion when the complex forms at the W/RTIL interface. A surface coverage of 311 pmol cm^{-2} was obtained for 50 μM of lysozyme in the bulk solution when subjected to adsorption at the W/RTIL interface for a

period of 600 s. These surface coverage values are in agreement with those obtained at the water-organogel μITIES array (550 pmol cm^{-2}), see Chapter 3. Determining the surface coverage from voltammograms following adsorption from more concentrated aqueous phases (e.g. 75 and 100 μM lysozyme) was not possible due to the distorted voltammograms produced. Nevertheless, the results suggest a multilayer formation of lysozyme at the water-[$P_{14,6,6,6}$][FAP] micro-interfaces, assuming a single layer of lysozyme adsorbed at the W/[$P_{14,6,6,6}$][FAP] is 13 pmol cm^{-2} (see Chapter 3, Section 3.3.7).

By varying the protein concentration in the aqueous phase while implementing a constant adsorption potential and constant adsorption time, the voltammetric desorption peak current was seen to vary linearly with the aqueous phase concentration of lysozyme. The slope of the linear relationship between current and lysozyme concentration was 0.022 nA μM^{-1} and the calculated limit of detection (LOD) was 2.5 μM for a 60 s adsorption period; the corresponding values obtained for experiments at the water/gelled (1,6-DCH) μITIES array were 0.91 nA μM^{-1} and 0.06 μM, respectively (Chapter 3, Section 3.3.6). This lower sensitivity and higher LOD at the W/RTIL interface may be a result of the lower potentials that can be applied during the adsorption step at the W/RTIL interface, however a contribution from increased background current is also likely. Hydronium desorption from RTIL to the aqueous phase is visible at -0.15 V in the voltammogram (Figure 5.3.19) which also contributes to the distortion of the background signal. This process appears to co-exist with lysozyme-FAP disruption at the interface as both steps occur at different potentials (ca. 100 mV separation potential). It may be possible to lower the LOD by the use of a more hydrophobic ionic liquid, as this may lead to a wider potential window enabling more efficient adsorptive accumulation of the protein at the W/RTIL interface. Longer pre-concentration times may also be of benefit.

The electrochemical behaviour of protonated lysozyme at the W/RTIL microinterface array displayed here is very similar to that reported by Scanlon et al.[78, 79] and Hartvig et al.[88] for lysozyme at the water/organic ITIES. Two steps are believed to take place: charged lysozyme adsorbs at the W/RTIL interface under the influence of positive applied potentials; the adsorbed protein facilitates the transfer of RTIL phase anions to form a lysozyme-[FAP] complex at the interface (Figure

5.3.20). The influence of simultaneous hydronium transfer does not seem to interfere significantly in the protein detection.

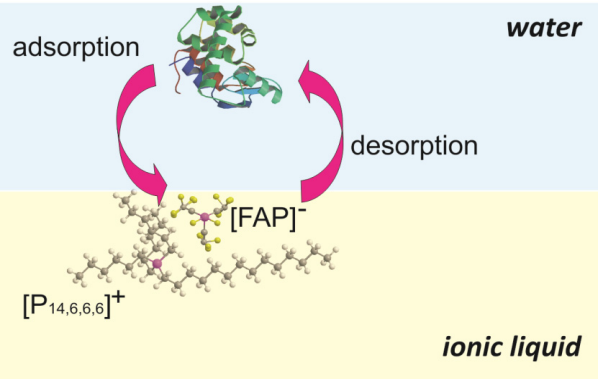

Figure 5.3.20. Proposed lysozyme adsorption-desorption mechanism at the water / ionic liquid ($[P_{14,6,6,6}][FAP]$) microinterfaces with facilitated anion transfer.

5. 4. Conclusions

Hydronium - tris(pentafluorethyl)trifluorphosphate $[FAP]^-$ interactions have been observed at the water – room temperature ionic liquid microinterfaces. Electrochemical studies such as impedance spectroscopy and voltammetric analysis suggest that H_3O^+ transfers across the $W/[P_{14,6,6,6}][FAP]$ forming a neutral capacitive thin film layer. Additional techniques have shown their limitations to provide extra information of this process although the biphasic electrospray ionisation – mass spectrometry studies seem to confirm the neutralisation of $[FAP]^-$ ions in the presence of H_3O^+ in a biphasic environment.

Moreover, the electrochemical behaviour of a protein, lysozyme, has been studied for the first time at a W/RTIL interface. An approach based on constant-potential adsorption followed by voltammetric desorption enables the detection of lysozyme in acidic aqueous solution down to 2.5 µM (following 60 s adsorption), where cyclic voltammetry was unable to detect the presence of the protein. The reaction is attributed to lysozyme adsorption at the interface, in conjunction with facilitated transfer of $[FAP]^-$ anions across the interface to form a complex with positively charged lysozyme, similar to the behaviour seen at water-organic[79] and water-organogel interfaces (Chapter 3).

Both processes take place at the W/RTIL micro-interfaces and hydronium-[FAP] interactions are compatible in the detection of lysozyme.

The challenge remains in using a more hydrophobic ionic liquid which is maintained in its liquid state at room temperature for electrochemical studies at liquid-liquid interfaces. A good example is trihexyltetradecylphosphonium tetrakis(pentafluorophenyl)borate, $[P_{14,6,6,6}][TB]$, which has been proven to provide a larger potential window (ca. 0.8 V)[200] at a μ-W/IL interface although this is achieved at 60ºC since it solidifies at room temperature.

6 Adsorptive stripping voltammetry of haemoglobin at a liquid – liquid microinterface array

The behaviour of haemoglobin (Hb) at the interface between two immiscible electrolyte solutions (ITIES) has been examined for analytical purposes. When Hb is fully protonated under acidic conditions (pH < pI) in the aqueous phase, it undergoes a potential-dependent adsorption and complexation, at the interface, with the anions of the organic phase electrolyte. This can be utilised as a simple and fast preconcentration step, consisting of adsorbing the protein at the interface, in conjunction with voltammetric desorption. This opens up the ITIES to the adsorptive stripping voltammetry (AdSV) approach. Utilising a 60 s adsorption step and linear sweep voltammetry, a linear response to Hb concentration in aqueous solution over the range 0.01 – 0.5 μM was achieved. The equation of the best-fit straight-line was I_p = 7.46 C - 0.109, R = 0.996, where I_p is the peak current (nA) and C is haemoglobin concentration (μM). The calculated detection limit (3σ) was 48 nM for a 60 s preconcentration period, while the relative standard deviation was 13.3 % for 6 successive measurements at 0.1 μM Hb. These results illustrate the prospects for simple, portable and rapid label-free detection of biomacromolecules offered by electrochemistry at arrays of liquid-liquid microinterfaces.

6. 1. Introduction

Haemoglobin is a metalloprotein from red blood cells responsible for oxygen transport in the blood of vertebrates. It possesses a quaternary structure comprised of four subunits, two α and two β polypeptide chains, in a tetrahedral arrangement. Each of these subunits is associated with a haem group.[216] The study of haemoglobin is especially relevant as it is an important biomolecule particularly in the fields of medicine, pharmacology and diagnostics. Studies on this molecule may also be transposed to other important molecules of biological significance such as glycated haemoglobin (HbA1c), myoglobin and cytochrome c. Simple and rapid determination of low concentrations of haemoglobin is desirable as the biomacromolecule may be present in samples, either as an analyte of interest that indicates an incidence of disease, or as a possible interferent in the measurement of other analytes. For instance, Shi et al. developed a non-invasive micro-sensor to diagnose gastrointestinal bleeding based on an electron transfer microelectromechanical system (MEMS) which achieved a detection limit of 0.1 mg/mL (1.6 μM) of Hb under physiological conditions (phosphate buffered saline).[217]

To-date, the detection of a wide range of haemoglobin molecules such as glycated (HbA1c), fetal (HbF), and C (HbC) haemoglobin has been performed mostly by colourimetric assays or immunoassays. For instance, several point-of-care testing (POCT) devices are commercially available for HbA1c detection in diabetes diagnosis.[218] Colourimetric assays are constrained by the detection limits and the interference of other biomolecules, while immunoassays require expensive reagents, several pre-treatment steps and longer periods of time from the collection of the sample until final analytical results are available. However, over recent decades electrochemistry has shown its potential as a possible selective, sensitive, portable, disposable, inexpensive and relatively simple technology for biomedical applications. The best example is the commercially-available glucose sensor for monitoring of blood glucose levels in diabetic patients. This biosensor represents about 85 % of the biosensor market.[219] Additionally, determination of blood electrolytes using ion selective electrodes is another important group of sensors

widely accepted and under continuous development for biomedical diagnosis purposes.[220]

Electrochemistry at the liquid-liquid interface (or at the interface between two immiscible electrolyte solutions, ITIES) has been developed over the last 40 years.[6, 12] Processes studied at the ITIES do not necessarily depend on electron transfer, but more generally charge transfer involving either ion transfer or electron transfer (or both) can be studied and manipulated for detection and determination purposes. The electrochemistry and electrochemical determination at the ITIES of a range of biomolecules such as dopamine,[221] heparin,[222] insulin,[77] lysozyme,[78] cytochrome c,[85] myoglobin[74] haemoglobin,[80] small peptides[34] and DNA[53] has been explored by diverse groups worldwide. The latest studies have focused attention towards reaching lower limits of detection basing the detection on voltammetric techniques combined with pre-treatment steps. For example, Collins et al. reported the detection of propranolol in artificial saliva using differential pulse stripping voltammetry.[17, 59] Previous work (see Chapter 3 and 4) has already shown the potential of adsorptive stripping voltammetry (AdSV) as an important tool for achieving lower limits of detection at the microITIES.

The aim of the present work was to investigate whether the adsorptive stripping voltammetry approach at the microITIES was generically applicable to biomacromolecules, with haemoglobin chosen as a protein that has been studied at the ITIES previously, but not subjected to adsorptive accumulation, and that is also of interest as a possible biomarker for disease. The present work provides the basis for a new reagentless, simple, fast and competitive technique with the capability to be miniaturised and integrated other analytical technologies.

6. 2. Experimental Section

6. 2. 1. Reagents

All reagents were purchased from Sigma-Aldrich Australia Ltd, and used as received. The electrolyte salt of the organic phase, bis (triphenylphosphoranylidene) ammonium tetrakis (4-chlorophenylborate) ($BTPPA^+$ $TPBCl^-$) was prepared by metathesis of bis (triphenylphosphoranlidene) ammonium chloride ($BTPPA^+Cl^-$) and

potassium tetrakis (4-chlorophenyl) borate (K^+TPBCl^-). The organic phase consisted of 10 mM $BTPPA^+$ $TPBCl^-$ in 1,6-dichlorohexane, which was gelled using low molecular weight poly(vinyl chloride),[79, 114] see Appendix A. Aqueous stock solutions of haemoglobin (from bovine blood) were prepared in 10 mM HCl on a daily basis. All aqueous solutions were prepared in purified water from a USF Purelab Plus UV (resistivity: 18 MΩ cm).

6. 2. 2. Apparatus

All measurements were performed using an Autolab PGSTAT302N analyser (Metrohm, The Netherlands). The micropore membranes, used to form an array of microITIES, were fabricated using photolithographic patterning and a combination of wet and dry silicon etching. Deep reactive ion etching was used for pore drilling and produces hydrophobic fluorocarbon-coated internal pore walls which subsequently are filled with the organic phase. The array employed here consisted of 30 micropores in a hexagonal close-packed arrangement, each with a diameter of 22.4 μm and a pore centre-to-centre distance of 200 μm.[33, 35] The microporous silicon membranes were sealed onto a glass cylinder using silicone rubber (acetic acid curing Selleys glass silicone, Selleys Australia & New Zealand). Then the gelled organic phase solution was introduced into the silicon micropore arrays, and the organic reference solution was placed on top of the gelled organic phase.[34] The gel/membrane/glass assembly was then inserted into the aqueous phase (10 mM HCl or haemoglobin in 10 mM HCl) and voltammetric experiments implemented. Transfer of tetraethylammonium (TEA^+) across the interface was performed to characterise the array and confirm the correct filling of the pores. TEA^+ transfer at the microITIES (data not shown) exhibited steady-state voltammetry on the forward scan (ion transfer from aqueous to organic phase) and peak-shaped voltammetry on the reverse scan (organic to aqueous phase), consistent with pores filled with organic phase, as previously reported.[33, 35]

6. 2. 3. Electrochemical measurements

A two-electrode electrochemical cell was employed, whereby, the micro-interface array was polarised by applying a potential difference between two Ag/AgCl

electrodes (one in each phase). Scheme 6.2.1 represents the electrochemical cell used, where *x* is the concentration of haemoglobin in the aqueous phase.

| Ag | AgCl | *x* μM Hb in 10 mM HCl || 10 mM $BTPPA^+TPBCl^-$ in gellified 1,6-DCH | 10 mM $BTPPA^+Cl^-$ in 10 mM LiCl | AgCl | Ag |

Scheme 6.2.1. Schematic representation of the electrochemical cell.

Cyclic voltammetry (CV) and adsorptive stripping voltammetry (AdSV) were carried out at a sweep rate of 5 mV s^{-1}. Parameters such as protein concentration, applied potential, and duration of the adsorption stage were varied.

6. 3. Results and Discussion

The experiments presented below have been performed at pH 2, which is below the isoelectric point (pI = 6.8)[216] of haemoglobin and where it is assumed to be fully protonated with a charge z_i of +62.[80] It is reported that at pH < 2.5, haemoglobin retains a large amount of tertiary structure and is only partially denatured.[223] Under these conditions, this protein has shown electroactivity at liquid-liquid interfaces and can be detected via the facilitated anion transfer mechanism at the micro-interface array, in agreement with previous reports.[80] CV analysis (Figure 6.3.1) confirmed this proposed mechanism at the gelled microITIES array, involving adsorption of the positively-charged haemoglobin on the interface at the more positive potentials in conjunction with facilitated transfer of organic phase anions. The sharp peak observed on the reverse sweep at ca. 0.65 V is characteristic of a desorption process, whereas on the forward sweep, an increase in current, relative to the background, and the presence of a pair of shoulders are indicative of charge transfer occurring. However the latter processes (shoulders) are insufficiently defined to be used for analytical purposes. Thus, Hb is electroactive at the microITIES array, but implementation of an advanced voltammetric strategy may offer better detection capability and that is the focus of this paper.

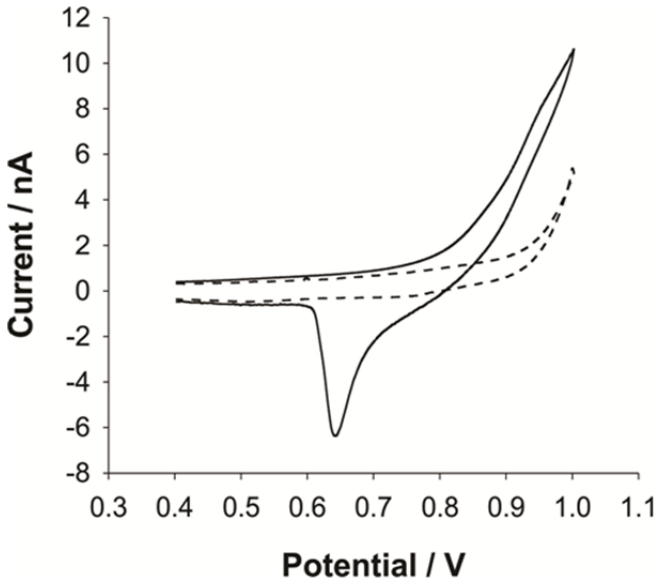

Figure 6.3.1. Cyclic voltammetry of 10 μM Hb (solid line) at the microITIES array. Sweep rate: 5 mV s^{-1}. The dashed line is the response in the absence of haemoglobin. The full cell description is given in Scheme 6.2.1.

6. 3. 1. Potential dependence

AdSV is an electroanalytical technique that involves two steps: first, preconcentration of the analyte by adsorption at the electrified interface, and second, the voltammetric desorption of the analyte from the interface. This methodology has been proven to enhance the detection capability in electrochemical analysis[224] and specifically at the micro-ITIES when employing lysozyme (Chapter 3), a model globular protein. Previous reports on haemoglobin behaviour at the ITIES have suggested that the protein undergoes a complex process consisting of adsorption and facilitated anion transfer of the organic electrolyte.[80, 81] In order to optimise the conditions where haemoglobin is maximally adsorbed, a series of applied potentials across a range from 0.45 to 1.1 V was investigated (see Figure 6.3.2). When the applied potential was greater than that required for the protein to adsorb, haemoglobin facilitated an ion transfer involving charged protein and organic anion interactions. This is followed by desorption of the biomacromolecule from the interface and back transfer of the organic electrolyte anion to the organic phase during the subsequent voltammetric scan. As can be seen from Figure 6.3.2, Hb adsorption starts at 0.8 V, reaching the maximum current peak height at 0.975 V with

a peak current of -15 nA. When increasing the potential beyond this optimum value, organic electrolyte transfer across the interface without complexation of the protein dominates this process. Additional peak analysis (not shown here) confirms an optimum potential applied of 0.975 V when the ratio between the half-width and the peak height of the reverse peak was also analysed. Moreover, this optimum potential differs to that obtained for lysozyme (0.950 V) under the same conditions (see Chapter 3, Section 3.3.2), indicating some selectivity of the system in the electrochemical adsorption. Furthermore, the voltammetric peak during the desorption process was also different, 0.65 V for Hb and 0.7 V for lysozyme. Nevertheless, the possible interference of other proteins, such as serum albumin present in blood samples, must be addressed in order to determine the capability of this method within a more complex sample matrix.

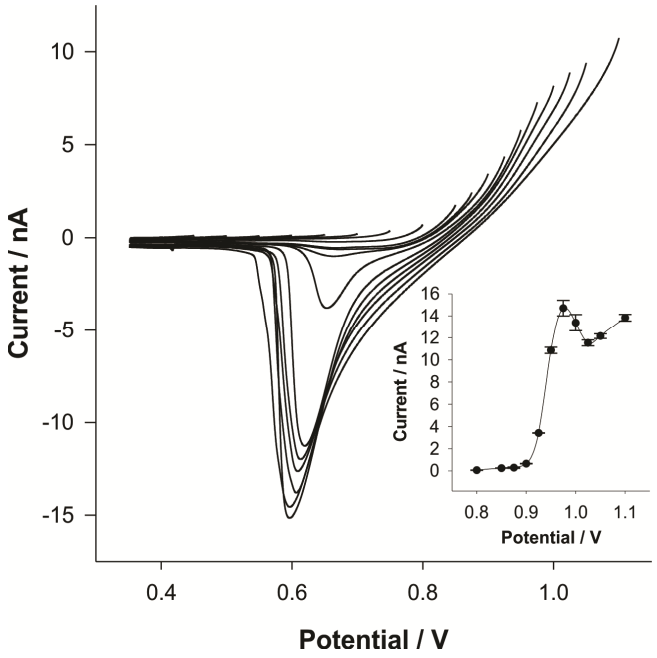

Figure 6.3.2. AdSV of 5 μM Hb at the microITIES array following application of different applied potentials (between 0.45 and 1.10 V) for the adsorption step of 60 s. Inset: evolution of the peak current with the applied potential of the adsorption step. Electrochemical cell composition as indicated in Scheme 6.3.1. Error bars represent ±1 standard deviation (n = 3).

6. 3. 2. Preconcentration time dependence

The influence of the preconcentration time at a fixed haemoglobin concentration also investigated. Figure 6.3.3 shows the evolution of the desorptive voltammograms with preconcentration time following adsorption of the protein at 0.975 V for different periods of time, from 0 to 1800 s. The inset in Figure 6.3.3 shows a hyperbolic increase of the desorption peak current when the preconcentration time is increased. However, adequate sensitivity to Hb is obtained at short preconcentration times. Furthermore, it can be seen that the peak shape becomes skewed at the longer times, indicating a possible loss of sensitivity or resolution.

Thus both the applied potential and time for adsorption have an impact on the detection signal and were fully characterised before studying the performance potential of the approach under different concentrations of the protein in the aqueous phase. The electrochemical response suggests that the adsorption of haemoglobin at the μITIES can be controlled by the solution concentration and the preconcentration time.

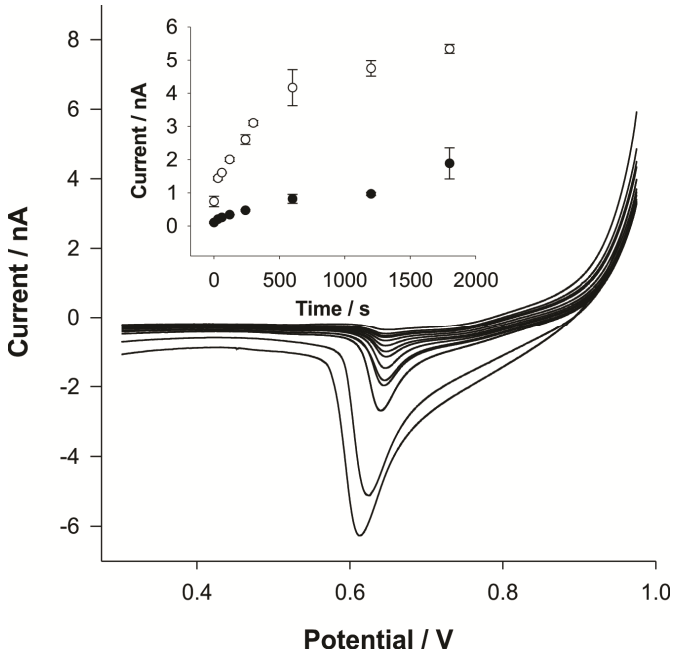

Figure 6.3.3. AdSV of 1 μM Hb at different preconcentration times, from 0 to 1800 s. Inset: plot of peak current versus preconcentration time for (○) 1 μM and (●) 0.1 μM Hb. Electrochemical cell composition as given in Scheme 6.3.1. Error bars represent ±1 standard deviation (n = 3).

6. 3. 3. Concentration range for haemoglobin detection

AdSV of haemoglobin was performed using fixed adsorption times (0, 60, 120 and 300 s) across an extensive concentration range (0.005 – 7.5 μM). Figure 6.3.4 shows the resultant voltammograms for (A) 0 s and (B) 60 s preconcentration times. The minimum measurable desorptive (stripping) peak corresponds to a concentration in the aqueous phase of 30 nM, for a preconcentration time of 60 s, whilst without pre-treatment (i.e. 0 s preconcentration) this value increased up to 70 nM, in line with previous studies by CV. A common feature was noticed in all of the voltammograms at 2 μM Hb in the bulk aqueous phase (see Figure 6.3.4). At that critical concentration, a crossover at 0.8 V is observed and the peak current regresses significantly. This process breaks the linearity observed at lower protein concentration in the aqueous solution. As noted in Chapter 3 and 4, multilayer formation has been demonstrated to occur at the liquid-liquid interfaces when protein is concentrated at the interface. Consequently, protein conformational changes are possible within the multilayers that built up at the microITIES, and perhaps there is less interaction between haemoglobin and the organic phase anion at higher concentrations due to the difference between interfacial and bulk concentration. Further studies on this observation are required for a fuller explanation.

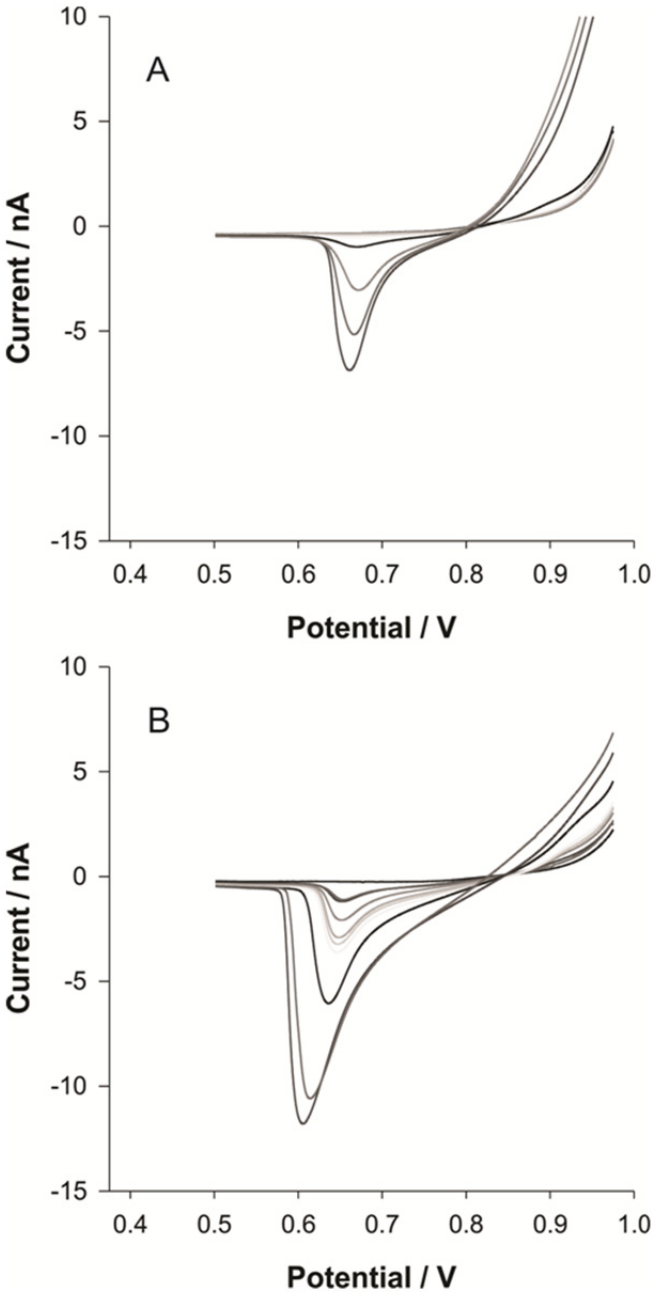

Figure 6.3.4. AdSV of different concentrations of Hb, 0.01, 0.05, 0.1, 0.25, 0.5, 1, 1.5, 2.5, 5 and 7 μM. (A) with 0 s preconcentration step and (B) after 60 s preconcentration.

The build-up of multilayers was characterised by determining the interfacial coverage of the adsorbed protein at the microITIES. Interfacial coverage (Γ) values were estimated using equation (6.3.1) where Q is the charge under the desorption peaks, assuming the charge of the protein z_i is +62 when fully protonated at pH 2, F is the Faraday constant and A is the geometric area of the microinterface array (1.18 x 10^{-4} cm^2).

$$Q = z_i F A \Gamma \qquad (6.3.1)$$

Taking into account that a molecule of haemoglobin occupies a cross-sectional area of 30 nm^2 and that for the formation of a single monolayer,[81] only 87 % of the interface is occupied by haemoglobin in a close-packed hexagon configuration,[225] then 3.4 x 10^8 molecules would be absorbed and occupying the available geometric area of the micro-interface array (1.18 x 10^{-4} cm^2). Without preconcentration conditions, the experimental interfacial coverage values for Hb bulk concentrations lower than 2.5 μM correspond to less than a monolayer, while the formation of multilayers occurs at higher concentrations (between 8 to 19 monolayers in the concentration range 5-10 μM, without preconcentration).

Subsequently linearity was investigated at low concentration of haemoglobin in the bulk aqueous solution. Table 6.3.1 summarises the analytical behaviour of this method over the range from 5 to 500 nM Hb using four different preconcentration times (0, 60, 120 and 300 s). At 0 s preconcentration time, the calculated limit of detection (LOD) was 0.265 μM, while amongst the results obtained from the longer preconcentration times, 60 s preconcentration gave best performance in terms of LOD, linearity, minimum observable peak and enhanced peak current (at 0.5 μM). The calibration curve obtained after the 60 s preconcentration step was: I_p *(nA) = 7.46 (nA* μM^{-1}*)* · *C (μM) - 0.109 (nA), R = 0.996*, where i_p is current of the desorptive voltammetry peak and *C* is the concentration of the protein in bulk aqueous solution (see Figure 6.3.5). The relative standard deviation was 13.3 % for 6 successive measurements at 0.1 μM of haemoglobin following 60 s preconcentration. This experiment showed that haemoglobin was completely stripped away from the interface, with intermediary blank scans displaying no peaks. The lowest observable and measurable desorption peak corresponded to 30 nM while the calculated limit of detection (LOD) was 48 nM for a preconcentration period of 60 s. This calculated LOD is based on three times the standard deviation of the intercept and the value larger than the experimentally detectable concentration reflects the precision of the measurements. Previous work based on cyclic voltammetry reported by Herzog et al. presented a non-linear behaviour[80] of Hb at a millimetre-sized ITIES (not gelled as in the present work) whilst the detection of 0.55 μM Hb was achieved after haemoglobin digestion and the use of differential pulse stripping voltammetry as a

more sensitive voltammetric technique.[83] However, the LOD under similar conditions to those presented here (AdSV for 60 s) was 60 nM of lysozyme (Chapter 3, Table 3.3.1). Based on these results, AdSV at arrays of liquid-liquid microinterfaces is a viable analytical approach for simple, fast and label-free detection of haemoglobin.

Table 6.3.1. Analytical characteristics of Hb at different pre-concentration times.

Pre-concentration times / s	*$[Hb]_{min}$ observable / nM*	*Peak current of $[Hb]_{min}$ / nA*	*Peak current at 0.5 µM Hb / nA*	*Calibration graph slope / nA μM^{-1}*	*Linear range / µM*	*Number of points (N)*	*Limit of detection (LOD)/ nM*	*Correlation coefficient (r)*
0	70	0.04	0.63	1.32	0.07 - 0.5	8	265	0.997
60	30	0.04	3.41	7.46	0.03 – 0.5	12	48	0.996
120	30	0.05	4.47	9.07	0.03 – 0.5	12	68	0.991
300	30	0.08	6.72	13.5	0.03 – 0.5	12	89	0.984

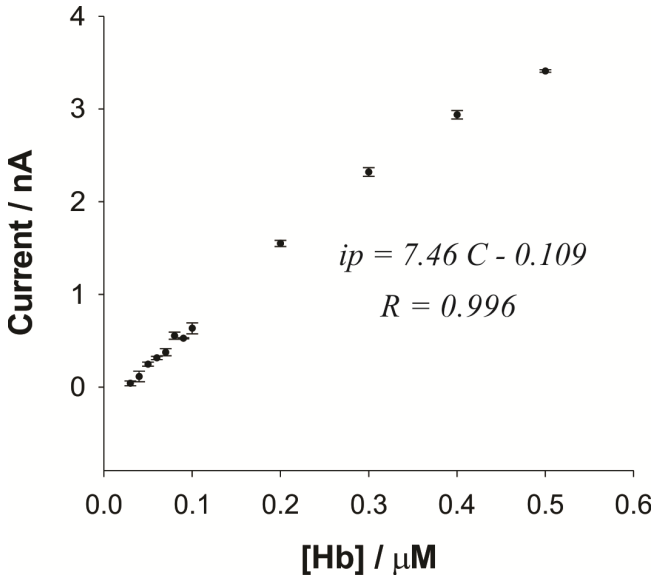

Figure 6.3.5. Current versus concentration curve of haemoglobin (0.01-0.5 µM) for 60s preconcentration time. Error bars represent ±1 standard deviation (n = 3).

6. 4. Conclusions

An analytical approach based on constant-potential adsorption of protein followed by voltammetric desorption enables the detection of lower levels of haemoglobin in aqueous solution. A calculated detection limit of 48 nM was achieved following 60 s adsorption at the aqueous-organogel micro-interface array. Previous studies have highlighted that protein detection at the ITIES may be attributed to a combination of adsorption and protein-facilitated transfer of organic phase electrolyte anions. The results of this study show that this adsorption event may be exploited for analytical purposes, in this case within a thirty-member array of micro-interfaces. The improvement in detection limit is two orders of magnitude better than has been achieved by cyclic voltammetry at macro liquid-liquid interfaces[83] and the same order of magnitude as obtained when applying the strategy to lysozyme detection. A lower measurable peak was obtained when analysing haemoglobin than lysozyme, which can be attributed to haemoglobin's higher positive charge (+17 in the case of lysozyme, +62 for haemoglobin). A higher degree of charge of the biomacromolecule enables a higher interaction with the anions from the organic phase, increasing the sensitivity of the system. The interference of other proteins in matrices such as blood must be addressed. Nevertheless, this report presents the fundamentals for a new area based on the capability of this technology which may be extrapolated to an extensive range of molecules.

7 Enzymatic digestion of proteins prior to electrochemical analysis at liquid – liquid microinterfaces

Electrochemical analysis of different protein fragments at liquid – liquid interfaces was implemented as a new methodology for protein identification. For this purpose, the effect of several proteases was investigated for lysozyme digestion. Complementary studies such as matrix-assisted laser desorption ionisation – time of flight - mass spectrometry (MALDI/TOF-TOF-MS), liquid and gas chromatography - mass spectrometry (LC-MS and GC-MS) were also performed for an extensive analysis of the lysozyme digest composition which would affect the voltammetric signal. The results indicate that the protein digest signal varies with the enzyme used, which cleaves in different parts of the amino acid sequence of the protein. Additionally, the degree of pepsinisation is influenced by the acidity of the aqueous solution. Subsequently, lysozyme, myoglobin, bovine serum albumin and haemoglobin were investigated under identical conditions for pepsin and trypsin digestions resulting in eight unique voltammograms which showed the potential of electrochemistry at the μ-ITIES as a tool for the identification of proteins. The results presented in this chapter open up a new avenue for a simple, label-free identification and biosensing tool.

7. 1. Introduction

Proteins are formed in the ribosomes which transcribe the messenger-ribonucleic acid (mRNA) into polypeptides. These polypeptides are the precursors of the protein which then undergo post-translational modifications (chemical and structural changes) to form the final protein. Transcription increases enormously the complexity of the proteins generated within cells as a single gene is capable to generate multiple proteins as a result of various factors such as different single-nucleotide polymorphism, splicing in the transcription and post-translational modifications. Therefore, the amino acid sequence and structure in a protein is directly link to the genetic code which highlights the significance of protein determination.[124]

Proteomics is the science that investigates systematically gene and cellular functions through protein analysis. The breakthrough in the late 1980s with the development of techniques for soft ionisation (electrospray ionisation[90] and matrix-assisted laser desorption ionisation[92]) of biomacromolecules made accessible the accurate measurement of protein and peptide masses as this soft ionisation is performed prior to mass spectrometric analysis. Shotgun proteomics requires proteolysis of the protein and then the mass spectra of the peptide fragments generated can be analysed through suitable software to deduce the amino acid sequence in the protein.[94] This makes possible the detection of amino acid substitutions or post-translational modifications and also provides high resolution measurements with capability to be integrated with separation techniques such as liquid chromatography and capillary electrophoresis.[226] However, tedious, inefficient and time consuming pre-treatments steps, costly instrumentation and low sequence coverage of the proteolysed protein are the disadvantages of this technology.[95, 99]

Biomolecule detection via electrochemistry became popular with the development and commercialisation of the glucose biosensor.[219] Numerous attempts with the view to developing selective and sensitive sensors focused on the surface modification of metal electrodes.[227] One strategy was primarily based on the formation of self-assemble monolayer to immobilise, for example, an antibody to detect specific interactions (antigen-antibody binding) in order to avoid interferences from complex matrices and enhance the electrochemical signal.[227] Nonetheless from the

commercial point of view, none of these approaches have been successful in terms of its application in the medical community or general public.

An alternative to conventional solid electrode electrochemistry is electrochemistry at the liquid-liquid interface. This method has been developed over the last 40 years[6, 12] and is able to detect charge transfer processes, not necessarily redox, which provided a label-free platform for protein detection. In the last decade, a range of proteins such as protamine,[69, 73] insulin,[77] lysozyme,[78] cytochrome c,[85] myoglobin[74] and haemoglobin[80] has been explored at the liquid - liquid interfaces (or at the interface between two immiscible electrolyte solutions, ITIES). The detection mechanism has been proposed to undergo a two step process, (1) protein adsorption and(2) facilitated transfer of the anion from the organic phase via positively charge protein-anion complexation which was discussed in previous chapters and confirmed for lysozyme in Chapter 4 via ESI-MS analysis. Also small oligopeptides[34, 228] and amino acids[66] have been detected at the ITIES in the presence of an ionophore in the organic phase. This ionophore is a crown-ether ligand that complexes these biomolecules hence facilitating their transfer across the interface. This is possible as there is hydrogen bonding between the oxygen atoms in the macrocycle and the protonated amines from amino acids. Moreover, protein folding and unfolding has been studied at the liquid – liquid interfaces by Herzog et al.[82, 229] and the first attempt to study the digestion of proteins as a pre-step before electrochemical analysis at the ITIES was also performed by Herzog et al.[83] The aim of this work reported here was to investigate the analytical utility of enzymatic digestions prior to electrochemical measurements with a calculated limit of detect of 0.55 μM when using differential pulse voltammetry. Following this line of research, several enzymes have been characterised to digest lysozyme before performing electrochemical analysis at liquid – liquid micro – interfaces. In addition, a series of mass spectrometry techniques was used to determine the peptide fragments and amino acids present in the proteolysed mixture to complement the electrochemical analysis. In order to examine the perspectives of this methodology as a label-free fingerprinting tool, four different proteins in terms of size and structure were also evaluated in this chapter.

7. 2. Experimental Section

7. 2. 1. Reagents

All reagents were purchased from Sigma-Aldrich Australia Ltd. and used as received. Hen-egg-white-lysozyme, equine heart myoglobin, haemoglobin from bovine blood, bovine serum albumin, trypsin (from porcine pancreas), pepsin (from porcine gastric mucosa) and endoproteinase Glu-C (from Staphylococcus Aureus V8) were stored at 4ºC or -21ºC as specified.

Protein and enzyme solutions were freshly prepared in the corresponding electrolyte solution (hydrochloric acid, phosphate buffer saline, ethylenediaminetetraacetic acid or ammonium bicarbonate) for the enzymatic digestion (see Section 7.2.2). Tetraethylammonium (TEA^+) chloride was prepared in 10 mM HCl of pH 2.

Electrochemical measurements required an organic phase which was gelled (10 % w/v) and prepared using bis(triphenylphosphoranylidene) tetrakis(4-chlorophenyl)borate ($BTPPA^+TPBCl^-$, 10mM) in 1,6-dichlorohexane (1,6-DCH) and low molecular weight poly(vinyl chloride) (PVC)[79, 114]. $BTPPA^+TPBCl^-$ is a hydrophobic salt used as the organic electrolyte and was prepared by metathesis of bis(triphenylphosphoranylidene)ammonium chloride ($BTPPA^+Cl^-$) and potassium tetrakis(4-chlorophenyl)borate (K^+TPBCl^-) as detailed in Appendix A.

All the aqueous solutions were prepared in purified water, from a USF Purelab plus UV, with a resistivity of 18 MΩ cm.

7. 2. 2. Proteolysis and denaturation

The enzyme-to-protein molar ratio was fixed to 1:25 for the different enzymatic reactions. When using pepsin, hydrochloric acid (HCl) was the acidic aqueous solution employed during the incubation at 37 °C for 2 h. In the case of tryptic digestion, the enzyme solution was prepared in 0.2 g L^{-1} of ethylenediaminetetraacetic acid (EDTA) at pH 7.0-7.6 which was then incubated at 37 °C for 16 h (overnight). Endoproteinase Glu-C was prepared in phosphate buffered saline (PBS) at pH 7.8 or 10 mg mL^{-1} of ammonium bicarbonate at pH 8 and left in a circulating bath at 37 °C for 16 h. The protein fragments were then separated from undigested material by filtration using 3 kDa centrifugal filter devices (amicon ultra 0.5 from Millipore Corporation, Billerica, USA) in a microcentrifuge

(Gyrospin, Thermo Fisher Scientific Australia Pty Ltd.). Aliquots of the filtered digest material were added to the acidic aqueous phase (10 mM HCl, pH 2) in order to protonate completely the peptides or amino acids formed.

Denaturation of the protein was carried out by incubating the protein (1 mM) with 9.5 M urea overnight at room temperature in either PBS or 0.15 M KCl + 0.15 M HCl. Then an aliquot (10 μL) was added to 10 mM HCl for electrochemical analysis.

7. 2. 3. Protein sequences

The amino acid sequence of hen-egg-white-lysozyme (129 residues) and myoglobin (153 residues) are illustrated in Sequences 7.2.1 and 7.2.2, respectively. For more detail see Appendix D where the single amino acids (individual letters) are defined.

KVFGRCELA AAMKRHGLDN YRGYSLGNWV CAAKFESNFN TQATNRNTDG STDYGILQIN SRWWCNDGRT PGSRNLCNIP CSALLSSDIT ASVNCAKKIV SDGNGMNAWV AWRNRCKGTD VQAWIRGCRL

Sequence 7.2.1. Lysozyme amino acid sequence.

GLSDGEWQQ VLNVWGKVEA DIAGHGQEVL IRLFTGHPET LEKFDKFKHL KTEAEMKASE DLKK**H**GTVVL TALGGILKKK GHHEAELKPL AQS**H**ATKHKI PIKYLEFISD AIIHVLHSKH PGDFGADAQG AMTKALELFR NDIAAKYKEL GFQG

Sequence 7.2.2. Myoglobin amino acid sequence. **H** is the distal histidine and **H** is the proximal.

The isoelectric point (pI) of lysozyme is 11.4[215] and possesses +17[150] charges when fully protonated, whilst myoglobin pI is 7.3[230] and is charged with positively 32 charges under acidic conditions. Myoglobin is lysine and histidine rich with 19 and 11 residues, respectively while lysozyme has 11 arginine residues in its sequence. In myoglobin, the hemin group is held by two histidine residues: H64 is known as the distal histidine and H93 is the primal histidine which binds via a covalent bond to the hemin group. However the distal histidine stabilizes the protein structure because it protects it from oxidation in the presence of O_2.

7. 2. 4. Electrochemical measurements

All electrochemical experiments were performed using an Autolab PGSTAT302N electrochemical analyser (Metrohm Autolab, Utrecht, The Netherlands). Cyclic

voltammetry was conducted at a scan rate of 5 mV s^{-1}. The microinterface was formed using a silicon membrane consisted of 30 micropores of 22.4 μm diameter which provides a total area of $1.18x10^{-4}$ cm^2. The fabrication process of these membranes combines dry and wet etching with hydrophobic micropore walls. The micro-arrays were then sealed to a hollow glass cylinder using silicone rubber (Acetic acid curing glass silicone (Selleys Australia & New Zealand)) where the gelled 1,6-DCH was introduced. Then the glass cylinder with the microarray membrane sealed on one edge was immersed in a beaker containing the aqueous solution. Therefore the microinterfaces are formed when both phases come in contact. Finally two silver/silver chloride wires act as reference electrode in each of the phases. See Figure 2.1.2 (Chapter 2 Section 2.1) which summarises the components of the two-electrode electrochemical cell set-up used in all voltammetric measurements.

| Ag | AgCl | *x* μM digest protein in 10 mM HCl || 10 mM $BTPPA^+TPBCl^-$ in gelled 1,6-DCH | 10 mM $BTPPA^+Cl^-$ in 10 mM LiCl | AgCl | Ag |

Scheme 7.2.1. Electrochemical cell.

7. 2. 5. Gas chromatography – mass spectrometry (GC-MS)

Free amino acid content of the protein digest was evaluated by GC-MS after its extraction and derivatisation. This process was performed using Kit:EZFaast (Phenomenex Inc. Australia) which is designed to accomplish the extraction of free amino acids and their derivatisation in 15 minutes preceding GC-MS analysis. This kit provides a chloroformate agent in order to derivatise the amines, carboxylic and hydroxyl group in the amino acid sample resulting in a more volatile product. GC-MS was carried out using a gas chromatograph from Agilent equipped with a ZB-AAA (10 m x 0.25 mm) Amino Acid Analysis GC Column that was directly connected to a 7000 Series GC/Triple Quad mass spectrometer. The injection volume was 2 μL at a carrier gas flow of 1.1 mL min^{-1} helium with a split ratio of 1:15 with hot needle (250 °C). The initial oven temperature of 110 °C was raised to 320 °C at 30 °C min^{-1}. Other settings were 240 °C ion source temperature and auxiliary of 310 °C. Mass spectra were analysed in the range of 45-450 *m/z* at a sampling rate of 2^2, 3.5 scans s^{-1}. MS data were processed using the program MassHunter from Agilent.

Technologies Australia Pty. For quantification purposes, a mixture of 23 amino acid standards was prepared as described previously using the EZFaast kit. In addition, an internal standard (norvaline, 23.43 ng/μL) was added at the beginning of the sample treatment which undergoes the same derivatisation reactions and extraction than the amino acids in the sample. For quantitative analysis, a mixture of 23 amino acid standards was prepared as described in the EZFaast kit.

Mass spectrometry work was performed by the Centre for Metabolomics at the faculty of Life and Physical Sciences at the University of Western Australia.

7. 2. 6. Matrix-assisted laser desorption ionisation / time of flight – time of flight (MALDI/TOF-TOF)

Peptides obtained after protein digestion (see Section 7.2.2) were analysed by MALDI/TOF-TOF mass spectrometer using a 5800 Proteomics Analyser from AB Sciex Australia Pty Ltd. (Mt Maverley, Victoria, Australia). Spectra were analysed to identify the protein of interest using Mascot sequence matching software (Matrix Science Ltd., London, UK) with Ludwig NR Database and Taxonomy set to metazoa (June 2012, 3831323 sequences). The search parameters for use on the mass spectrometer were: ± 0.4 of peptide tolerance (tol) and MS/MS tol ± 0.4, peptide charge of +1, monoisotopic, one miss cleavage and trypsin digestion.

7.2.7. Liquid Chromatography - Mass Spectrometry (LC-MS)

LC-MS was carried out using an Ultimate 3000 nano HPLC system (Dionex, Thermo Fisher Scientific) coupled to a 4000 Q TRAP mass spectrometer from Applied Biosystems (Life Technologies Australia Pty Ltd., Mulgrave, Australia). Tryptic peptides were loaded onto a C18 PepMap100, 3 μm (LC Packings) and separated with a linear gradient of water/acetonitrile/0.1% formic acid (v/v). Spectra were analysed to identify proteins of interest using Mascot sequence matching software with Ludwig NR database and Taxonomy set to metazoa (September 2012, 3958669 sequences).

The proteomics analyses were performed in facilities funded by the (WA) Lotterywest State Biomedical Facility – Proteomics Node, Western Australian

Institute for Medical Research, Perth, Australia. The proteomics data analyses were performed with the support of the facilities at the Australian Proteomics Computational Facility.

Figure 7.2.1 illustrates the steps performed before any analysis.

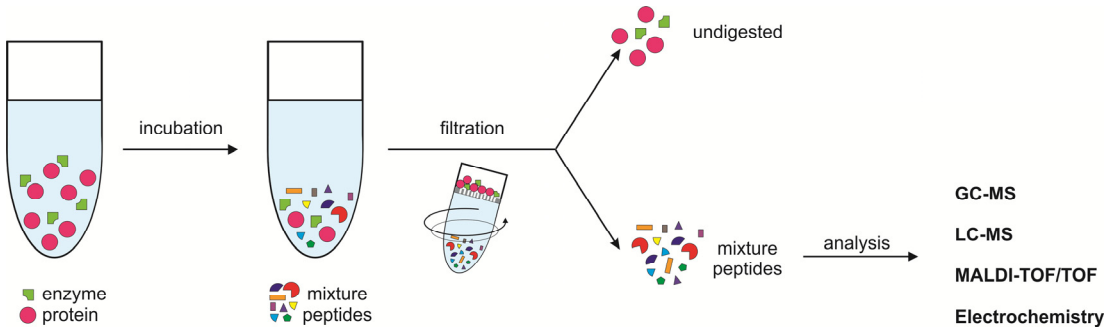

Figure 7.2.1. Sketch of the procedure prior to peptides or free amino acids measurements: protein digestion, separation and analysis performed.

7. 3. Results and Discussion

7. 3. 1. Effect of enzymes in the digestion of lysozyme

In the literature, the preferential cleavage sites of the enzymes employed for this study has been reported.[118, 119, 231] A general diagram (Figure 7.3.1) shows the importance of the amino acid sequence for the specific cleavage performed by the enzyme and the specific residues of cleavage for pepsin, trypsin and endoproteinase Glu-C.

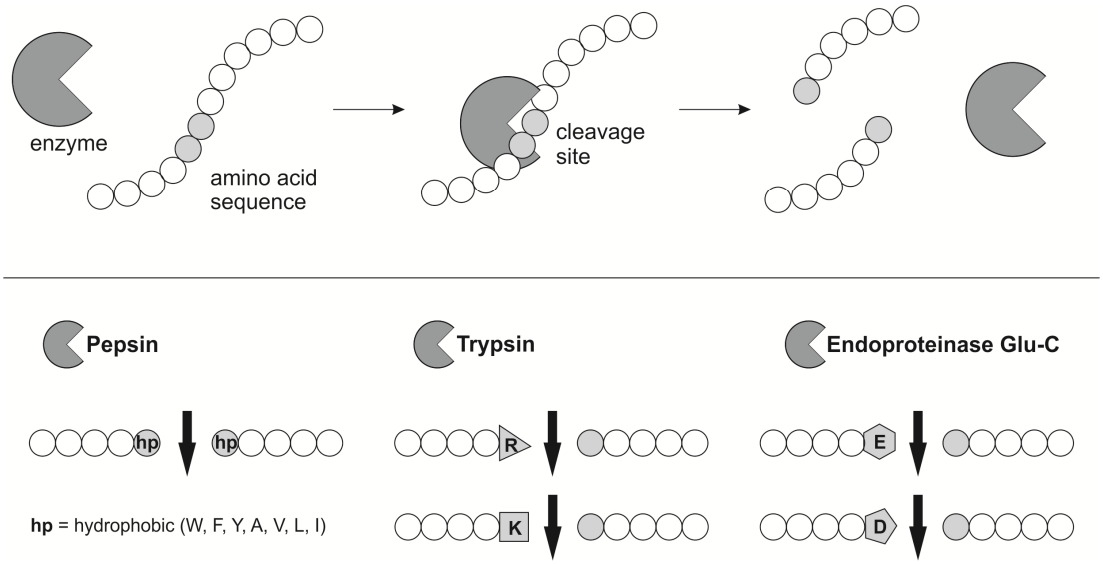

Figure 7.3.1. Sketch of enzyme digestion of an amino acid sequence. The cleavage sites are highlighted for the different enzyme used in this thesis. Note that the abbreviations correspond to amino acids: tryptophan (*W*), phenylalanine (*F*), tyrosine (*Y*), alanine (*A*), valine (*V*), leucine (*L*), isoleucine (*I*), arginine (*R*), lysine (*K*), aspartic acid (*D*) and glutamic acid (*E*).

Pepsin exhibits a broad specificity. Hydrophobic residues are the preferential cleavage sites, in particular aromatic amino acids such as tryptophan, phenylalanine, tyrosine, alanine, valine, leucine and isoleucine. Trypsin cleaves predominantly at the carboxylic site of arginine and lysine except when they are bound to a C-terminal proline. However, in the case of endoproteinase Glu-C, the enzyme also hydrolyses peptide bonds at the carboxylic site in the presence of ammonium at the glutamic and aspartic acid. And endoproteinase Glu-C cleaves only at aspartic acid residues, in the absence of ammonium ions in solution.[118, 119] Figure 7.3.2 illustrates the molecular structure of the amino acids involved in the digestions carried out when using pepsin, trypsin and endoproteinase Glu-C.

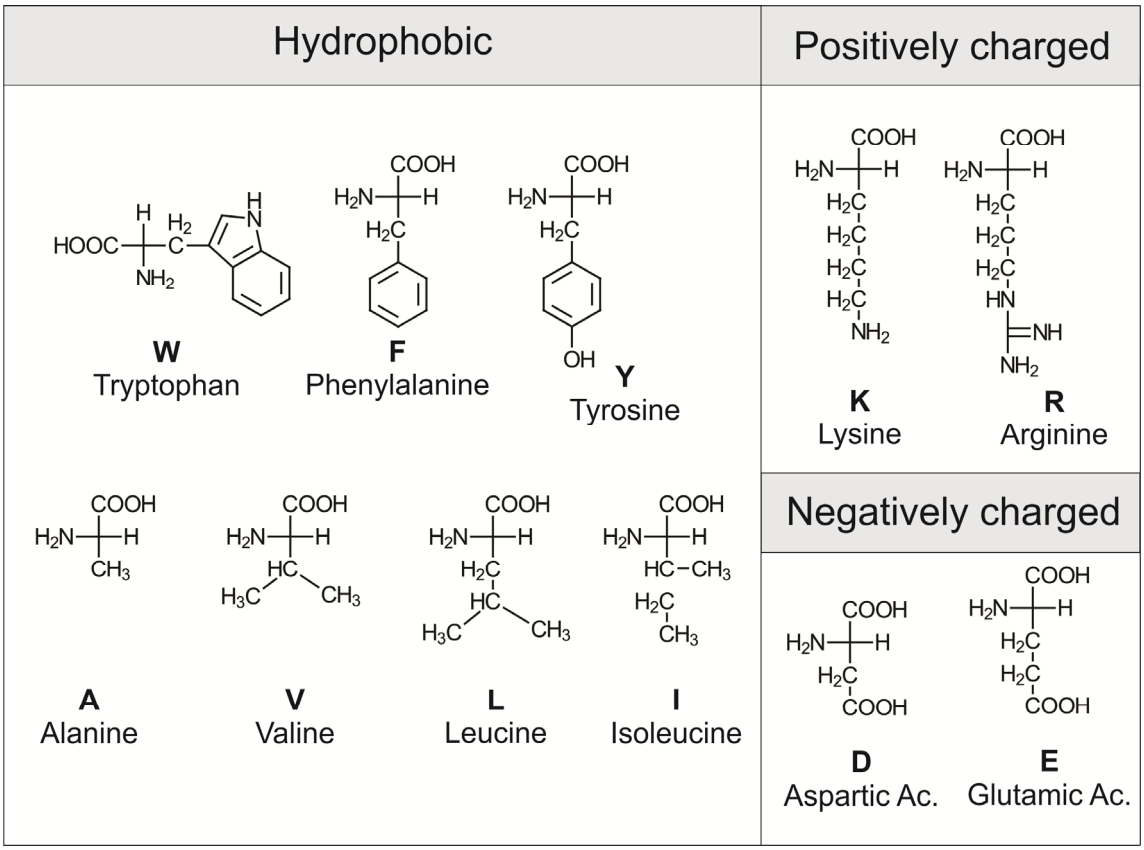

Figure 7.3.2. Representation of 11 amino acids that are crucial in the cleavage performed by pepsin, trypsin and endoproteinase Glu-C and these are divided into 3 groups (hydrophobic, positively and negatively charged amino acids).

In this study, the fragmentation of hen-egg-white-lysozyme (HEWL) resulted from digestion by several enzymes was implemented. Based on this principle, a wide variety of oligopeptides and free amino acids were formed for the same protein under different conditions. Figure 7.3.3 shows six cyclic voltammograms obtained for lysozyme after being digested with: pepsin at pH 1.3 and 2; trypsin; pepsin digestion followed by trypsinisation; and finally, endoproteinase Glu-C in phosphate buffered saline and ammonium bicarbonate. These results were obtained after the appropriate incubation time at 37ºC, filtration of the mixture in order to separate the undigested protein and the enzyme and finally, the addition of different aliquots of the reaction product mixture to 10 mM HCl which results in concentrations of 5, 10, 15, 30, 60, 100 μM of the initial lysozyme. Analysis of the buffers used during the incubation time was carried out to evaluate possible interference of these salts on the electrochemical detection. Ammonium bicarbonate was the only buffer which showed electrochemical activity within the concentration studied. For 1.12 mg/mL

NH_4HCO_3 (14 mM), a new feature is observed at 0.9 V on the reverse scan which can be attributed to NH_4^+ transfer across the interface. Therefore, this phenomenon could explain the voltammogram obtained when lysozyme is digested with endoproteinase Glu-C in ammonium bicarbonate, as it became distorted at 60 and 100 μM of lysozyme. At 60 μM lysozyme, the reverse peak became wider and shifted from 0.70 V to 0.75 V (Figure 7.3.3f). In addition, when lysozyme aqueous concentration is 100 μM and NH_4HCO_3 reaches 14 mM, then the electrochemical contribution of both charge transfer processes overlaps resulting in an unresolved peak at *ca.* 0.92 V on the reverse scan. However for remaining electrolyte solutions employed during digestion (HCl, PBS and EDTA), there was no observable change in the voltammetry which therefore provided a better platform for peptide analysis.

Pepsin

For pepsin digestion, two acidic solutions were investigated (pH 1.3 and 2) as this enzyme is known to cleave at hydrophobic sites and the degree of pepsinisation depends on the pH studies.[231] As confirmed by the voltammograms in Figure 7.3.3a and 7.3.3b, the more acidic pH enhances the cleavage performed by pepsin. This results in higher currents in Figure 7.3.3a, 15 nA on the forward scan for 100 μM lysozyme compared to 10 nA in pH 2. The reverse peak also becomes wider at pH 1.3 and the peak intensity reaches 13 nA for 100 μM concentration, while the peak at pH 2 was 8 nA.

Pepsin and trypsin

Another digestion approach was the sequential combination of pepsin and trypsin for a further digestion of the initial protein. This mimics the process in the mammalian digestive tract that starts in the saliva followed by further digestion in the stomach (pepsinogen), pancreas (trypsinogen) and intestine.[232] This double digestion resulted in a single peak (Figure 7.3.3c) at 0.94 V of 1.6 nA height. If the extended digestion resulted in a higher fragmentation where the neutral components were higher and the positively charged peptides or amino acids were reduced or become more hydrophilic, then the energy of transfer from the aqueous to the organic phase would be higher and in the case of too small molecules, undetectable due to a possible overlap the background signal.

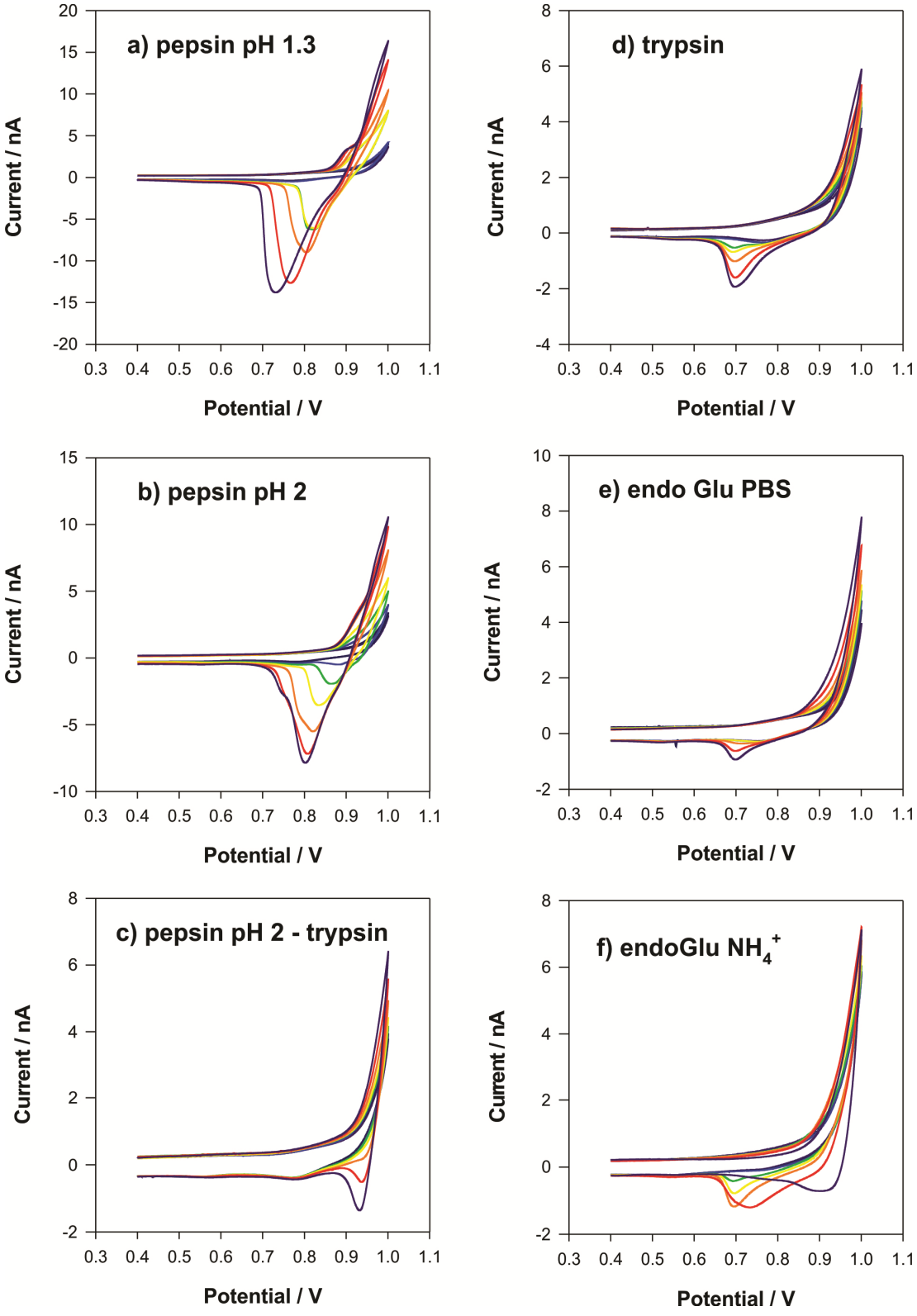

Figure 7.3.3. CVs of lysozyme digested using a) pepsin at pH 1.3, b) pepsin at pH 2, c) pepsin (pH 2) followed by trypsin, d) trypsin, e) endoproteinase Glu-C in PBS and f) endoproteinase Glu-C in NH_4HCO_3. Note that all the voltammograms are at 5 mV/s and the electrochemical signal increases with the peptide concentration (from 5, 10, 15, 30, 60, 100 µM).

Trypsin

Figure 7.3.3d corresponds to trypsinised lysozyme which shows a slight increase in the forward current but a peak-shaped voltammetry on the reverse (*ca.* 1.8 nA peak height at 0.7 V).

Endoproteinase Glu-C

Finally endoproteinase Glu-C was studied in PBS and NH_4HCO_3. Both voltammograms (Figure 7.3.3e and f) showed limited activity and, in the case of the incubation in the presence of ammonium, the electrochemical signal was compromised by the background transfer of ammonium at very positive potential. In both cases, there is a reverse peak at 0.7 V which showed higher currents for the sample incubated in phosphate buffered saline. A higher signal was expected for the digestion in PBS solution because under these conditions, the protease is able to fragment the protein at 9 sites[118] whereas in the presence of ammonium cations, lysozyme is cleaved in position 6 and 17 producing 3 fragments. After the digestion under these conditions, theoretically the peptide mixture obtained is formed by 3 peptides of *ca.* 0.7, 3.1 and 10.5 kDa. Thus after the filtration the only peptide in solution correspond to a 6 amino acid sequence (KVFGRC). However in phosphate buffered saline conditions, 10 fragments under 3 kDa were potentially in solution which was expected to present larger voltammograms. The potential peptide-peptide interaction and the ammonium interference could be sources of which would be discuss in the next sections.

The main observation from the above is the fact that each of the enzymes employed produces different voltammetry for a single protein. Accordingly, Figure 7.3.4 has been plotted to summarize the results obtained for the different enzymatic conditions for an initial protein concentration of 30 μM. In this figure, the differences in CVs produced by the various conditions are clearly distinguishable by visual inspection. The signal measured for the samples digested with trypsin and endoproteinase Glu-C present a similar reverse peak. Nevertheless, there is an increase of current on the forward wave in the case of the protein being fragmented at the glutamic and aspartic acid residues (NH_4CO_3 media). Pepsinised lysozyme in two acidic solutions (pH 1.3 and 2) also presents a significant increase of current on the forward scan. From approximately 0.85 to 0.93 V a shoulder was found for both

voltammograms although the CV run in a lower pH appears to produce higher current intensity during the full cycle (forward and reverse wave) and also showed a sharper shoulder *ca.* 0.9 V. The particular shape of each voltammogram has been assessed and it is described in section 7.3.2 in order to elucidate the detection mechanism of these matrices composed of single amino acids and oligopeptides.

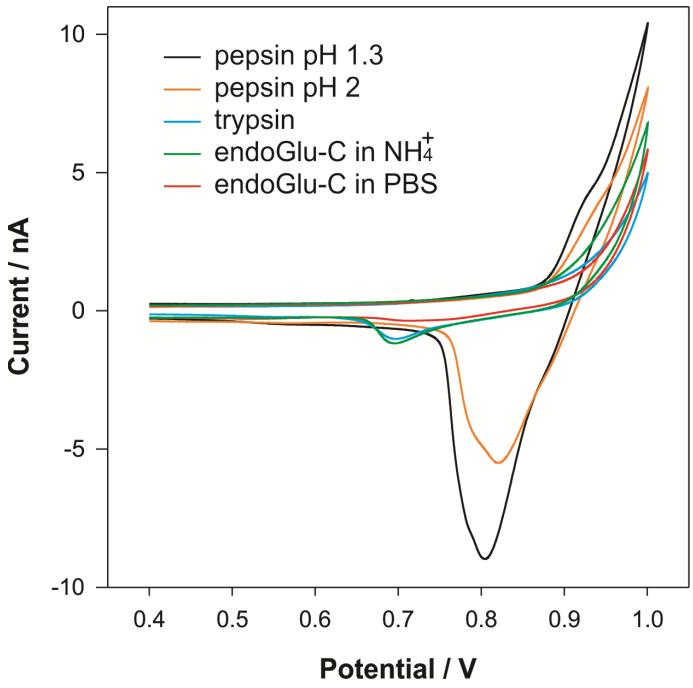

Figure 7.3.4. Cyclic voltammetry of 30µM of initial lysozyme after digestion with pepsin at pH 1.3 (—), at pH 2 (—), trypsin (—), endoproteinase Glu-C (—) in ammonium bicarbonate and phosphate buffer saline (—). CV of lysozyme digested with pepsin followed by trypsin is not shown in this graph due to its voltammetry did not differ from the blank signal for 30 µM of the protein digested.

As the data for endoproteinase Glu-C and the sequential digestion (pepsin followed by trypsin) present low currents for 30 µM lysozyme, the voltammograms of 100 µM lysozyme fragments under those conditions were illustrated in Figure 7.3.5. A qualitative analysis of these data demonstrate, as in the case of Figure 7.3.4, the ability of this methodology to provide unique voltammograms based on label-free charge transfer of digested biomolecules across liquid-liquid interfaces. However, the sensitivity has been found to be compromised when the protein undergoes enzymatic digestion. The lowest concentration that produces an observable change in current is at least one order of magnitude higher than the obtained for the native protein (lysozyme) via cyclic voltammetry.[79]

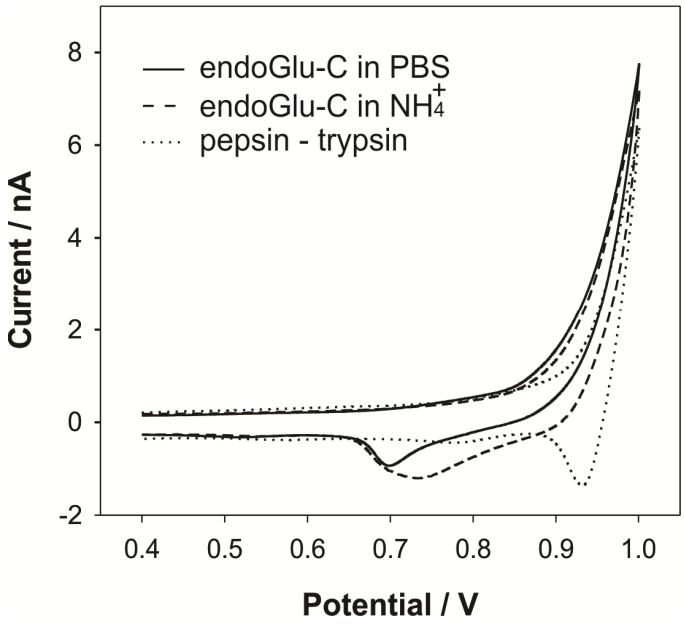

Figure 7.3.5. Cyclic voltammetry of 100μM pepsin-trypsin, 100μM PBS, 600μM NH_4^+ of initial lysozyme after digestion.

For these measurements, 3 experiments were run under identical conditions (buffer solution, incubation time and μ-ITIES design) but on different days and with different micropore membranes. These reproducibility studies showed a relative standard deviation (RSD) of approximately 17.5% when the reverse peak height was measured and 9.7 % for the evaluation of the peak area for lysozyme. Relative standard deviation for the reverse peak height and area are summarised in Table 7.3.1.

Table 7.3.1. Summary of the relative standard deviation for the reverse peak height and area measured by cyclic voltammetry.

Lysozyme	Relative standard deviation (RSD) / %		
	Pepsin pH 1.3	Pepsin pH 2	Trypsin
Peak height	9.2	13.4	30
Peak area	13.4	8.9	6.8

These results are in agreement with previous relative standard deviation values reported in Chapter 6 (Section 6.3.3) for these water/organogel micro-interface arrays.

In addition, the theoretical peptide sequences formed by the digestion process were evaluated. Table 7.3.2 summarises the expected small sequences or free amino acids and their hydrophilicity values omitting fragments larger than 3 KDa. In appendix C (Table appendix C1 to C6), the lysozyme digest are detailed for each of the enzymatic reactions.

Table 7.3.2. Summary of the theoretical number of small oligopeptides, amino acids, total number of digest fragments, average and total hydrophilicity of their mixture in solutions.

Lysozyme	Pep 1.3	Pep 2	Tryp	Pep 2 + Tryp	Endo PBS	Endo NH4+
single amino acids	12	5	4	13	0	0
di-peptides	6	1	1	3	0	0
tri-peptides	1	1	1	3	0	0
average hydrophilicity [a] (STD)	-0.97 (1.50)	-0.09 (0.86)	0.53 (1.34)	0.35 (1.40)	0.06 (0.39)	0.2 (NA)
sum hydrophilicity [b]	-28.1	-1.1	9.5	11	0.6	0.2
Average GRAVY (STD)[c]	0.47 (2.08)	1.49 (2.09)	-1.08 (2.08)	-0.82 (2.14)	-0.56 (0.69)	-0.4 (NA)
total amino acids and oligopeptides	29	14	18	31	10	3

[a] average value of the hydrophilicity data allocated for each digest fragment produced for 1 molecule of lysozyme based on the Hop-Woods scale.[233]

[b] sum of all the hydrophilicity values corresponding to for each digest fragment produced for 1 molecule of lysozyme, also based on the Hop-Woods scale.[233]

[c] grand average of hydropathy index[234] for each digest fragment produced for 1 molecule of lysozyme

STD is the standard deviation of the hydrophilicity or hydropathy index values of the total number of fragments employed to calculate the corresponding average value.

**data assuming 100% cleavage efficiency*

The hydrophilicity values quoted in Table 7.3.2 represent the hydrophilicity or lipophobicity of single amino acids, being tryptophan, the most hydrophobic with -

3.4 (hydrophilicity value), and arginine, lysine, aspartic and glutamic acid which present positive value of 3 as the four are highly ionisable amino acids (see Table appendix D1 in Appendix D).[233] These values are the hydrophilicity values in Hopp-Woods scale[233] which are based on the experimental energy of transfer of amino acids from water to ethanol or estimated values reported by Levitt.[235] Grand average of hydropathy index (GRAVY) is also another way to estimate the solubility of peptides or amino acids based on their sequence which was proposed by Kyte and Doolittle.[234] The hydropathy index values allocated to each amino acid in the Kyte-Doolittle are summarised in Table appendix D1 (Appendix D) and were also based on the partition coefficient of amino acids between water and ethanol as the ethanol phase was estimated to resemble the interior of the protein.[236]

Evaluation of current intensity (forward or reverse signal) and charge under the voltammetric peaks versus the number of di-peptides, tri-peptides, average hydrophilicity, total number of digest fragments, hydrophobic single residues and average hydrophilicity of the mixture were investigated. There was no noticeable trend in most of the cases, although the effect of hydrophobic single residues and the average hydrophilicity seemed to play an important role in the electrochemical detection of these complex mixtures. Figure 7.3.6 a and b illustrate the effect of the number of hydrophobic single amino acids in solution and the average hydrophilicity of the mixtures on the forward current of the voltammograms (see CVs in Figure 7.3.4)

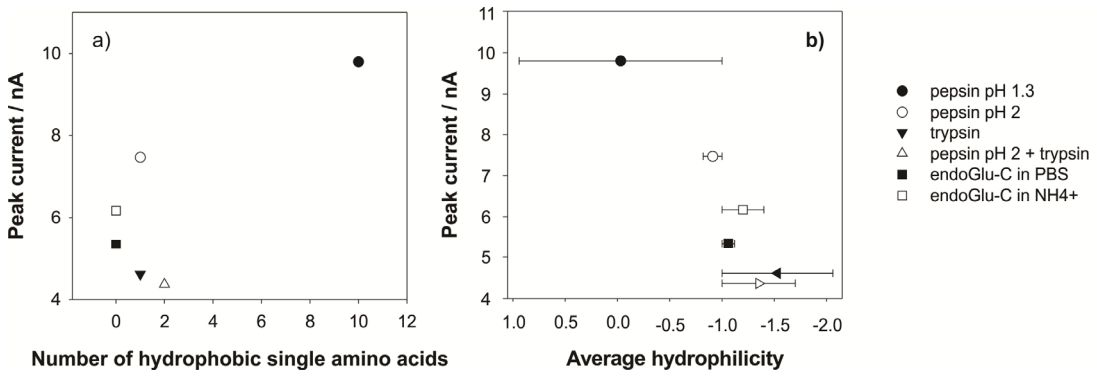

Figure 7.3.6. Peak height of the forward sweep of the CVs represented versus the number of hydrophobic amino acids and average hydrophilicity after several digestions.

From Figure 7.3.6, the increase of peak current is clear when there is higher presence of hydrophobic amino acids in solution or higher hydrophobic contribution from the mixture. This is the case of pepsinisation at a low pH which is known to cleave at hydrophobic residues points in the amino acid sequence of the protein. However, when a sequential enzymatic digestion is implemented, the size of the peptides decreases significantly leading to a dramatic diminution of the current peak. Therefore, this could translate into a more electrochemically significant contribution of the oligopeptides in comparison to the single amino acids in solution or their co-existence in the aqueous phase.

7. 3. 2. Mass spectrometry

In an attempt to identify the composition of the samples after enzymatic digestion and thus better understanding the contribution to electrochemical signal, complementary techniques such as liquid chromatography - mass spectrometry and gas chromatography mass spectrometry were employed. In addition, the theoretical composition of each of the samples was predicted assuming that the enzyme is 100% efficient and cleaves at the residues described in the literature.

Matrix-assisted laser desorption ionisation time of flight/time of flight (MALDI/TOF-TOF) was the first technique employed to identify peptide sequences. The disadvantage of MALDI is that the peptide coverage is low which limits the identification of a protein. Trypsinised lysozyme was the only sample that provided significant matches. This could be attributed to the small peptide size when pepsin is used to digest lysozyme. The sequences found via MALDI are shown below for lysozyme after trypsin digestions which correspond to 26% peptide coverage.

32 – 39	K.RHGLDNYR.G
32 – 41	K.RHGLDNYRGY.S
33 – 39	R.HGLDNYR.G
33 – 41	R.HGLDNYRGY.S
52 – 63	K.FESNFNTQATNR.N
53 – 63	F.ESNFNTQATNR.N
72 – 79	S.GILQINSR.W
135 – 143	K.GTDVQAWIR.G

For the rest of the fragmentation via enzymatic reactions, the matches were not significant. Then, nano-high performance liquid chromatography - mass spectrometry (nanoHPLC-MS) was carried out to improve the sequence coverage for the trypsinised lysozyme. However the percentage was within the same range as the previous measurements (19%, corresponding to the oligopeptides 32 – 39, 52 – 63 and 135 – 143).

One of the factors to consider for this lack of sequence coverage is that the enzymes used were not proteomics grade, except for the endoproteinase Glu-C. In addition, denaturation (either chemical or thermal), reduction and alkylation were not performed prior to the enzymatic digestion of the protein. These pre-treatments are well established to enhance the peptide coverage in MALDI, although they were not implemented before electrochemical analysis in an attempt to simplify the steps required for a successful protein identification and detection at the liquid-liquid interfaces.

Single amino acid content was also studied by GC-MS. Derivatisation was required to increase the volatility of the residues for detection via GC-MS. Table 7.3.3 shows the concentration of free amino acids in the sample after digestion of 1 mM lysozyme in a 1:25 enzyme-to-protein ratio. These values as expressed in micromoles per liter. The raw data obtained via GC-MS for 100 µL of the digested protein (1 mM) is summarised in Table appendix E1 (see Appendix E) and presented as the amount of free amino acid detected in nanomoles. Then the amino acid concentration in the initial sample of lysozyme was calculated and illustrated in Table 7.3.3.

Table 7.3.3. Free amino acid concentration of 1 mM lysozyme digested in the presence of 40 μM enzyme and measured via GC-MS after derivatisation.

Amino acid	Amino acid concentration / μM							
	Pep pH 1.3	**Pep pH 2**	**Pep pH 3**	**Tryp**	**Pep pH 1.3 - Tryp**	**Pep pH 2 - Tryp**	**Endo PBS**	**Endo NH_4^+**
Alanine	875	390	34	7	93	71	23	23
Sarcosine**	9	7	8	9	9	8	12	10
Glycine	75	51	20	13	26	55	26	33
Valine	29	35	44	0.0	6	8	6	4
Leucine	6058	2840	237	30	646	501	44	29
Isoleucine	0	0	6	0	0	0	5	0
Threonine	11	15	10	0	0	0	7	4
Serine	20	25	0	0	0	11	14	12
Proline	6	6	0	1	2	2	4	8
Asparagine	224	89	5	0	29	12	29	73
Aspartic acid	75	41	5	3.0	14	7	58	81
Methionine	68	62	20	0	0	7	0	0
Glutamic acid	30	30	0	0	5	4	15	17
Phenylalanine	563	320	80	5	77	50	6	1
Glutamine	201	134	82	113	118	108	120	170
Ornithine*	13	12	9	0	0	0	6	0
Lysine	16	13	10	20	12	30	11	8
Histidine	0	0	0	0	0	0	0	0
Tyrosine	494	254	82	4	44	50	6	0
Tryptophan	4325	2162	187	2	819	437	2	4

**Ornithine is the degradation product of arginine*

***Sarcosine is the degradation product of glycine.*

In the actual electrochemical cell the measurement were performed with a 1/10 dilution of the samples represented by the data in Table 7.3.3, which corresponds to a maximum of 100 μM of the starting protein. High concentrations of hydrophobic amino acids such as tryptophan (4.3 mM), leucine, (6.1 mM), tyrosine (0.50 mM) and phenylalanine (0.56 mM) were present in the digest obtained when lysozyme was cleaved by pepsin under acidic conditions (pH 1.3). It was also noticed that the higher the pH the lower the hydrophobic amino acid content in the samples when digesting lysozyme via pepsin. Moreover, the content of lysine is slightly higher in trypsinised lysozyme although the content of amino acids is a lot lower than pepsinised samples, specifically hydrophobic residues. Sequential digestions (pepsin

+ trypsin) resulted in lower concentration of amino acids compared to the lysozyme digested with pepsin. One of the possible reasons for this unexpected observation could be the change of buffer conditions. Lastly, histidine levels are undetectable via GC-MS. The reason is the low amount of this residue in the amino acid sequence of the lysozyme (1 out of 129).

The electrochemistry of free amino acids in solution was conducted to elucidate the nature of the signal produced by the lysozyme fragments. In order to mimic the single amino acid concentrations determined via GC-MS, a solution containing the most relevant amino acids such as tryptophan, tyrosine, lysine, phenylalanine, glutamic acid, aspartic acid, proline, leucine, valine, glycine and alanine was prepared. These amino acids were selected for electrochemical characterisation as they showed significantly high concentrations in the GC-MS data obtained after derivatisation (see Table 7.3.3). For this study, a solution was prepared simulating the digestion with pepsin (pH 1.3) in hydrochloric acid. Then a 1/10 dilution of the free amino acid mixture was electrochemically characterised via cyclic voltammetry (data not shown) in the same way as the protein digest were previously. The CV of pepsinised lysozyme showed a slight increase (1.6 nA) on the forward current at the most positive applied potential which is in accordance with the increase of current when using pepsin which cleaves at hydrophobic sites, but it does not fully explain the features observed in the CV obtained for the lysozyme digested with pepsin. Tryptophan and leucine were spiked in this solution. The additional 4.2 mM of tryptophan increased the forward current by 1.6 nA and leucine by 0.85 nA for the same concentration although neither of them presented any reverse peak.

7. 3. 2. Detection mechanism of lysozyme peptides

In terms of the detection mechanism, there are many different factors that affect the Gibbs energy of transfer for each the biomolecules present in solution. As mentioned before, size, charge, hydrophobic component and protein-peptide, peptide-peptide, protein-amino acid, peptide-amino acid and amino acid-amino acid interactions have to be taken into account.

As a first approach, tetraethylammonium transfer at the μ-ITIES in the presence of digested biomolecules was examined. In previous studies, the distortion of simple ion transfer has been used to follow adsorption processes at the ITIES.[78] In Figure 7.3.7, tetraethyl ammonium (TEA^+) transfer is shown (from a to f) after being added to a 100 μM solution of lysozyme digest.

The experimental data illustrates the distortion of the steady-state profile expected for radial diffusion-controlled TEA^+ transfer from the aqueous phase to the organogel. This is the case for Figure 7.3.7a, b, e and f. These four CVs have different degrees of distortion, with Figure 7.3.7b being the most affected which could be due to the digest being composed of large peptide sequences that might adsorb at the micro-ITIES. For Figure 7.3.7c and d, the voltammogram of TEA^+ in the presence of the lysozyme digest mixture overlaps no interfering with the signal from the digest. The forward scan for TEA^+ presents steady-state current and peak shaped at 0.64 V on the reverse which corresponds to radial and linear diffusion from the aqueous to the organogel and its back transfer respectively. These data suggest that digestion of lysozyme produces peptide mixtures that adsorb differently at the μITIES.

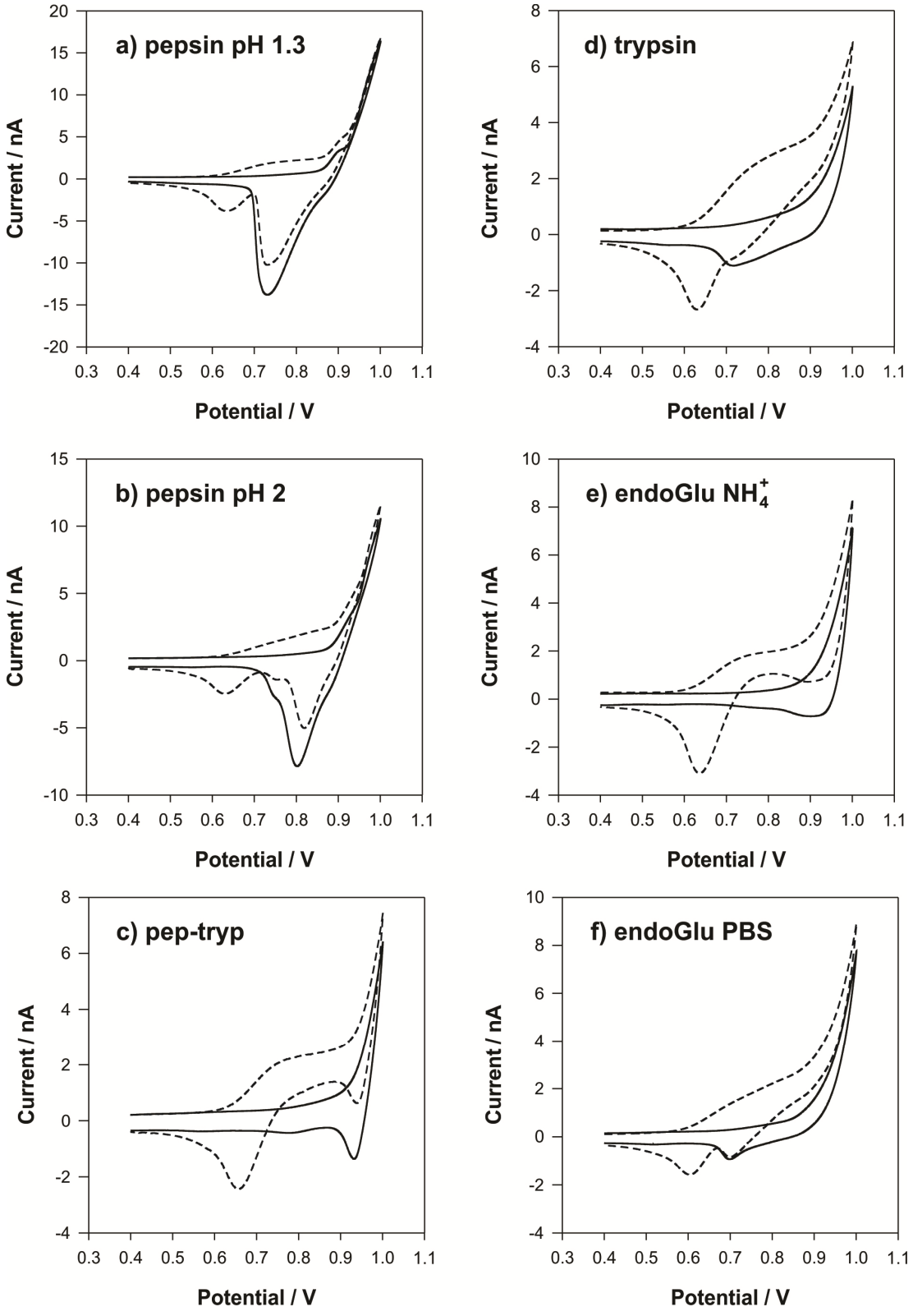

Figure 7.3.7. CVs of 100 µM lysozyme after digestion (solid line) and following addition of 10 µM TEA+ for different enzymatic conditions: a) pepsin at pH 1.3, b) pepsin at pH 12, c) pepsin followed by trypsin, d) trypsin, e) endoproteinase Glu-C in the presence of ammonium and f) endoproteinase Glu-C in PBS.

7. 3. 3. Influence of temperature and filtration step

In order to determine the influence of temperature, filtration and the continuous cycling of applied potential on the voltammetry, the pepsinisation process was followed via cyclic voltammetry for 2 hours at room temperature and 37˚C with measurements taken every 5 minutes. Figure 7.3.8a shows the last CV after the 2h digestion. The voltammograms obtained every 5 minutes are not shown but the reverse peak observed at approximately 0.76 V increased progressively from *ca.* -2.1 nA to -3.2 nA and from ~ -6 nA to -9.2 nA at room temperature and 37ºC, respectively. Comparing Figure 7.3.8a and 7.3.8b, it is clear that the increase of temperature promotes faster and more efficient digestion and the filtration of unreacted molecules prevents the interference of these for the digest detection. The effect of protein and enzyme separation from the aqueous reaction mixture was also investigated as those unreacted molecules could alter the electrochemistry of the new complex mixture via adsorption at the liquid-liquid interface. This is illustrated in Figure 7.3.8b.

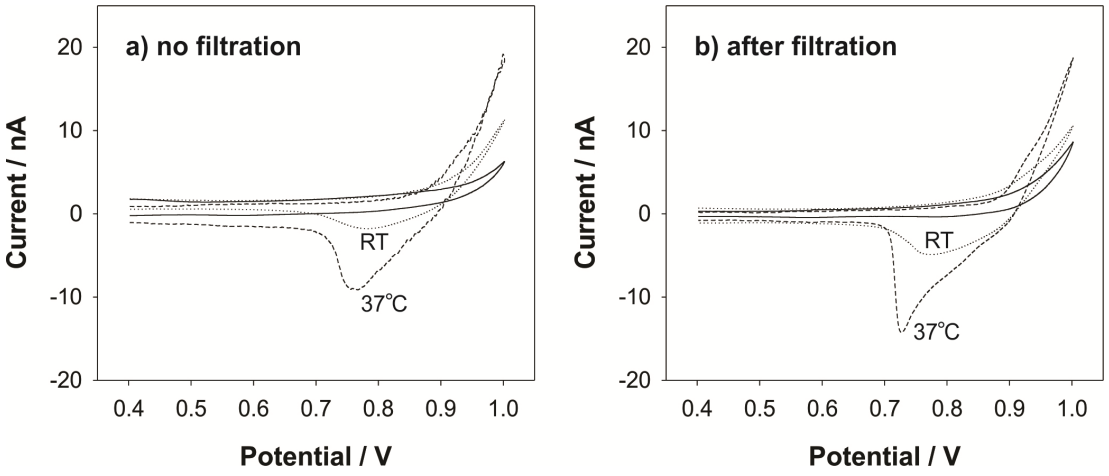

Figure 7.3.8. CV of 10 mM HCl (—), 100 µM lysozyme + 4 µM pepsin after 2h incubation at room temperature (RT) (···) and 100 µM lysozyme + 4 µM pepsin after 2h incubation at 37˚C (- - -); a) without filtration and be after filtration (3 KDa filters).

This demonstrates the importance of the temperature in achieving the optimum performance of the enzyme since the temperature modifies the rate constant (k) of a reaction (Equation 7.3.2).

$$k = Ae^{-\Delta G/RT} \qquad (7.3.2)$$

where A is frequency factor, ΔG is the Gibbs energy (activation energy), R the gas constant and T the temperature.

This preliminary data also bring the possibility to study the kinetics of the enzymatic reaction, the influence of multiple scans (every 5 minutes) and the effect of the undigested protein.

7. 3. 1. Protein identification

Following the detailed characterisation of lysozyme by enzymatic digestion, other proteins were evaluated to study the potential of the ITIES as a label-free biomolecule identification technique in combination with enzyme digestion prior to electrochemical measurements.

Firstly, myoglobin was investigated as it presents a similar molecular size than the lysozyme but it possesses a higher charge (+32) in the acidic conditions than lysozyme. Figure 7.2.9 shows the current intensity versus applied potential of myoglobin digests corresponding to protein concentrations of 1, 5, 10, 15, 30, 60 and 100 μM after enzyme (pepsin and trypsin) digestion.

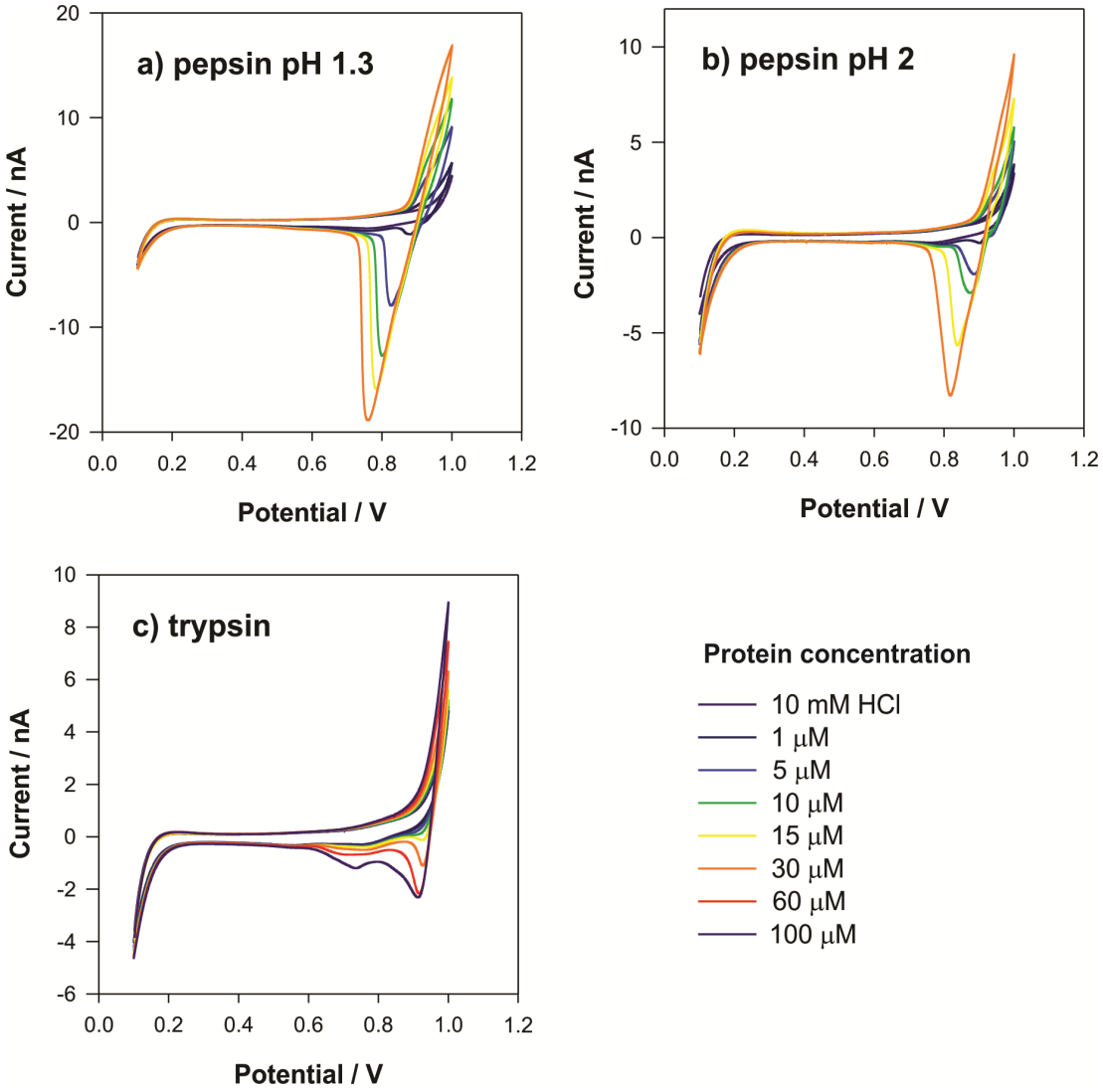

Figure 7.3.9. CV of myoglobin after enzymatic digestion with a) pepsin at pH 1.3, b) pepsin at pH 2 and c) trypsin followed by filtration prior to electrochemical analysis.

As expected for myoglobin, the electrochemical signal is larger than for lysozyme voltammetry for the same aqueous concentrations, which is attributed to how the higher positive charge enhances the interactions between the charged residues in the oligopeptides with the anions from the organic phase ($TPBCl^-$).

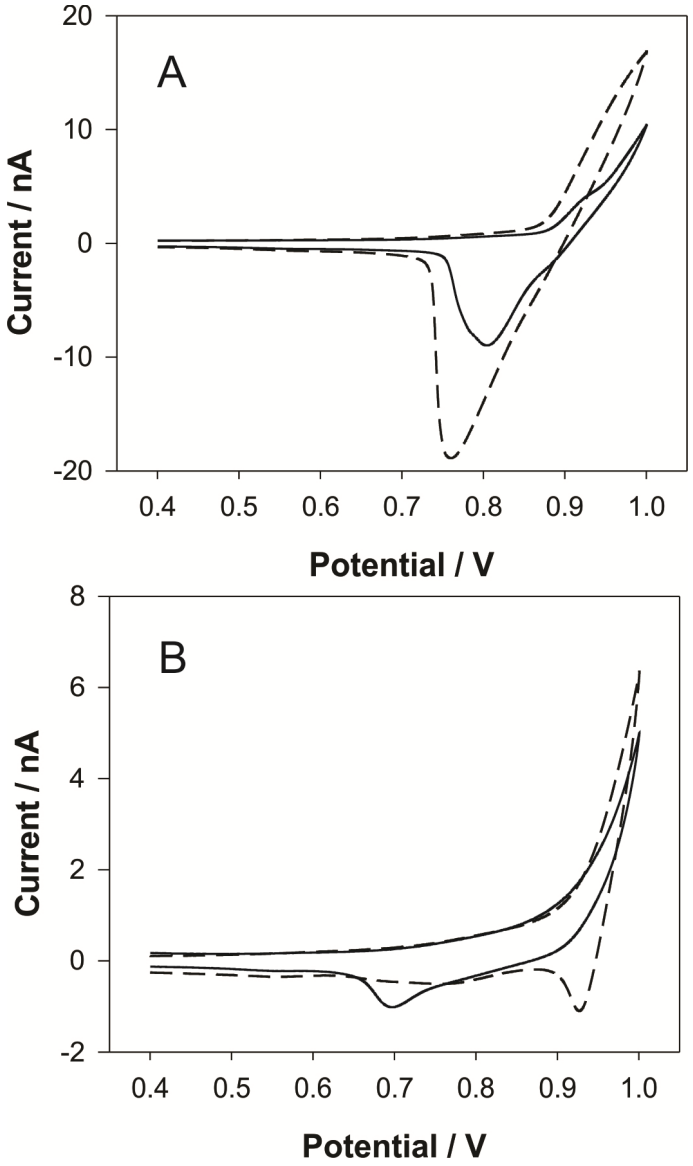

Figure 7.3.10. CV of 30μM lysozyme (—) and myoglobin (- - -) after enzymatic digestion with A) pepsin at pH 2 and B) trypsin followed by filtration prior to electrochemical analysis.

Figure 7.3.10 shows a comparison between 30 μM lysozyme and 30 μM myoglobin digested with pepsin and trypsin, (Figure 7.3.10a and 7.3.10b respectively). A similar approach for the extensive characterisation and comparison to lysozyme was also applied to myoglobin. MALDI/TOF-TOF-MS analysis was carried out for this protein digested with (pepsin at pH 1.3, 2 and 3, trypsin and pepsin (pH 1.30 and pepsin pH 2 followed by trypsin). This time pepsinisation at pH 3 was also carried out in order to determine the effect of the pH in the activity of pepsin therefore in the electroactivity of the digest fragment which would translate in

different voltammetric response. The peptide coverage ranged between 9% and 34 % for these 6 types of digestions. The lack of disulfide bonds in the structure of myoglobin could facilitate the enzymatic digestion and the impossibility to re-fold as the disulfides bonds were not reduced in the lysozyme sample. The sequences identified via MALDI/TOF-TOF-MS were as follows:

Pepsin (pH 1.3): 21 – 30, 22 – 30, 34 – 41, 111 – 124, 111 – 126, 111 – 127, 112 – 124 and 112 – 127

Pepsin (pH 2): 13 – 20, 34 – 52 and 139 – 154

Pepsin (pH 3): 139 – 154

Decreasing the acidity of the digestion solution limited the protein digestion so that the number of cleavages was dramatically reduced, as shown by MALDI/TOF-TOF-MS.

When using trypsin, the peptide coverage was 9% peptide. The peptides identified are:

18 – 32	K.VEADIAGHGQEVLIR.L
26 – 32	H.GQEVLIR.L

From the theoretical point of view, the cleavage of lysozyme or myoglobin by the same enzyme (either pepsin or trypsin), results in a higher number of free amino acids for myoglobin and higher number of small oligopeptides (2 or 3 residues) which translates into a higher total variety of molecules in solution (see Table 7.3.4). These values support the electrochemical fingerprint of lysozyme and myoglobin (Figure 7.3.10). See Appendix C where all the myoglobin digest fragments (Table appendix C7 to C9) produced after enzymatic digestion are summarised.

Table 7.3.4. Comparison of lysozyme and myoglobin digest fragments content.

Peptide mixture Composition	Lysozyme		Myoglobin	
	Pepsin pH 2	Trypsin	Pepsin pH 2	Trypsin
single amino acids	6	4	16	3
di-peptides	1	2	8	3
tri-peptides	1	1	3	2
total amino acids and oligopeptides	15	18	38	21

**data assuming 100% cleavage efficiency*

Again, the free amino acid content in the aqueous phase following digestion was determined via GC-MS. For this purpose, 1 mM myoglobin was incubated with the corresponding enzyme (40 μM) for either 2h or overnight (*ca.* 16 h). The results obtained via GC-MS for 100 μL of the digested protein (1 mM) are summarised in Table appendix E2 (see Appendix E) and presented as the amount of free amino acid detected in nanomoles. Then the amino acid concentration in the initial sample was calculated and illustrated in Table 7.3.5. A higher content of hydrophobic amino acids at pH 2 comparing to the concentrations obtained for the pH 3 digestion confirms the importance of the pH in enzyme activity. Moreover the content of lysine is substantially higher in the trypsinised sample than in the other digests. In the case of trypsinisation, the levels of histidine increased which could be due to a higher component of histidine residues in the amino acid sequence (11 out of 153 in myoglobin to 1 in 129 in the case of lysozyme) but also because histidine groups in positions 48, 64, 97 and 119 are bonded to lysine residues which is one of the specific targets for trypsin. All the amino acid levels in solution are summarised in Table 7.3.5.

Table 7.3.5. Free amino acid concentration of 1 mM myoglobin digested in the presence of 40 μM enzyme and measured via GC-MS after derivatisation.

Amino Acid	Amino acid concentration / μM				
	Pepsin pH 2	**Pepsin pH 3**	**Trypsin**	**Pepsin pH 1.3 - Trypsin**	**Pepsin pH 2 - Trypsin**
Alanine	92	31	60	237	149
Sarcosine	13	9	11	12	15
Glycine	47	22	245	37	39
Valine	38	156	37	21	8
Leucine	494	27	687	174	217
Isoleucine	26	13	0	7	0
Threonine	19	10	50	23	88
Serine	15	8	20	0	0
Proline	4	0	0	14	0
Asparagine	0	0	29	0	0
Aspartic acid	22	5	43	39	8
Methionine	50	0	32	66	13
4-Hydroxyproline	0	13	0	0	0
Glutamic acid	91	50	154	108	40
Phenylalanine	434	0	508	240	141
Glutamine	333	691	396	369	175
Ornithine	20	13	0	0	0
Lysine	76	24	7808	190	828
Histidine	0	0	406	0	0
Tyrosine	130	0	1572	66	209
Tryptophan	32	1	28	104	11

Mechanistically, the mixture measured is a complex matrix difficult to elucidate due to all the possible interactions within the molecules which can affect their transfer across the liquid – liquid interfaces. As a rough attempt to understand the contribution of these molecules to the electrochemical signal, TEA^+ was spiked to a final concentration of 10 μM in the final digest solution. Thus, a qualitative analysis could prove the co-transfer of several molecules with TEA^+ and/or the adsorption of some which would alter the TEA^+ voltammetry. Figure 7.3.11 summarizes this information. It was found that for the mixture obtained after trypsinisation of myoglobin, the TEA^+ transfer peak was distorted, which is due to the adsorption of the large peptides at the micro-interfaces.

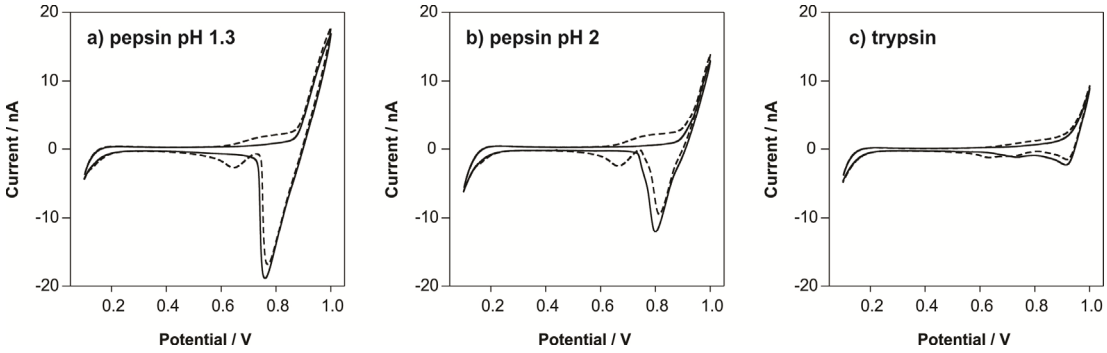

Figure 7.3.11. CV of 30μM lysozyme (—) and myoglobin (- - -) after enzymatic digestion with A) pepsin at pH 2 and B) trypsin followed by filtration prior to electrochemical analysis.

Two larger proteins were also investigated, bovine serum albumin (BSA) and haemoglobin. Four different CVs for 30 μM of protein incubated at 37˚C for 2h in a pepsin-to-protein 1:25 ratio at pH 2 (10 mM HCl), are illustrated in Figure 7.3.12.

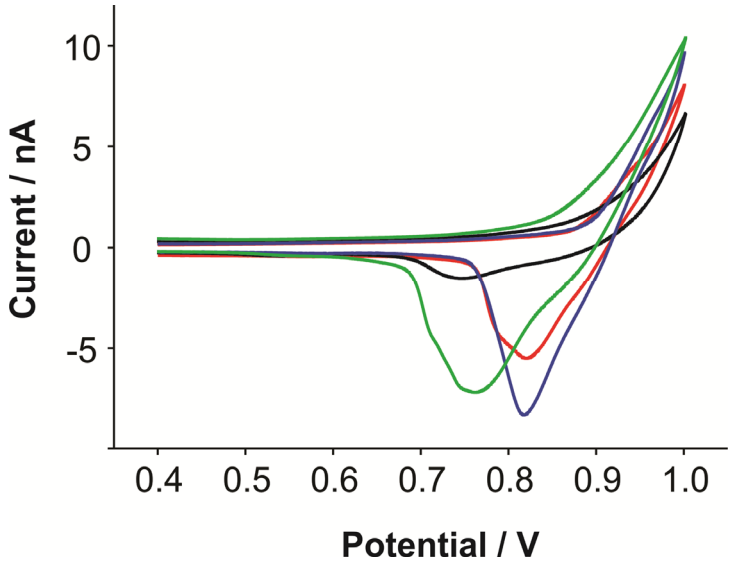

Figure 7.3.12. CV of pepsin digest lysozyme (—), myoglobin (—), BSA (—) and haemoglobin (—). Concentrations correspond to 30μM of initial protein.

The analogous voltammograms for trypsinisation of lysozyme, myoglobin, albumin and haemoglobin are plotted in Figure 7.3.13.

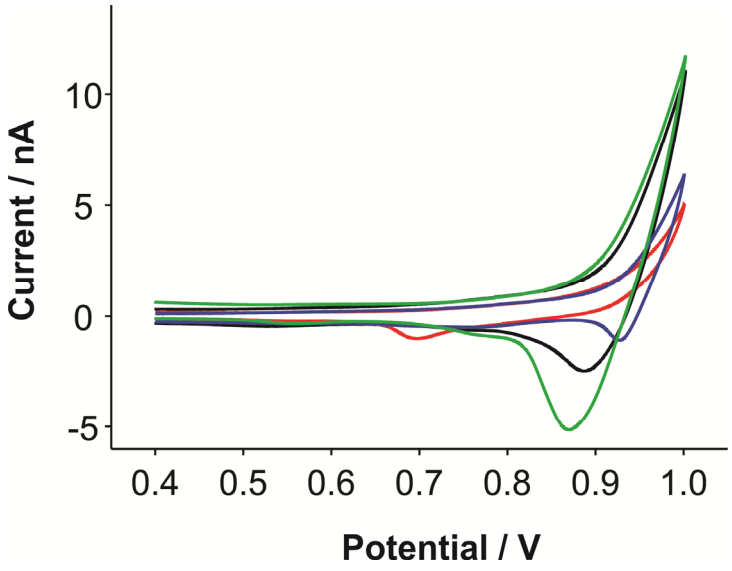

Figure 7.3.13. CV of 30μM lysozyme (—), myoglobin (—), BSA (—) and haemoglobin (—) after trypsination and filtration.

The extension of the mixtures voltammograms relies on the protein configuration and charge. The degree of unfolding is linked to the content of disulfide (S-S) bridges in the protein. Therefore, when comparing lysozyme to myoglobin and albumin to haemoglobin, it was expected to measure higher current for myoglobin and haemoglobin respectively, as both lack S-S bonds which leads to a more unstable conformation in acidic conditions exposing larger parts of the protein which facilitates its protonation. Nonetheless, when comparing the four proteins together other factors have to be taken into account as for instance size and structure. In Table 7.3.6, the number of digest fragments, free amino acids, di-peptides and tri-peptides for the four proteins studied have been reported. As expected, the total number of digest fragments increased for proteins such as albumin and haemoglobin as their amino acid content is approximately 4-fold larger than lysozyme and myoglobin. As pointed previously, values such as the small oligopeptides or free amino acids are only one of the factors that influence the voltammetry of the digested proteins. This is confirmed as the albumin signal when trypsinised is significantly lower than the other three proteins which is contradictory to the number of small fragments expected (see Table 7.3.6).

Table 7.3.6. Comparison of the digest composition of the four proteins when digested with pepsin or trypsin.

Peptide mixture composition	Lysozyme		Myoglobin		Albumin		Haemoglobin	
	Pepsin pH 2	Trypsin	Pepsin pH 2	Trypsin	Pepsin pH 2	Trypsin	Pepsin pH 2	Trypsin
single amino acids	6	4	16	3	56	3	56	2
di-peptides	1	2	8	3	18	6	22	8
tri-peptides	1	1	3	2	8	7	21	0
total amino acids and oligopeptides	15	18	38	21	146	79	160	63

**data assuming 100% cleavage efficiency*

On the contrary, these preliminary results seem promising as each of the protein presents different signatures under the same conditions and also different features when varying the enzyme to cleave the amino acid sequence of the protein.

Mathemical examination of the current measured over a period of time when a potential difference is applied across the μ-liquid – liquid interfaces was proposed as an alternative methodology to obtain more information from the electrochemical signature of the digest mixtures. In a cyclic voltammogram, the current measured is represented versus applied potential (5 mV/s in the experiments shown in this chapter). In this case, the first and second derivative[237] were calculated for the current measured versus applied potential. Figure 7.3.14 and 7.3.15 correspond to the first derivative of the electrochemical data obtained for lysozyme, myoglobin, albumin and haemoglobin after pepsin digestion (pH 2) for the forward (Figure 7.3.14) and the reverse scan (Figure 7.3.15). The first derivative illustrates the tangent of the curve ($\Delta i/\Delta E$) over time which shows the inflexion points in the original data.

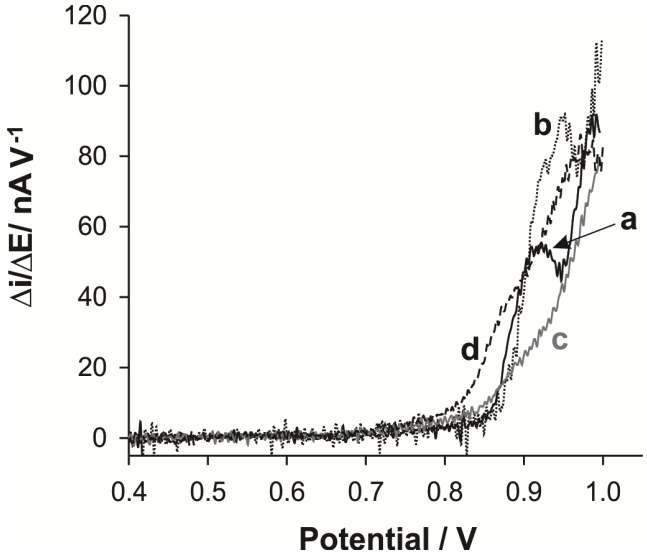

Figure 7.3.14. First derivative of the forward current versus the applied potential of a) lysozyme, b) myoglobin, c) BSA and d) haemoglobin after pepsinisation at pH 2. Concentrations correspond to 30μM of initial protein.

In Figure 7.3.14, lysozyme showed a maximum in Δi/ΔE values at 0.91 V, and myoglobin and haemoglobin at 0.94 and 0.97 V, respectevily. Albumin, however, presents an exponentional increase in the tangent value of the voltammogram data with no maximum or inflexion point within the potential range measured. On the reverse scan of the voltammetric analysis of the digest fragments produced after pepsinisation, the first derivative provides higher resolution of the process characterisefd via cyclic voltammetry (see Figure 7.3.15). Whilst in the standard CV performed for the four different samples (lysozyme, myoglobin, albumin and haemoglobin) only one single reverse peak was observed (Figiure 7.3.12).

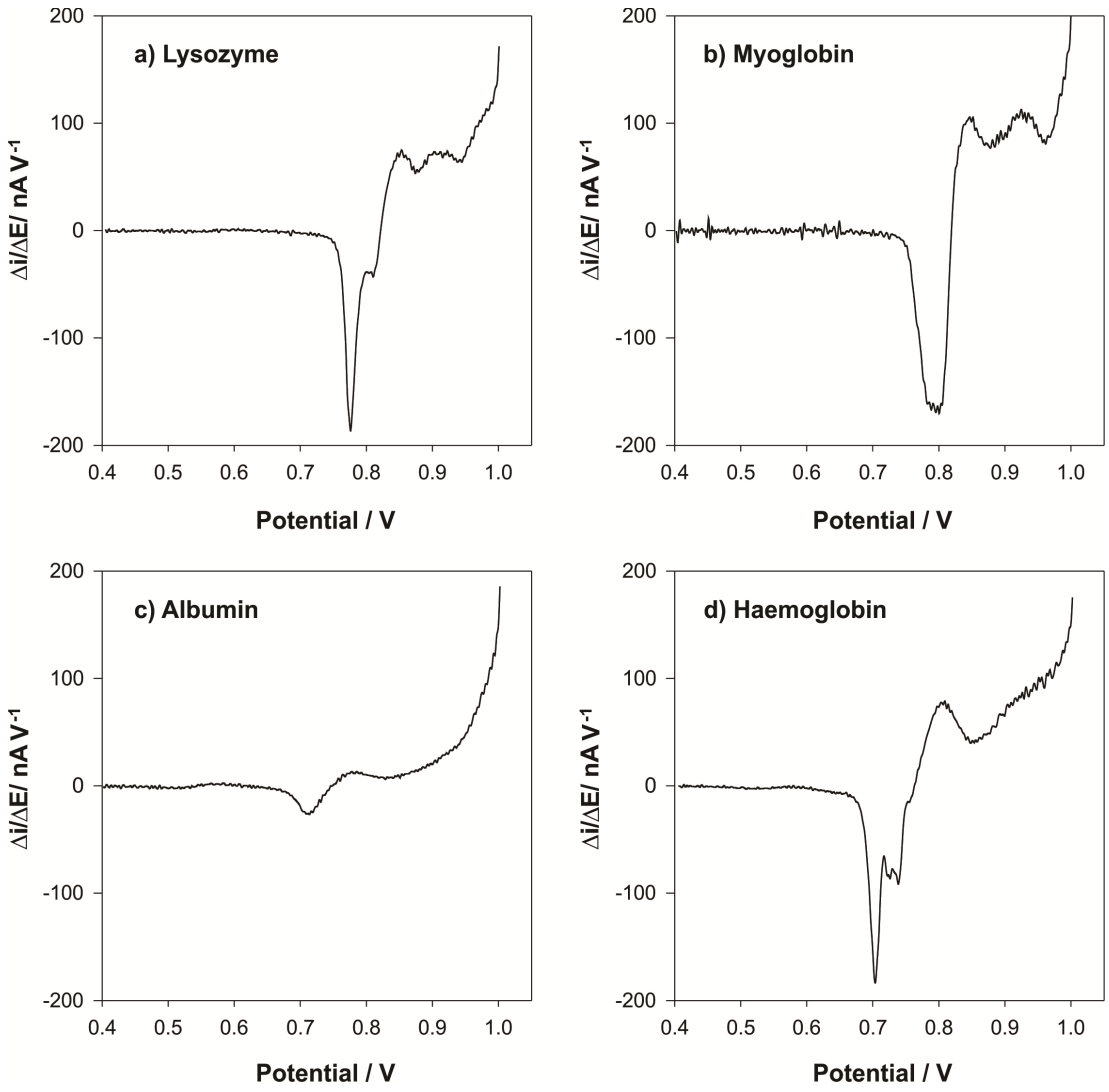

Figure 7.3.15. First derivative of the reverse current over time of a) lysozyme, b) myoglobin, c) BSA and d) haemoglobin after pepsinisation at pH 2. Concentrations correspond to 30µM of initial protein.

Higher derivatives such as the second derivative of current versus applied potential were also investigated. The second derivative ($\Delta\left(\frac{\Delta i}{\Delta E}\right)/\Delta E$ versus time) gives the minimum or maximum values of the tangent of the first derivative (Figure 7.3.14 and 7.3.15) over applied potential. Herein the second derivative of the reverse scan is illustrated in Figure 7.3.16 as the results when evaluating the forward sweep showed insignificant changes (see Figure appendix F1).

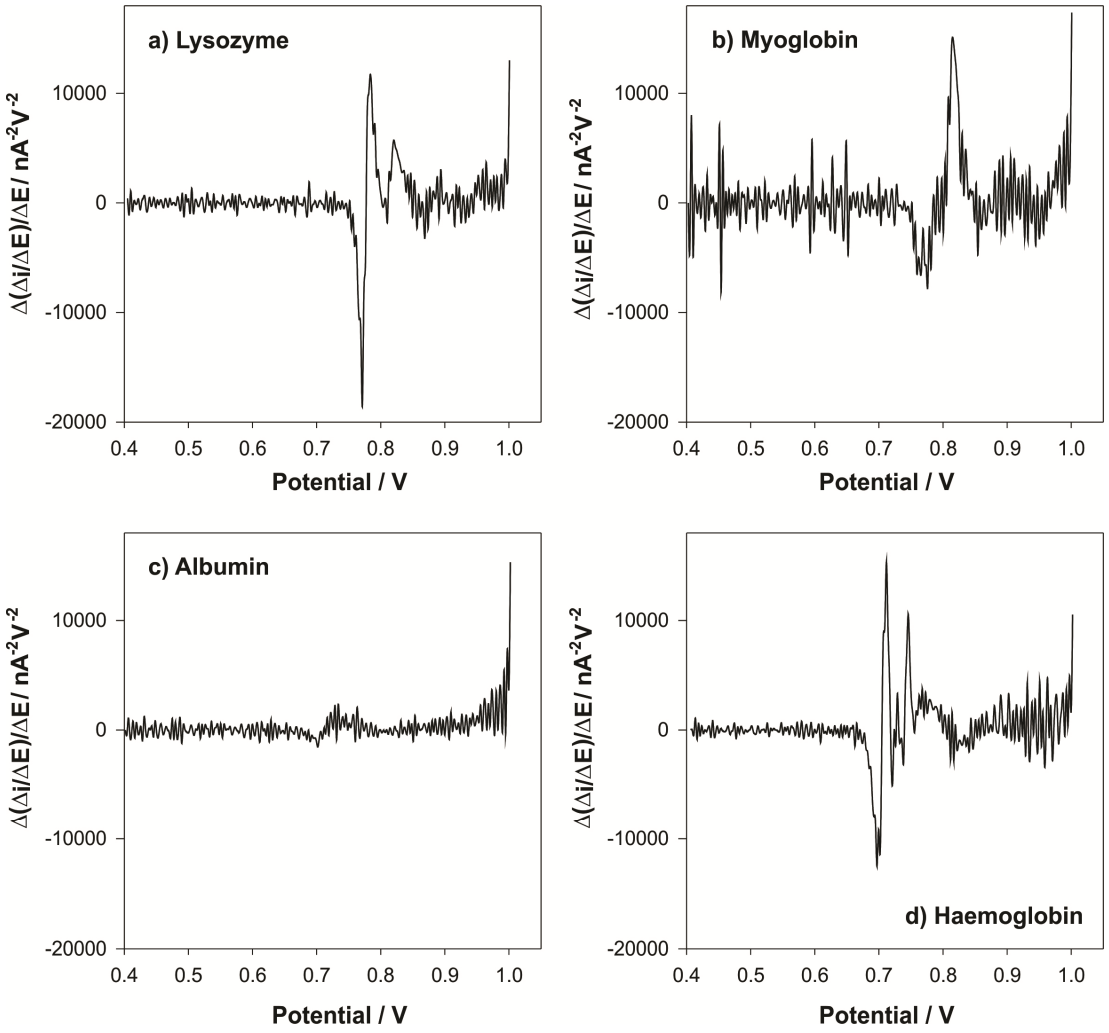

Figure 7.3.16. Second derivative of the reverse voltammogram obtained for 30 μM pepsin digest (pH 2) of a) lysozyme, b) myoglobin, c) albumin and d) haemoglobin.

The same approach was applied for the digestion of four proteins (lysozyme, myoglobin, BSA and haemoglobin) with trypsin. The CVs from Figure 7.3.13 were also derivatised. The first order derivatives are shown in Figure 7.3.17 and Figure 7.3.18.

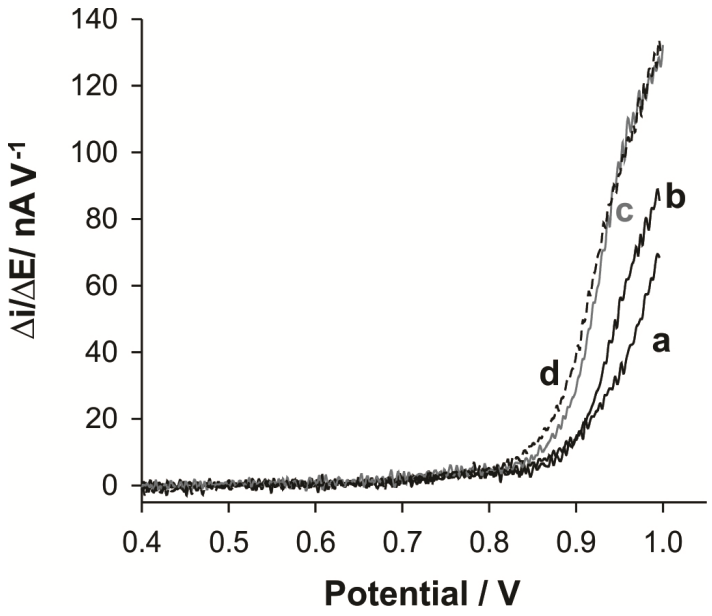

Figure 7.3.17. First derivative of the forward sweep voltammetry obtained for 30 μM trypsin digest of a) lysozyme, b) myoglobin, c) albumin and d) haemoglobin.

Figure 7.3.17 presents less characteristic features compared to the previous derivatives from the digestion performed using pepsin at pH 2 (Figure 7.3.14), which is in agreement with the voltammetry of these proteins. Nonetheless, there is a significant difference in the Δi/ΔE values for the four samples providing a certain degree of resolution between the first derivatives of the proteins studied. Again as in the case of pepsin digestion, the first derivative of the reverse voltammogram provided more significant changes. In Figure 7.3.18, lysozyme posses a minimum Δi/ΔE value at 0.68 V, myoglobin at 0.92 V, albumin at 0.87 V and haemoglobin at 0. 85 V.

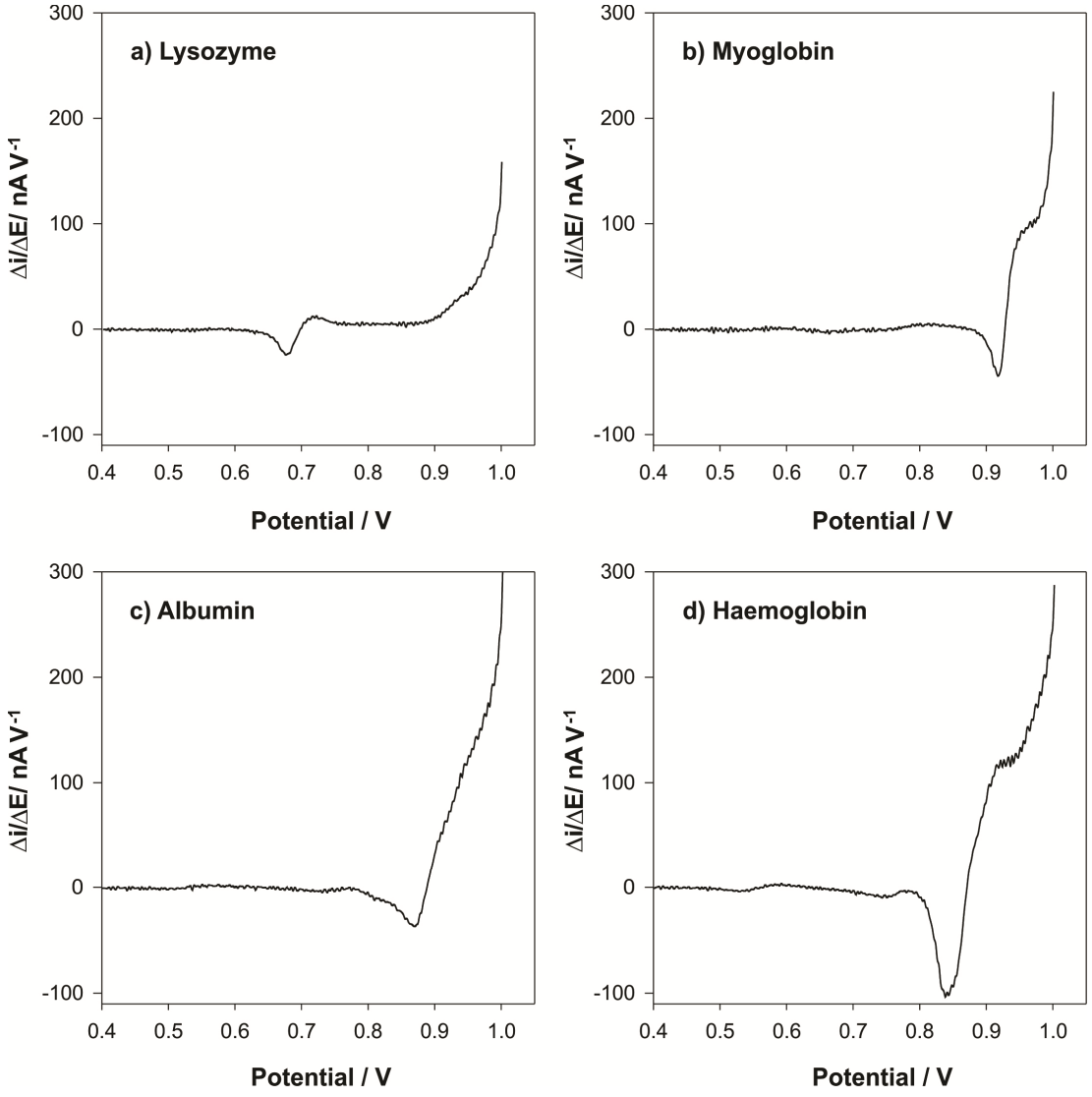

Figure 7.3.18. First derivative of CVs obtained for 30 μM pepsin digest (pH 2) of a) lysozyme, b) myoglobin, c) albumin and d) haemoglobin.

Lastly the second derivative was also evaluated for the tryptic digestion of the four proteins. The analysis performed on the forward scan is represented in Figure appendix F2 and the corresponding to the reverse is illustrated in Figure 7.3.19.

The second derivatives (Figure 7.3.16 and 7.3.19) could complement the analysis of the results obtained when performing the first derivative although based on the data presented here, the first derivatives of the voltammograms might provide enough evidence of differences in the charge transfer processes at the ITIES which are undistinguishable in the voltammetric analysis (current versus potential).

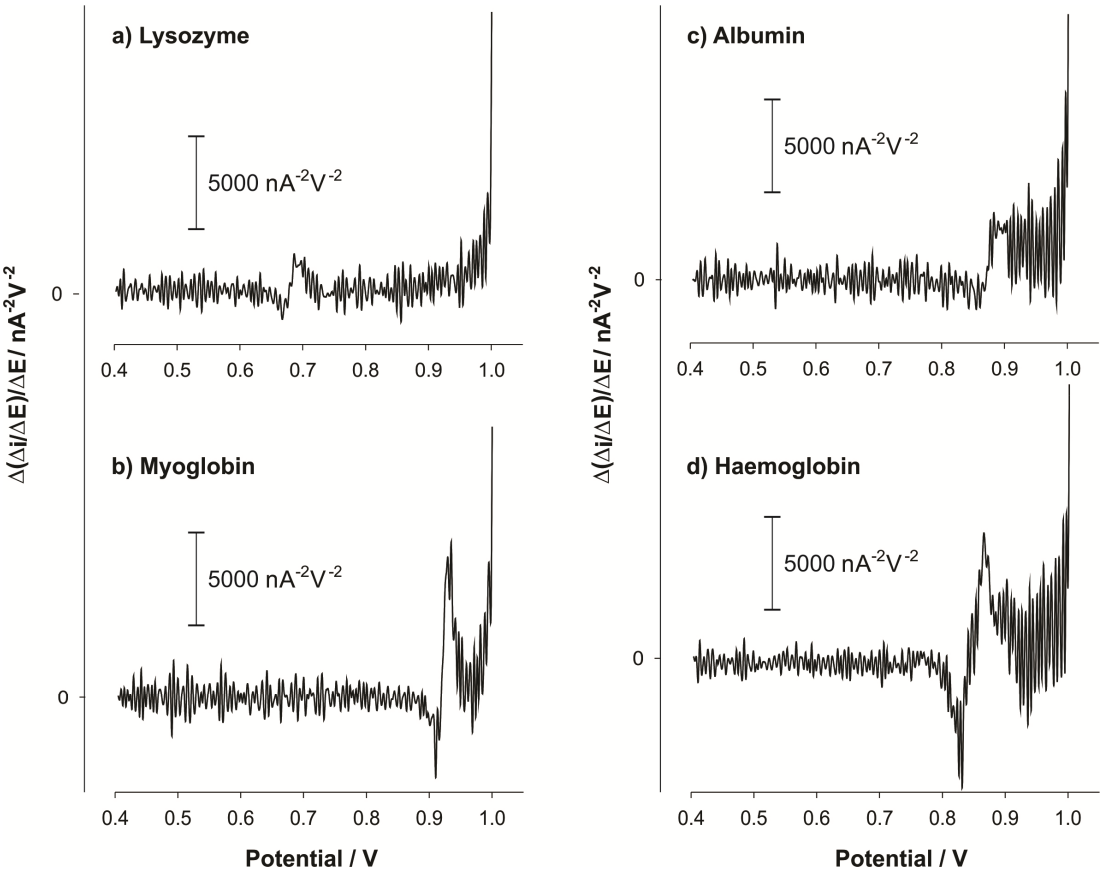

Figure 7.3.19. Second derivative of current versus time of a) lysozyme, b) myoglobin, c) BSA and d) haemoglobin after trypsinisation. Concentrations correspond to 30μM of initial protein.

This mathematical approach could be of use for protein identification in a protein mixture where cyclic voltammetry is incapable of discerning inflexion point characteristic of the specific analytes.

7.3.4. Denaturation with urea

The effect of chemical denaturation (presence of urea in the aqueous solution) was evaluated as an alternative or complementary characterisation of different proteins. Urea can interact with polar residues in the protein, stabilizing non-native conformation.

The experiment carried out consisted in a preliminary incubation of the protein with urea overnight at room temperature followed by electrochemical analysis. Therefore the possible electroactivity of urea was evaluated as a control experiment. For the experiments performed to denature the protein, an aliquot of protein + urea

was added to the 10 mM HCl resulting in 10 μM of the protein + 0.095M urea in 10 mM HCl. There was no measurable change in the voltammetry for 0.095 M of urea in 10 mM HCl. Only ion transfer was observed when the urea concentration in the aqueous solution was higher than 0.23 M (see Figure 7.3.20).

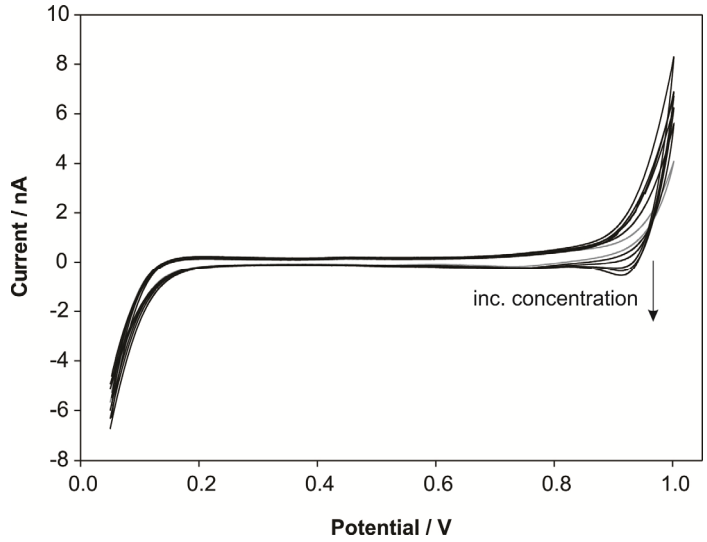

Figure 7.3.20. CV of increasing concentrations of urea in 10 mM HCl (0/ 0.095/ 0.238/ 0.475/ 0.713/ 0.950 M).

When lysozyme was incubated with urea prior to the voltammetric analysis, the electrochemical signal did not vary significantly in comparison to the native protein in 10 mM HCl (see Figure 7.3.21). In addition, 5 μM haemoglobin was also incubated with 9.5 M urea in 0.15 M KCl and 0.15 M HCl prior to the electrochemical analysis. The voltammetry before and after chemical denaturation with urea is shown in Figure 7.3.21. There is a slight decrease in the peak intensity (1 nA) but the voltammetric shape is very similar to haemoglobin in 10 μM in its native form. This could be due to partial re-folding of the protein after changing aqueous conditions, from 9.5 M urea in the media to 0.095 M. Moreover, the different structural nature of the lysozyme and haemoglobin can also explain the voltammetry (Figure 7.3.21) for these proteins. Lysozyme is a compact globular protein and haemoglobin is a large metalloprotein which contains four globular subunits. Lysozyme possesses four disulphide bonds[238] that keep the protein in its folded state therefore maintaining lysozyme in its native configuration. However the lack of disulphide bonds in haemoglobin[124] makes the protein more susceptible to unfolding. This is believed to disturb the voltammetry of haemoglobin after it has been

denatured via urea-protein destabilization, which is in agreement with Herzog's work.[82]

Herzog et al. performed electrochemistry of haemoglobin in the presence of urea[229] or after urea and guanidine denaturation[82] at a water/1,2-dichloroethane interface. These studies introduced the potential of this technique for the investigation of protein denaturation.

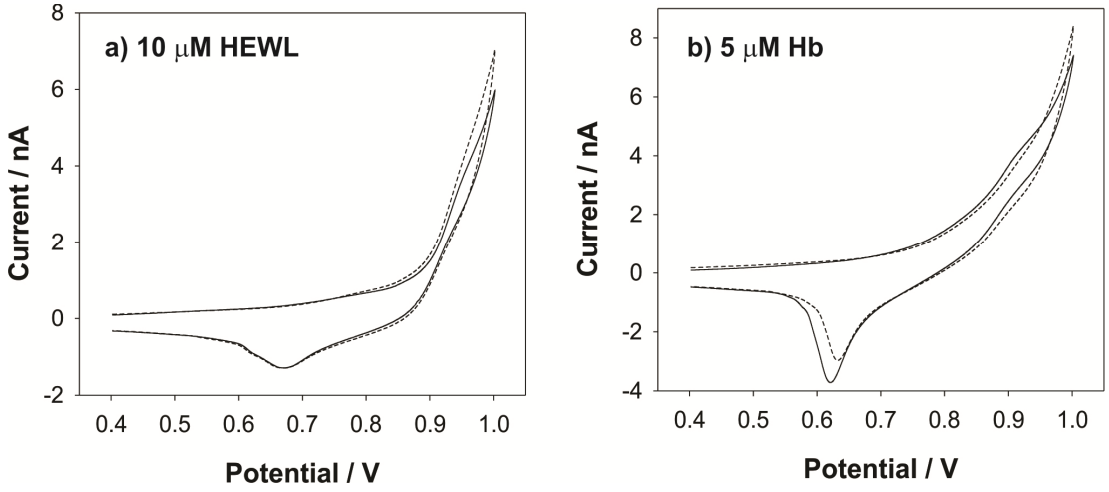

Figure 7.3.21. CV of a) 10 μM lysozyme in 10 mM HCl after being incubated in PBS + urea overnight and b) 5 μM haemoglobin after incubation in 0.15 M KCl and 0.15 M HCl then measured in 10 mM HCl.

Further investigation of denaturation prior to enzymatic digestion could enhance the enzymatic efficiency and affect the voltammetry, as the unfolded state of the protein exposes the hydrophobic core and inaccessible parts of the protein to further digestion.

7.3.4. The use of ionophores to enhance the peptide signal

As an attempt to enhance the electrochemical signal of the digested protein, dibenzo-18-crown-6 (see Figure 7.3.22) was studied because this macrocycle is able to complex single amino acids and peptides via their protonated states. This is via interaction of the crown ether through hydrogen bonding between the oxygen atoms in the crown and the protonated amine.[34, 66] DB18C6 has also been proven to complex several metal ions such as K^+,[239] Li^+ by electrostatic interactions at liquid-liquid interfaces.[240]

Consequently, the effect of the aqueous electrolyte was under examination as a potential interference in the detection of oligopeptides or single amino acids. Initially, 10 mM HCl, 10 mM LiCl and 10 mM HNO_3 were evaluated at the water/gelled-1,6-DCH micro-interfaces when 10 mM DB18C6 was present in the organic phase in combination with 10 mM TPPBA TPBCl.

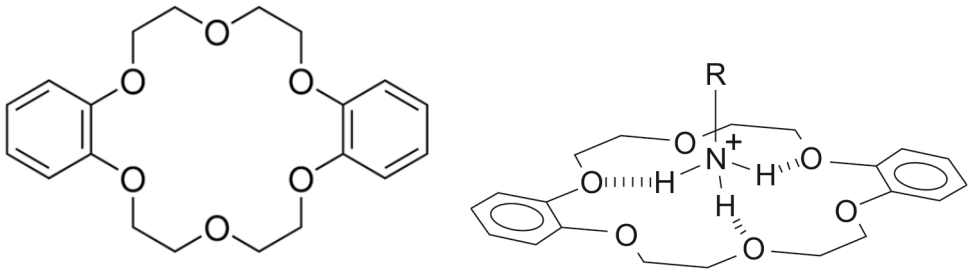

Figure 7.3.22. Ionophore dibenzo-18-crown-6 (DB18C6) structure on the left hand side and primary ammonium cations interacting via hydrogen binding to DB18C6.

Figure 7.3.23 shows the CVs obtained for the different aqueous electrolytes. The nitrate starts transferring at 0.4 V from the aqueous to the organic phase whilst the chlorine transfers at *ca.* 0.1 V. However, HCl and LiCl present two different features in their corresponding voltammograms. Both showed a peak at 0.6 V on the reverse scan which can be attributed to complexation of DB18C6 to either H^+ or Li^+ respectively via electrostatic interactions. In the case of HNO_3, the potential window shortened which makes difficult the direct comparison to the HCl and LiCl voltammetry.

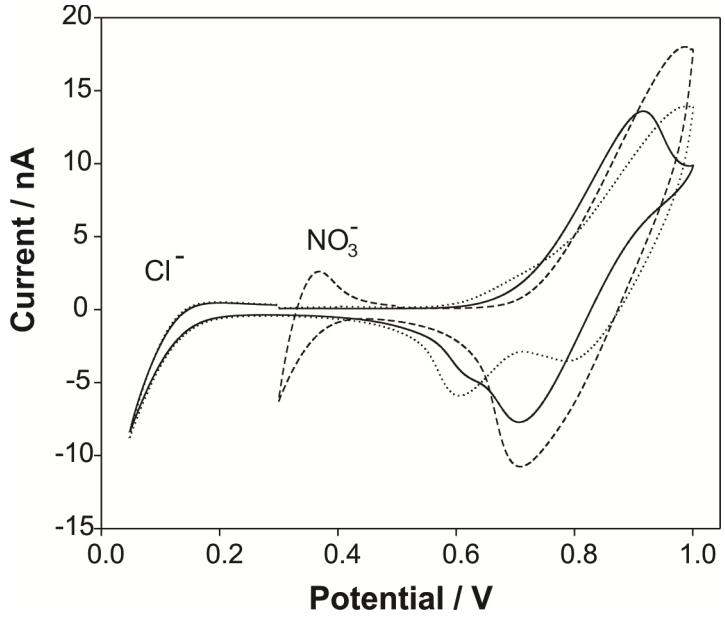

Figure 7.3.23. CV of 10 mM of HCl (—), LiCl (···) and HNO_3 (- - -) at the W/gelled DB18C6-1,6-DCH microinterfaces.

Even though the background electrolyte signal is quite significant and the complexation observed for DB18C6-H^+ could interfere the protein detection, the lysozyme digest was measured via cyclic voltammetry at these new gelled microinterfaces. In Figure 7.3.24, the different voltammograms for several lysozyme digestions in 10 mM HCl are presented. These results are compared with the native protein (lysozyme) at the W/gelled DB18C6-1,6-DCH microinterfaces (Figure 7.3.24 inset) and the background signal (10 mM HCl, solid black line in Figure 7.3.24 inset).

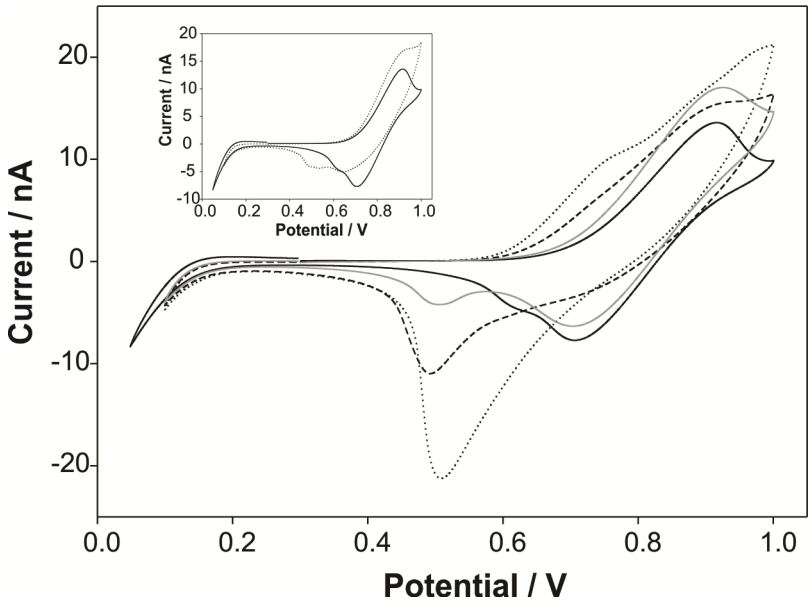

Figure 7.3.24. CV of 10 mM HCl (—), 30 μM lysozyme in pepsin pH 1.3 (···), pH 2(- - -), and trypsin (—) at the W/gelled DB18C6-1,6-DCH microinterfaces. Inset corresponds to CV of 10 mM HCl (solid line) and 30 μM of native lysozyme with no digestion at the same micro-interfaces at a scan rate of 5 mV/s.

From an analytical point of view, the use of dibenzo-18-crown-6 enables signal enhancement via biomolecule complexation to DB18C6. However, there was no gain in resolution of the voltammetric peaks, which agrees with the low selectivity reported by Chen when using DB18C6 at the water/dichloroethane interface.[66] They attributed this to steric effects from the hindrance by the side group of the amino acids and lipophilic stabilization in the bulk solution.

The above experiments repeated in a shorter potential window to avoid the background signal associated with the organic phase electrolyte and ionophore, and also the complexation of the aqueous electrolyte by DB18C6. Figure 7.3.25 illustrates similar data to Figure 7.3.24 but in a shorter potential range (0.05 – 0.75 V) as reported in several publications.[34, 66, 228, 241]

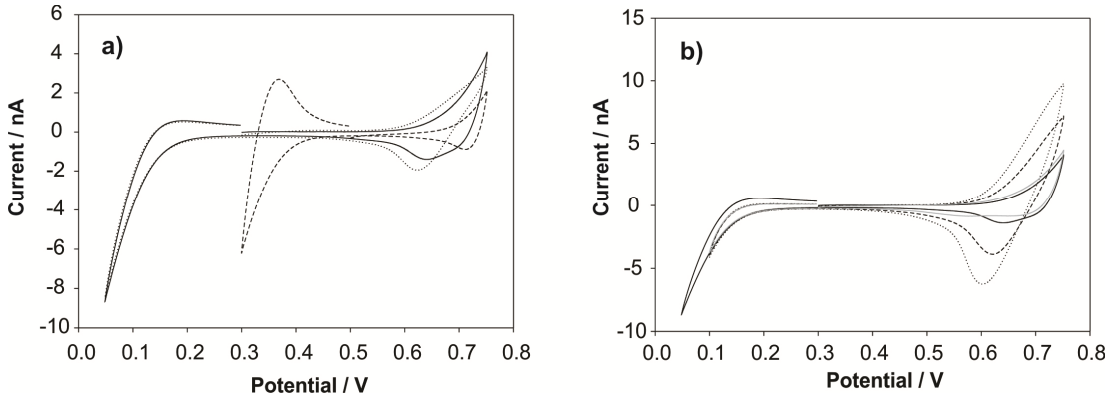

Figure 7.3.25. a) CV of 10 mM of HCl (—), LiCl (···) and HNO_3 (- - -) and b) CV of 10 mM HCl (—), 30 µM lysozyme in pepsin pH 1.3 (···), pH 2(- - -), and trypsin (—). Inset CV of 10 mM HCl (solid line) and 30 µM of lysozyme with no digestion.

In this situation (Figure 7.3.25), the current generated in the presence of complex peptide mixtures is substantially lower than that in a wider potential range (Figure 7.3.24). For instance, for trypsinised lysozyme, the CV is indistinguishable from the background signal (HCl). As a result, dibenzo-18-crown-6 has been shown to enhance the electrochemical signal of complex peptide mixtures. However, the resolution was limited.

7.3.5. SV of protein digest

Pre-concentration of the protein digest followed by Stripping voltammetry (SV) was assessed in order to achieve lower limit of detections as performed in previous Chapters (3, 4, 5 and 6). Protein digestion resulted in a decrease current intensity when the new matrix is present in the aqueous solution compared to the signal of the native protein. For example, Figure 7.3.26a illustrates the differences in the cyclic voltammetry of bovine serum albumin and its digest product. The data reveal that changes in the aqueous matrix after digestion were not measurable for higher concentration of the initial protein (5 µM of BSA and 10 µM of BSA digest). Here the importance of supplementary analysis either to enhance the signal by pre-concentration or a better understanding of the detection mechanism of these complex matrices. Figure 7.3.26b presents stripping voltammograms of different applied potentials for the native BSA. Then Figure 7.3.26c and Figure 7.3.26d consist of SV of 10 µM BSA after pepsinisation and trypsinisation respectively at several applied potentials for a pre-concentration time fixed to 60 seconds. These two last graphs

show the different behaviour of the digested albumin when its fragmentation occurs at different residues. In the case of albumin, its structure is stabilized by 17 disulfide bridges[242] in the molecule which holds three homologous domains and can reduce the degree of digestion. As mention in Section 7.3.4, denaturation should be evaluated as a pre-treatment step before enzyme incubation and reduction of the disulfide bonds for a further residue exposure when the protein is in its unfolded conformation.

Figure 7.3.26. a) CV of 5 μM BSA (—), 10 μM BSA after pepsin digest (pH 2) (···) and 10 μM BSA after trypsin digest (- - -), b) SV of 5 μM BSA of different applied potential, c) SV of 10 μM BSA after pepsin digestion (pH 2) at different applied potential and d) SV of 10 μM BSA after trypsinisation at different applied potential. All SV were implemented at 60 s pre-concentration time and 5 mV/s scan rate.

Similar results are presented in Figure 7.3.27 for haemoglobin which is a disulfide free protein. The conformation of the protein in acidic conditions seems to play a key

role in the detection of the molecules, as the theoretical number of charges at acidic pH based on the amino acid sequence should be higher for albumin than haemoglobin, as both are similar in size (average ~65 kDa). However, the 17 disulfide bonds stabilize the protein in a more compact conformation than haemoglobin which is partially unfolded at pH 2. Figure 7.3.27b and Figure 7.3.27c-d illustrate the loss of sensitivity when haemoglobin is fragmented by pepsin and trypsin.

Figure 7.3.27. a) CV of 10 μM Hb (—), 10 μM Hb after pepsin digest (pH 2) (···) and 10 μM Hb after trypsin digest (- - -), b) SV of 5 μM Hb different applied potential, c) SV of 10 μM Hb after pepsin digestion (pH 2) at different applied potential and d) SV of 10 μM Hb after trypsinisation at different applied potential. All SV were implemented at 60 s pre-concentration time and 5 mV/s scan rate.

These preliminary results which are a continuation of the work performed in Chapters 3, 5 and 6 present the potential of stripping voltammetry as a possible tool

after electrochemical pre-concentration by tuning the applied potential and pre-concentration time prior to further analyses. Cyclic voltammetry presented the limitation of sensitivity when the protein of interest is digested which could be overcome by the application of this technique. Herzog et al. have already reported the improvement in protein digest detection when implementing differential pulsed stripping voltammetry at liquid – liquid interfaces. The lowest concentration reported was 0.55 μM haemoglobin tryptic digest at micro-interfaces[83] which agrees with the presented work here.

7. 7. Conclusions

Four proteins (lysozyme, myoglobin, albumin and haemoglobin) were proteolised with several enzymes prior to electrochemistry at water/gelled 1,6-dichlorohexane micro-interfaces. It has been observed that unique voltammetry is obtained for the distinctive protein fragment mixtures. The use of various enzymes such as pepsin, trypsin and endoproteinase Glu-C, has been also shown to increase the selectivity of the protein electrochemical signal as it increases the specific signatures obtained for a unique protein, in this case lysozyme. However, the gain in selectivity has compromised the sensitivity of the system, as the minimum detectable concentration has increased relative to the voltammetry of the native protein. For instance, the minimum digest detectable for lysozyme varied from 10 μM to 30 μM via CV, 1-3 orders of magnitude higher than reported values of the native protein at the liquid – liquid interfaces.[78] These results follow up on previous work carried out by Herzog et al.[83] and show the potential of this approach as a label-free identification by electrochemical analysis. This could lead to a new methodology that could be nominated as *'electroproteomics',* the combination of proteomics and electrochemistry.

Mass spectroscopy data revealed the importance of proteolysis in the electrochemical signature. When using pepsin at low pH, the concentration of free amino acids and smaller oligopeptides was higher than when employing trypsin or endoproteinase Glu-C. Also, by GC-MS, it was proven that the hydrophobic content of the digest mixture enhances the electrochemical signal. Preliminary experiments confirmed how this is not the unique factor as isolated amino acids in the aqueous

solutions only provided a slight change in the forward voltammetric scan. Therefore, amino acid-peptide interactions should be considered. Moreover, MALDI-TOF confirmed the activity of pepsin which was correlated to the corresponding voltammetry.

In terms of proteolysis by endoproteinase Glu-C, the unique oligopeptide in solution when using ammonium bicarbonate as buffer and after filtration, is KVFGRC, a 6 residue peptide with a charge of 2+ (lysine and arginine) under acidic conditions. When the different buffer conditions were compared, similar reverse peaks were observed in both (0.7 V). This could be explained as the same peptide (KVFGRC) is present in both solutions but for digestion in PBS, the forward signal increases. This increase could be due to larger oligopeptides (1.2 – 2.5 kDa) in solution which can adsorb at the interface and distort at the same time the reverse peak magnitude.

As there are still open questions at the time of submission of this thesis, further studies are recommended for a better understanding of the protein digest at the ITIES. Firstly, address the electrochemical signal of isolated peptides from the digest. For instance, the three main peptides (32 – 39, 52 – 63 and 135 – 143) obtained for lysozyme when trypsinised, should be characterised in the presence and absence of amino acids and other oligopeptides. Secondly, pre-concentration steps to enhance the signal should be also optimised with either several stripping techniques following previous work (see Chapter 3 and 6) or the use of solid phase extraction columns after digesting the protein prior to electrochemistry at the ITIES. As mentioned in this chapter, chemical and thermal denaturation and disulfide bridge (S-S) reduction to prevent re-folding of the peptides/proteins before protein digestion should also be evaluated. For this, several mutations including addition or removal of S-S bonds in a single protein such as lysozyme could provide significant information regarding parameters such as hydrophobicity, size, total charge, exposed charge, number of disulfide bonds and interactions (amino acid-amino acid, amino acid-peptide and peptide-peptide) of the digest components in solution. Moreover, enzymes of proteomic grade should be also investigated to determine their effect in the electrochemical signal as the digestion efficiency can be compromised.

Finally, identification of proteins in a protein mixture could potentially require more advanced data analysis techniques than those introduced in this chapter (first and second derivatives), such as principal component analysis or other chemometric approaches.

8 Conclusions

This final section summaries the findings through the investigation shown in this thesis and points out some further studies that could be implemented for a better understanding of soft polarisable interfaces and particularly as a label-free biosensing platform.

General conclusions

The work presented in this thesis attempts to bring proteomics and electrochemistry at the interface between two immiscible electrolyte solutions (ITIES) together. Pre-treatment steps widely used in proteomics such as pre-concentration and proteolysis have been implemented. The first, electrochemical pre-concentration via adsorption has been investigated at gelled liquid – liquid micro-interfaces and water/RTIL interfaces for lysozyme detection. Haemoglobin has also shown to be susceptible to pre-concentration when using adsorptive stripping voltammetry to achieve lower limits of detection. Secondly, proteolysis prior to electrochemical analysis at the liquid – liquid interfaces has been shown its potential as the analogous process carried out in shotgun proteomic for protein identification. Complementary mass spectrometry analyses have been also performed at these soft interfaces to characterise interfacial processes and peptide composition.

Adsorption of lysozyme has been investigated at micro liquid-liquid interfaces. Electrochemical pre-concentration followed by voltammetric detection has been implemented to enhance the electrochemical signal. The pre-concentration step corresponds to adsorption of the protein at the gelled liquid – liquid interface. This process occurs at highly positive potentials, just below the potential where the background electrolyte transfers. The influence of time in the adsorption process indicates that this is a slow process which could be associated to multilayer formation and molecular re-orientation of lysozyme within the adsorbed film. Using a pre-concentration (adsorption) time of 300 s at 0.95 V, a limit of detection of 30 nM lysozyme was achieved which is more than 15-fold lower than the reported in the literature for lysozyme at the ITIES. Differential pulse voltammetry and square wave voltammetry are more sensitive techniques than in combination with adsorptive pre-concentration may lead to achieve lower limits of detection.

Moreover, hydrophobic gelled liquid – liquid interfaces were characterised for the first time by electrostatic spray – mass spectrometry (ESTASI-MS) after electrochemical pre-concentration of lysozyme. Interfacial complexes such as $[\text{Lysozyme-2TPBCl+12H}]^{+10}$ have been observed between lysozyme and one or two anions from the organic electrolyte (tetrakis(4-chlorophenyl)borate -TPBCl^--) at the

gelled liquid-liquid interfaces. These data confirms the proposed mechanism for the detection of lysozyme at the ITIES. In addition, ESTASI-MS spectra support the behaviour observed when electrochemical adsorptive accumulation of lysozyme was followed by stripping voltammetry. The limit of detection reported when implementing ESTASI-MS on polyacrylamide corresponds to approximately 1.6 pmol and the estimated amount of protein adsorbed on the organogel for a single monolayer of lysozyme is *ca.* 3-folds lower. This data confirms the formation of several layers of protein at the hydrophobic gel after electrochemical adsorption. Integration of ITIES and ESTASI-MS may improve the resolution and the limit of detection for the elucidation of interfacial reactions.

Lysozyme, has been also investigated at water / room temperature ionic liquid (RTIL) micro-interfaces. This is the first time a macrobiomolecule has been reported electroactive at these interfaces. While cyclic voltammetry is unable to detect the presence of lysozyme, AdSV enables the detection of this protein in a short potential window (*ca.* 400 mV) with a limit of detection of 2.5 μM when adsorbing lysozyme at the W/RTIL for 60 s. This process is also attributed to protein adsorption at the interface, in conjunction with facilitated transfer of $[FAP]^-$ anions across the interface to form a complex with positively charged lysozyme. These data reveal the similar behaviour seen at liquid – liquid and gelled liquid – liquid interfaces to the presented in this thesis. Simultaneously, interactions between the anion of the RTIL (tris(pentafluorethyl)trifluorphosphate $[FAP]^-$) and hydronium molecules have been observed at the W/RTIL microinterfaces when applying an electrochemical potential difference. Electrochemical characterisation studies such as impedance spectroscopy and several voltammetric techniques suggest that H_3O^+ transfers across the W/$[P_{14,6,6,6}][FAP]$ forming a neutral capacitive thin film layer. In addition, biphasic electrospray ionisation – mass spectrometry data suggest the neutralisation of $[FAP]^-$ ions in the presence of H_3O^+ in a biphasic environment as the mass-to-charge ration decreases in more than 99% when $[P_{14,6,6,6}][FAP]$ is sprayed with hydrochloric acid or acetic acid. However, both processes take place at the W/RTIL micro-interfaces and hydronium-[FAP] interactions are compatible in the detection of lysozyme. The use of more hydrophobic RTILs may provide a better platform for protein detection if the energy of adsorption can be lower down or the potential window increased.

Additionally, haemoglobin was studied in order to evaluate the analytical utility of AdSV for label-free protein detection. A detection limit of 48 nM was estimated following 60 s adsorption at 0.975V at the gelled liquid - liquid micro-interfaces. The improvement in detection limit is two orders of magnitude better than has been achieved by cyclic voltammetry at millimetre size interfaces. The enhancement of the signal for similar conditions than the implemented for lysozyme can be explained taking into account the degree of protonation of the proteins. A higher degree of charge of the biomacromolecule (+17 in the case of lysozyme, +62 for haemoglobin) enables a higher interaction with the anions from the organic phase, increasing the sensitivity of the system. The results show the capability of this label-free methodology which present some degree of selectivity as it is based on the Gibbs energy of transfer of different molecules although the influence of interferences must be addressed.

Finally, four proteins (lysozyme, myoglobin, albumin and haemoglobin) were proteolised prior to electrochemical analysis at the gelled liquid – liquid micro-interfaces with several enzymes. The results have evidenced the unique signature obtained for the distinctive protein fragments under the same conditions. Enzymes such as pepsin, trypsin and endoproteinase Glu-C have shown to produce specific fragments for a unique protein (lysozyme) which may be used as a label-free cheap fingerprint technology which that could be denominated *'electroproteomics'* as a combination between proteomics and electrochemistry. However, the main disadvantage is the fact that detection limit is significantly higher than the electrochemical signal obtained when analysing the native protein. Furthermore, mass spectroscopy data confirmed the electrochemical data were in agreement with the degree of digestion by pepsin when changing the pH. When the concentration of small oligopeptides and free amino acids was higher, the exposed hydrophobic content enhances the electrochemical signal. Experimental data confirmed how this is not the unique factor as isolated amino acids in the aqueous solutions only provided a slight change in the forward scan. Therefore, amino acid-peptide and peptide-peptide interactions should be considered.

Future perspective

Future work to enhance the electrochemical signal therefore achieving more competitive limits of detection for label-free protein detection includes more sensitive techniques such as differential pulse voltammetry and square wave voltammetry. This, in combination with adsorptive pre-concentration steps may lead to sub-nanomolar concentration which is within the levels of biomarker present in the blood stream for early disease diagnosis. The use of more hydrophobic room temperature ionic liquids could also improve its analytical utility for protein detection although the gelled liquid possesses a larger potential window which translated into more sensitive measurements.

Moreover, the integration of electrochemistry at the polarisable soft interfaces and mass spectrometry via electrospray ionisation may improve elucidation of interfacial processes which are vital in cell membrane understanding which have relevant implications in biological processes and pharmaceutical industry (drug delivery). This technique could provide further information to optimise the counterion that complexes with the charge protein which might result in a more selective analysis of biomolecules by tuning the organic phase components. In addition, a four-electrode set-up for the characterisation of millimetre-size gelled liquid-liquid interfaces might improve the ESTASI-MS spectra resolution after pre-concentrating the protein at these liquid-liquid interfaces. Combination of both techniques might also increase the detection limits and resolution as the interfacial complexes would be characterised via MS straight after the electrochemical pre-concentration with no time to undergo through disassociation when there is no electric field applied.

Regarding the work performed when mimicking the shotgun proteomics methodology, the isolated peptides must be fully characterised for a better understanding of the electrochemical signal produced as the work presented here (Chapter 7) requires further analysis which has not been possible to address before the submission of this thesis. The use of enzymes of proteomic grade is one of the recommendations to improve the digestion efficiency. Moreover the use of different filter sizes after digestion to collect different fractions of the digest fragments and evaluate their influence in the voltammetric response. Pre-treatment steps such as pre-concentration via solid phase extraction and electrochemical pre-concentration should be optimised to improve the sensitivity of this approach. Protein denaturation

prior digestion should be also evaluated as this process could provide a more efficient proteolysis step which will result in lower detectable concentrations. Finally, parameters such as hydrophobicity, size, total charge, exposed charge, number of disulfide bonds and interactions should be studied using a unique protein with modifications in its amino acid sequence.

References

1. A. J. Bard, L. R. Faulkner, *Electrochemical methods : fundamentals and applications*. 2nd ed.; Wiley: New York, **2001**; p xxi, 833 p.

2. P. W. Atkins, *Physical chemistry*. 5th ed.; W.H. Freeman: New York, **1994**.

3. Y. X. Wang, T. Kakiuchi, Y. Yasui, M. V. Mirkin, Kinetics of Ion Transfer at the Ionic Liquid/Water Nanointerface. *J. Am. Chem. Soc.* **2010**, *132*. 16945-16952.

4. C. G. Zoski, *Handbook of electrochemistry*. 1st ed.; Elsevier: Amsterdam ; Boston, **2007**; p xx, 892 p., 19 p. of plates.

5. J. Wang, *Analytical Electrochemistry*. 2nd ed.; Wiley-VCH: New York, **2000**.

6. Z. Samec, Electrochemistry at the interface between two immiscible electrolyte solutions. *Pure Appl. Chem.* **2004**, *76*. 2147-2180.

7. W. Nersnt, E. H. Risenfield, Ueber elektrolytische Erscheinungen an der Grenzfläche zweier Lösungsmittel. *Annalen der Physik* **1902**, *313*. 600 - 608.

8. C. Gavach, P. Seta, B. Depenoux, Double-Layer and Ion Adsorption at Interface between 2 Non-Miscible Solutions .1. Interfacial-Tension Measurements for Water-Nitrobenzene Tetraalkylammonium Bromide Systems. *J. Electroanal. Chem.* **1977**, *83*. 225-235.

9. J. Koryta, Electrochemical Polarization Phenomena at the Interface of 2 Immiscible Electrolyte-Solutions .2. Progress since 1978. *Electrochim. Acta* **1984**, *29*. 445-452.

10. Z. Samec, V. Marecek, J. Koryta, M. W. Khalil, Investigation of Ion Transfer across Interface between 2 Immiscible Electrolyte-Solutions by Cyclic Voltammetry. *J. Electroanal. Chem.* **1977**, *83*. 393-397.

11. M. Blank, S. Feig, Electric Fields across Water-Nitrobenzene Interfaces. *Science* **1963**, *141*. 1173-4.

12. D. W. M. Arrigan, Bioanalytical Detection Based on Electrochemistry at Interfaces between Immiscible Liquids. *Anal. Lett.* **2008**, *41*. 3233-3252.

13. D. W. M. Arrigan, Voltammetry of proteins at liquid-liquid interfaces. *Annual Reports Section "C" (Physical Chemistry)* **2013**.

14. A. Berduque, R. Zazpe, D. W. M. Arrigan, Electrochemical detection of dopamine using arrays of liquid–liquid micro-interfaces created within micromachined silicon membranes. *Anal. Chim. Acta* **2008**, *611*. 156-162.

15. E. Alvarez de Eulate, S. O'Sullivan, S. Fletcher, P. Newsholme, D. W. M. Arrigan, Ion-Transfer Electrochemistry of Rat Amylin at the Water–Organogel Microinterface Array and Its Selective Detection in a Protein Mixture. *Chemistry – An Asian Journal* **2013**, *8*. 2096-2101.

16. S. O'Sullivan, E. Alvarez de Eulate, Y. H. Yuen, E. Helmerhorst, D. W. M. Arrigan, Stripping voltammetric detection of insulin at liquid-liquid microinterfaces in the presence of bovine albumin. *Analyst* **2013**.

17. C. J. Collins, D. W. M. Arrigan, Ion-Transfer Voltammetric Determination of the Beta-Blocker Propranolol in a Physiological Matrix at Silicon Membrane-Based Liquid vertical bar Liquid Microinterface Arrays. *Anal. Chem.* **2009**, *81*. 2344-2349.

18. M. Velicky, K. Y. Tam, R. A. W. Dryfe, Hydrodynamic voltammetry at the liquid-liquid interface: Application to the transfer of ionised drug molecules. *J. Electroanal. Chem.* **2012**, *683*. 94-102.

19. Y. Wang, K. Kececi, J. Velmurugan, M. V. Mirkin, Electron transfer/ion transfer mode of scanning electrochemical microscopy (SECM): a new tool for imaging and kinetic studies. *Chem Sci* **2013**, *4*. 3606-3616.

20. X. Bian, M. D. Scanlon, S. Wang, L. Liao, Y. Tang, B. Liu, H. H. Girault, Floating conductive catalytic nano-rafts at soft interfaces for hydrogen evolution. *Chem Sci* **2013**, *4*. 3432-3441.

21. N. Younan, M. Hojeij, L. Ribeaucourt, H. H. Girault, Electrochemical properties of gold nanoparticles assembly at polarised liquid|liquid interfaces. *Electrochem. Commun.* **2010**, *12*. 912-915.

22. P. Ge, A. J. Olaya, M. D. Scanlon, I. Hatay Patir, H. Vrubel, H. H. Girault, Photoinduced Biphasic Hydrogen Evolution: Decamethylosmocene as a Light-Driven Electron Donor. *ChemPhysChem* **2013**, *14*. 2308-2316.

23. E. L. W. Verwey, K. F. Niessen, *Phil. Mag.* **1939**. 435.

24. H. H. J. Girault, D. J. Schiffrin, Theory of the kinetics of ion transfer across liquid/liquid interfaces. *Journal of Electroanalytical Chemistry and Interfacial Electrochemistry* **1985**, *195*. 213-227.

25. C. M. Pereira, W. Schmickler, F. Silva, M. J. Sousa, Ion association at liquid|liquid interfaces. *J. Electroanal. Chem.* **1997**, *436*. 9-15.

26. M. L. Schlossman, Liquid–liquid interfaces: studied by X-ray and neutron scattering. *Curr. Opin. Colloid Interface Sci.* **2002**, *7*. 235-243.

27. G. Luo, S. Malkova, J. Yoon, D. G. Schultz, B. Lin, M. Meron, I. Benjamin, P. Vanysek, M. L. Schlossman, Ion distributions near a liquid-liquid interface. *Science* **2006**, *311*. 216-8.

28. N. Laanait, M. Mihaylov, B. Y. Hou, H. Yu, P. Vanysek, M. Meron, B. H. Lin, I. Benjamin, M. L. Schlossman, Tuning ion correlations at an electrified soft interface. *Proc. Natl. Acad. Sci. U. S. A.* **2012**, *109*. 20326-20331.

29. D. M. Mitrinović, A. M. Tikhonov, M. Li, Z. Huang, M. L. Schlossman, Noncapillary-Wave Structure at the Water-Alkane Interface. *Phys. Rev. Lett.* **2000**, *85*. 582-585.

30. J. Strutwolf, A. L. Barker, M. Gonsalves, D. J. Caruana, P. R. Unwin, D. E. Williams, J. R. P. Webster, Probing liquid-liquid interfaces using neutron reflection measurements and scanning electrochemical microscopy. *J. Electroanal. Chem.* **2000**, *483*. 163-173.

31. H. H. Girault, Electrochemistry at Liquid-Liquid Interfaces. *Electroanalytical Chemistry, Vol 23* **2010**. 1-104.

32. G. Taylor, H. H. J. Girault, Ion Transfer-Reactions across a Liquid Liquid Interface Supported on a Micropipette Tip. *J. Electroanal. Chem.* **1986**, *208*. 179-183.

33. R. Zazpe, C. Hibert, J. O'Brien, Y. H. Lanyon, D. W. M. Arrigan, Ion-transfer voltammetry at silicon membrane-based arrays of micro-liquid-liquid interfaces. *Lab Chip* **2007**, *7*. 1732-1737.

34. M. D. Scanlon, G. Herzog, D. W. M. Arrigan, Electrochemical detection of oligopeptides at silicon-fabricated micro-liquid-liquid interfaces. *Anal. Chem.* **2008**, *80*. 5743-5749.

35. J. Strutwolf, M. D. Scanlon, D. W. M. Arrigan, Electrochemical ion transfer across liquid/liquid interfaces confined within solid-state micropore arrays - simulations and experiments. *Analyst* **2009**, *134*. 148-158.

36. M. l. D. Scanlon, J. r. Strutwolf, A. Blake, D. Iacopino, A. J. Quinn, D. W. M. Arrigan, Ion-Transfer Electrochemistry at Arrays of Nanointerfaces between Immiscible Electrolyte Solutions Confined within Silicon Nitride Nanopore Membranes. *Anal. Chem.* **2010**, *82*. 6115-6123.

37. S. J. Liu, Q. Li, Y. H. Shao, Electrochemistry at micro- and nanoscopic liquid/liquid interfaces. *Chem. Soc. Rev.* **2011**, *40*. 2236-2253.

38. H. J. Lee, P. D. Beattie, B. J. Seddon, M. D. Osborne, H. H. Girault, Amperometric ion sensors based on laser-patterned composite polymer membranes. *J. Electroanal. Chem.* **1997**, *440*. 73-82.

39. S. N. Faisal, C. M. Pereira, S. Rho, H. J. Lee, Amperometric proton selective sensors utilizing ion transfer reactions across a microhole liquid/gel interface. *Phys Chem Chem Phys* **2010**, *12*. 15184-15189.

40. S. J. Liu, Y. T. Dong, W. B. Zhao, X. Xie, T. R. Ji, X. H. Yin, Y. Liu, Z. W. Liang, D. Momotenko, D. H. Liang, H. H. Girault, Y. H. Shao, Studies of Ionic Current Rectification Using Polyethyleneimines Coated Glass Nanopipettes. *Anal. Chem.* **2012**, *84*. 5565-5573.

41. Y. H. Shao, B. Liu, M. V. Mirkin, Studying ionic reactions by a new generation/collection technique. *J. Am. Chem. Soc.* **1998**, *120*. 12700-12701.

42. C. G. Zoski, M. V. Mirkin, Steady-state limiting currents at finite conical microelectrodes. *Anal. Chem.* **2002**, *74*. 1986-1992.

43. A. M. Bond, D. Luscombe, K. B. Oldham, C. G. Zoski, A Comparison of the Chronoamperometric Response at Inlaid and Recessed Disk Microelectrodes. *J. Electroanal. Chem.* **1988**, *249*. 1-14.

44. D. W. M. Arrigan, Nanoelectrodes, nanoelectrode arrays and their applications. *Analyst* **2004**, *129*. 1157-65.

45. T. J. Davies, S. Ward-Jones, C. E. Banks, J. del Campo, R. Mas, F. X. Munoz, R. G. Compton, The cyclic and linear sweep voltammetry of regular arrays of microdisc electrodes: Fitting of experimental data. *J. Electroanal. Chem.* **2005**, *585*. 51-62.

46. T. J. Davies, R. G. Compton, The cyclic and linear sweep voltammetry of regular and random arrays of microdisc electrodes: Theory. *J. Electroanal. Chem.* **2005**, *585*. 63-82.

47. Y. Saito, Theoretical study on the diffusion current at the stationary electrodes of circular and narrow band types. *Rev. Polarogr.* **1968**. 177 - 187.

48. S. Fletcher, M. D. Horne, Random assemblies of microelectrodes (RAM™ electrodes) for electrochemical studies. *Electrochem. Commun.* **1999**, *1*. 502-512.

49. P. Vanýsek, J. D. Reid, M. A. Craven, R. P. Buck, Properties of the Interface Between Two Immiscible Electrolytes in the Presence of Proteins. *J. Electrochem. Soc.* **1984**, *131*. 1788-1791.

50. B. R. Horrocks, M. V. Mirkin, Cation Binding to DNA Studied by Ion-Transfer Voltammetry at Micropipets. *Anal. Chem.* **1998**, *70*. 4653-4660.

51. T. Osakai, H. Komatsu, M. Goto, Cationic-surfactant transfer facilitated by DNA adsorbed on a polarized 1,2-dichloroethane/water interface. *J Phys-Condens Mat* **2007**, *19*.

52. M. Y. Vagin, S. A. Trashin, A. A. Karyakin, M. Mascini, Label-free detection of DNA hybridization at a liquid|liquid interface. *Anal. Chem.* **2008**, *80*. 1336-1340.

53. F. Kivlehan, M. Lefoix, H. A. Moynihan, D. Thompson, V. I. Ogurtsov, G. Herzog, D. W. M. Arrigan, Interaction of acridine-calix[4]arene with DNA at the electrified liquid liquid interface. *Electrochim. Acta* **2010**, *55*. 3348-3354.

54. T. Osakai, H. Jensen, H. Nagatani, D. J. Fermín, H. H. Girault, Mechanistic aspects associated with the oxidation of l-ascorbic acid at the 1,2-dichloroethane - water interface. *J. Electroanal. Chem.* **2001**, *510*. 43-49.

55. H. Ohde, K. Maeda, Y. Yoshida, S. Kihara, Redox reactions between NADH and quinone derivatives at a liquid/liquid interface. *Electrochim. Acta* **1998**, *44*. 23-28.

56. D. Zhan, S. Mao, Q. Zhao, Z. Chen, Hu, P. Jing, M. Zhang, Z. Zhu, Y. Shao, Electrochemical Investigation of Dopamine at the Water/1,2-Dichloroethane Interface. *Anal. Chem.* **2004**, *76*. 4128-4136.

57. V. Beni, M. Ghita, D. W. M. Arrigan, Cyclic and pulse voltammetric study of dopamine at the interface between two immiscible electrolyte solutions. *Biosens. Bioelectron.* **2005**, *20*. 2097-2103.

58. J. A. Ribeiro, I. M. Miranda, F. Silva, C. M. Pereira, Electrochemical study of dopamine and noradrenaline at the water/1,6-dichlorohexane interface. *Phys. Chem. Chem. Phys.* **2010**, *12*. 15190-15194.

59. C. J. Collins, C. Lyons, J. Strutwolf, D. W. M. Arrigan, Serum-protein effects on the detection of the beta-blocker propranolol by ion-transfer voltammetry at a micro-ITIES array. *Talanta* **2010**, *80*. 1993-1998.

60. P. Lopes, R. Kataky, Chiral Interactions of the Drug Propranolol and α1-Acid-Glycoprotein at a Micro Liquid–Liquid Interface. *Anal. Chem.* **2012**, *84*. 2299-2304.

61. Z. Samec, A. Trojánek, J. Langmaier, E. Samcová, Cyclic voltammetry of biopolymer heparin at PVC plasticized liquid membrane. *Electrochem. Commun.* **2003**, *5*. 867-870.

62. J. D. Guo, Y. Yuan, S. Amemiya, Voltammetric detection of heparin at polarized blood plasma/1,2-dichloroethane interfaces. *Anal. Chem.* **2005**, *77*. 5711-5719.

63. J. Langmaier, Z. Samec, E. Samcova, P. Tuma, Transfer of heparin polyion across a polarized water/ionic liquid membrane interface. *Electrochem. Commun.* **2012**, *24*. 25-27.

64. M. A. Mendez, M. Prudent, B. Su, H. H. Girault, Peptide-Phospholipid Complex Formation at Liquid-Liquid Interfaces. *Anal. Chem.* **2008**, *80*. 9499-9507.

65. M. A. Méndez, Z. Nazemi, I. Uyanik, Y. Lu, H. H. Girault, Melittin Adsorption and Lipid Monolayer Disruption at Liquid–Liquid Interfaces. *Langmuir* **2011**, *27*. 13918-13924.

66. Y. Chen, Y. Yuan, M. Q. Zhang, F. Li, P. Sun, Z. Gao, Y. H. Shao, Systematic study of the transfer of amino acids across the water/1,2-dichloroethane interface facilitated by dibenzo-18-crown-6. *Sci China Ser B* **2004**, *47*. 24-33.

67. P. Vanýsek, Z. Sun, Bovine serum albumin adsorption on a water/nitrobenzene interface. *Bioelectrochem. Bioenerg.* **1990**, *23*. 177-194.

68. G. C. Lillie, S. M. Holmes, R. A. W. Dryfe, Electrochemistry of cytochrome c at the liquid-liquid interface. *J. Phys. Chem. B* **2002**, *106*. 12101-12103.

69. S. Amemiya, X. T. Yang, T. L. Wazenegger, Voltammetry of the phase transfer of polypeptide protamines across polarized liquid/liquid interfaces. *J. Am. Chem. Soc.* **2003**, *125*. 11832-11833.

70. Y. Yuan, S. Amemiya, Facilitated Protamine Transfer at Polarized Water/1,2-Dichloroethane Interfaces Studied by Cyclic Voltammetry and Chronoamperometry at Micropipet Electrodes. *Anal. Chem.* **2004**, *76*. 6877-6886.

71. M. Y. Vagin, E. V. Malyh, N. I. Larionova, A. A. Karyakin, Spontaneous and facilitated micelles formation at liquid vertical bar liquid interface: towards amperometric detection of redox inactive proteins. *Electrochem. Commun.* **2003**, *5*. 329-333.

72. M. Shinshi, T. Sugihara, T. Osakai, M. Goto, Electrochemical extraction of proteins by reverse micelle formation. *Langmuir* **2006**, *22*. 5937-5944.

73. A. Trojanek, J. Langmaier, E. Samcova, Z. Samec, Counterion binding to protamine polyion at a polarised liquid-liquid interface. *J. Electroanal. Chem.* **2007**, *603*. 235-242.

74. S. O'Sullivan, D. W. M. Arrigan, Electrochemical behaviour of myoglobin at an array of microscopic liquid-liquid interfaces. *Electrochim. Acta* **2012**, *77*. 71-76.

75. S. O'Sullivan, D. W. M. Arrigan, Impact of a Surfactant on the Electroactivity of Proteins at an Aqueous–Organogel Microinterface Array. *Anal. Chem.* **2012**, *85*. 1389-1394.

76. R. Matsui, T. Sakaki, T. Osakai, Label-Free Amperometric Detection of Albumin with an Oil/Water-type Flow Cell for Urine Protein Analysis. *Electroanalysis* **2012**, *24*. 1164-1169.

77. F. Kivlehan, Y. H. Lanyon, D. W. M. Arrigan, Electrochemical study of insulin at the polarized liquid-liquid interface. *Langmuir* **2008**, *24*. 9876-9882.

78. M. D. Scanlon, E. Jennings, D. W. M. Arrigan, Electrochemical behaviour of hen-egg-white lysozyme at the polarised water/1,2-dichloroethane interface. *Phys. Chem. Chem. Phys.* **2009**, *11*. 2272-2280.

79. M. D. Scanlon, J. Strutwolf, D. W. M. Arrigan, Voltammetric behaviour of biological macromolecules at arrays of aqueous-organogel micro-interfaces. *Phys. Chem. Chem. Phys.* **2010**, *12*. 10040-10047.

80. G. Herzog, V. Kam, D. W. M. Arrigan, Electrochemical behaviour of haemoglobin at the liquid/liquid interface. *Electrochim. Acta* **2008**, *53*. 7204-7209.

81. G. Herzog, W. Moujahid, J. Strutwolf, D. W. M. Arrigan, Interactions of proteins with small ionised molecules: electrochemical adsorption and facilitated ion transfer voltammetry of haemoglobin at the liquid vertical bar liquid interface. *Analyst* **2009**, *134*. 1608-1613.

82. G. Herzog, P. Eichelmann-Daly, D. W. M. Arrigan, Electrochemical behaviour of denatured haemoglobin at the liquid/liquid interface. *Electrochem. Commun.* **2010**, *12*. 335-337.

83. G. Herzog, A. Roger, D. Sheehan, D. W. M. Arrigan, Ion-Transfer Voltammetric Behavior of Protein Digests at Liquid-Liquid Interfaces. *Anal. Chem.* **2010**, *82*. 258-264.

84. A. E. Thomsen, H. Jensen, L. Jorgensen, M. van de Weert, J. Ostergaard, Studies on human insulin adsorption kinetics at an organic-aqueous interface determined using a label-free electroanalytical approach. *Colloid Surface B* **2008**, *63*. 243-248.

85. T. Osakai, Y. Yuguchi, E. Gohara, H. Katano, Direct Label-free Electrochemical Detection of Proteins Using the Polarized Oil/Water Interface. *Langmuir* **2010**, *26*. 11530-11537.

86. M. Y. Vagin, S. A. Trashin, S. Z. Ozkan, G. P. Karpachova, A. A. Karyakin, Electroactivity of redox-inactive proteins at liquid/liquid interface. *J. Electroanal. Chem.* **2005**, *584*. 110-116.

87. M. Rimboud, K. Charreteur, V. Sladkov, C. Elleouet, F. Quentel, M. L'Her, Effect of the supporting electrolytes on voltammetry at liquid/liquid microinterfaces

between water and nitrobenzene, 1,2-dichloroethane or 1,6-dichlorohexane. *J. Electroanal. Chem.* **2009**, *636*. 53-59.

88. R. A. Hartvig, M. A. Mendez, M. van de Weert, L. Jorgensen, J. Ostergaard, H. H. Girault, H. Jensen, Interfacial Complexes between a Protein and Lipophilic Ions at an Oil-Water Interface. *Anal. Chem.* **2010**, *82*. 7699-7705.

89. K. Tanaka, H. Waki, Y. Ido, S. Akita, Y. Yoshida, T. Yoshida, T. Matsuo, Protein and polymer analyses up to m/z 100 000 by laser ionisation time-of-flight mass spectrometry. *Rapid Commun. Mass Spectrom.* **1988**, *2*. 151-153.

90. J. B. Fenn, M. Mann, C. K. Meng, S. F. Wong, C. M. Whitehouse, Electrospray ionisation for mass spectrometry of large biomolecules. *Science* **1989**, *246*. 64-71.

91. J. B. Fenn, Electrospray Wings for Molecular Elephants (Nobel Lecture). *Angewandte Chemie International Edition* **2003**, *42*. 3871-3894.

92. M. Karas, F. Hillenkamp, Laser desorption ionisation of proteins with molecular masses exceeding 10,000 daltons. *Anal. Chem.* **1988**, *60*. 2299-2301.

93. R. Aebersold, M. Aebersold, R. Mann, Aebersold, Mass spectrometry-based proteomics. *Nature* **2003**, *422*. 198-207.

94. D. A. Wolters, M. P. Washburn, J. R. Yates, An Automated Multidimensional Protein Identification Technology for Shotgun Proteomics. *Anal. Chem.* **2001**, *73*. 5683-5690.

95. J. v. Hagen, *Proteomics sample preparation*. Wiley-VCH: Darmstadt, Germany, **2008**; p 453.

96. C. Wang, A. B. Jemere, D. J. Harrison, Multifunctional protein processing chip with integrated digestion, solid-phase extraction, separation and electrospray. *Electrophoresis* **2010**, *31*. 3703-3710.

97. R. Aebersold, D. R. Goodlett, Mass spectrometry in proteomics. *Chem. Rev.* **2001**, *101*. 269-95.

98. G. L. Glish, R. W. Vachet, The basics of mass spectrometry in the twenty-first century. *Nat. Rev. Drug Discov.* **2003**, *2*. 140-50.

99. M. Mann, R. C. Hendrickson, A. Pandey, Analysis of proteins and proteomes by mass spectrometry. *Annu. Rev. Biochem.* **2001**, *70*. 437-473.

100. M. J. Stump, R. C. Fleming, W. H. Gong, A. J. Jaber, J. J. Jones, C. W. Surber, C. L. Wilkins, Matrix-assisted laser desorption mass spectrometry. *Appl. Spectrosc. Rev.* **2002**, *37*. 275-303.

101. L. A. McDonnell, R. M. A. Heeren, Imaging mass spectrometry. *Mass Spectrom. Rev.* **2007**, *26*. 606-643.

102. K. Chughtai, R. M. Heeren, Mass spectrometric imaging for biomedical tissue analysis. *Chem. Rev.* **2010**, *110*. 3237-77.

103. L. Qiao, E. Tobolkina, B. Liu, H. H. Girault, Coupling isoelectric focusing gel electrophoresis to mass spectrometry by electrostatic spray ionisation. *Anal. Chem.* **2013**, *85*. 4745-52.

104. A. L. Dill, L. S. Eberlin, D. R. Ifa, R. G. Cooks, Perspectives in imaging using mass spectrometry. *Chem. Commun.* **2011**, *47*. 2741-2746.

105. L. Qiao, R. Sartor, N. Gasilova, Y. Lu, E. Tobolkina, B. H. Liu, H. H. Girault, Electrostatic-Spray Ionisation Mass Spectrometry. *Anal. Chem.* **2012**, *84*. 7422-7430.

106. P. J. Todd, T. G. Schaaff, P. Chaurand, R. M. Caprioli, Organic ion imaging of biological tissue with secondary ion mass spectrometry and matrix-assisted laser desorption/ionisation. *J. Mass Spectrom.* **2001**, *36*. 355-369.

107. A. Brunelle, D. Touboul, O. Laprévote, Biological tissue imaging with time-of-flight secondary ion mass spectrometry and cluster ion sources. *J. Mass Spectrom.* **2005**, *40*. 985-999.

108. B. Johansson, ToF-SIMS imaging of lipids in cell membranes. *Surf. Interface Anal.* **2006**, *38*. 1401-1412.

109. L. S. Eberlin, I. Norton, D. Orringer, I. F. Dunn, X. Liu, J. L. Ide, A. K. Jarmusch, K. L. Ligon, F. A. Jolesz, A. J. Golby, S. Santagata, N. Y. R. Agar, R. G. Cooks, Ambient mass spectrometry for the intraoperative molecular diagnosis of human brain tumors. *Proceedings of the National Academy of Sciences* **2013**, *110*. 1611-1616.

110. M.-J. Kang, J.-C. Pyun, J.-C. Lee, Y.-J. Choi, J.-H. Park, J.-G. Park, J.-G. Lee, H.-J. Choi, Nanowire-assisted laser desorption and ionisation mass spectrometry for quantitative analysis of small molecules. *Rapid Commun. Mass Spectrom.* **2005**, *19*. 3166-3170.

111. A. Tata, A. M. A. P. Fernandes, V. G. Santos, R. M. Alberici, D. Araldi, C. A. Parada, W. Braguini, L. Veronez, G. Silva Bisson, F. H. Z. Reis, L. C. Alberici, M. N. Eberlin, Nanoassisted Laser Desorption-Ionisation-MS Imaging of Tumors. *Anal. Chem.* **2012**, *84*. 6341-6345.

112. J. Laskin, B. S. Heath, P. J. Roach, L. Cazares, O. J. Semmes, Tissue Imaging Using Nanospray Desorption Electrospray Ionisation Mass Spectrometry. *Anal. Chem.* **2011**, *84*. 141-148.

113. R. J. Cotter, *Time-of-Flight Mass Spectrometry*. American Chemical Society: **1993**; Vol. 549, p 16-48.

114. T. Osakai, T. Kakutani, M. Senda, Ion-Transfer Voltammetry and Amperometric Chemical Sensors. *J. Electrochem. Soc.* **1987**, *134*. C520-C520.

115. D. S. Silvester, D. W. M. Arrigan, Array of water|room temperature ionic liquid micro-interfaces. *Electrochem. Commun.* **2011**, *13*. 477-479.

116. R. G. Compton, C. E. Banks, *Understanding voltammetry*. World Scientific: Singapore ; Hackensack, NJ, **2007**; p xii, 371 p.

117. E. Barsoukov, J. R. Macdonald, Impedance Spectroscopy: Theory, Experiment, and Applications, 2nd Edition. *Impedance Spectroscopy: Theory, Experiment, and Applications, 2nd Edition* **2005**. 1-595.

118. P. Sweeney, J. Walker, in *Enzymes of Molecular Biology*, ed. M. Burrell. Humana Press, **1993**, vol. 16, pp 277-303.

119. L. Fothergill-Gilmore, in *Protein Biotechnology*, ed. F. Franks. Humana Press, **1993**, pp 237-249.

120. A. El-Aneed, A. Cohen, J. Banoub, Mass Spectrometry, Review of the Basics: Electrospray, MALDI, and Commonly Used Mass Analyzers. *Appl. Spectrosc. Rev.* **2009**, *44*. 210-230.

121. R. Cooks, A. Rockwood, The Thomson - A suggested unit for mass spectroscopists. *Rapid Commun. Mass Spectrom.* **1991**, *5*. 93-93.

122. V. Gobry, J. van Oostrum, M. Martinelli, T. C. Rohner, F. Reymond, J. S. Rossier, H. H. Girault, Microfabricated polymer injector for direct mass spectrometry coupling. *Proteomics* **2002**, *2*. 405-12.

123. L. Qiao, Y. Lu, B. Liu, H. H. Girault, Copper-catalyzed tyrosine nitration. *J. Am. Chem. Soc.* **2011**, *133*. 19823-31.

124. A. L. Lehninger, D. L. Nelson, M. M. Cox, *Lehninger Principles of Biochemistry*. 5th ed.; W. H. Freeman: New York, **2008**.

125. R. E. Canfield, The Amino Acid Sequence of Egg White Lysozyme. *J Biol Chem* **1963**, *238*. 2698-707.

126. R. E. Canfield, A. K. Liu, The Disulfide Bonds of Egg White Lysozyme (Muramidase). *J Biol Chem* **1965**, *240*. 1997-2002.

127. R. D. Jones, K. Lee, Y. C. Lee, T. K. Samec, Monte-Carlo Simulation of the Non-Linear Fokker - Planck Equation. *B Am Phys Soc* **1980**, *25*. 985-985.

128. C. C. Blake, D. F. Koenig, G. A. Mair, A. C. North, D. C. Phillips, V. R. Sarma, Structure of hen egg-white lysozyme. A three-dimensional Fourier synthesis at 2 Angstrom resolution. *Nature* **1965**, *206*. 757-61.

129. K. Kubiak, P. A. Mulheran, Molecular Dynamics Simulations of Hen Egg White Lysozyme Adsorption at a Charged Solid Surface. *J. Phys. Chem. B* **2009**, *113*. 12189-12200.

130. L. R. Wetter, H. F. Deutsch, Immunological studies on egg white proteins. IV. Immunochemical and physical studies of lysozyme. *J Biol Chem* **1951**, *192*. 237-42.

131. G. D. Shockman, J. F. Barrett, Structure, function, and assembly of cell walls of gram-positive bacteria. *Annu. Rev. Microbiol.* **1983**, *37*. 501-527.

132. J. Mestecky, M. E. Iamm, W. Strober, J. Bienenstock, J. R. McGhee, M. L., *Mucosal Immunology*. Third ed.; Elsevier Academic Press: Burlington, **2005**; p 2064.

133. K. R. Falchuk, J. L. Perrotto, Serum Lysozyme in Diagnosis and Follow-up of Patients with Crohns-Disease. *Gastroenterology* **1975**, *68*. 890-890.

134. C. Serra, F. Vizoso, L. Alonso, J. C. Rodriguez, L. O. Gonzalez, M. Fernandez, M. L. Lamelas, M. Sanchez, J. L. Garcia-Muniz, A. Baltasar, J. Medrano, Expression and prognostic significance of lysozyme in male breast cancer. *Breast Cancer Res* **2002**, *4*. -.

135. E. Tahara, H. Ito, F. Shimamoto, T. Iwamoto, K. Nakagami, H. Niimoto, Lysozyme in Human Gastric-Carcinoma - a Retrospective Immunohistochemical Study. *Histopathology* **1982**, *6*. 409-421.

136. O. P. Mishra, P. Batra, Z. Ali, S. Anupurba, B. K. Das, Cerebrospinal fluid lysozyme level for the diagnosis of tuberculous meningitis in children. *J. Trop. Pediatr.* **2003**, *49*. 13-16.

137. S. Lee-Huang, P. L. Huang, Y. T. Sun, H. F. Kung, D. L. Blithe, H. C. Chen, Lysozyme and RNases as anti-HIV components in beta-core preparations of human chorionic gonadotropin. *P Natl Acad Sci USA* **1999**, *96*. 2678-2681.

138. G. Sava, A. Benetti, V. Ceschia, S. Pacor, Lysozyme and Cancer - Role of Exogenous Lysozyme as Anticancer Agent - (Review). *Anticancer Res.* **1989**, *9*. 583-591.

139. P. Vanysek, L. B. Ramirez, Interface between two immiscible liquid electrolytes: A review. *J. Chil. Chem. Soc.* **2008**, *53*. 1455-1463.

140. Z. Samec, Electrochemistry at the interface between two immiscible electrolyte solutions. *Pure Appl. Chem.* **2004**, *76*. 2147-2180.

141. R. A. W. Dryfe, The Electrified Liquid-Liquid Interface. *Advances in Chemical Physics, Vol 141* **2009**, *141*. 153-215.

142. A. J. Bard, C. G. Zoski, *Electroanalytical Chemistry*. Taylor & Francis Group: New York, **2010**; Vol. 23, p 304.

143. M. Y. Vagin, S. A. Trashin, G. P. Karpachova, N. L. Klyachko, A. A. Karyakin, Protein extracting electrodes: Insights in the mechanism. *J. Electroanal. Chem.* **2008**, *623*. 68-74.

144. Z. Samec, A. Trojanek, J. Langmaier, E. Samcova, Counterion binding to protamine polyion at a polarised liquid-liquid interface. *J Electroanal Chem* **2007**, *603*. 235-242.

145. D. W. M. Arrigan, G. Herzog, V. Kam, Electrochemical behaviour of haemoglobin at the liquid/liquid interface. *Electrochim Acta* **2008**, *53*. 7204-7209.

146. M. Thompson, J. S. Ellis, S. Q. Xu, X. Wang, G. Herzog, D. W. M. Arrigan, Interaction of surface-attached haemoglobin with hydrophobic anions monitored by on-line acoustic wave detector. *Bioelectrochemistry* **2010**, *79*. 6-10.

147. R. Kaldova, M. Kopanica, Adsortive stripping voltammetry in trace analysis. *Pure and Applied Chemistry (IUPAC)* **1989**, *61*. 97-112.

148. B. Pihlar, P. Valenta, H. W. Nurnberg, New High-Performance Analytical Procedure for the Voltammetric Determination of Nickel in Routine Analysis of Waters, Biological-Materials and Food. *Fresen Z Anal Chem* **1981**, *307*. 337-346.

149. A. Berduque, M. D. Scanlon, C. J. Collins, D. W. M. Arrigan, Electrochemistry of Non-Redox-Active Poly(propylenimine) and Poly(amidoamine) Dendrimers at Liquid−Liquid Interfaces. *Langmuir* **2007**, *23*. 7356-7364.

150. S. Kuramitsu, K. Hamaguchi, Analysis of the Acid-Base Titration Curve of Hen Lysozyme. *J. Biochem. (Tokyo)* **1980**, *87*. 1215-1219.

151. T. J. Su, R. J. Green, Y. Wang, E. F. Murphy, J. R. Lu, R. Ivkov, S. K. Satija, Adsorption of lysozyme onto the silicon oxide surface chemically grafted with a monolayer of pentadecyl-1-ol. *Langmuir* **2000**, *16*. 4999-5007.

152. J. M. Kleijn, D. Barten, M. A. C. Stuart, Adsorption of charged macromolecules at a gold electrode. *Langmuir* **2004**, *20*. 9703-9713.

153. F. Scheller, M. Janchen, H. J. Prumke, Adsorption Behavior of Globular Proteins at Water-Mercury Interface. *Biopolymers* **1975**, *14*. 1553-1563.

154. W. R. Jin, L. Xiao, The mechanism of the electrochemical reaction of lysozyme at the mercury electrode. *J Electroanal Chem* **1997**, *434*. 37-41.

155. J. Etheve, P. Dejardin, Adsorption kinetics of lysozyme on silica at pH 7.4: Correlation between streaming potential and adsorbed amount. *Langmuir* **2002**, *18*. 1777-1785.

156. J. R. Lu, M. J. Swann, L. L. Peel, N. J. Freeman, Lysozyme adsorption studies at the silica/water interface using dual polarization interferometry. *Langmuir* **2004**, *20*. 1827-1832.

157. T. Wei, S. Kaewtathip, K. Shing, Buffer Effect on Protein Adsorption at Liquid/Solid Interface. *J. Phys. Chem. C* **2009**, *113*. 2053-2062.

158. V. Ball, J. J. Ramsden, Analysis of hen egg white lysozyme adsorption on Si(Ti)O-2 vertical bar aqueous solution interfaces at low ionic strength: a biphasic reaction related to solution self-association. *Colloid Surface B* **2000**, *17*. 81-94.

159. C. A. Haynes, E. Sliwinsky, W. Norde, Structural and Electrostatic Properties of Globular-Proteins at a Polystyrene Water Interface. *J Colloid Interf Sci* **1994**, *164*. 394-409.

160. D. T. Kim, H. W. Blanch, C. J. Radke, Direct imaging of lysozyme adsorption onto mica by atomic force microscopy. *Langmuir* **2002**, *18*. 5841-5850.

161. C. F. Schmidt, R. M. Zimmermann, H. E. Gaub, Multilayer Adsorption of Lysozyme on a Hydrophobic Substrate. *Biophys. J.* **1990**, *57*. 577-588.

162. M. A. Brusatori, Y. Tie, P. R. Van Tassel, Protein adsorption kinetics under an applied electric field: An optical waveguide lightmode spectroscopy study. *Langmuir* **2003**, *19*. 5089-5097.

163. M. Przybylski, M. O. Glocker, Electrospray mass spectrometry of biomacromolecular complexes with noncovalent interactions - New analytical perspectives for supramolecular chemistry and molecular recognition processes. *Angewandte Chemie-International Edition in English* **1996**, *35*. 807-826.

164. M. Prudent, M. A. Mendez, H. H. Girault, Biphasic Electrospray Ionisation for the Study of Interfacial Complexes. *Anal. Sci.* **2008**, *24*. 1399-1404.

165. H. Watarai, A. Matsumoto, T. Fukumoto, Direct electrospray ionisation mass spectroscopic measurement of micro-flow oil/water system. *Anal. Sci.* **2002**, *18*. 367-368.

166. P. Liu, M. Lu, Q. Zheng, Y. Zhang, H. D. Dewald, H. Chen, Recent advances of electrochemical mass spectrometry. *Analyst* **2013**, *138*. 5519-5539.

167. D. S. Gross, P. D. Schnier, S. E. RodriguezCruz, C. K. Fagerquist, E. R. Williams, Conformations and folding of lysozyme ions in vacuo. *Proc. Natl. Acad. Sci. U. S. A.* **1996**, *93*. 3143-3148.

168. M. Xu, V. A. Shashilov, V. V. Ermolenkov, L. Fredriksen, D. Zagorevski, I. K. Lednev, The first step of hen egg white lysozyme fibrillation, irreversible partial unfolding, is a two-state transition. *Protein Sci.* **2007**, *16*. 815-832.

169. R. E. Canfield, The Amino Acid Sequence of Egg White Lysozyme. *J. Biol. Chem.* **1963**, *238*. 2698-2707.

170. K. Strupat, Molecular weight determination of peptides and proteins by ESI and MALDI. *Methods Enzymol.* **2005**, *405*. 1-36.

171. P. V. Bondarenko, D. Chelius, T. A. Shaler, Identification and relative quantitation of protein mixtures by enzymatic digestion followed by capillary reversed-phase liquid chromatography-tandem mass spectrometry. *Anal. Chem.* **2002**, *74*. 4741-4749.

172. W. H. Zhu, J. W. Smith, C. M. Huang, Mass Spectrometry-Based Label-Free Quantitative Proteomics. *Journal of Biomedicine and Biotechnology* **2010**.

173. S. Saraswat, B. Snyder, D. Isailovic, Quantification of HPLC-separated peptides and proteins by spectrofluorimetric detection of native fluorescence and mass spectrometry. *Journal of Chromatography B-Analytical Technologies in the Biomedical and Life Sciences* **2012**, *902*. 70-77.

174. D. S. Silvester, R. G. Compton, Electrochemistry in room temperature ionic liquids: A review and some possible applications. *Z Phys Chem* **2006**, *220*. 1247-1274.

175. L. E. Barrosse-Antle, A. M. Bond, R. G. Compton, A. M. O'Mahony, E. I. Rogers, D. S. Silvester, Voltammetry in room temperature ionic liquids: comparisons and contrasts with conventional electrochemical solvents. *Chem.--Asian J.* **2010**, *5*. 202-30.

176. M. Armand, F. Endres, D. R. MacFarlane, H. Ohno, B. Scrosati, Ionic-liquid materials for the electrochemical challenges of the future. *Nat. Mater.* **2009**, *8*. 621-629.

177. N. V. Ignat'ev, U. Welz-Biermann, A. Kucheryna, G. Bissky, H. Willner, New ionic liquids with tris(perfluoroalkyl)trifluorophosphate (FAP) anions. *J. Fluorine Chem.* **2005**, *126*. 1150-1159.

178. N. Nishi, S. Imakura, T. Kakiuchi, Wide electrochemical window at the interface between water and a hydrophobic room-temperature ionic liquid of tetrakis[3,5-bis(trifluoromethyl)phenyl]borate. *Anal. Chem.* **2006**, *78*. 2726-2731.

179. D. R. MacFarlane, J. H. Huang, M. Forsyth, Lithium-doped plastic crystal electrolytes exhibiting fast ion conduction for secondary batteries. *Nature* **1999**, *402*. 792-794.

180. R. Kemp, K. Fraser, K. Fujita, D. MacFarlane, G. Elliott, Biocompatible Ionic Liquids: A New Approach for Stabilizing Proteins in Liquid Formulation. *Proceedings of the Asme Summer Bioengineering Conference 2008, Pts a and B* **2009**. 947-948.

181. X. W. Chen, J. W. Liu, J. H. Wang, Ionic liquids in the assay of proteins. *Anal Methods-Uk* **2010**, *2*. 1222-1226.

182. C. Lange, G. Patil, R. Rudolph, Ionic liquids as refolding additives: N '-alkyl and N '-(omega-hydroxyalkyl) N-methylimidazolium chlorides. *Protein Sci.* **2005**, *14*. 2693-2701.

183. J. P. Mann, A. McCluskey, R. Atkin, Activity and thermal stability of lysozyme in alkylammonium formate ionic liquids-influence of cation modification. *Green Chem.* **2009**, *11*. 785-792.

184. R. M. Vrikkis, K. J. Fraser, K. Fujita, D. R. MacFarlane, G. D. Elliott, Biocompatible Ionic Liquids: A New Approach for Stabilizing Proteins in Liquid Formulation. *J Biomech Eng-T Asme* **2009**, *131*.

185. D. Corradini, I. Nicoletti, G. K. Bonn, Co-electroosmotic capillary electrophoresis of basic proteins with 1-alkyl-3-methylimidazolium tetrafluoroborate ionic liquids as non-covalent coating agents of the fused-silica capillary and additives of the electrolyte solution. *Electrophoresis* **2009**, *30*. 1869-1876.

186. D. H. Cheng, X. W. Chen, Y. Shu, J. H. Wang, Selective extraction/isolation of hemoglobin with ionic liquid 1-butyl-3-trimethylsilylimidazolium hexafluorophosphate (BtmsimPF(6)). *Talanta* **2008**, *75*. 1270-1278.

187. X. Lin, Y. Wang, Q. Zeng, X. Ding, J. Chen, Extraction and separation of proteins by ionic liquid aqueous two-phase system. *Analyst* **2013**.

188. G. Zhao, S. Chen, X.-W. Chen, R.-H. He, Selective isolation of hemoglobin by use of imidazolium-modified polystyrene as extractant. *Anal. Bioanal. Chem.* **2013**, *405*. 5353-5358.

189. K. Shimojo, K. Nakashima, N. Kamiya, M. Goto, Crown ether-mediated extraction and functional conversion of cytochrome c in ionic liquids. *Biomacromolecules* **2006**, *7*. 2-5.

190. K. Shimojo, N. Kamiya, F. Tani, H. Naganawa, Y. Naruta, M. Goto, Extractive solubilization, structural change, and functional conversion of cytochrome c in ionic liquids via crown ether complexation. *Anal. Chem.* **2006**, *78*. 7735-7742.

191. D. W. Armstrong, L.-K. Zhang, L. He, M. L. Gross, Ionic Liquids as Matrixes for Matrix-Assisted Laser Desorption/Ionisation Mass Spectrometry. *Anal. Chem.* **2001**, *73*. 3679-3686.

192. Y. L. Li, M. L. Gross, Ionic-liquid matrices for quantitative analysis by MALDI-TOF mass spectrometry. *J. Am. Soc. Mass Spectrom.* **2004**, *15*. 1833-1837.

193. S. Wang, Z. Guo, H. Zhang, Direct electrochemistry of cytochrome c entrapped in agarose hydrogel in room temperature ionic liquids. *Bioelectrochemistry* **2011**, *82*. 55-62.

194. T. Chen, H. Xiong, W. Wen, X. Zhang, S. Wang, Electrochemistry of heme proteins entrapped in DNA films in two imidazolium-based room temperature ionic liquids. *Bioelectrochemistry* **2013**, *91*. 8-14.

195. D. Abd El-Hady, A. K. Youssef, Hyphenation of ionic liquid albumin glassy carbon biosensor or protein label-free sensor with differential pulse stripping voltammetry for interaction studies of human serum albumin with fenoprofen enantiomers. *Anal. Chim. Acta* **2013**, *772*. 68-74.

196. B. M. Quinn, Z. F. Ding, R. Moulton, A. J. Bard, Novel electrochemical studies of ionic liquids. *Langmuir* **2002**, *18*. 1734-1742.

197. J. Langmaier, Z. Samec, Cyclic voltammetry of ion transfer across a room temperature ionic liquid membrane supported by a microporous filter. *Electrochem. Commun.* **2007**, *9*. 2633-2638.

198. Z. Samec, J. Langmaier, T. Kakiuchi, Charge-transfer processes at the interface between hydrophobic ionic liquid and water. *Pure Appl. Chem.* **2009**, *81*. 1473-1488.

199. T. Kakiuchi, N. Tsujioka, Electrochemical polarizability of the interface between an aqueous electrolyte solution and a room-temperature molten salt. *J. Electroanal. Chem.* **2007**, *599*. 209-212.

200. T. J. Stockmann, J. Zhang, J. C. Wren, Z. F. Ding, Hydrophobic alkylphosphonium ionic liquid for electrochemistry at ultramicroelectrodes and micro liquid vertical bar liquid interfaces. *Electrochim. Acta* **2012**, *62*. 8-18.

201. E. S. Medvedev, A. A. Stuchebrukhov, Proton diffusion along biological membranes. *J Phys-Condens Mat* **2011**, *23*.

202. Y. Shao, H. H. Girault, Kinetics of the Transfer of Acetylcholine across the Water + Sucrose 1,2-Dichloroethane Interface - a Comparison between Ion-Transport and Ion Transfer. *J. Electroanal. Chem.* **1990**, *282*. 59-72.

203. C. Wakai, A. Oleinikova, M. Ott, H. Weingartner, A. Oleinikova, M. Ott, H. Weingrtner, How polar are ionic liquids? Determination of the static dielectric constant of an imidazolium-based ionic liquid by microwave dielectric spectroscopy. *The journal of physical chemistry. B* **2005**, *109*. 17028-17030.

204. C. Daguenet, P. Dyson, I. Krossing, A. Oleinikova, J. Slattery, C. Wakai, H. Weingrtner, Dielectric response of imidazolium-based room-temperature ionic liquids. *The journal of physical chemistry. B* **2006**, *110*. 12682-12688.

205. M. V. Fedorov, N. Georgi, A. A. Kornyshev, Double layer in ionic liquids: The nature of the camel shape of capacitance. *Electrochem Commun* **2010**, *12*. 296-299.

206. N. Georgi, A. A. Kornyshev, M. V. Fedorov, The anatomy of the double layer and capacitance in ionic liquids with anisotropic ions Electrostriction vs lattice saturation. *J Electroanal Chem* **2010**, *649*. 261-267.

207. X. Li, Z. Z. Yang, Study of lithium cation in water clusters: Based on atom-bond electronegativity equalization method fused into molecular mechanics. *J. Phys. Chem. A* **2005**, *109*. 4102-4111.

208. J. Mahler, I. Persson, A Study of the Hydration of the Alkali Metal Ions in Aqueous Solution. *Inorg. Chem.* **2012**, *51*. 425-438.

209. O. N. Ventura, J. P. Bartolucci, On the Application of Some Solvation Models to the Water Dimer. *Theor. Chim. Acta* **1984**, *64*. 229-248.

210. P. Choi, N. H. Jalani, R. Datta, Thermodynamics and proton transport in Nafion - II. Proton diffusion mechanisms and conductivity. *J. Electrochem. Soc.* **2005**, *152*. E123-E130.

211. M. S. Silberberg, *Chemistry The molecular nature of matter and change*. Second ed.; McGraw Hill: Sydney, Australia, **2000**; p 1086.

212. H. Jensen, D. J. Fermin, J. E. Moser, H. H. Girault, Organization and reactivity of nanoparticles at molecular interfaces. Part 1. Photoelectrochemical responses involving TiO(2) nanoparticles assembled at polarizable water vertical bar 1,2-dichloroethane junctions. *J. Phys. Chem. B* **2002**, *106*. 10908-10914.

213. G. D. Sisk, G. Herzog, J. D. Glennon, D. W. M. Arrigan, Assessment of ion transfer amperometry at liquid-liquid interfaces for detection in CE. *Electrophoresis* **2009**, *30*. 3366-3371.

214. D. Silvester, K. Ward, L. Aldous, C. Hardacre, R. Compton, The electrochemical oxidation of hydrogen at activated platinum electrodes in room temperature ionic liquids as solvents. *J Electroanal Chem* **2008**, *618*. 53-60.

215. L. R. Wetter, H. F. Deutsch, Immunological studies on egg white proteins. IV. Immunochemical and physical studies of lysozyme. *J. Biol. Chem.* **1951**, *192*. 237-242.

216. R. H. Garrett, C. M. Grisham, *Biochemistry*. 4th Edition ed.; Brooks / Cole: Boston, **2010**; p 1059.

217. J. Shi, G. Z. Yan, K. D. Wang, Y. Fang, Non-invasive method to detect and locate haemorrhagic focus of GI tract. *J. Med. Eng. Technol.* **2007**, *31*. 123-8.

218. A. Warsinke, Point-of-care testing of proteins. *Anal Bioanal Chem* **2009**, *393*. 1393-405.

219. J. Wang, Electrochemical glucose biosensors. *Chem. Rev.* **2008**, *108*. 814-825.

220. G. Dimeski, T. Badrick, A. St John, Ion Selective Electrodes (ISEs) and interferences-A review. *Clin. Chim. Acta* **2010**, *411*. 309-317.

221. J. A. Ribeiro, I. M. Miranda, F. Silva, C. M. Pereira, Electrochemical study of dopamine and noradrenaline at the water/1,6-dichlorohexane interface. *Phys Chem Chem Phys* **2010**, *12*. 15190-4.

222. S. Amemiya, Y. Kim, R. Ishimatsu, B. Kabagambe, Electrochemical heparin sensing at liquid/liquid interfaces and polymeric membranes. *Anal Bioanal Chem* **2011**, *399*. 571-9.

223. H. G. Kristinsson, Acid-induced unfolding of flounder hemoglobin: Evidence for a molten globular state with enhanced pro-oxidative activity. *J. Agric. Food Chem.* **2002**, *50*. 7669-7676.

224. R. Kalvoda, Review of Adsorptive Stripping Voltammetry - Assessment and Prospects. *Fresen J Anal Chem* **1994**, *349*. 565-570.

225. G. Herzog, S. Flynn, C. Johnson, D. W. M. Arrigan, Electroanalytical Behavior of Poly-L-Lysine Dendrigrafts at the Interface between Two Immiscible Electrolyte Solutions. *Anal. Chem.* **2012**, *84*. 5693-5699.

226. B. Sarg, K. Faserl, L. Kremser, B. Halfinger, R. Sebastiano, H. H. Lindner, Comparing and Combining CE-ESI-MS and nano-LC-ESI-MS for the Characterisation of Post-translationally Modified Histones. *Mol. Cell. Proteomics* **2013**.

227. T. Wink, S. J. vanZuilen, A. Bult, W. P. vanBennekom, Self-assembled monolayers for biosensors. *Analyst* **1997**, *122*. R43-R50.

228. T. Osakai, T. Hirai, T. Wakamiya, S. Sawada, Quantitative analysis of the structure-hydrophobicity relationship for di- and tripeptides based on voltammetric measurements with an oil/water interface. *Phys. Chem. Chem. Phys.* **2006**, *8*. 985-993.

229. G. Herzog, M. T. Nolan, D. W. M. Arrigan, Haemoglobin unfolding studies at the liquid-liquid interface. *Electrochem. Commun.* **2011**, *13*. 723-725.

230. E. Blanco, J. M. Ruso, J. Sabin, G. Prieto, F. Sarmiento, Thermal stability of lysozyme and myoglobin in the presence of anionic surfactants. *J. Therm. Anal. Calorim.* **2007**, *87*. 211-215.

231. B. Keil, *Specificity of Proteolysis*. First edition ed.; Springer-Verlag: New York, **1992**; p 336.

232. A. C. Guyton, J. E. Hall, *Textbook of medical physiology*. Eleventh ed.; Elsevier In.: Pennsylvania, **2006**.

233. T. P. Hopp, K. R. Woods, Prediction of Protein Antigenic Determinants from Amino-Acid-Sequences. *P Natl Acad Sci-Biol* **1981**, *78*. 3824-3828.

234. J. Kyte, R. F. Doolittle, A Simple Method for Displaying the Hydropathic Character of a Protein. *J. Mol. Biol.* **1982**, *157*. 105-132.

235. M. Levitt, A simplified representation of protein conformations for rapid simulation of protein folding. *J. Mol. Biol.* **1976**, *104*. 59-107.

236. Y. Nozaki, C. Tanford, The solubility of amino acids and two glycine peptides in aqueous ethanol and dioxane solutions. Establishment of a hydrophobicity scale. *J. Biol. Chem.* **1971**, *246*. 2211-7.

237. J. Stewart. Thomson Learning Inc.: Southbank, Australia, Fifth edition edn., **2003**, p 1204.

238. R. E. Canfield, A. K. Liu, The Disulfide Bonds of Egg White Lysozyme (Muramidase). *J. Biol. Chem.* **1965**, *240*. 1997-2002.

239. S. N. Tan, H. H. Girault, Potassium transfer facilitated by monoaza-18-crown-6 across the water—1,2-dichloroethane interface. *J. Electroanal. Chem.* **1992**, *332*. 101-112.

240. D. P. Zhan, Y. Yuan, Y. J. Xiao, B. L. Wu, Y. H. Shao, Alkali metal ions transfer across a water/1,2-dichloroethane interface facilitated by a novel monoaza-B15C5 derivative. *Electrochim. Acta* **2002**, *47*. 4477-4483.

241. S. Sawada, T. Osakai, Hydrophobicity of oligopeptides: a voltammetric study of the transfer of dipeptides facilitated by dibenzo-18-crown-6 at the nitrobenzene/water interface. *Phys. Chem. Chem. Phys.* **1999**, *1*. 4819-4825.

242. D. Fass, Disulfide Bonding in Protein Biophysics. *Annu Rev Biophys* **2012**, *41*. 63-79.

Every reasonable effort has been made to acknowledge the owners of copyright material. I would be pleased to hear from any copyright owner who has been omitted or incorrectly acknowledge.

APPENDIX A

BTPPA·TPBCl metathesis

Metathesis of bis(triphenylphosphoranylidene)ammonium chloride ($BTPPA^+Cl^-$) and potassium tetrakis(4-chlorophenyl)borate (K^+TPBCl^-) to form bis(triphenylphosphoranylidene)ammonium tetrakis(4-chlorophenyl)borate BTPPA·TPBCl was performed as follows:

- $BTPPA^+$ Cl^- (1.157 g) was dissolved in 10 mL of H_2O/MeOH (1:2 v/v) solution and added drop-wise to a 20mL solution of K^+ $TPBCl^-$ (1 g) in H_2O/MeOH solution (1:2 v/v).
- The product formed BTPPA·TPBCl (see Figure appendix A) is filtered under vacume using a Buchner funnel and covered with parafilm with holes pierced in it. This process takes approximately 2 hours. Then the product is placed in a dessicator over night.

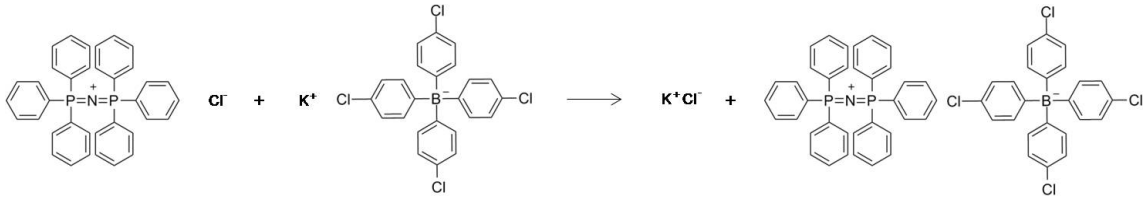

Figure appendix A. Chemical equation of the metathesis reaction between $BTPPA^+Cl^-$ and K^+TPBCl^- which occurs at a 1 to 1 molar ratio.

- BTPPA·TPBCl is re-crystallised by its dissolution in acetone. The acetone solution is filtered under gravity.
- The beaker containing the product is covered with parafilm, holes are pierced in the parafilm and the beaker placed in a fume-hood to allow the acetone to evaporate (~ 1 day).
- The resulting precipitate is washed in H_20/Acetone solution (1:1 v/v) and allowed to dry overnight in a desicator.

The final product (BTPPA·TPBCl) must be stored in a refrigerator and covered with aluminium foil as the product is photo- and thermo-sensitive.

Gelled organic phase

To improve mechanical stability, the organic solution is gelled by adding low molecular weight polyvinyl chloride in 10% w/v.

Firstly, 10mM BTPPA·TPBCl (0.025 g) solution is prepared in 2.5 ml of 1,6-dichlorohexane. The solution is stirred at 50-70°C until the organic electrolyte is completely dissolved. Then polyvinyl chloride (0.25 g) is added in stoges to form the gel (10% w/v). The temperature is increased to 100°C over 30min until solution is clean. This procedure requires the sealing of the container with parafilm to avoid solvent evaporation. Then added while is hot into the glass cylinder which has been modified previously by sealing the pores membrane onto one of the hollow sides. One hour of cooling is required before performing any electrochemical measurements.

APPENDIX B

Infrared (iR)

Figure appendix B shows the infrared spectra of $[P_{14,6,6,6}][FAP]$ and the same ionic liquid after its saturation with water and 1 M HCl.

Some of the more characteristic absorption bands for this ionic liquid are illustrated here: C-H stretch are in 3000 – 2850 cm^{-1} range, C-F in 1000 – 1360 cm^{-1}, C-P within 1400 – 900 cm^{-1} and P-F around 900 cm^{-1} (See Figure appendix B). The infrared spectra do not present any difference when the ionic liquid is saturated with water or hydrochloric acid. This means that under these conditions there is no change in the chemical structure of the RTIL.

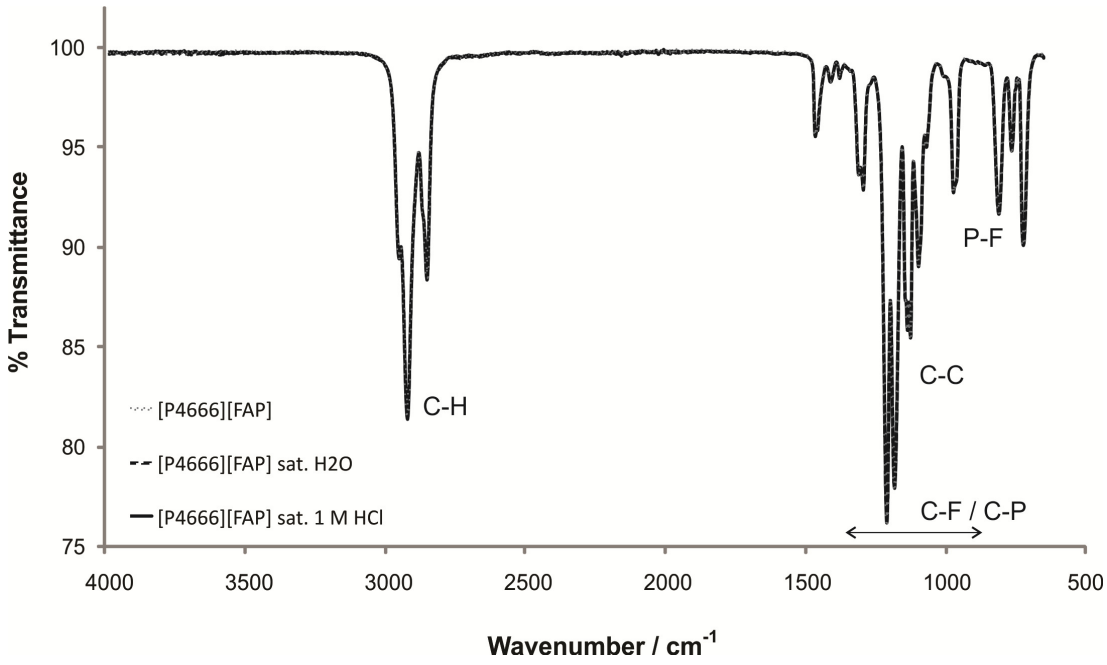

Figure appendix B1. iR of $[P_{14,6,6,6}][FAP]$ before (···), after saturation of the ionic liquid with water (- -) and 1 M HCl (—). The spectra are difficult to distinguish as they three overlap.

Nuclear magnetic resonance (NMR)

^{1}H, ^{19}F and ^{31}P NMR spectra were measured on a Bruker Avance III 400 MHz spectrometer (400.13 MHz for 1H and 376.46 for 19F) and $CDCl_3$ was used as internal reference for ^{19}F NMR and the proton spectra correspondingly. The room temperature ionic liquid (trihexyl(tetradecyl)phosphonium tris(pentafluorethyl)trifluorphosphate, $[P_{14,6,6,6}][FAP]$) was analysed before and after being saturated with H_2O or HCl in order to analyse the proton - $[(C_2F_5)_3PF_3]^-$ interactions. In the case of proton and phosphorous NMR, the net sample was measured although in the case of fluorine NMR the RTIL was dissolved with $CDCl_3$ due to its high viscosity. Once the ionic liquid was dissolved (10% v/v), the ionic liquid was saturated with H_2O or HCl.

The NMR details are summarised below:

^{1}H NMR

1H NMR spectrum, d, ppm: 0.860 – 0.912 m (4CH3), 1.257 – 1.304 (16CH2), broad peak 1.459 m (8CH2), 1.953 – 1.993 m (4CH2).

^{31}P NMR

31P NMR, d, ppm: 31.6 m (1P); 149.0 d, t, m (1P).

^{19}F NMR

19F NMR spectrum, d, ppm: 43.5 d, m (PF); 80.1 m (CF3); 81.7 m (2CF3); 86.7 d, m (PF2); 115.3 d, m (1CF2); 115.8 d, m (2CF2); 1JP,F = 892 Hz; 1JP,F = 1208 Hz; 2JP,F = 83 Hz; 2JP,F = 98 Hz.

The data presented are in agreement with Ignat'ev's NMR spectra corresponding to the same ionic liquid, trihexyl(tetradecyl)phosphonium tris(pentafluorethyl)trifluorphosphate.[177]

APPENDIX C

Tables of cleavage sites and peptide sequences after digestion

Lysozyme

Table appendix C1. Lysozyme fragments using pepsin (pH 1.3).

Position of cleavage site	Peptide sequence	Peptide length (number of amino acids)	Molecular weight / g mol^{-1}
2	KV	2	245.3
8	FGRCEL	6	723.8
19	AAAMKRHGLDN	11	1183.4
20	Y	1	181.2
22	RG	2	231.3
24	YS	2	268.3
25	L	1	131.2
27	GN	2	189.2
28	W	1	204.2
33	VCAAK	5	490.6
34	F	1	165.2
37	ESN	3	348.3
38	F	1	165.2
52	NTQATNRNTDGSTD	14	1494.5
53	Y	1	181.2
55	GI	2	188.2
56	L	1	131.2
62	QINSRW	6	802.9
74	WCNDGRTPGSRN	12	1362.4
82	LCNIPCSA	8	820.
83	L	1	131.2
84	L	1	131.2
107	SSDITASVNCAKKIVSDGNGMNA	23	2282.5
108	W	1	204.2
110	VA	2	188.2
111	W	1	204.2
122	RNRCKGTDVQA	11	1247.4
123	W	1	204.2
129	IRGCRL	6	716.9

Table appendix C2. Lysozyme peptides after pepsinisation at pH 2.

Position of cleavage site	Peptide sequence	Peptide length (number of amino acids)	Molecular weight / g mol^{-1}
2	KV	2	245.3
8	FGRCEL	6	723.8
24	AAAMKRHGLDNYRGYS	16	1810.0
25	L	1	131.2
33	GNWVCAAK	8	848.0
34	F	1	165.2
37	ESN	3	348.3
38	F	1	165.2
55	NTQATNRNTDGSTDYGI	17	1827.8
56	L	1	131.2
74	QINSRWWCNDGRTPGSRN	18	2147.3
82	LCNIPCSA	8	820.0
83	L	1	131.2
84	L	1	131.2
129	SSDITASVNCAKKIVSDGNGMNAWVAWRNRCKGTDVQAWIRGCRL	45	4939.6

Table appendix C3. Lysozyme fragments when trypsinised.

Position of cleavage site	Peptide sequence	Peptide length (number of amino acids)	Molecular weight / g mol^{-1}
1	K	1	146.2
5	VFGR	4	477.6
13	CELAAAMK	8	836.0
14	R	1	174.2
21	HGLDNYR	7	873.9
33	GYSLGNWVCAAK	12	1268.5
45	FESNFNTQATNR	12	1428.5
61	NTDGSTDYGILQINSR	16	1753.8
68	WWCNDGR	7	936.0
73	TPGSR	5	516.6
96	NLCNIPCSALLSSDITASVNCAK	23	2337.7
97	K	1	146.2
112	IVSDGNGMNAWVAWR	15	1675.9
114	NR	2	288.3
116	CK	2	249.3
125	GTDVQAWIR	9	1045.2
128	GCR	3	334.4
129	L	1	131.2

Table appendix C1. Lysozyme fragments in pepsin pH 2 and tryptic digestion.

Position of cleavage site	Peptide sequence	Peptide length (number of amino acids)	Molecular weight / g mol^{-1}
1	K	1	146.2
2	V	1	117.1
5	FGR	3	378.4
8	CEL	3	363.4
13	AAAMK	5	490.6
14	R	1	174.2
21	HGLDNYR	7	873.9
22	G	1	75.1
23	Y	1	181.2
31	SLGNWVCA	8	849
32	A	1	89.1
33	K	1	146.2
35	FE	2	294.3
36	S	1	105.1
45	NFNTQATNR	9	1065.1
53	NTDGSTDY	8	871.8
54	G	1	75.1
61	ILQINSR	7	843
68	WWCNDGR	7	936
72	TPGS	4	360.4
73	R	1	174.2
80	NLCNIPC	7	775.9
81	S	1	105.1
96	ALLSSDITASVNCAK	15	1492.7
97	K	1	146.2
112	IVSDGNGMNAWVAWR	15	1675.9
114	NR	2	288.3
116	CK	2	249.3
125	GTDVQAWIR	9	1045.2
128	GCR	3	334.4
129	L	1	131.2

Table appendix C5. Lysozyme peptides when endoproteinase Glu-C in PBS.

Position of cleavage site	Peptide sequence	Peptide length (number of amino acids)	Molecular weight / g mol^{-1}
6	KVFGRCE	6	708.9
17	LAAAMKRHGLD	11	1196.4
34	NYRGYSLGNWVCAAKFE	17	1964.2
47	SNFNTQATNRNTD	13	1496.5
51	GSTD	4	378.3
65	YGILQINSRWWCND	14	1768
86	GRTPGSRNLCNIPCSALLSSD	21	2161.4
118	ITASVNCAKKIVSDGNGMNAWV AWRNRCKGTD	24	2464.8
129	VQAWIRGCRL	11	1316.6

Table appendix C6. Lysozyme digest using endoproteinase Glu-C in NH_4^+.

Position of cleavage site	Peptide sequence	Peptide length (number of amino acids)	Molecular weight / g mol^{-1}
6	KVFGRCE	6	708.9
17	LAAAMKRHGLDNYRGYSLGNW VCAAKFE	28	3142.6
129	SNFNTQATNRNTDGSTDYGILQI NSRWWCNDGRTPGSRNLCNIPCS ALLSSDITASVNCAKKIVSDGNG MNAWVAWRNRCKGTDVQAWIR GCRL	95	10497.7

Myoglobin

Table appendix C7. Myoglobin fragments using pepsin (pH 1.3).

Position of cleavage site	Peptide sequence	Peptide length (number of amino acids)	Molecular weight / g mol^{-1}
1	G	1	75.1
2	L	1	131.2
6	SDGE	4	406.3
7	W	1	204.2
10	QQV	3	373.4
11	L	1	131.2
13	NV	2	231.3
14	W	1	204.2
28	GKVEADIAGHGQEV	14	1409.5
29	L	1	131.2
32	IRL	3	400.5
39	FTGHPET	7	787.8
40	L	1	131.2
42	EK	2	275.3
43	F	1	165.2
45	DK	2	261.3
46	F	1	165.2
47	K	1	146.2
48	H	1	155.2
60	LKTEAEMKASED	12	1351.5
61	L	1	131.2
68	KKHGTVV	7	767.9
69	L	1	131.2
71	TA	2	190.2
72	L	1	131.2
75	GGI	3	245.3
76	L	1	131.2
85	KKK GHHEAE	9	1063.2
88	LKP	3	356.5
102	LAQSHATKHKIPIK	14	1571.9
103	Y	1	181.2
105	LE	2	260.3
106	F	1	165.2
114	ISDAIIHV	8	867
122	LHSKHPGD	8	890
123	F	1	165.2
134	GADAQGAMTKA	11	1020.1
136	LE	2	260.3

137	L	1	131.2
138	F	1	165.2
145	RNDIAAK	7	786.9
146	Y	1	181.2
148	KE	2	275.3
150	LG	2	188.2
151	F	1	165.2
153	QG	2	203.2

Table appendix C8. Myoglobin peptides obtained after pepsinisation (pH 2).

Position of cleavage site	Peptide sequence	Peptide length (number of amino acids)	Molecular weight / g mol^{-1}
1	G	1	75.1
2	L	1	131.2
10	SDGEWQQV	8	948.0
11	L	1	131.2
28	NVWGKVEADIAGHGQEV	17	1809.0
29	L	1	131.2
32	IRL	3	400.5
39	FTGHPET	7	787.8
40	L	1	131.2
42	EK	2	275.3
43	F	1	165.2
45	DK	2	261.3
46	F	1	165.2
48	KH	2	283.3
60	LKTEAEMKASED	12	1351.5
61	L	1	131.2
68	KKHGTVV	7	767.9
69	L	1	131.2
71	TA	2	190.2
72	L	1	131.2
75	GGI	3	245.3
76	L	1	131.2
85	KKKGHHEAE	9	1063.2
88	LKP	3	356.5
103	LAQSHATKHKIPIKY	15	1735.1
105	LE	2	260.2
106	F	1	165.2
114	ISDAIIHV	8	867.0
122	LHSKHPGD	8	890.0
123	F	1	165.2

134	GADAQGAMTKA	11	1020.1
136	LE	2	260.3
137	L	1	131.2
138	F	1	165.2
148	RNDIAAKYKE	10	1207.4
150	LG	2	188.2
151	F	1	165.2
153	QG	2	203.2

Table appendix C9. Myoglobin digest after trypsinisation.

Position of cleavage site	Peptide sequence	Peptide length (number of amino acids)	Molecular weight / g mol^{-1}
16	GLSDGEWQQVLNVWGK	16	1816.0
31	VEADIAGHGQEVLIR	15	1606.8
42	LFTGHPETLEK	11	1271.4
45	FDK	3	408.5
47	FK	2	293.4
50	HLK	3	396.5
56	TEAEMK	6	707.8
62	ASEDLK	6	661.7
63	K	1	146.2
77	HGTVVLTALGGILK	14	1378.7
78	K	1	146.2
79	K	1	146.2
96	GHHEAELKPLAQSHATK	17	1854.1
98	HK	2	283.3
102	IPIK	4	469.6
118	YLEFISDAIIHVLHSK	16	1885.2
133	HPGDFGADAQGAMTK	15	1502.6
139	ALELFR	6	747.9
145	NDIAAK	6	630.7
147	YK	2	309.4
153	ELGFQG	6	649.7

APPENDIX D

Hydrophilicity scales

Table appendix D1. Amino acid hydrophilicity in the Hopp-Woods and Kyte-Doolittle scales.

Amino acid	Amino acid abbreviation	Amino acid letter	Hopp-Woods scale[233]	Kyte-Doolittle scale[234]
Alanine	Ala	A	-0.5	1.8
Arginine	Arg	R	3.0	-4.5
Asparagine	Asn	N	0.2	-3.5
Aspartic acid	Asp	D	3.0	-3.5
Cysteine	Cys	C	-1.0	2.5
Glutamic acid	Glu	E	0.2	-3.5
Glutamine	Gln	Q	3.0	-3.5
Glycine	Gly	G	0.0	-0.4
Histidine	His	H	-0.5	-3.2
Isoleucine	Ile	I	-1.8	4.5
Leucine	Leu	L	-1.8	3.8
Lysine	Lys	K	3.0	-3.9
Methionine	Met	M	-1.3	1.9
Phenylalanine	Phe	F	-2.5	2.8
Proline	Pro	P	0.0	-1.6
Serine	Ser	S	0.3	-0.8
Threonine	Thr	T	-0.4	-0.7
Tryptophan	Trp	W	-3.4	-0.9
Tyrosine	Tyr	Y	-2.3	-1.3
Valine	Val	V	-1.5	4.2

APPENDIX E

Free amino acid content (GC-MS data)

Table appendix E1. Free amino acid amount in 100 µL of sample (1 mM lysozyme digested in 40 µM enzyme) treated with the EZ:faast GC kit and measured via GC-MS after derivatisation.

Amino acid	Amino acid concentration / nmol							
	Pep pH 1.3	Pep pH 2	Pep pH 3	Tryp	Pep pH 1.3 - Tryp	Pep pH 2 - Tryp	Endo PBS	Endo NH_4^+
Alanine	87.52	39.03	3.38	0.7	9.33	7.14	2.29	2.25
Sarcosine	0.93	0.73	0.76	0.92	0.92	0.75	1.19	1.03
Glycine	7.54	5.13	2.01	1.34	2.6	5.52	2.6	3.33
Valine	2.88	3.54	4.41	0	0.64	0.81	0.63	0.38
Leucine	605.83	283.97	23.73	3.03	64.61	50.1	4.37	2.93
Isoleucine	0	0	0.6	0	0	0	0.49	0
Threonine	1.14	1.54	0.98	0	0	0	0.67	0.39
Serine	2.02	2.46	0	0	0	1.11	1.36	1.17
Proline	0.57	0.57	0	0.14	0.18	0.16	0.4	0.82
Asparagine	22.44	8.9	0.54	0	2.94	1.23	2.87	7.29
Aspartic acid	7.45	4.07	0.52	0.3	1.42	0.68	5.78	8.14
Methionine	6.76	6.23	1.96	0	0	0.74	0	0
Glutamic acid	3	2.98	0	0	0.45	0.37	1.53	1.73
Phenylalanine	56.27	31.99	8	0.51	7.74	4.96	0.56	0.12
Glutamine	20.05	13.39	8.16	11.34	11.77	10.75	12	17.04
Ornithine	1.33	1.23	0.94	0	0	0	0.57	0
Lysine	1.59	1.29	1.04	2.04	1.22	3.02	1.09	0.79
Histidine	0	0	0	0	0	0	0	0
Tyrosine	49.35	25.36	8.23	0.44	4.44	4.95	0.56	0
Tryptophan	432.46	216.24	18.69	0.22	81.86	43.67	0.17	0.37

**Ornithine is the degradation product of arginine*

***Sarcosine is the degradation product of glycine.*

Table appendix E2. Free amino acid amount in 100 µL of sample (1 mM myoglobin digested in 40 µM enzyme) treated with the EZ:faast GC kit and measured via GC-MS after derivatisation.

Amino Acid	Amino acid concentration / nmol				
	Pepsin pH 2	**Pepsin pH 3**	**Trypsin**	**Pepsin pH 1.3 - Trypsin**	**Pepsin pH 2 - Trypsin**
Alanine	9.18	3.09	5.99	23.68	14.86
Sarcosine	1.25	0.94	1.12	1.2	1.49
Glycine	4.74	2.15	24.47	3.71	3.93
Valine	3.8	15.64	3.72	2.12	0.83
Leucine	49.41	2.65	68.68	17.38	21.71
Isoleucine	2.55	1.25	0	0.66	0
Threonine	1.94	0.98	5.03	2.32	8.82
Serine	1.5	0.78	1.96	0	0
Proline	0.44	0	0	1.37	0
Asparagine	0	0	2.88	0	0
Aspartic acid	2.19	0.46	4.33	3.87	0.75
Methionine	5.02	0	3.21	6.64	1.3
4-Hydroxyproline	0	1.27	0	0	0
Glutamic acid	9.12	4.95	15.36	10.82	3.97
Phenylalanine	43.45	0	50.8	23.95	14.12
Glutamine	33.26	69.07	39.63	36.92	17.48
Ornithine	2	1.27	0	0	0
Lysine	7.61	2.43	780.77	19.02	82.83
Histidine	0	0	40.61	0	0
Tyrosine	12.95	0	157.23	6.58	20.94
Tryptophan	3.23	0.1	2.8	10.41	1.07

**Ornithine is the degradation product of arginine*

***Sarcosine is the degradation product of glycine.*

APPENDIX F

Second derivative graphs

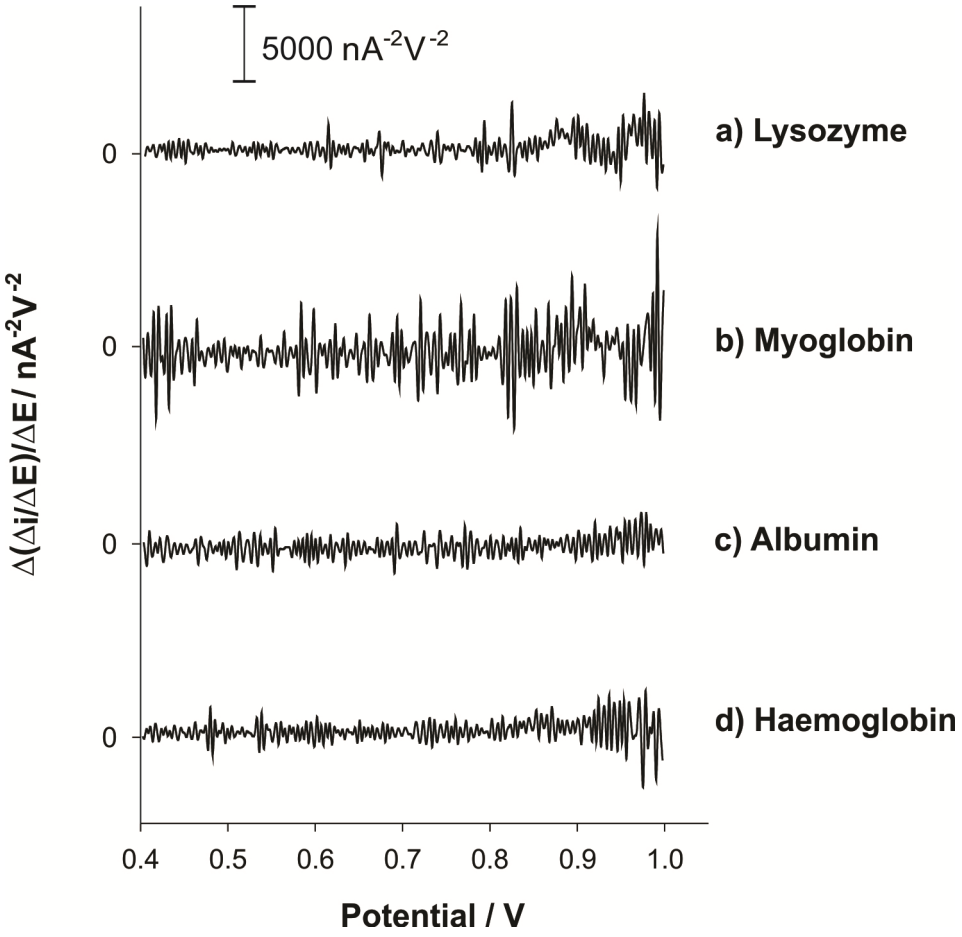

Figure appendix F1. Second derivative of forward current versus potential of a) lysozyme, b) myoglobin, c) BSA and d) haemoglobin after pepsinisation at pH 2. Concentrations correspond to 30μM of initial protein.

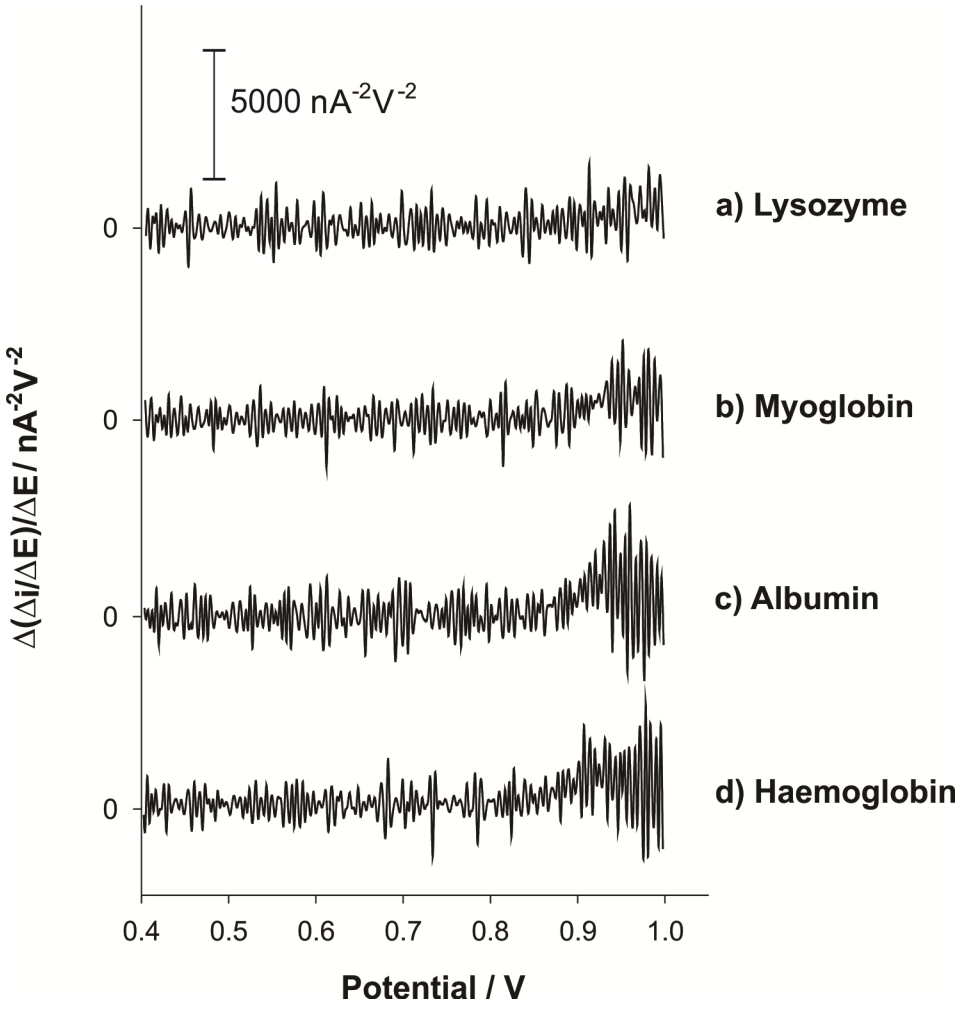

Figure appendix F2. Second derivative of forward current versus potential of a) lysozyme, b) myoglobin, c) BSA and d) haemoglobin after tryptic digestion. Concentrations correspond to 30μM of initial protein.

APPENDIX G

Journal Publications

1. Stripping voltammetric detection of insulin at liquid-liquid microinterfaces in the presence of bovine albumin

S. O'Sullivan, E. Alvarez de Eulate, Y. H. Yuen, E. Helmerhorst, D. W. M. Arrigan

*Analyst (**2013**), 138, 6192-6196*

2. Ion transfer electrochemistry of rat amylin at the water-organogel microinterface array and its selective detection in a protein mixture

E. Alvarez de Eulate, S. O'Sullivan, S. Fletcher, P. Newsholme, D. W. M. Arrigan

*Chemistry an Asian Journal (**2013**), 8 (9), 2096-2101*

Back cover (Chemistry an Asian Journal, page, (2013))

3. Detection of haemoglobin using an adsorption approach at a liquid–liquid microinterface array

E. Alvarez de Eulate, L. Serls, D. W. M. Arrigan

*Analytical & Bioanalytical Chemistry (**2012**), 405 (11), 3801-3806*

4. Behaviour of Lysozyme at the Electrified Water / Room Temperature Ionic Liquid Interface

E. Alvarez de Eulate, D. S. Silvester, D. W. M. Arrigan

*Chemistry an Asian Journal (**2012**), 7 (11), 2559-2561,*

Inside cover (Chemistry an Asian Journal, page 2462, (2012))

5. Adsorptive stripping voltammetry of hen-egg-white-lysozyme via adsorption-desorption at an array of liquid-liquid microinterfaces

E. Alvarez de Eulate, D. W. M. Arrigan

*Analytical Chemistry (**2012**), 84 (5), 2505–2511*

Kali-Alexander HDR Publication Prize (2012)

Oral presentations

1. Electrochemical protein pre-concentration at the gelled liquid/liquid interface followed by mass spectrometry via electrostatic spray ionisation

E. Alvarez de Eulate, D. W. M. Arrigan

19th Australia/New Zealand Electrochemistry Symposium (19ANZES)

Melbourne (Australia) November 2013

2. Protein detection and identification via electrochemistry at liquid – liquid interfaces

E. Alvarez de Eulate, D. W. M. Arrigan

Seminar at Institute of Bioengineering of Catalonia (IBEC)

Barcelona (Spain) July 2013

3. Adsorptive stripping voltammetry of lysozyme via adsorption-desorption at liquid/liquid microinterfaces

E. Alvarez de Eulate, D. W. M. Arrigan

18th Australian Electrochemistry Symposium (18AES)

Perth (Australia) April 2012

4. Adsorptive stripping voltammetry of lysozyme via adsorption-desorption at liquid/liquid microinterfaces

E. Alvarez de Eulate, D. W. M. Arrigan

19th Annual RACI Analytical and Environmental Divisions Research and Developments Topics Conference for 2011

Melbourne (Australia) December 2011

**Oral Presentation Awards, Honourable mention*

Poster presentations

1. Protein detection and identification via electrochemistry at liquid – liquid interfaces

E. Alvarez de Eulate, D. W. M. Arrigan

Biological Surfaces and Interfaces, FEBS workshop

Sant Feliu de Guixols (Spain) July 2013

2. Proton and protein voltammetry at a water/ionic liquid microinterface array

E. Alvarez de Eulate, D. S. Silvester D. W. M. Arrigan

5th Australian Symposium on Ionic Liquids (ASIL-5)

Melbourne (Australia) May 2012

3. Proton and protein voltammetry at a water/ionic liquid microinterface array

E. Alvarez de Eulate, D. S. Silvester D. W. M. Arrigan

10th Spring meeting of International Society of Electrochemistry (ISE)

Perth (Australia) April 2012